NORTHWESTERN UNIVERSITY

Mechanisms of Bone Morphogenetic Protein Regulation of Neural Progenitor Cell Fate Specification

A DISSERTATION

SUBMITTED TO THE GRADUATE SCHOOL
IN PARTIAL FULFILLMENT OF THE REQUIREMENTS

for the degree

DOCTOR OF PHILOSOPHY

Field of Life Sciences

By

Jessie Chen

EVANSTON, ILLINOIS

September 2020

ABSTRACT

Mechanisms of Bone Morphogenetic Protein Regulation of Neural Progenitor Cell Fate Specification

Jessie Chen

Neural stem and progenitor cell (NPC) fate specification is a crucial component of central nervous system development, and the myriad signaling pathways that guide it are poorly understood. In my thesis work, I aimed to elucidate signaling mechanisms of the bone morphogenetic protein family (BMP) and some of its targets on astrocyte differentiation and neural stem cell maintenance. While BMP signaling was initially identified in ossification processes, it has subsequently been discovered to play a major role in NPC fate determination. However, these effects change over the course of development, and the ranges of effects are extremely wide. To address this, my lab has focused our studies on identifying downstream targets and mechanisms of BMP signaling. Here, we first utilized a microarray to identify genes upregulated in astrocytes generated from BMP4 treatment, and enriched in comparison to neural stem cells. We identified HtrA1 as one such gene, and found it to be expressed in astrocytes but not stem cells, indicating its potential use as an astrocytic marker. Additionally, we found HtrA1 to regulate astrocyte maturation rate, as well as injury response. To identify immediate regulators of BMP4 signaling effects on NPC fate, we then conducted RNA sequencing on neural progenitor cells with different BMP receptor subunits deleted, which were treated with BMP4 for a short duration. The large number of different genes that are differentially regulated in the absence of individual BMP receptors indicate unique functions that have not been properly parsed apart in the past. BMP receptor type 1 subunits may be responsible for some of the variation in BMP effects. Our identification of short-term BMP signaling targets flagged several

pathways as BMP-regulated, including Hippo signaling. Our last section of studies described here therefore sought to examine the intersection of BMP and Hippo signaling at the level of Hippo pathway transcriptional factors. BMP upregulates the Hippo effector Ww-domain containing transcription regulator 1 (TAZ), but not the effector Yes-associated protein (YAP). TAZ, but not YAP, promotes astrocyte differentiation of NPCs, and YAP and TAZ together regulate the morphology of BMP-generated astrocytes. Altogether, these studies demonstrate some of BMP's signaling targets and their effects on NPC fate specification, particularly towards astrocyte differentiation, as well as the need for further studies to identify other downstream BMP mechanisms.

ACKNOWLEDGEMENTS

My deepest gratitude to my partner, Marco Ravaglia, for his unwavering patience and support (and years of home-cooked meals and desserts).

LIST OF ABBREVIATIONS

Aldh1L1	aldehyde dehydrogenase 1 family member L1
ANOVA	analysis of variance
BMP	Bone morphogenetic protein
BMPR1a	bone morphogenetic protein receptor subunit 1a, also abbreviated as R1a
BMPR1b	bone morphogenetic protein receptor subunit 1b, also abbreviated as R1b
BMPR2	bone morphogenetic protein receptor subunit 2, also abbreviated as R2
CARASIL	cerebral autosomal recessive arteriopathy with subcortical infarcts and leukoencephalopathy
CDC	Centers for Disease Control and Prevention
CNS	central nervous system
CNTF	ciliary neurotrophic factor
Ctgf	connective tissue growth factor
DCX	doublecortin
DIV1	days in vitro 1
DIV3	days in vitro 3
DMEM	Dulbecco’s minimum essential medium
ECM	extracellular matrix
EdU	5-ethynyl-2’-deoxyuridine
EGF	epidermal growth factor
FDA	Food and Drug Administration
FDR	False discovery rate
GFAP	glial fibrillary acidic protein

HtrA1	high temperature requirement A serine protease 1
Id	Inhibitor of differentiation
ILK	Integrin-linked kinase
JAK-STAT	Janus kinase-signal transducer and activator of transcription
LIF	leukemia inhibitory factor
mRNA	messenger ribonucleic acid
NPC	neural progenitor cell
NSC	neural stem cell
P1	postnatal day 1
P3	postnatal day 3
P4	postnatal day 4
P7	postnatal day 7
PCR	polymerase chain reaction
qPCR	quantitative RT-PCR
Rasgrf1	ras guanine nucleotide releasing factor 1
S100β	S100 Calcium-Binding Protein, Beta
SEM	standard error of the mean
Shh	Sonic hedgehog
TAZ	WW-domain containing transcriptional regulator 1
TGFβ	Transforming Growth Factor Beta
Vcl	Vinculin
YAP	Yes-associated protein
Wwtr1	WW-domain containing transcriptional regulator 1 (alternate name)

“The question isn’t whether it’s doable; it is. It’s just whether we’ll have the focus and the persistence to actually do it. Powerful enemies make for a big, difficult fight. But you can’t win if you don’t play, and in this fight it’s the stakes that should motivate us: Democracy either wins this one or disappears. It oughtta be a blowout.”

— Rachel Maddow, Blowout

TABLE OF CONTENTS

TABLE OF FIGURES AND TABLES

Chapter 1

General Introduction

I. Bone Morphogenetic Protein Overview

Bone morphogenetic protein signaling (BMP) plays a central role in multiple aspects of development, from the earliest stages of embryogenesis through adult life. Despite the name indicating a primary role in ossification and skeletal formation, BMPs exert a myriad of effects on many biological systems. BMPs, which are part of the larger transforming growth factor beta (TGFβ) family of ligands, have a wide array of functions in multiple cell types and serve as critical morphogens that are particularly important for their role in developing and regulating the nervous system. Within the BMP subgroup, there are a number of different BMP ligands, which themselves have varying functions. Of particular interest are BMP2 and BMP4, which play a major role in the central nervous system (CNS).

Even within the CNS, BMPs influence a wide arrange of processes, from neural tube patterning during early development to neural stem cell (NSC) maintenance through adulthood. In embryogenesis, BMPs direct embryonic patterning and cell fate specification (Bond, Bhalala, & Kessler, 2012). In the adult nervous system, BMP signaling regulates neurogenesis and hippocampal-dependent cognitive function, and alterations in BMP signaling mediate aging-related decreases in cognition (Bond et al., 2014; Meyers et al., 2016). BMPs are one of the primary signals that govern gliosis after injury to the nervous system (Sahni et al., 2010). The central role of BMP signaling in regulating nervous system formation as well as responses to injury or disease makes it important to understand the cellular and molecular events downstream of activation of BMP receptors.

BMP2/4 signaling has been traditionally referred to as either canonical or non-canonical. Signaling is mediated through tetrameric receptor complexes composed of dimers of both type 2 serine/threonine kinase receptor subunits (BMPR2) (F. Liu, Ventura, Doody, & Massagué, 1995) and type 1 serine/threonine kinase subunits (either BMPR1a or BMPR1b) (Dijke, Yamashita, Ichijo, et al., 1994a; Dijke, Yamashita, Sampath, et al., 1994b; Koenig et al., 1994) (Figure 1.1). In canonical BMP signaling, a BMP2/4 ligand binds to the pre-formed receptor complex due to type 1 receptor ligand affinity. Through this heteromeric complex (Attisano, Wrana, Montalvo, & Massagué, 1996; Marom, Heining, Knaus, & Henis, 2011; Nohno et al., 1995; Wrana, Attisano, Wieser, Ventura, & Massagué, 1994), the BMPR2 subunits phosphorylate the type 1 receptor subunits. In turn, the BMP type 1 receptor subunits phosphorylate SMADs 1/5/8 on serine residues (Hoodless et al., 1996; Kretzschmar, Liu, Hata, Doody, & Massagué, 1997; F. Liu et al., 1996; Nakayama et al., 1998b; Newfeld et al., 1997; Suzuki, Chang, Yingling, Wang, & Hemmati-Brivanlou, 1997; Wieser, Wrana, & Massagué, 1995), and then associate with co-SMADs (SMAD4) and translocate to the nucleus to stimulate transcriptional activity (Lagna, Hata, Hemmati-Brivanlou, & Massagué, 1996; F. Liu et al., 1996). This leads to regulation of downstream signaling targets such as glial fibrillary acidic protein (GFAP) (Bonaguidi et al., 2005) and the inhibitor of differentiation (ID) proteins (Ying, Nichols, Chambers, & Smith, 2003a). BMP-activated SMADs likely associate with other transcriptional co-activators, such as CBP/p300, to exert their effects (Waltzer & Bienz, 1999).

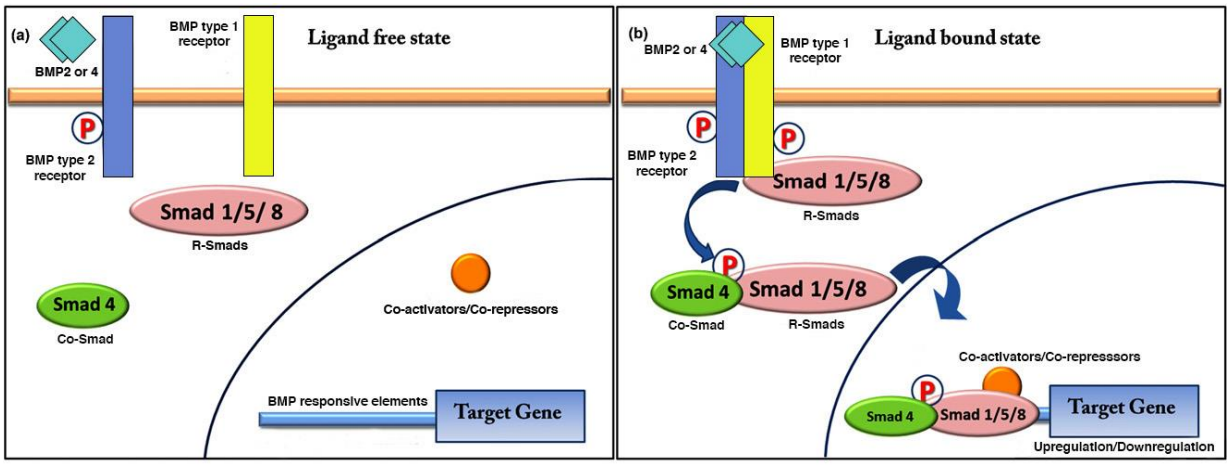

Figure 1.1 Diagram of BMP2/4 signaling
Adapted from Bandyopadhyay 2013 *Biochem Pharmacol* (Bandyopadhyay, Yadav, & Prashar, 2013). BMP2/4 signaling is mediated through heterodimers of type 1 and type 2 receptors. When BMP2 or BMP4 binds to the BMP receptor complex, type 2 receptor subunits phosphorylate the type 1 receptors, which go on to activate SMAD 1/5/8. These receptor SMADs (R-Smads) recruit the Co-Smad SMAD4, and translocate to the nucleus to exert transcriptional effects.

BMP2/4 also has non-canonical downstream effects, which are frequently mediated by ligand-induced formation of receptor complexes (Guzman et al., 2012; Nohe et al., 2002). BMPs have a wide variety of non-canonical signaling pathways, including the MAP kinase p38 (Bond et al., 2012; Hassel et al., 2003; Kendall et al., 2005; Nohe et al., 2002), although many other downstream targets are likely unknown. One such identified non-canonical pathway is mediated by TAK1, which is a mitogen-activated protein kinase kinase kinase (MAPKKK) downstream of both BMP and TGFβ (Yamaguchi et al., 1995). TAK1 activation is enhanced by TAK1 binding protein (TAB1) (Sakurai, Miyoshi, Mizukami, & Sugita, 2000; Shibuya et al., 1996), and X-linked inhibitor of apoptosis (XIAP) links the BMP receptors to TAB1 and TAK1 (Yamaguchi et al., 1999). This signaling pathway has been implicated in BMP-mediated embryonic development, as well as regulation of apoptosis.

BMP signaling moderates a wide variety of processes through both canonical and non-canonical pathways. Here we outline some of those processes, starting from early embryonic

patterning through late embryogenesis and adulthood. We also cover the role BMP signaling may play during injury and inflammation, and delve into some of the mechanisms of BMP signaling and crosstalk with other pathways.

II. BMP effects on embryonic patterning

BMP signaling plays a critical role in multiple phases of embryonic development, and is highly conserved across species, indicating its importance. In the earliest stages of mouse embryonic development, BMPs and their receptor subunits are expressed pre-gastrulation (Beppu et al., 2000; Lawson et al., 1999; Mishina, Suzuki, Ueno, & Behringer, 1995). Ablation of BMP4, BMPR1a, or BMPR2 results in early embryonic lethality and gross embryonic defects (Beppu et al., 2000; Lawson et al., 1999; Mishina et al., 1995; Winnier, Blessing, Labosky, & Hogan, 1995).

BMP2/4 signaling through BMPR1a is necessary to maintain embryonic cell pluripotency (Di-Gregorio et al., 2007), and may do so through inhibition of the extracellular receptor kinase (ERK) and p38 MAPK pathways (Qi et al., 2004). BMP also acts in combination with leukemia inhibitory factor (LIF) and transcription factor STAT3 to activate Id gene expression through canonical SMAD signaling (Ying, Nichols, Chambers, & Smith, 2003b). BMP signaling through SMAD1/5/8 phosphorylation regulates cell cleavage in the preimplantation phases (Reyes de Mochel et al., 2015). At these early stages, BMP serves to inhibit premature neuralization of vertebrate tissue and promote ventralization of the embryo, as well as induce formation of the epidermis from ectoderm (C. M. Jones, Dale, Hogan, Wright, & Smith, 1996; Weinstein & Hemmati-Brivanlou, 1999; Wilson & Hemmati-Brivanlou, 1995). Expression of SMAD1, SMAD5, or a constitutively active version of BMPR1a similarly cause embryonic ventralization

of dorsally located tissue (Shibuya et al., 1998), and several components of the non-canonical BMP-XIAP-TAB1-TAK1 signaling pathway have similar effects on embryonic ventralization (Shibuya et al., 1996; 1998; Yamaguchi et al., 1999).

BMP signaling is critical during embryonic gastrulation, and different ligand doses regulate terminal cell type specification (Dosch, Gawantka, Delius, Blumenstock, & Niehrs, 1997). Ordinarily, the BMP signaling inhibitors noggin, follistatin, and chordin function as inducers of neural tissue from dorsal ectoderm by blocking BMP-mediated induction of ectoderm to mesoderm, as aberrant BMP4 expression results in disrupted embryonic patterning and irregular germ layer formation (Fainsod, Steinbeisser, & De Robertis, 1994; Hemmati-Brivanlou, Kelly, & Melton, 1994; Lamb et al., 1993; Sasai, Lu, Steinbeisser, & De Robertis, 1995). Inhibition of BMP signaling through overexpression of the inhibitory SMADs SMAD6 or SMAD7 is sufficient to induce ectoderm neutralization (Casellas & Brivanlou, 1998; A. Hata, Lagna, Massagué, & Hemmati-Brivanlou, 1998; Nakayama, Gardner, Berg, & Christian, 1998a). Conversely, in *Xenopus* embryos, disruption of normal BMP activity through swirl/bmp2b mutation results in excessive embryo dorsalization and floorplate tissue expansion (Barth et al., 1999).

Ablation of BMP signaling through BMPR1a knockout leads to impairment of mesoderm formation, although embryonic survival until E9.5 indicates that there may be at least some overlapping function between BMP receptors (Mishina et al., 1995). Dominant negative BMP receptor constructs are able to achieve a similar disruption in BMP signaling, leading to excessive mesoderm dorsalization (Graff, Thies, Song, Celeste, & Melton, 1994). In studies examining the role of BMP signaling in human embryonic stem cells (hESCs), a delicate balance between BMP signaling and its inhibitors is necessary to regulate spontaneous differentiation

into endoderm cells, with the antagonist Noggin potentiating hESCs into a neural lineage (Pera et al., 2004). Studies of BMP-deficient chimeric embryos post-gastrulation indicate that BMP deficient tissues may still form all three germ layers (ectoderm, mesoderm, and endoderm) of an embryo in which the epiblast is wild-type (S. Davis, Miura, Hill, Mishina, & Klingensmith, 2004). However, patterning of all three layers is highly irregular, including a dramatically expanded neuroectoderm, indicating that BMP plays critical roles in tissue organization.

Following the establishment of neuroectoderm, the neural tube is formed. BMPs then direct dorsal-ventral patterning (Barth et al., 1999). A high level of BMPs, including BMP4, is established in the neural plate on the dorsal side of the neural tube (Liem, Tremml, Roelink, & Jessell, 1995). Higher BMP concentrations elicit dorsal fates and lower concentrations occur ventrally, where they may regulate responses to Sonic hedgehog (Shh) signaling (Liem, Jessell, & Briscoe, 2000), since Shh is necessary for establishment of the ventral neural tube floorplate (Bond et al., 2012; Chiang et al., 1996).

In addition to dorsal-ventral patterning, BMPs affect left-right asymmetry. Many components of BMP signaling, including SMAD1 and BMP4, are expressed asymmetrically in Hensen's node of the primitive streak during early chick development (Monsoro-Burq & Le Douarin, 2000). BMP presence regulates the asymmetrical distribution of Shh (Monsoro-Burq & Le Douarin, 2001), and BMP is necessary for expression of left-right determinants, including the left-right patterning genes *nodal* and *lefty2* (Fujiwara, Dehart, Sulik, & Hogan, 2002). Similarly, ablation of SMAD5 results in embryonic lethality, abnormal heart development, and irregular expression of *nodal* and its antagonists *lefty-1* and *lefty-2* (H. Chang, Zwijsen, Vogel, Huylebroeck, & Matzuk, 2000). BMP signaling through SMAD5 appears to act on left-right patterning through regulation of *nodal* in particular, although studies conflict as to the exact

mechanism of BMP-Nodal interaction and it is likely there is both a spatial and temporal component to BMP orchestration of signals ((Schlange, Arnold, & Brand, 2002), reviewed in (Capdevila, Vogan, Tabin, & Izpisúa Belmonte, 2000)).

II. BMP effects on cell fate specification during early development

During development, BMP signaling impacts not only embryonic patterning and organization, but also cellular proliferation and apoptosis. BMPs promote proliferation in the earliest embryonic stages, with receptor ablation resulting in proliferative defects (Beppu et al., 2000; Di-Gregorio et al., 2007; Mishina et al., 1995). Ablation of BMPR1a dramatically decreases proliferation in mouse embryos before gastrulation and before any embryonic structural anomalies are visibly detected (Mishina et al., 1995). Overexpression of constitutively active BMPR type 1 receptors results in increased proliferation in chondrogenic areas of the embryo (Zou, Wieser, Massagué, & Niswander, 1997a).

BMP4 promotes apoptosis of the neural crest in certain rhombomeres during chick hindbrain development (Graham, Francis-West, Brickell, & Lumsden, 1994). Relatedly, during mouse embryonic development, multiple BMPs are expressed in the dorsomedial neuroectoderm, coinciding with reduced tissue expansion. Application of BMP4 to explants removed at this stage reduces proliferation and increases apoptosis (Furuta, Piston, & Hogan, 1997), perhaps indicative of a changing role for BMP signaling in regulating cell cycle dynamics in comparison to the earliest embryonic stages. Conditional disruption of BMPR1a expression under a Foxg1-driven Cre recombinase removes BMPR1a throughout the developing telencephalon, inhibiting formation of the choroid plexus and maintaining cells in a more proliferative, less differentiated state (Hébert, Mishina, & McConnell, 2002).

As with neuroectoderm formation, within limb development, BMPR1a expression is necessary for proper ventral limb identity formation (Ahn, Mishina, Hanks, Behringer, & Crenshaw, 2001). BMP continues to regulate apoptosis during limb formation as well. Ordinarily, limb buds extend into digits, which require apoptosis for proper formation. In chick embryos, overexpression of a dominant negative BMPR1b receptor (dnBMPR1b), which cannot be phosphorylated to transduce BMP signaling intracellularly, results in webbing between digits, as well as abnormally truncated digits (Zou & Niswander, 1996). BMP regulation of apoptosis is suggested due to presence of BMP in these webbed areas in wild-type embryos, as well as a decrease in TUNEL staining in dnBMPR1b-infected limbs (Zou & Niswander, 1996). Conversely, overexpression of a constitutively activated version of BMPR1b promotes cell death (Zou, Wieser, Massagué, & Niswander, 1997a).

BMP also has profound effects on cell lineage specification. In early embryonic development, BMP signaling serves to inhibit premature neural differentiation (Di-Gregorio et al., 2007; Finley, Devata, & Huettner, 1999). In cultures of murine mesencephalon tissue, BMPs promote neuronal survival, proliferation, and GFAP immunoreactivity (Jordan, Böttner, Schluesener, Unsicker, & Krieglstein, 1997). BMP treatment of neuronal precursors dissected from the mouse telenecephalon at embryonic day E12-13 leads to increased MAP2+ and Tuj1+ neuronal differentiation, while overexpression of a dominant negative BMPR1a in impairs neurite extension *in vitro* and cell migration in neocortical explant cultures (W. Li, Cogswell, & LoTurco, 1998).

BMP signaling inhibits astrocyte differentiation of dorsal neurepithelial progenitors during early development, and instead promotes neuronal differentiation (Agius, Decker, Soukkarieh, Soula, & Cochard, 2010) while suppressing overexpansion of specific neuronal

subtypes in the dorsal spinal cord (Nguyen et al., 2000). BMP signaling also directs neuronal subtype differentiation during early development. BMP4 suppresses differentiation of GABAergic inhibitory interneurons in the dorsal telencephalon, with addition of BMP4 decreasing interneurons grown in dorsolateral telencephalon cells and decreasing proliferation (Gulacsi & Lillien, 2003). Multiple populations of neurons arise whose markers are regulated in a BMP-dependent fashion (Timmer, Wang, & Niswander, 2002; Wine-Lee et al., 2004). The absence of both BMPR1a and BMPR1b results in a loss of neural progenitors that ordinarily differentiate into Lhx2+, Lhx9+, and Foxd3+ interneurons, and causes neural tube populations to shift to a more dorsal spatial location (Wine-Lee et al., 2004).

BMP impacts non-neuronal cell type development as well. Deletion of BMP signaling through BMPR1a in Olig1-expressing cells in the developing embryo results in a decrease in immature CNPase marked oligodendrocytes present at birth, and a marked increase CNPase+ oligodendrocytes at P20, indicating that BMP signaling plays a critical role in regulating oligodendrocyte maturation and myelin formation, although BMP receptors are not absolutely necessary for oligodendrocyte formation (Samanta et al., 2007; See et al., 2007). Strikingly, ablation of BMPR1a from Olig1+ cells does not affect the numbers of GFAP+ or S100b+ astrocytes, nor the number of NeuN+ neurons. The presence of phosphorylated SMAD1/5/8 in BMPR1a-ablated cells may indicate that either other signaling pathways are responsible for mediating differentiation of those cell types, or other BMP receptors are the critical pathway components (Samanta et al., 2007). However, deletion of BMPR1a does appear to reduce cell cycle length as indicated through the percentage of cells in S-phase (Samanta et al., 2007).

III. BMP in stem cells and astrocytes during late development through adulthood

BMP continues to play an important role in stem cell maintenance and cell cycle dynamics past early development. Postnatally, BMP suppresses proliferation through canonical signaling elements (Yao et al., 2014). In adolescent mice, ablation of the BMP signaling effector SMAD4 results in an increase of SVZ cells with NSC-like properties as well as the presence of a larger number of dividing cells *in vivo*. Cultured SMAD4-knockout NSCs demonstrate increased proliferative capacity and decreased differentiation (Kawaguchi-Niida, Shibata, & Furuta, 2017). This regulation of proliferation is not limited to the CNS, as ablation of BMPR1a in hair follicles results in decreased proliferation of hair follicle epithelial cells in adolescent and adult mice (Yuhki et al., 2004). It is likely that BMP cooperates with other pathways to regulate proliferation in different systems, as BMP is far from the only signal that is involved in stem cell regulation (detailed in later sections). This necessary role of SMAD4 and BMP signaling in regulation of NSCs continues through adulthood. *In situ hybridization* and immunocytochemistry shows multiple BMP ligands, receptors, and canonical SMAD signaling effectors present in adult NSCs (Colak et al., 2008; Lim, Tramontin, Trevejo, Herrera, Garcia-Verdugo, et al., 2000a; D. Zhang, Mehler, Song, & Kessler, 1998), and the BMP4 target Id4 promotes NSC quiescence (R. Zhang et al., 2019) through downregulation of Ascl1 (Blomfield et al., 2019).

During late embryonic and early postnatal development, BMP signaling plays a greater role in astrogliogenesis as well, which is partially due to a downregulation of non-astrocytic lineage pathways. Neural precursor cells dissected from the lateral ganglionic eminence at E17 treated with BMP4 demonstrate suppressed oligodendrocytic differentiation through ID4 and ID2 (Samanta & Kessler, 2004). When added to NSCs and NPCs in culture, BMP4 results in the generation of terminally differentiated GFAP+ astrocytes at all stages of development through adulthood (Bonaguidi et al., 2005; Zhu, Mehler, Mabie, & Kessler, 1999a). Ablation of BMP

signaling through deletion of type 1 receptors impairs numbers of GFAP+ and S100β+ astrocytes by birth (See et al., 2007). BMP signaling acts in conjunction with LIF to activate a STAT3-SMAD1-p300 transcriptional complex to activate GFAP expression and induce astrocyte differentiation (Nakashima, Yanagisawa, et al., 1999c). This BMP-LIF/CNTF signaling cooperation is mediated through the membrane protein gp130, which is necessary for astrocyte differentiation of neurepithelial progenitors (Nakashima, Wiese, et al., 1999a; Nakashima, Yanagisawa, Arakawa, & Taga, 1999b).

While BMP signaling promotes lineage specification from NPCs at these later stages of development, it also impacts astrocyte properties. BMP4 and its effector SMAD1 are upregulated after birth, and promote both neuronal and GFAP+ astroglial differentiation of postnatal cerebellar cell cultures (Angley, Kumar, Dinsio, Hall, & Siegel, 2003).Within astrocytes, BMP ligand promotes a more mature astrocyte phenotype, with more processes, less proliferation, and higher levels of aquaporin-4 and other astrocytic markers, including serine protease high temperature requirement A1 (HtrA1) and S100β in GFAP-expressing cortical astrocytes (J. Chen et al., 2018; Scholze, Foo, Mulinyawe, & Barres, 2014). Upregulated BMP ligands in reactive astrocytes may inhibit oligodendrocyte differentiation and promote astrocyte fate specification instead (Y. Wang et al., 2011).

During adulthood, BMP continues to play important lineage specification roles in the CNS. Ablation of SMAD4 impairs SVZ neurogenesis but potentiates oligodendrogliogenesis (Colak et al., 2008). Viral overexpression of BMP ligand reduces proliferation in the SVZ (Lim, Tramontin, Trevejo, Herrera, García-Verdugo, et al., 2000b), while overexpression of BMP4 ligand under control of a neuron-specific enolase (NSE) promoter results in increased astrocyte and decreased oligodendrocyte numbers in the adult (Gomes, Mehler, & Kessler, 2003).

BMP signaling plays a particularly important role in adult neurogenesis. Ependymal cells of the SVZ produce Noggin, which promotes neuronal differentiation of NSCs by blocking BMP signaling. BMP4 also promotes the survival of SVZ neurons in culture (Lim, Tramontin, Trevejo, Herrera, Garcia-Verdugo, et al., 2000a), and hippocampal adult NSCs are reliant on BMP signaling for regulation. Application of Noggin to the subgranular zone of the hippocampus results in increased expression of doublecortin, an immature neuronal marker, and increased cell proliferation (Brooker, Gobeske, Chen, Peng, & Kessler, 2017). As hippocampal NSCs progress in cell fate commitment, BMP signaling pushes cells from activation into quiescence, slowing neurogenesis. Inhibition of BMP signaling increases NSC and NPC activation, pushing cells from quiescence into activation, as well as accelerates the pace of neurogenesis while increasing NSC proliferation (Bond et al., 2014; Mira et al., 2010). With age, BMP ligand concentrations increase in the adult brain, including the hippocampus. These increases in BMP signaling correlate with cognitive impairment, which can be reversed through overexpression of the BMP inhibitor Noggin as well as through environmental enrichment and exercise (Gobeske et al., 2009; Meyers et al., 2016).

Aside from regulation of cell cycle dynamics, BMPs also affect cellular morphology throughout development. BMPs regulate neurite extension and outgrowth in multiple models, likely indicating an effect on cytoskeletal elements. For instance, *in vivo*, BMPs regulate extension of neurites in the hypothalamus (Peng, Mukhopadhyay, Jarrett, Yoshikawa, & Kessler, 2012). Signaling through SMAD1 promotes axonal growth in dorsal root ganglion (DRG) neurons, both in culture and in a spinal cord injury model (Parikh et al., 2011). Axons of commissural neurons from the developing spinal cord grown *in vitro* are repelled by a chemical signal secreted from the roof plate, likely BMP7 ligand, which when applied in culture can

destroy axon growth cones (Augsburger, Schuchardt, Hoskins, Dodd, & Butler, 1999). *In vivo*, the extension of commissural axons towards the ventral floorplate is mediated by both BMP7 and distant family member GDF7, with ablation of BMP7 resulting in aberrant axon extension medially and dorsally (Butler & Dodd, 2003). In cultured *Xenopus* spinal neurons, BMP ligand acts as a chemoattractant for axons, but longer stimulation results in repulsion (Wen et al., 2007).

There are a number of potential mechanisms for BMP-mediated cytoskeletal regulation. For example, in neurons derived from PC12 cells, BMP2 promotes neurite outgrowth through the p38 MAP kinase pathway (Iwasaki et al., 1999). Another established non-canonical pathway for cytoskeletal regulation is through BMP's effects on LIM kinase and cofilin. BMPR2 interacts with LIM kinase (Eaton & Davis, 2005; Foletta et al., 2003; Lee-Hoeflich et al., 2004). In developing spinal neuron cultures, BMP signaling acts through LIM kinase to exert its chemoattractant effects by phosphorylating cofilin in growth cones (Wen et al., 2007). A kinase-dead version of LIM kinase results in abolition of BMP growth cone attraction (Wen et al., 2007). To regulate repulsion, BMP signaling regulates the Slingshot family of phosphatases through the transient receptor potential channel TRPC1 to dephosphorylate cofilin (Niwa, Nagata-Ohashi, Takeichi, Mizuno, & Uemura, 2002; Wen et al., 2007). LIM kinase 1 is also required for BMP-mediated promotion of dendritogenesis in cultured embryonic cortical neurons (Lee-Hoeflich et al., 2004), and regulates synaptic stability at the neuromuscular junction in *Drosophila* (Eaton & Davis, 2005). Further downstream, LIM kinase regulates the actin cytoskeleton by phosphorylating cofilin, a protein necessary in actin depolymerization. Phosphorylation of cofilin leads to accumulation of actin filaments, and impairment of normal cytoskeletal changes and fluctuations (Arber et al., 1998). This BMP-LIMK1-cofilin-actin

signaling axis is one mechanism by which BMP presence may modulate CNS cell processes, although there are likely others.

IV. BMP during injury, inflammation, and disease

As a morphogen that is present in a wide variety of systems through adulthood, it is no surprise that irregular BMP activity occurs in many diseases. BMPs were first discovered for their osteogenic roles (Urist, 1965; Urist & Strates, 1971), and overexpression of BMP leads to heterotopic ossification. In the disease Fibrodysplasia ossificans progressive (FOP), in which connective tissues inappropriately ossify (F. S. Kaplan et al., 2009), genetic targeting of the BMP receptor ALK2 has shown some therapeutic promise (J. Kaplan, Kaplan, & Shore, 2012; Shore et al., 2006). In childhood-onset schizophrenia, aberrant downregulation of astrocyte differentiation is seen, with progenitor cells arrested earlier in development. BMP repressors are found to be upregulated in glial progenitor cells derived from these schizophrenia patients. Inhibition of SMAD4 expression alleviates this repressor-mediated inhibition by downregulating repressor transcription (Z. Liu et al., 2019). BMPs also play a role in depression, with BMP overexpression emulating depressive-like behavior and blocking the antidepressant action of fluoxetine (Brooker et al., 2017).

Irregular regulation of BMP signaling is a hallmark of multiple cancer types, including glioblastoma, and modulation of BMP levels in cancer may be a potential therapy. *In vitro* and *in vivo* exposure of human glioblastoma (GBM) cells to BMP4 results in decreased GBM proliferation, inhibition of tumor growth, and a decrease in mortality of mice with transplanted GBMs (Piccirillo et al., 2006). Variation seen in GBM response to BMP ligand challenge may be attributable to the BMP receptor types expressed – for example, BMPR1b levels in stem-like

GBM cells are lower than in normal neural stem cells, and overexpression of BMPR1b promotes differentiation and loss of tumor-like characteristics (J. Lee et al., 2008). Within oligodendroglioma stem cells, BMP signaling reduces proliferation and increases astrocyte differentiation, indicating a potential target for future therapeutic development (Srikanth, Kim, Das, & Kessler, 2014).

BMPs have been clinically approved for use during spinal surgery to induce bone growth. However, there are a number of side effects associated with BMP use, including inflammation and ectopic bone formation, indicating that a better understanding of how to modulate BMP signaling is needed (reviewed in (James et al., 2016)). BMPs are implicated in modulating the response to CNS injury, as signaling is upregulated following spinal cord injury and traumatic brain injury (J. Chen et al., 2018; Jian Chen, Leong, & Schachner, 2005; Divolis, Stavropoulos, Brain, 2019, n.d.; Hart et al., 2020; Setoguchi et al., 2001; Yan et al., 2012). In the spinal cord, lesion healing has two waves of gliosis – the initial hypertrophic response, and the later hyperplastic phase. Ablation of BMPR1a results in reduction of hypertrophic astrocytes generated, resulting in increased inflammation and poor neuronal repair. Ablation of BMPR1b results in smaller glial scars and lesion volumes, indicating that while BMP signaling modulates multiple phases of CNS injury recovery, it does so in a receptor-dependent manner and potentially through differentially regulated downstream targets such as miR-21 (Bhalala et al., 2012; Sahni et al., 2010). Blanket inhibition of BMP through administration of Noggin or the BMP inhibitor LDN193189 following spinal cord injury assists in axonal regrowth, myelin repair, and oligodendrogliosis, as well as lowers acute cell death measured through Caspase3 staining, though results on effects on long-term functional recovery are mixed (Hart et al., 2020; Matsuura, Taniguchi, Hata, Saeki, & Yamashita, 2008; Y. Wang et al., 2011). A better

understanding of how different BMPs and their receptor subtypes regulate physiologic processes would assist in resolving this confusion.

Modulation of BMP signaling following brain injury also impacts recovery. Overexpression of Noggin in the brain increases microglia numbers and reduces infarct volume in mice in an ischemic stroke model, although the glial scar is not altered in size (Samanta, Alden, Gobeske, Kan, & Kessler, 2010). Inhibition of BMP signaling effectors, such as fibrinogen, have been shown to ameliorate generation of reactive astrocytes differentiated due to CNS injury (Petersen et al., 2017; Pous et al., 2020). Stab wound injury (SWI) increases BMP signaling downstream effectors, including Id3, while also increasing local cell proliferation and astrocyte differentiation. Deletion of Id3 impairs the proliferative and astroglial response (Bohrer et al., 2015).

BMP2 and BMP4 are expressed by astrocytes *in vitro*, which may explain the influence that BMP signaling has on response to inflammation in the CNS, since gliosis is a part of the CNS injury response (J.-G. Hu et al., 2012; Lü & Hu, 2009). Additionally, increases in BMP4 have been observed with age in the human hippocampus (Meyers et al., 2016). An age-related increase in reactive-like astrocytes has also been found in humans, and experiments in mice have shown that reduction in microglial-associated cytokines ameliorates this increase (Clarke et al., 2018). Given that BMP is also linked to inflammation, it is possible that increases in astrocyte reactivity and cognition impairment are an effect of BMP with age.

The molecular mechanisms by which BMP signaling promotes inflammation are unclear. There are a number of potential transcriptional targets of BMP that are associated with inflammation and microglia. TAK1, downstream of BMP, has been linked to activation of pro-

inflammatory signaling pathways mediated by interleukin-1 (Takaesu et al., 2000). Within endothelial cells, inflammatory cytokines such as tumor necrosis factor α (TNFα) induce BMP ligand expression (Csiszar et al., 2005). BMP ligands themselves are regulated by inflammatory stimuli in endothelial cells as well (Csiszar et al., 2006). A more detailed examination of BMP signaling mechanisms related to inflammatory signaling pathways would assist in understanding how to apply BMPs in a clinical setting, as well as understand potential side effects of BMP-related treatments.

V. Mechanisms of regulation and signaling crosstalk

BMPs themselves are varied in nature, comprised of two main family groups, the 60A ligands and DPP ligands, the latter of which includes BMP2 and BMP4. When the ligands are initially synthesized, they dimerize as either homo- or heterodimers and are cleaved for secretion. The ability of a dimer to activate different BMP receptor configurations will depend on which monomers it is comprised of, as well as the receptor subunits to which the ligand dimer binds (Mueller & Nickel, 2012). BMP signaling can be opposed by multiple antagonists such as noggin, follistatin (Nakamura et al., 1990), and chordin (Piccolo, Sasai, Lu, & De Robertis, 1996), all of which play important roles in counteracting BMP signaling during embryonic development. The most prominent of these antagonists is noggin, due to its ability to directly bind the BMP4 ligand and abolish its receptor-binding ability (Zimmerman, De Jesús-Escobar, & Harland, 1996), as well as the large body of literature detailing the presence and role of noggin during mammalian CNS development. For many laboratories, experimental manipulation of BMP signaling can be achieved by addition of noggin to *in vitro* cultures, or through infusion of noggin or viral injection for *in vivo* studies.

BMP signaling may also be inhibited by upregulation of the inhibitory SMADs, or i-SMADs. SMAD6 and SMAD7 bind to BMP type 1 receptors, thereby inhibiting phosphorylation of SMAD1/5 and transduction of BMP signaling (Imamura et al., 1997; Ishisaki et al., 1999; Nakao et al., 1997). However, blanket inhibition of BMP or SMADs may have unintended consequences, given that BMP has links to many other signaling pathways and a myriad of downstream effectors. Here we discuss potential mechanisms of more finely tuned BMP regulation, as well as signaling cross-talk.

a. BMP Receptors

BMPR1a and BMPR1b have a great deal of sequence similarity, and are often considered to have many overlapping functions (Hirschhorn, Levi-Hofman, Danziger, Smorodinsky, & Ehrlich, 2017; Qin, Wine-Lee, Ahn, & Crenshaw, 2006; Yoon et al., 2005). However, there is also an increasing body of literature that suggests they also have different and often opposing effects, and it is possible that developments of drug candidates that target one or the other with greater specificity may help in regulating BMP signaling in a more precise manner.

BMPR1a and BMPR1b are expressed at different time points during embryonic development, with BMPR1a inducing expression of BMPR1b (Panchision et al., 2001; Zou, Wieser, Massagué, & Niswander, 1997a). During development, while constitutive ablation of BMPR1a results in embryonic lethality (Mishina et al., 1995), ablation of BMPR1b still results in viable mice that grow to adulthood, although they are infertile (Edson et al., 2010; Yi et al., 2001; Yoon et al., 2005). In the adult, immunohistochemical staining appears to show the two type 1 receptor subunits expressed in different cell populations in the dentate gyrus (Mira et al., 2010). After spinal cord injury, BMPR1a signaling promotes reactive gliosis and enhances recovery,

whereas BMPR1b signaling inhibits lesion healing (Sahni et al., 2010). Additionally, BMPR1a signaling decreases post-transcriptional processing of microRNA 21 in NPCs but BMPR1b does not, indicating that the two type 1 receptor subunits activate different downstream targets in NSCs (Bhalala et al., 2012). BMPR1b, but not BMPR1a, guides commissural axon guidance and growth rate during spinal cord development by regulating cofilin and its effects on cytoskeletal regulation (Yamauchi, Phan, & Butler, 2008; Yamauchi, Varadarajan, Li, & Butler, 2013). Nevertheless, despite these observations as well as other evidence of divergent effects of the two receptor subunits in NSCs (Panchision et al., 2001; Peng et al., 2012; Yamauchi et al., 2008; 2013), there is little understanding of the underlying mechanisms by which the receptor subunits regulate their effects. BMPR1a and BMPR1b even have different ligand affinities and are themselves processed and modified differently in the cell (Hirschhorn et al., 2017; Wegleiter et al., 2019). These differences likely extend to crosstalk with other signaling pathways. Future studies wanting to better understand the myriad of effects that BMP has on different cell types may choose to focus on not only the different BMP ligands, but also the receptor subunits expressed.

During development, BMPR1a and BMPR1b play both overlapping and independent roles. BMPR1b is implicated in proper formation of limb buds as previously discussed in studies utilizing a dominant negative form, while a dominant negative version of BMPR1a did not induce similar results (Zou & Niswander, 1996). Expression patterns for the two type 1 receptors also differ within the developing limb, as BMPR1b predominantly is expressed in less mature areas of cartilage development, while *in situ* reveals BMPR1a mRNA to be located in areas of cartilage maturation (Zou, Wieser, Massagué, & Niswander, 1997a). Inappropriate expression of

constitutively active BMPR1a (caBMPR1a) may delay chondrocyte differentiation, a phenotype not observed with caBMPR1b (Zou, Wieser, Massagué, & Niswander, 1997a).

Although the role of BMPR1a in pushing NSCs into quiescence in the dentate gyrus has been examined in adult mice (Mira et al., 2010), the role of BMPR1b in NSCs has not been studied as thoroughly. Limited analysis on gene expression in SVZ NSCs incubated in noggin has revealed differential expression of genes linked to cell cycle and lineage commitment (Morell, Tsan, & O'Shea, 2015), but the difference in BMPR1a and BMPR1b downstream signaling remains unclear. Phenotypic differences attributed to different signaling mechanisms between these two receptor subunits have been observed in other systems but sometimes conflict in their roles in cell differentiation, with BMPR1b responsible for cell differentiation in embryonic nervous system development but BMPR1a playing a similar role in osteo- and chondrogenesis (Kaps et al., 2004; Panchision et al., 2001). An overall picture of their differences in downstream effects is lacking, particularly in neural stem cells, but necessary for a better understanding of BMP signaling.

b. Wnt Signaling

Wnt signaling is a commonly studied pathway known to act in opposition to BMP signaling in many contexts. In *Xenopus* embryonic development, Wnt signaling promotes ectoderm neuralization while repressing BMP4 expression during gastrulation, a process reversible through overexpression of a constitutively active form of BMPR1a (Baker, Beddington, & Harland, 1999). Beta-catenin, a downstream effector of Wnt signaling, promotes neural precursor proliferation and cell cycle re-entry in the SVZ of embryonic mice to regulate

size of the cerebral cortex (Chenn & Walsh, 2002). This stands in contrast to BMP's known effect in promoting cell cycle exit during late development and postnatally (Bond et al., 2014).

BMP signaling may have a positive feedback loop with components of the Wnt pathway. Our own data indicate that there is a more complicated relationship between BMP and Wnt signaling, with BMP4 ligand inducing increased mRNA levels of some Wnt ligands, such as Wnt4 and Wnt11, but decreased levels of others such as Wnt5a and Wnt5b (our unpublished observations). In the developing spinal cord, ablation of both BMPR1a and BMPR1b receptor subunits decreases *Wnt1* and *Wnt3a* expression in the roof plate (Wine-Lee et al., 2004).

Interestingly, BMP and Wnt signaling share common downstream targets. Among these is Id2 (Rockman et al., 2001; Wine-Lee et al., 2004). Beta-catenin is downstream of canonical Wnt signaling, and activation of downstream BMP signaling effector TAK1 suppresses beta-catenin mediated transcription (Ishitani et al., 1999). BMP and Wnt signaling also have a common antagonistic regulator, Cerebrus (Piccolo et al., 1999), which suppresses both signaling pathways to induce head formation. Given that Wnt is a critical morphogen involved in a wide variety of developmental and diseases processes, BMP interaction with components of the Wnt cascade may explain some of the diverse effects of BMP non-canonical signaling.

c. Sonic Hedgehog signaling

Sonic hedgehog and BMP signaling frequently interact with each other during development. Among non-neural tissues, they have opposing effects during cartilage development of vertebrae (Watanabe, Duprez, Monsoro-Burq, Vincent, & Le Douarin, 1998). Disruption in Shh during development results in skeletal abnormalities (Chiang et al., 1996). Given that BMP signaling is crucial for chondrogenesis and osteogenesis, it seems likely that these two signaling pathways are highly coordinated during skeleton patterning and limb

formation. During somite patterning in chick embryos, Shh induces Noggin expression to suppress BMP signaling, thereby preventing excessive lateralization patterning (Hirsinger et al., 1997). As previously mentioned, BMP4 moderates Shh expression in Hensen's node, regulating left-right asymmetry in chick embryos (Fujiwara et al., 2002; Monsoro-Burq & Le Douarin, 2001).

Within the CNS, Shh signaling acts in opposition to BMP during neural tube formation, with Shh necessary for ventral floorplate establishment, and BMP critical to the dorsal side and neural crest formation (Bond et al., 2012; Chiang et al., 1996). Moreover, BMP and Shh interact to regulate ventral-dorsal identity specification (Liem et al., 2000; Nguyen et al., 2000). Both BMP and Shh can regulate the expression of Pax family genes that indicate dorsoventral patterning, and they may do so in opposing ways as with Pax7, in order to establish regional boundaries (Timmer et al., 2002). Low doses of BMP signaling appear to modulate neurectoderm response to Shh signaling, as Shh alone acting on caudal neurectoderm cells induces gene expression similar to that of floor plate cells, but BMP addition results in rostral diencephalic midline cells (J. K. Dale et al., 1997). A balance between BMP and Shh signaling regulates interneuron generation in the dorsomedial telencephalon (Gulacsi & Lillien, 2003).

In vitro, the opposing effects of BMP and Shh within the context of NPC fate specification are laid out even more clearly. Shh treatment of embryonically dissected forebrain NPCs increases O4+ and β-tubulin+ cells, with no effect on GFAP expression, while BMP treatment results in more GFAP+ and fewer O4+ cells. Moreover, when both factors are applied simultaneously, an intermediate phenotype between the two occurs (Zhu, Mehler, Zhao, Yu Yung,

& Kessler, 1999b). BMP's effects on NPC fate specification may be dependent on or exerted through downregulation of certain Shh signaling elements.

d. Integrin Signaling

Integrin signaling is another pathway that intersects with BMP signaling. β1-integrin was first identified as a regulator of neural stem cell maintenance by the Ffrench-Constant group in 2005, and has since been shown to promote neurepithelial progenitor proliferation *in vivo* and NPC proliferation in culture (Leone et al., 2005; Long, Moss, Laursen, Boulter, & Ffrench-Constant, 2016). In vivo, SVZ NPCs show low levels of β1-integrin, and blockage of β1-integrin through infusion of an antibody promotes proliferation, which may be indicative that regulation of proliferation by integrins depends on the context of other signaling or extracellular matrix cues (Kazanis et al., 2010). Our lab has more recently shown that β1-integrin is present in adult hippocampal neural stem cells, and contributes to their maintenance through integrin-linked kinase (ILK) signaling. Ablation of β1-integrin results in greater astrocyte differentiation in cultured SVZ NPCs, spinal cord ependymal stem cells, and hippocampal NPCs (Brooker, Bond, Peng, & Kessler, 2016; L. Pan et al., 2014).

β1-integrin signaling in NPCs activates a MAP kinase signaling pathway, which may indicate convergence with BMP signaling in this system (Campos et al., 2004). In fact, there are multiple biologic systems in which integrins and BMP signaling converge. In vascular endothelial cells, integrin and BMP receptors cooperate to regulate the Runx2/mTOR/p70S6K pathway and moderate cellular proliferation (J. Zhou et al., 2013). β3-integrin has been shown to be induced by BMP2 signaling in cell spreading dynamics, and to conversely regulate BMP2-mediated SMAD activity through receptor regulation (Fourel et al., 2016). In bone marrow,

reduction of β1-integrin levels results in a reduction of phosphorylated SMAD1/5 and impairs BMP-mediated transcription of certain bone-related genes (Brunner et al., 2018). In human osteoblasts, BMP signaling increases integrin expression at the cell surface to modulate extracellular matrix adhesion, and integrins associate with BMP type 1 and type 2 receptor subunits (Lai & Cheng, 2005). In bone marrow mesenchymal stem cells, knockdown of β1-integrin by siRNA results in decreased BMPR1a receptor internalization, suggesting a role for integrin in BMP signaling regulation through receptor localization dynamics (Du et al., 2011).

In the CNS, ablation of β1-integrin from ependymal stem cells and SVZ NPCs results in an increase in multiple BMP signaling targets, including phospho-SMADs, GFAP, and pp38. Moreover, β1-integrin physically associates with both BMPR1a and BMPR1b, although with differing interaction dynamics for different receptors (North, Pan, McGuire, Brooker, & Kessler, 2015). These studies indicate that BMPs and integrins interact on common physiologic processes in multiple systems, and frequently regulate each other. It is likely that they act upon common signaling effectors to influence cell fate and differentiation.

e. Hippo Signaling

BMP signaling has recently been linked to the Hippo signaling regulators Yes-associated protein (YAP) and WW domain-containing transcription regulator 1 (Wwtr1, or TAZ). YAP and TAZ are transcriptional co-activators that were initially identified as inhibitors of the Hippo pathway and characterized as binding partners of 14-3-3. Although they cannot directly bind DNA themselves, they recruit other transcription factors to exert their downstream effects. They were identified as pro-proliferative factors that regulate organ size, although numerous studies have since found roles for YAP and TAZ as mechanosensors that integrate extracellular stiffness cues into cellular fate determinations.

Early work on their biological roles focused on their pro-proliferative and pro-tumorigenic capabilities, as both have been identified as aberrantly upregulated in multiple types of cancers. In multiple cell types, overexpression of either YAP and/or TAZ promotes proliferative capacity. BMP regulation of YAP through SMAD phosphorylation has been identified as a mediator of embryonic NPC proliferation (Yao et al., 2014). Postnatally, BMP has been identified as acting through YAP to modulate cortical astrocyte differentiation (Z. Huang, Hu, et al., 2016a).

Overexpression of TAZ has also been demonstrated to increase cellular proliferation and promote epithelial to mesenchymal transition (EMT), similarly to BMP signaling in other cell types (Choi et al., 2019; Q.-Y. Lei et al., 2008). However, TAZ's impact on NPC proliferation and differentiation has not been the subject of much study, as its paralog YAP is usually considered the primary effector of the Hippo pathway. Nevertheless, YAP and TAZ effects appear to differ by cell type, and have frequently been studied in combination, due to a lack of tools (until recently) that can individually address their effects. Recent evidence and the emergence of tools able to tease apart their roles has pointed to non-overlapping effects, including in their actions as downstream effectors of BMP signaling in some systems.

YAP and TAZ are well known as mechanosensors (Aragona et al., 2013; Dupont et al., 2011; Low et al., 2014). Given β1-integrin's well-known role in modulating extracellular mechanical inputs, and BMP's known role in regulating cytoskeletal components for axonal growth during development and cell morphology during astrocytic differentiation, as well as previously described ties to integrin signaling, it is likely that YAP and TAZ are downstream effectors of the mechanical aspects of BMP signaling, and may even be related to integrin. The

intricacies of how these various signaling pathways intersect is important to understand to tease apart how each of them plays a role in NPC fate determination.

VI. Conclusion

Although there are a number of clinically approved uses of BMPs and some of their downstream targets, broad activation or inhibition of the BMP signaling pathway can lead to unwanted side effects due to the variety of effects that BMP's downstream signaling effectors have (Gautschi, Frey, & Zellweger, 2007; James et al., 2016). The vast clinical potential of different BMPs on multiple disorders is extremely promising (M. Kim & Choe, 2011), but when considering the myriad of influences that BMP and its targets play on important biological processes within the CNS such as development, responses to injury, and aging, it is clear that a more fine-tuned approach and a better understanding of how BMP regulates neural stem cells and astrocytes and how BMP signaling converges with other pathways is critical.

In the following studies described, I focus on BMP signaling and its downstream regulators' impacts on neural stem and progenitor cell fate specification and astrocytic properties. Beginning with chapter 2, I first examine BMP regulation of HtrA1, a gene identified through a microarray screen. We found that HtrA1 is a novel astrocyte marker, and regulates astrocyte differentiation during development as well as astrocyte response to cortical injury. In chapter 3, I delve into the different transcriptional targets of BMP receptors through RNA sequencing. In chapter 4, I examine BMP regulation of the Hippo pathway mechanosensors YAP and TAZ, as well as their effects on NPC fate specification. Finally, in chapter 5, I summarize the findings of the previous chapters, as well as describe the limitations of studies conducted and future directions that may be taken by our lab or others.

Chapter 2

BMP-Responsive Protease HtrA1 Is Differentially Expressed in Astrocytes and Regulates Astrocytic Development and Injury Response

This chapter has previously been published as J. Chen, S Van Gulden, T. McGuire, A.C. Fleming, C. Okia, J.A. Kessler, and C.-Y. Peng. BMP-Responsive Protease HtrA1 Is Differentially Expressed in Astrocytes and Regulates Astrocytic Development and Injury Response. *Journal of Neuroscience* 11 April 2018, 38 (15) 3840-3857; DOI: https://doi.org/10.1523/JNEUROSCI.2031-17.2018.

I. Introduction

Although there are many molecular labels that identify morphologically, biochemically, and functionally diverse populations of neurons, molecular markers that label subpopulations of astrocytes are limited, and mechanisms that generate distinct astrocyte subtypes remain unclear. Astrocytes, stereotypically defined by their stellate morphology, are classically categorized as “fibrous” or “protoplasmic” based on morphological differences and anatomical locations (Golgi, 1886; Kimelberg, 2009). Molecular and electrophysiological analyses of developing and mature astrocytes have demonstrated heterogeneity among the astroglial population(Batter & Kessler, 1991; Chvátal, Pastor, Mauch, Syková, & Kettenmann, 1995; Sosunov et al., 2014; M. Zhou, Schools, & Kimelberg, 2006) which was made more evident by genomic scale expression profiling of astrocytes from different developmental time points and brain regions (Bachoo et al., 2004; Cahoy et al., 2008; Yeh, Lee, Gianino, & Gutmann, 2009; Y. Zhang et al., 2014). However, molecular markers that identify functionally unique, or disease-associated astroglial subtypes are just beginning to emerge (Ben Haim & Rowitch, 2017; Liddelow et al., 2017; Lin et

al., 2017). Further expansion of functionally relevant molecular markers is essential for the understanding of astrocyte subtype development and function.

Molecular mechanisms of astrocyte specification and diversity have been studied extensively using cultured neural stem cells (NSCs) and glial restricted progenitors (GRPs) (J. Herrera et al., 2001; Raff, Abney, & Miller, 1984; Rao, Noble, & Mayer-Proschel, 1998). Cells expressing the astrocytic intermediate filament Glial Fibrillary Acidic Protein (GFAP) can be generated from NSCs and GRPs by two different classes of cytokines, the leukemia inhibitory factor (LIF) / ciliary neurotrophic factor (CNTF) family and the Bone Morphogenetic Proteins (BMPs) (Gross et al., 1996; Johe, Hazel, Muller, Dugich-Djordjevic, & McKay, 1996; Lillien, Sendtner, Rohrer, Hughes, & Raff, 1988; Richards et al., 1996; Takizawa et al., 2001). Upon ligand binding, LIF/CNTF activate JAK-STAT pathways whereas BMPs signal primarily through SMAD pathways (F. Liu et al., 1996; N. Stahl et al., 1994). A transcriptional complex that contains both STAT and SMAD proteins regulates GFAP expression, leading to the conclusion that both pathways contribute to astrogliogenesis through convergent mechanisms (Nakashima, Yanagisawa, et al., 1999c; Y. Sun et al., 2001). However, while BMP signaling promotes the generation of stellate, post-mitotic astrocytes from NSCs, LIF signaling promotes a bipolar, radial glia-like cell that maintains a stem cell phenotype (Bonaguidi et al., 2005). In addition to cellular and molecular differences, BMP and CNTF signaling generate functionally and molecularly distinct astrocytes that respond differently to injury when transplanted (Davies et al., 2008). These findings suggest that differential cytokine responsiveness plays an important role in astrocyte specification as well as in astrocyte diversity.

Our goals in this study were to find novel molecular markers that are expressed specifically in differentiated astrocytes, and to reveal genes that participate in cytokine-specific

generation of astrocyte diversity during development. We identified the serine protease High temperature requirement A 1 (HtrA1) as an astrocyte-specific BMP signaling responsive molecular marker of astrocytes in the adult mouse forebrain. Here we show that HtrA1 is important for postnatal astrogliogenesis as well as for astrocytic morphology and extracellular matrix (ECM) protein regulation. In addition, deletion of HtrA1 increases microglia and endothelial cell proliferation post brain injury. Mutation in HtrA1 has been linked to the human small blood vessel disease Cerebral Autosomal Recessive Arteriopathy with Subcortical Infarcts and Leukoencephalopathy (CARASIL). Our demonstration of astrocyte specificity of HtrA1 also suggests CARASIL may be astrocytic in origin, and that HtrA1 functions in astrocytes may play important roles in cerebrovascular health.

II. Materials and Methods

Animals For the microarray analysis and subsequent expression characterization, CD1 mice (Harlan Laboratories) of either sex at the appropriate ages were used for neural stem cell isolation and mRNA *in situ* hybridization. HtrA1 null mice (Supanji, Shimomachi, Hasan, Kawaichi, & Oka, 2013) were maintained as heterozygotes in a C57BL/6J background and genotyped by PCR with tail DNA. Generation of GFAP-Cre; $BMPR1^{fx/fx}$ mice has been previously described (Garcia, Doan, Imura, Bush, & Sofroniew, 2004; Sahni et al., 2010). All mice were housed in groups and maintained on a 12-hour light/dark cycle with *ad libitum* access food and water. All experiments were performed with both male and female mice in each condition and analyzed without sex separation. Handling and treatment of animals were in accordance with Northwestern University IACUC regulations and policies.

Transcriptome profiling by Microarray Passage 1 dissociated NSCs were infected with retrovirus expressing GFP under the control of either CMV or GFAP promoters as

previously described (Bonaguidi et al., 2005). 3 days after infection, GFP-expressing cells in CMV-GFP retrovirus transduced neurospheres were isolated by fluorescent-activated cell sorting (FACS) and processed for total RNA collection. GFAP-GFP retrovirus transduced cells were plated for differentiation in EGF (1ng/ml) with BMP4 (20ng/ml) or LIF (20ng/ml) plus Noggin (250ng/ml; to block endogenous BMPs) for 7 days before GFP expressing cells were isolated by FACS. Total RNA was immediately extracted after FACS from GFP-expressing cells using an RNAqueous Micro RNA isolation kit (Thermo Fisher). RNA from 4 replicates of all experimental conditions was examined by Nanodrop-1000 (Nanodrop Technologies) and Bioanalyzer (Agilent Technologies) before proceeding to cDNA amplification and labeling using the Ovation kit (NuGEN) according to the manufacturer's protocols. Gene expression profiles amongst the treatment groups were compared using the mouse WG-6 v1.1 microarray beadchip (Illumina). Hybridization and scanning of the beadchip array was performed by the Northwestern University genomic core facility with an Illumina BeadArray reader and preprocessed by the Illmina BeadStudio software. The microarray data has been deposited in the NCBI Gene Expression Omnibus (GEO; http://ncbi.nlm.nih.gov/geo/) and is accessible through GEO accession number GSE67942.

Quantitative Real-Time PCR Total RNA was isolated from mouse brain tissue or cultured cells using RNAqueous-4PCR RNA isolation kit (Thermo Fisher). cDNA was generated with 1μg of total RNA using thermoscript reverse transcriptase (Thermo Fisher), and used in quantitative RT-PCR reactions with primers specific to desired candidate genes and SYBR Green master mix (Applied Biosystems). PCR reactions were performed in a Realplex2 thermal cycler (Eppendorf). Gene expression levels were standardized with GAPDH as the internal control, compared among experimental groups, and represented as fold changes relative to

expression in the control group. At least three independent experiments were performed for all qPCR studies.

Stab Wound Injury Eight to 10-week-old age-matched HtrA1 wild type and mutant mice of both sexes were secured on a stereotaxic injection frame (Kopf Model 900) and anesthetized with isofluorane. The skull opening was made with a dental drill. Stab wound injury was performed with a scalpel in the right neocortex (Bregma from -0.8 to -2.8mm, latero-lateral 1.5mm, 0.9mm deep). Mice were sacrificed at 3 days and 7 days post injury for immunohistochemical analyses. Post-injury proliferation was measured with the injection of a single dose of EdU (50mg/kg body weight; Thermo Fisher) 4 hours before sacrifice. To analyze the lesion area, coronal cryostat sections of 400μm distance rostral and distal of the injury site were collected and examined to identify the lesion center, the location with the largest lesion area. Four sections 50μm apart surrounding the lesion center were quantified for changes in lesion area, neurovascular morphology, and proliferation.

Neural Stem Cell and Astrocyte Cultures NSCs from the subventricular zone (SVZ) of postnatal day 1 (PN1) mice were isolated and cultured as neurospheres using standard protocols (Bonaguidi et al., 2005). Primary astrocytes were dissected from PN2 mice and cultured as monolayers as previously described (McCarthy & de Vellis, 1980; Sahni et al., 2010). For coculture studies, astrocytes transduced with GFP-tagged scrambled shRNA or HtrA1 shRNA lentivirus were FACS purified then plated at 50,000 cells/well onto 12mm Poly-D-Lysine (PDL) coated glass coverslips in 10% fetal bovine serum (FBS) containing astrocyte growth media as described. At 7 days after FACS, astrocytes were either harvested for western blot analyses or used for neuronal coculture studies. Prior to the start of cocultures, astrocytes were adapted for serum free conditions by culturing in astrocyte growth media containing 5% FBS for 16hrs. On

the following day, 20,000 freshly dissected cortical neurons from postnatal day 1 C57BL6 mice were plated on top of the astrocytes, and cultured without serum in neurobasal media with N2 and B27 supplements along with Pen/Strep/Glutamine (Thermo Fisher) for 7 days before fixing with 4% paraformaldehyde (PFA) and proceeding with further analysis. For treatment of cultured astrocytes with recombinant HtrA1 (R&D Systems), serum- derived cultured astrocytes were adapted for serum-free conditions as described and incubated in serum-free astrocyte media with or without recombinant HtrA1 (250ng/ml) for 3hrs. Protein was then extracted and analyzed by western blots. For generating human NSCs and astrocytes from embryonic stem cells or induced pluripotent stem cells, we followed the protocol described in Duan et al. (2015) with the following modifications: Before passage 6 (day 165), NSCs are treated with LIF (20ng/ml) for 7 days to enrich for glial progenitors. Cells are then dissociated and plated at 100,000 cells/well on PDL coated 12mm glass coverslips for 3 days before switching to differentiation media with BMP4 (10ng/ml) for 7 days followed by FGF1 (50ng/ml) for 7 days. Cells are fixed (on day 185) with 4% PFA and used for Immunocytochemical analyses.

Bioinformatics Analysis Raw signal intensity data from Illumina BeadStudio version 3 for individual probes were analyzed by the Northwestern University bioinformatics core facility using the R/Bioconductor *lumi* package, which corrected for small sample size variance via an empirical Bayesian method and performed normalization with internal controls. Probes with all samples values near or at background levels were marked “absent” and removed, leaving 21217 probes for further analysis. Probes marked as “Present” were examined for differential expression among experimental groups using stringent statistical criteria with Bonferroni false discovery rate (FDR) p values less than 0.05 and fold-change greater than 2 fold.

***In situ* hybridization (ISH)** Brain tissue was collected from mice that were transcardially perfused with cold phosphate buffer saline (PBS) and 4% PFA followed by 2 hours postfix with 4% PFA. Brains were cryo-protected in 30% sucrose overnight, and stored at -80°C in OCT compound (Tissue-Tek) until use. 20μm cryo-sections (Leica CM3050) from desired brain regions were washed 3 times with PBS with 0.02% Triton-X 100 (PBST) and treated with Proteinase K (1μg/ml) for 5min. Sections were then washed 3 times in PBST and fixed in 4% paraformaldehyde (PFA) and 0.1% glutaraldehyde for 30min. Following 3 PBST washes, Digoxygenin (DIG) labeled antisense mRNA probes (1:150 in hybridization buffer) were added onto the slides which were then covered with siliconized glass coverslips and placed in a humidified hybridization chamber at 68°C overnight. Slides were washed at 68°C on day 2 with high stringency wash buffer (5xSSC with 50% formamide and 0.1% SDS) twice and low stringency wash buffer (2xSSC with 50x formamide) 3 times, followed by 3 Tris-buffered saline with 0.1% Tween (TBST) washes before incubation overnight in anti-DIG alkaline phosphotase antibody (Roche, 1:2000) in 5% goat serum. On day 3, slides were washed in TBST+2mM levamasole for 3 times and transferred into NBT-BCIP (Roche) containing developing solution from 6hr to overnight. Upon signal detection, slides were dehydrated through an ethanol gradient, cleared in xylene, and mounted in Histomount (Zymed) for storage and analysis.

Immunohistochemistry (IHC) 10μm tissue sections were prepared and washed with PBST as described for the ISH protocol before incubation with primary antibodies diluted in PBST with 5% Goat Serum at 4°C overnight. Primary antibodies used were: rabbit anti-GFAP (1:1000, Dako Cytomation); Mouse anti-GFAP (1:1000, Sigma), chicken anti-GFAP (1:1000, Abcam) rabbit anti-GFP (1:1000, Thermo Fisher), chicken anti-GFP (1:1000, Abcam), mouse anti-CSPG (CS-56 1:1000, Sigma), Rabbit anti-Collagen IV (1:500, Abcam), rat anti-CD31

(1:500, Millipore), mouse anti-PDGFRβ (1:1000, Abcam), rabbit anti-HtrA1 (1:200, Abcam). Following primary incubation, tissue sections were washed 3 times in PBST and then incubated in fluorescent secondary antibody (1:500, Thermo Fisher) in PBST with 5% normal Goat Serum and DAPI nuclear stain for one hour at room temperature. After a second set of PBST washes, sections were mounted in ProLong Gold antifade reagent (Thermo Fisher). EdU staining followed secondary antibody washes and was performed according to manufacturer's instructions (Thermo Fisher). Stained sections were imaged on a confocal microscope (Leica SP5).

Protein extraction and Western blotting Protein was extracted from astrocyte cultures using M-PER protein extraction reagent (Pierce) with HALT protease and phosphatase inhibitor cocktail (Thermo Scientific) and stored at -80°C until use. To correctly resolve CSPGs including Neurocan, samples were treated with Chondroitinase ABC (1:20 of 10U/ml stock, Seikagaku Bioscience) at 37°C for 90min before further processing. 10ug of protein was boiled in strong denaturing conditions for 10 minutes and loaded onto 4-20% polyacrylamide gels (Biorad). Protein was transferred onto polyvinylidene difluoride membranes at 4°C for one hour, followed by blocking in 5% nonfat dry milk in TBST for one hour at room temperature. Membranes were then incubated with primary antibody in blocking solution overnight at 4°C. After washing, membranes were incubated with the appropriate horseradish peroxidase-conjugated secondary antibody (1:2000 in blocking solution; Santa Cruz Biotechnology) and developed using Pierce Enhanced Chemiluminescent Western Blotting Substrate (Thermo Fisher). The following primary antibodies were used: sheep anti-Neurocan (1:500, R&D), mouse anti-CSPG (CS-56, 1:1000, Sigma), rabbit anti-HtrA1 (1:500, Abcam), mouse anti-BMP4 (1:1000, Millipore), rabbit anti-TGF□ (1:1000, Abcam) mouse anti-GAPDH (1:5000, Millipore).

Lentiviral construct production and transduction Plasmid DNA (pGIPz) containing short hairpin RNA (shRNA) sequences targeted to mouse HtrA1 were purchased (GE Dharmacon) and used to produce lentiviral particles as previously described (Bond et al., 2014). Viral transductions were performed on PN1 NSCs that were dissociated into single cells at a density of $5x10^4$/ml in 50ml of neurosphere growth media for 12 hours before lentivirus was added (at a titer of $1x10^8$ cfu/ml) and incubated at 37°C for 48hrs. The transduced cells were then isolated by FACS and plated for differentiation studies or protein isolation as previously described. Lentiviral transduction of PN2 astrocytes was performed in 80% confluent monolayer cultures before passage 2 for 48hrs. Cells were then shaken and dissociated for FACS isolation, followed by plating at $5x10^4$/ml in astrocyte growth media for subsequent studies.

Quantification and Statistical Analyses Images acquired on a confocal microscope (Leica SP5) were exported to NIH ImageJ for cell counting and integrated pixel density analysis. Measurement of astrocyte morphological properties was performed with Cell Profiler software (Carpenter et al., 2006) using the *MeasureObjectSizeShape* module. Quantification of endothelial cell density, branching, length, and uniformity in the neocortex is performed using the Angiotool software (Zudaire, Gambardella, Kurcz, & Vermeren, 2011) with intensity threshold of 11/255, vessels diameter of 15, and remove small particle setting of 40. Quantification results were presented as mean ± standard error of the mean (SEM), generated from at least three independent trials per experimental condition. Differences among experimental groups were evaluated with unpaired Student's t-test for two group experiments and 1-way ANOVA with Tukey *post-hoc* test for pairwise comparisons in three group experiments using Microsoft Excel with XL Toolbox plugin.

III. Results

BMP and LIF generate morphologically and molecularly distinct astrocytes.

Previous work has demonstrated that BMP and LIF generate molecularly and morphologically distinct astrocytes (Bonaguidi et al., 2005). To examine the genome-wide molecular differences between astrocytes specified by BMP or LIF signaling, we cultured NSCs derived from postnatal day 1 mouse brain, during the period of active cortical astrogliogenesis. NSCs were transduced with a retrovirus containing green fluorescent protein (GFP) under the control of the mouse GFAP promoter, then differentiated in the presence of either BMP4 or LIF with noggin, a BMP signaling inhibitor (Fig. 2-1A). After 7 days in culture, GFP-expressing cells in each experimental condition displayed clearly distinctive morphologies (Fig. 2-1B). Total mRNA from GFP-expressing cells was collected and used for gene expression profiling by a cDNA microarray that contained 45281 probes for transcripts found in the mouse genome. To identify differentially expressed genes, probes with greater than a two-fold change in intensity and a false discovery rate (FDR) adjusted p-value less than 0.05 in pairwise comparisons were considered as positives and selected for further analysis. The number and the identities of differentially expressed genes in pairwise comparisons of each experimental group are summarized in Table 2-1 and detailed in Tables 2-3 to 2-5. Heatmap comparison of the 1108 differentially expressed genes amongst the three experimental groups revealed clearly opposing expression profiles between BMP4 induced astrocytes and the neurosphere derived progenitors (Fig. 2-1C). Examination of known astrocytic genes also confirmed that many accepted markers of astrocytes are more highly expressed in BMP4 treated group (Table 2-2), provide further support for candidates from BMP-induced genes as potential marker of differentiated astrocytes.

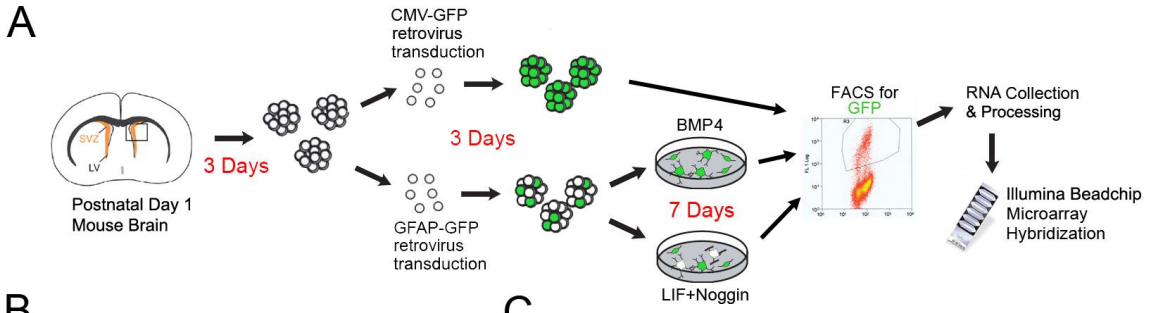

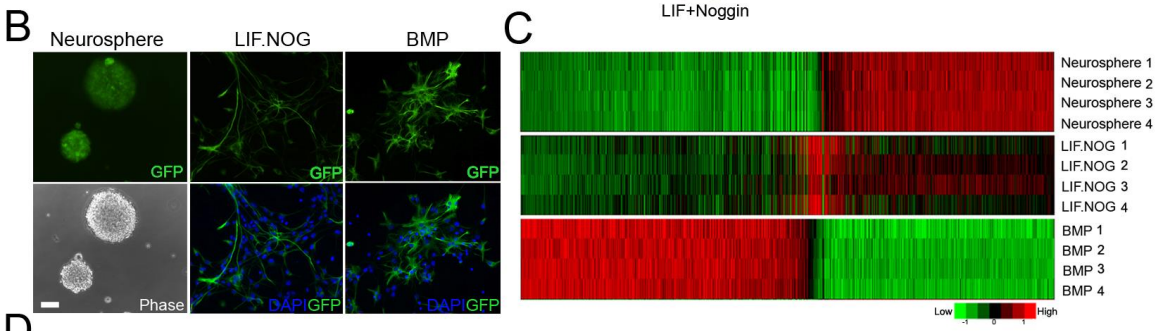

D

Symbol	BMP/NS fold change	BMP/LIF fold change	Astrocyte enriched #	ABA Expression Data	In House *in situ*
Gfap	85.712	7.089	84.9x	Astrocytes and NSCs	Astrocytes and NSCs
Aqp4	74.683	6.778	79.7	Astrocytes and NSCs	Astrocytes and NSCs
Hopx	14.964	15.21	17.3x	Hippocampal Astro & NSCs	Hippocampal Astro & NSCs
Kcne1L	10.385	12.055	25x	Not detected	Astrocytes, NSCs and Neurons
Aox1	8.7075	5.333	10.7x	Not detected	Not detected
Tmem166	8.6425	7.158	32.7x	Not detected	Not detected
HtrA1	8.6385	4.574	19x	Astrocytes but not in NSCs	Subsets of Astrocytes
Glud1	8.5282	2.9554	8.1x	Not detected	Astrocytes and Neurons
Emp2	8.421	3.651	19.5x	Neuronal	Neuronal
Igsf1	7.902	6.4977	10.1x	Not detected	Not detected
Pla2g7	6.606	3.595	65.1x	Astrocytes and NSCs	Astrocytes and NSCs
Aldoc	6.3343	3.297	52.9x	Astrocytes and NSCs	Astrocytes and NSCs
Slc1a2	5.2863	4.213	46.7x	Astrocytes and NSCs	Astrocytes and NSCs
F3	5.0299	2.24	40.6x	Astrocytes but not NSCs	Astrocytes but not NSCs

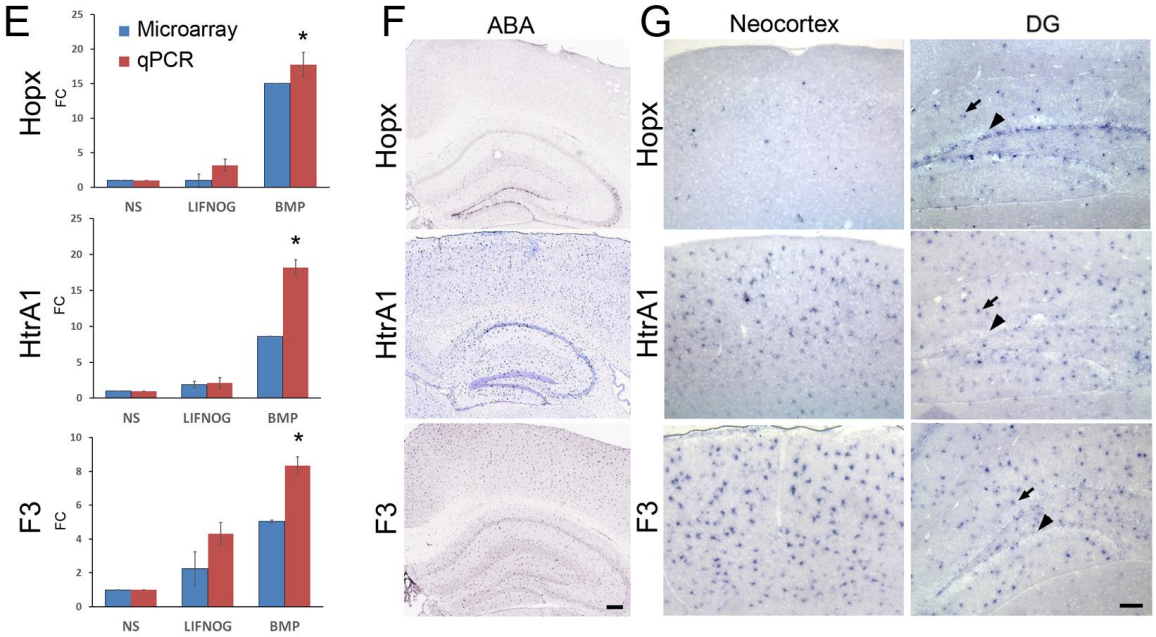

Figure 2.1 Genomic scale expression analysis by cDNA microarray reveals differential expression profiles of BMP and LIF-induced astrocyte subtypes and identified novel astrocyte markers

(A) Schematic diagram of gene expression microarray experimental design. (B) Cellular morphology of each experimental group as visualized by GFP expression after viral transduction. LIF-induced cells acquire a radial morphology whereas BMP-induced cells acquire a stellate morphology after seven days in culture. (C) Heatmap of the top 1108 genes that are differentially expressed during astrogliogenesis with experimental groups and replicate numbers listed on the right of the heatmap. Opposing expression profiles are found between BMP-induced astrocytes and NSCs in neurospheres. LIF-induced $GFAP^+$ cells are more similar to NSCs in overall profile than to BMP-induced astrocytes. Summary of differentially expressed genes, as well as expression of astrocytic genes, are listed in Extended Data Tables 1-1 to 1-5. (D) The list of 14 genes expressed by BMP4-induced astrocytes that show 10-fold or higher enrichment in astrocytes compared to neurons and oligodendrocytes. Blue highlights indicate genes that are known to be expressed by both astrocytes and NSCs, and grey highlights indicate genes that failed *in vivo* validation by *in situ* hybridization (ISH). Yellow highlights mark the final 3 candidates for further expression analyses. (E) Expression analysis by microarray and quantitative PCR (qPCR) of Hopx, HtrA1, and F3. Expression levels are presented as fold change relative to the neurosphere group (FC, n=4 per group). Comparison of qPCR results between BMP and neurosphere groups revealed significant increases (*) of the three candidates in BMP astrocytes. (F) Low magnification ISH of Hopx, HtrA1, and F3 mRNA in P56 mouse neocortex and hippocampus (Allen Brain Atlas). (G) High magnification view of Hopx, HtrA1, and F3 mRNA in the dorsal cortex and the dentate gyrus of P60 mice as validated by in house ISH. Hopx is found in both astrocytes (arrow) and NSCs in the subgranular zone (arrowhead) of the dentate gyrus (DG) but not in other cortical astrocytes. HtrA1 and F3 are found in astrocytes (arrows) but not in NSCs of the DG (arrowheads). All data presented as mean±SEM. ABA, Allen Brain Atlas; Scale bar: panel B, 50μmm, panel F, 400μm; panel G, 50μm. * = < 0.01. Figure created with Chian-Yu Peng.

Table 2-1. Summary of the number of differentially expressed genes identified by the microarray.

21217 probes that were identified as "present" were compared among experimental groups in pairwise fashion using listed criteria (N1, N2, N3). The number of differential expressed genes (N) was determined for each experimental group, which included genes that were induced (up) and suppressed (down).

	N1	N2	N3	N	up	down	min p	max FC
BMP-Neuro	1763	6327	1985	1108	591	517	4.89E-13	157.92
BMP-LIF.NOG	1080	4187	1026	536	342	194	4.86E-13	158.42
LIF.NOG-Neuro	481	2610	204	82	66	16	1.63E-07	34.543

Table 2-2 Expression of known astrocyte markers in Neurospheres, BMP induced, and LIF induced astrocytes.

A summary of gene expression levels for fourteen commonly used astrocytes markers. While every marker is expressed in all three experimental groups, majority of the genes show strongest expression in BMP induced astrocytes.

Gene Symbol	Gene Name	BMP	LIFNOG	Neuro
Gfap	Glial Fibrillary Acidic Protein	**13065.7**	**2217.775**	**139.1975**
Aqp4	Aquaporin 4	**28972.25**	**4467.45**	**388.6**
ApoE	Apo Lipoprotein E	**16827.75**	**7537.15**	**303.3675**
Glud1	Glutamate Dehydrogenase 1	**11855.75**	**4079.6**	**1392.5**
Aldoc	Aldolase C	**10605.05**	**3198.85**	**1617.475**
Slc1a2 (Glt1)	Glial high affinity glutamate transporter	**1237.35**	**291.45**	**232.3425**
Gja1	Gap Junction Protein Alpha 1, Connexin 43	**18538**	**6922.75**	**3977.525**
Gjb6	Gap Junction Protein Beta 6, Connexin 30	**272.1525**	**150.49**	**148.6375**
Acsbg1	Acyl-CoA synthetase bubblegum family member 1	**596.3425**	**301.415**	**336.2**
S100b	S100 Calcium Binding Protein B	**194.11**	**132.7925**	**136.385**
GLUL (GS)	Glutamine Synthase	**216.2725**	**160.175**	**153.605**
Vim	Vimentin	**14626.5**	**18975.75**	**10507.25**
Aldh1L1	Aldehyde dehydrogenase 1 family member L1	**428.0675**	**1302.845**	**457.1225**
slc1a3 (GLAST)	Glial high affinity glutamate transporter, member 3	**160.515**	**176.0775**	**215.3675**

Table 2-3 A list of differentially expressed genes identified by the comparison of BMP-induced astrocytes and neurospheres.

Genes are ordered based on largest to smallest fold difference. Genes that show less than two-fold change are excluded. A total of 830 genes are differentially expressed. 455 genes are expressed more highly in BMP-induced astrocytes compared to neurospheres. Conversely, 375 genes are expressed more highly in neurospheres compared to BMP-induced astrocytes

High in BMP

Symbol	Description	Fold Change	p.value	FDR
Serpinf1	serine (or cysteine) peptidase inhibitor, clade F, member 1	157.92	2.31E-17	4.89E-13
Gfap	glial fibrillary acidic protein	85.712	4.56E-07	0.0096839
Aqp4	aquaporin 4	74.683	7.71E-12	1.64E-07
Apoe	apolipoprotein E	56.749	2.12E-09	4.51E-05
Hspb8	heat shock protein 8	54.308	3.35E-11	7.11E-07
Cidea	cell death-inducing DNA fragmentation factor, alpha subunit-like effector A	38.771	4.65E-16	9.87E-12
Hspb1	heat shock protein 1	33.275	8.66E-09	0.00018379
Fos	FBJ osteosarcoma oncogene	29.375	1.18E-10	2.51E-06
Fbxo2	F-box protein 2	26.959	7.54E-13	1.60E-08
Clu	clusterin	26.51	1.11E-08	0.00023486
Man1c1	mannosidase, alpha, class 1C, member 1	26.312	5.05E-11	1.07E-06
Rgs9	regulator of G-protein signaling 9	25.343	2.05E-12	4.36E-08
Serpina3n	serine (or cysteine) peptidase inhibitor, clade A, member 3N	24.059	2.07E-07	0.0043834
Ctgf	connective tissue growth factor	20.574	2.36E-08	0.0005001
Kcnk13	potassium channel, subfamily K, member 13	18.803	4.56E-13	9.68E-09
Kcna6	potassium voltage-gated channel, shaker-related, subfamily, member 6	18.622	3.38E-08	0.00071659
Socs3	suppressor of cytokine signaling 3	18.614	4.26E-08	0.00090282
Plec1	plectin 1	17.411	1.06E-09	2.24E-05
Padi2	peptidyl arginine deiminase, type II	16.87	4.63E-09	9.82E-05
Ncan	neurocan	15.034	9.56E-14	2.03E-09
Slc6a8	solute carrier family 6 (neurotransmitter transporter, creatine), member 8	15.017	2.93E-10	6.22E-06
Hopx	homeobox only domain	14.964	4.14E-08	0.00087896
Cd59a	CD59a antigen	14.002	3.07E-09	6.52E-05
Adra2a	adrenergic receptor, alpha 2a	13.968	7.40E-12	1.57E-07
Scg5	secretogranin V	13.83	1.57E-08	0.0003322
Mt2	metallothionein 2	13.313	1.72E-07	0.00364
Id2	inhibitor of DNA binding 2	13.298	1.93E-10	4.10E-06
Lrp4	low density lipoprotein receptor-related protein 4	12.847	2.91E-07	0.0061723
Fxyd6	FXYD domain-containing ion transport regulator 6	12.684	2.69E-09	5.71E-05
Fgf1	fibroblast growth factor 1	12.465	4.87E-08	0.0010336
Scrg1	scrapie responsive gene 1	12.359	5.40E-09	0.00011465
Mt3	metallothionein 3	12.298	3.27E-08	0.00069481
Hrsp12	heat-responsive protein 12	12.001	2.37E-09	5.02E-05
Cryab	crystallin, alpha B	11.811	4.20E-07	0.0089197

Dbp	D site albumin promoter binding protein	10.99	1.97E-10	4.19E-06
Dhrs1	dehydrogenase/reductase (SDR family) member 1	10.773	6.41E-08	0.0013607
Dusp1	dual specificity phosphatase 1	10.753	6.32E-10	1.34E-05
ENSMUSG00000056615	predicted gene, ENSMUSG00000056615	10.521	1.03E-12	2.20E-08
Kcne1l	potassium voltage-gated channel, Isk-related family, member 1-like	10.385	9.64E-10	2.05E-05
Slc7a5	solute carrier family 7 (cationic amino acid transporter, y+ system), member 5	10.271	9.05E-11	1.92E-06
Fcgrt	Fc receptor, IgG, alpha chain transporter	10.176	1.96E-09	4.16E-05
Reln	reelin	9.954	3.54E-09	7.51E-05
Hey1	hairy/enhancer-of-split related with YRPW motif 1	9.9161	5.28E-08	0.0011199
Sphk1	sphingosine kinase 1	9.7492	2.35E-07	0.0049794
Timp3	tissue inhibitor of metalloproteinase 3	9.7317	4.55E-08	0.00096618
Tmem108	transmembrane protein 108	9.5037	5.69E-10	1.21E-05
Pygb	brain glycogen phosphorylase	9.4851	2.64E-07	0.0055916
Gstm6	glutathione S-transferase, mu 6	9.4289	3.96E-11	8.39E-07
Ndg2	Nur77 downstream gene 2	9.248	1.37E-09	2.90E-05
Pdgfrl	platelet-derived growth factor receptor-like	8.7829	3.35E-10	7.11E-06
Gbx2	gastrulation brain homeobox 2	8.7738	5.06E-10	1.07E-05
Gstm1	glutathione S-transferase, mu 1	8.7397	3.58E-09	7.59E-05
Aox1	aldehyde oxidase 1	8.7075	1.32E-07	0.0027979
Tmem166	transmembrane protein 166	8.6425	6.73E-09	0.0001428
Stk32a	serine/threonine kinase 32A	8.6423	2.91E-10	6.18E-06
Htra1	HtrA serine peptidase 1	8.6385	2.12E-12	4.50E-08
Glud1	glutamate dehydrogenase 1	8.5282	2.24E-10	4.74E-06
Sgk	serum/glucocorticoid regulated kinase	8.3653	4.63E-07	0.0098194
Ank	progressive ankylosis	8.2871	3.82E-10	8.10E-06
Itpk1	inositol 1,3,4-triphosphate 5/6 kinase	8.2384	2.69E-09	5.71E-05
C130076O07Rik	RIKEN cDNA C130076O07 gene	8.2185	2.53E-09	5.37E-05
Cadps	Ca<2+>dependent activator protein for secretion	8.1997	1.65E-08	0.00035008
Kif26b	kinesin family member 26B	7.99	3.26E-10	6.92E-06
Pfkm	phosphofructokinase, muscle	7.7809	7.32E-11	1.55E-06
Cyr61	cysteine rich protein 61	7.7624	1.92E-09	4.07E-05
Nsg2	neuron specific gene family member 2	7.5929	1.23E-06	0.025996
Lxn	latexin	7.4918	5.51E-09	0.00011698
Ctsd	cathepsin D	7.4597	5.49E-08	0.0011642
Hist1h2bc	histone cluster 1, H2bc	7.4279	5.71E-09	0.00012109
Hmox1	heme oxygenase (decycling) 1	7.23	1.30E-09	2.75E-05
Rcsd1	RCSD domain containing 1	7.1767	5.83E-13	1.24E-08
Ednrb	endothelin receptor type B	7.1408	5.04E-08	0.0010696
Pde4b	phosphodiesterase 4B, cAMP specific	7.0804	1.92E-09	4.07E-05
Cd9	CD9 antigen	7.0609	1.97E-11	4.17E-07
Slc2a1	solute carrier family 2 (facilitated glucose transporter), member 1	7.0193	2.67E-07	0.0056659
Id4	inhibitor of DNA binding 4	6.8306	2.79E-08	0.00059131
Pla2g7	phospholipase A2, group VII (platelet-activating factor acetylhydrolase, plasma)	6.606	9.58E-08	0.0020327
Wwc2	WW, C2 and coiled-coil domain containing 2	6.5171	6.37E-11	1.35E-06

Paqr8	progestin and adipoQ receptor family member VIII	6.5134	1.05E-10	2.22E-06
Slc8a1	solute carrier family 8 (sodium/calcium exchanger), member 1	6.501	3.54E-10	7.51E-06
Ifitm2	interferon induced transmembrane protein 2	6.4148	5.69E-09	0.00012079
Tst	thiosulfate sulfurtransferase, mitochondrial	6.3746	2.40E-07	0.0051003
Atp1a1	ATPase, Na+/K+ transporting, alpha 1 polypeptide	6.3134	9.98E-11	2.12E-06
Chgb	chromogranin B	6.2844	3.14E-15	6.66E-11
Axl	AXL receptor tyrosine kinase	6.2752	2.90E-08	0.00061605
Chst2	carbohydrate sulfotransferase 2	6.2599	1.30E-06	0.02765
Agl	amylo-1,6-glucosidase, 4-alpha-glucanotransferase	6.2102	2.51E-12	5.32E-08
Bag3	Bcl2-associated athanogene 3	6.1771	1.83E-08	0.00038814
Tmem100	transmembrane protein 100	6.1307	8.28E-10	1.76E-05
Lgals8	lectin, galactose binding, soluble 8	6.1226	2.35E-10	4.98E-06
Id1	inhibitor of DNA binding 1	6.0636	1.75E-10	3.71E-06
Ankrd15	ankyrin repeat domain 15	6.0141	9.15E-10	1.94E-05
Cyp2j9	cytochrome P450, family 2, subfamily j, polypeptide 9	5.9845	1.50E-09	3.19E-05
Fstl1	follistatin-like 1	5.9669	4.61E-08	0.00097768
Eef1a2	eukaryotic translation elongation factor 1 alpha 2	5.9374	6.53E-08	0.0013854
Sat1	spermidine/spermine N1-acetyl transferase 1	5.9213	9.97E-08	0.0021145
Mmd2	monocyte to macrophage differentiation-associated 2	5.8429	5.66E-07	0.012014
C1qtnf5	C1q and tumor necrosis factor related protein 5	5.8046	1.30E-09	2.75E-05
3-Sep	septin 3	5.7794	3.23E-07	0.0068518
Plp1	proteolipid protein (myelin) 1	5.7738	6.22E-07	0.01319
Evi5	ecotropic viral integration site 5	5.7591	2.65E-10	5.62E-06
Chst8	carbohydrate (N-acetylgalactosamine 4-0) sulfotransferase 8	5.7383	3.50E-11	7.42E-07
Pib5pa	phosphatidylinositol (4,5) bisphosphate 5-phosphatase, A	5.686	2.41E-10	5.12E-06
Timp4	tissue inhibitor of metalloproteinase 4	5.6712	3.66E-07	0.0077721
Rarres1	retinoic acid receptor responder (tazarotene induced) 1	5.6611	2.15E-09	4.56E-05
Gprc5b	G protein-coupled receptor, family C, group 5, member B	5.6573	1.62E-10	3.43E-06
Ctnnbip1	catenin beta interacting protein 1	5.6486	1.16E-09	2.45E-05
Nog	noggin	5.6464	2.60E-10	5.51E-06
Vasn	vasorin	5.5843	7.93E-08	0.001682
Ablim2	actin-binding LIM protein 2	5.5359	1.01E-09	2.14E-05
Cd44	CD44 antigen	5.4915	1.89E-07	0.0040188
Fgfr2	fibroblast growth factor receptor 2	5.4617	6.62E-08	0.001405
Smad6	MAD homolog 6 (Drosophila)	5.3977	8.55E-15	1.81E-10
Snta1	syntrophin, acidic 1	5.3842	2.43E-07	0.0051595
D12Ertd647e	DNA segment, Chr 12, ERATO Doi 647, expressed	5.3772	2.81E-10	5.96E-06
Pcsk1n	proprotein convertase subtilisin/kexin type 1 inhibitor	5.3295	1.97E-09	4.19E-05
Slc1a2	solute carrier family 1 (glial high affinity glutamate transporter), member 2	5.2863	3.62E-11	7.67E-07
E130203B14Rik	RIKEN cDNA E130203B14 gene	5.2305	2.44E-08	0.0005182
Pea15	phosphoprotein enriched in astrocytes 15	5.191	4.17E-07	0.0088553
Lgmn	legumain	5.0961	4.17E-08	0.00088403
Gm2a	GM2 ganglioside activator protein	5.0374	1.97E-06	0.041749
Ldb2	LIM domain binding 2	4.9994	1.86E-08	0.00039359

Nedd9	neural precursor cell expressed, developmentally down-regulated gene 9	4.9434	2.96E-09	6.29E-05
Caln1	calneuron 1	4.901	5.42E-07	0.011492
Ccpg1	cell cycle progression 1	4.898	9.33E-07	0.019801
Ctnnal1	catenin (cadherin associated protein), alpha-like 1	4.8171	8.66E-09	0.00018382
Spsb1	splA/ryanodine receptor domain and SOCS box containing 1	4.7854	1.52E-07	0.0032254
S100a13	S100 calcium binding protein A13	4.7705	1.76E-11	3.74E-07
Wnt9a	wingless-type MMTV integration site 9A	4.7588	2.26E-07	0.004787
Sparcl1	SPARC-like 1 (mast9, hevin)	4.7415	3.82E-08	0.0008103
Appl2	adaptor protein, phosphotyrosine interaction, PH domain and leucine zipper containing 2	4.718	1.86E-08	0.00039536
Slc6a6	solute carrier family 6 (neurotransmitter transporter, taurine), member 6	4.6425	4.84E-07	0.010266
Gja1	gap junction membrane channel protein alpha 1	4.6147	3.74E-08	0.00079322
Hist1h2bp	histone cluster 1, H2bp	4.6038	3.06E-09	6.49E-05
App	amyloid beta (A4) precursor protein	4.5632	1.26E-09	2.68E-05
Nav1	neuron navigator 1	4.4685	9.16E-11	1.94E-06
Cdh22	cadherin 22	4.4643	5.47E-07	0.011605
Hist1h2bm	histone cluster 1, H2bm	4.4557	6.31E-09	0.00013392
AI646023	expressed sequence AI646023	4.3572	2.75E-08	0.0005839
Slc44a1	solute carrier family 44, member 1	4.3232	3.91E-09	8.31E-05
Id3	inhibitor of DNA binding 3	4.3104	4.66E-09	9.88E-05
Stard10	START domain containing 10	4.2829	5.36E-07	0.011382
AI427515	expressed sequence AI427515	4.275	9.10E-08	0.0019313
9130213B05Rik	RIKEN cDNA 9130213B05 gene	4.2502	4.85E-08	0.0010297
Hist1h2bj	histone cluster 1, H2bj	4.2443	3.47E-08	0.00073648
Plekhb2	pleckstrin homology domain containing, family B (evectins) member 2	4.2186	2.48E-09	5.27E-05
Pon2	paraoxonase 2	4.2118	1.67E-08	0.0003535
Prdx6	peroxiredoxin 6	4.1937	1.25E-07	0.0026419
Pitpnc1	phosphatidylinositol transfer protein, cytoplasmic 1	4.1823	2.67E-08	0.00056744
Ssfa2	sperm specific antigen 2	4.1759	2.14E-06	0.045495
Gsta4	glutathione S-transferase, alpha 4	4.1442	1.25E-07	0.0026609
Cyhr1	cysteine and histidine rich 1	4.1414	1.18E-08	0.0002506
Tbcel	tubulin folding cofactor E-like	4.1348	8.78E-09	0.00018626
Grina	glutamate receptor, ionotropic, N-methyl D-asparate-associated protein 1	4.1339	1.05E-07	0.0022249
Aldh6a1	aldehyde dehydrogenase family 6, subfamily A1	4.1336	1.98E-07	0.0041908
Sgcb	sarcoglycan, beta (dystrophin-associated glycoprotein)	4.094	3.03E-09	6.42E-05
Atp1b1	ATPase, Na+/K+ transporting, beta 1 polypeptide	4.0548	5.48E-07	0.011617
Ctsb	cathepsin B	4.0488	2.20E-10	4.66E-06
Gpx4	glutathione peroxidase 4	3.9944	1.16E-11	2.46E-07
Prnp	prion protein	3.9793	5.29E-09	0.00011218
Ncam1	neural cell adhesion molecule 1	3.9672	1.37E-09	2.91E-05
Mgst1	microsomal glutathione S-transferase 1	3.9301	4.24E-07	0.0089882
Enpp5	ectonucleotide pyrophosphatase/phosphodiesterase 5	3.9264	3.13E-09	6.65E-05
Map1lc3a	microtubule-associated protein 1 light chain 3 alpha	3.9171	1.68E-06	0.035578
9130404D14Rik	RIKEN cDNA 9130404D14 gene	3.9101	5.24E-10	1.11E-05

Pstpip1	proline-serine-threonine phosphatase-interacting protein 1	3.8823	6.99E-09	0.0001483
Tapt1	transmembrane anterior posterior transformation 1	3.8477	1.81E-11	3.85E-07
Sdsl	serine dehydratase-like	3.8428	1.56E-10	3.31E-06
Abhd3	abhydrolase domain containing 3	3.83	2.54E-07	0.0053881
Cpxm1	carboxypeptidase X 1 (M14 family)	3.8256	1.29E-09	2.73E-05
Fth1	ferritin heavy chain 1	3.8132	5.86E-09	0.00012433
Hist1h2bf	histone cluster 1, H2bf	3.8131	4.42E-09	9.38E-05
AI593442	expressed sequence AI593442	3.7777	8.01E-08	0.0017003
Il11ra2	interleukin 11 receptor, alpha chain 2	3.7734	1.84E-06	0.039014
Zcchc18	zinc finger, CCHC domain containing 18	3.7628	9.63E-07	0.020436
S100a1	S100 calcium binding protein A1	3.7443	2.44E-08	0.00051749
Scrn1	secernin 1	3.7291	1.41E-09	2.99E-05
Mt1	metallothionein 1	3.7222	4.78E-07	0.010132
Ecm1	extracellular matrix protein 1	3.72	4.00E-07	0.0084873
Psap	prosaposin	3.7094	3.58E-07	0.0075914
Susd4	sushi domain containing 4	3.6999	1.86E-08	0.00039428
Ephx1	epoxide hydrolase 1, microsomal	3.6982	7.94E-08	0.0016848
Lrig1	leucine-rich repeats and immunoglobulin-like domains 1	3.683	1.91E-07	0.004042
Aldh2	aldehyde dehydrogenase 2, mitochondrial	3.6587	6.74E-08	0.001431
Tceal3	transcription elongation factor A (SII)-like 3	3.6537	5.40E-10	1.15E-05
Mfap3l	microfibrillar-associated protein 3-like	3.6448	2.86E-07	0.0060614
Selm	selenoprotein M	3.6429	1.11E-06	0.023591
Adcy8	adenylate cyclase 8	3.6392	1.07E-07	0.0022603
Ltbp3	latent transforming growth factor beta binding protein 3	3.6318	7.76E-08	0.0016465
Adora2b	adenosine A2b receptor	3.5911	1.64E-07	0.0034695
Rab7l1	RAB7, member RAS oncogene family-like 1	3.5745	5.88E-09	0.00012471
Rnf182	ring finger protein 182	3.5649	1.16E-10	2.45E-06
Loxl1	lysyl oxidase-like 1	3.5512	1.38E-06	0.02933
Aqp11	aquaporin 11	3.5474	1.92E-12	4.07E-08
Tmem117	transmembrane protein 117	3.5414	5.69E-08	0.0012077
Slc38a3	solute carrier family 38, member 3	3.5398	7.93E-11	1.68E-06
P2ry1	purinergic receptor P2Y, G-protein coupled 1	3.5358	1.63E-08	0.00034669
2900062L11Rik	RIKEN cDNA 2900062L11 gene	3.5351	1.78E-09	3.78E-05
Cd151	CD151 antigen	3.5331	4.72E-09	0.00010017
Emb	embigin	3.528	3.56E-12	7.55E-08
Ctsh	cathepsin H	3.525	7.57E-09	0.0001606
Cited2	Cbp/p300-interacting transactivator, with Glu/Asp-rich carboxy-terminal domain, 2	3.5083	2.81E-07	0.0059579
BC046404	cDNA sequence BC046404	3.4969	2.97E-08	0.00063006
Laptm4a	lysosomal-associated protein transmembrane 4A	3.4931	6.82E-08	0.0014465
Ddo	D-aspartate oxidase	3.4858	4.59E-08	0.00097289
Lhfpl2	lipoma HMGIC fusion partner-like 2	3.478	8.78E-09	0.00018625
AW125753	expressed sequence AW125753	3.4709	2.94E-07	0.0062384
Aktip	thymoma viral proto-oncogene 1 interacting protein	3.4577	2.99E-11	6.35E-07

Junb	Jun-B oncogene	3.4559	8.70E-07	0.01846
Ramp2	receptor (calcitonin) activity modifying protein 2	3.4371	4.85E-07	0.010296
Pdlim7	PDZ and LIM domain 7	3.406	1.20E-06	0.025491
1200015A19Rik	RIKEN cDNA 1200015A19 gene	3.381	2.95E-08	0.0006252
Ak3	adenylate kinase 3	3.3753	3.44E-07	0.0073009
Capzb	capping protein (actin filament) muscle Z-line, beta	3.3661	2.24E-08	0.00047512
Tmem66	transmembrane protein 66	3.3601	5.68E-08	0.0012052
Eps15	epidermal growth factor receptor pathway substrate 15	3.3595	1.24E-07	0.0026376
Hist2h2aa1	histone cluster 2, H2aa1	3.3561	2.47E-07	0.0052439
Osbpl1a	oxysterol binding protein-like 1A	3.3555	7.76E-07	0.016456
Usp2	ubiquitin specific peptidase 2	3.3504	1.23E-06	0.026184
Dner	delta/notch-like EGF-related receptor	3.3447	1.04E-08	0.00022077
Pink1	PTEN induced putative kinase 1	3.3381	1.68E-07	0.0035731
Pim3	proviral integration site 3	3.3243	5.41E-09	0.00011478
Gna13	guanine nucleotide binding protein, alpha 13	3.3225	8.57E-08	0.0018184
Cutl1	cut-like 1 (Drosophila)	3.3154	2.33E-06	0.049472
Sorbs1	sorbin and SH3 domain containing 1	3.3057	1.75E-08	0.00037182
Gas6	growth arrest specific 6	3.2894	5.00E-07	0.010607
Tceal5	transcription elongation factor A (SII)-like 5	3.2791	4.26E-07	0.0090349
Tmem86a	transmembrane protein 86A	3.2784	1.40E-08	0.00029635
BC065085	cDNA sequence BC065085	3.2773	9.79E-09	0.00020767
Cpe	carboxypeptidase E	3.2759	5.90E-07	0.012511
Mxra8	matrix-remodelling associated 8	3.2719	4.19E-07	0.0088853
Anxa5	annexin A5	3.2644	2.10E-08	0.00044506
Spon2	spondin 2, extracellular matrix protein	3.2613	5.98E-07	0.012698
Ghitm	growth hormone inducible transmembrane protein	3.2588	2.73E-07	0.0057861
Ppp1r3c	protein phosphatase 1, regulatory (inhibitor) subunit 3C	3.2323	8.89E-07	0.01886
Hist1h2bn	histone cluster 1, H2bn	3.2269	1.01E-08	0.00021483
Ugp2	UDP-glucose pyrophosphorylase 2	3.219	6.87E-09	0.0001458
Acadsb	acyl-Coenzyme A dehydrogenase, short/branched chain	3.193	7.58E-07	0.016092
Hist1h2bh	histone cluster 1, H2bh	3.1676	5.99E-08	0.0012715
Tspan3	tetraspanin 3	3.1619	2.01E-07	0.0042678
Slc24a6	solute carrier family 24 (sodium/potassium/calcium exchanger), member 6	3.1593	4.07E-10	8.64E-06
Tmem158	transmembrane protein 158	3.1427	1.97E-07	0.00418
H2afy	H2A histone family, member Y	3.1406	4.21E-09	8.92E-05
Prpsap1	phosphoribosyl pyrophosphate synthetase-associated protein 1	3.1404	3.63E-08	0.00076988
Arhgef4	Rho guanine nucleotide exchange factor (GEF) 4	3.1357	1.21E-06	0.025635
Gpr85	G protein-coupled receptor 85	3.1209	9.23E-10	1.96E-05
Ypel5	yippee-like 5 (Drosophila)	3.0888	9.37E-07	0.019888
Hist1h2bl	histone cluster 1, H2bl	3.0669	4.92E-09	0.00010449
Pmm1	phosphomannomutase 1	3.0627	1.09E-07	0.0023166
Slc36a2	solute carrier family 36 (proton/amino acid symporter), member 2	3.059	1.90E-10	4.03E-06
Tgfb2	transforming growth factor, beta 2	3.0542	5.86E-07	0.012434
Atox1	ATX1 (antioxidant protein 1) homolog 1 (yeast)	3.049	2.50E-07	0.0053025

AW049604	expressed sequence AW049604	3.0465	3.37E-08	0.00071506
Tmem47	transmembrane protein 47	3.0415	9.77E-07	0.020721
Il17rb	interleukin 17 receptor B	3.0278	5.97E-07	0.012675
Hspa2	heat shock protein 2	3.0191	9.99E-07	0.02119
Sqstm1	sequestosome 1	3.019	7.58E-08	0.0016085
Lyzs	lysozyme	3.0115	1.53E-09	3.24E-05
Myl4	myosin, light polypeptide 4	3.0007	2.70E-08	0.00057311
Pfkl	phosphofructokinase, liver, B-type	2.9907	3.99E-08	0.00084597
Dlgap1	discs, large (Drosophila) homolog-associated protein 1	2.9776	2.53E-07	0.0053709
Rtn1	reticulon 1	2.9774	9.53E-07	0.020223
Lrp10	low-density lipoprotein receptor-related protein 10	2.9708	1.57E-07	0.0033252
Csf1	colony stimulating factor 1 (macrophage)	2.9678	8.42E-07	0.017874
Rasl11b	RAS-like, family 11, member B	2.9669	2.65E-07	0.0056307
Cmtm5	CKLF-like MARVEL transmembrane domain containing 5	2.9647	7.49E-07	0.015884
4933426M11Rik	RIKEN cDNA 4933426M11 gene	2.9629	2.22E-07	0.0047042
Pax6	paired box gene 6	2.9629	7.75E-07	0.016443
Ormdl3	ORM1-like 3 (S. cerevisiae)	2.9615	4.40E-08	0.00093375
Omd	osteomodulin	2.9526	5.75E-12	1.22E-07
5730469M10Rik	RIKEN cDNA 5730469M10 gene	2.9516	1.01E-06	0.021403
Lamp1	lysosomal membrane glycoprotein 1	2.942	9.16E-07	0.019444
Bmpr1a	bone morphogenetic protein receptor, type 1A	2.9417	1.47E-10	3.11E-06
Tegt	testis enhanced gene transcript	2.9328	5.29E-08	0.0011224
Zfpm1	zinc finger protein, multitype 1	2.9309	4.69E-08	0.00099587
Rfx2	regulatory factor X, 2 (influences HLA class II expression)	2.9154	2.64E-07	0.0056039
Hist1h2bk	histone cluster 1, H2bk	2.9054	4.05E-08	0.00085823
Pcdh7	protocadherin 7	2.8955	1.54E-07	0.0032772
Ubl3	ubiquitin-like 3	2.8796	3.67E-08	0.00077877
Fhl1	four and a half LIM domains 1	2.8477	4.97E-08	0.0010551
Skp1a	S-phase kinase-associated protein 1A	2.8342	3.69E-09	7.83E-05
Nrxn3	neurexin III	2.8314	2.71E-09	5.74E-05
Reep5	receptor accessory protein 5	2.8312	2.24E-07	0.0047529
Tulp4	tubby like protein 4	2.8292	2.74E-10	5.81E-06
Bbox1	butyrobetaine (gamma), 2-oxoglutarate dioxygenase 1 (gamma-butyrobetaine hydroxylase)	2.8229	1.59E-08	0.00033756
Bcan	brevican	2.8161	1.15E-07	0.0024483
Nope	neighbor of Punc E11	2.8103	1.47E-07	0.0031264
Nfat5	nuclear factor of activated T-cells 5	2.8067	4.45E-09	9.43E-05
Elovl1	elongation of very long chain fatty acids (FEN1/Elo2, SUR4/Elo3, yeast)-like 1	2.8067	5.26E-08	0.0011159
2410166I05Rik	RIKEN cDNA 2410166I05 gene	2.8034	7.96E-11	1.69E-06
Hmgcs2	3-hydroxy-3-methylglutaryl-Coenzyme A synthase 2	2.795	8.97E-09	0.00019039
Rora	RAR-related orphan receptor alpha	2.7827	7.25E-08	0.0015381
2310016C16Rik	RIKEN cDNA 2310016C16 gene	2.7811	9.01E-08	0.0019108
Pls3	plastin 3 (T-isoform)	2.7786	1.17E-06	0.024719
Cyp4v3	cytochrome P450, family 4, subfamily v, polypeptide 3	2.7655	2.16E-07	0.0045784

Degs1	degenerative spermatocyte homolog 1 (Drosophila)	2.7425	9.79E-08	0.0020777
1200009O22Rik	RIKEN cDNA 1200009O22 gene	2.7242	6.75E-07	0.014318
BC010787	cDNA sequence BC010787	2.7077	8.86E-09	0.00018788
Lamb2	laminin, beta 2	2.6902	2.41E-07	0.0051198
Fzd5	frizzled homolog 5 (Drosophila)	2.6868	7.65E-08	0.0016241
Arsa	arylsulfatase A	2.6856	1.58E-06	0.033521
Rab31	RAB31, member RAS oncogene family	2.6684	1.45E-06	0.030825
Mpv17	Mpv17 transgene, kidney disease mutant	2.6625	1.09E-07	0.0023117
Zfp423	zinc finger protein 423	2.6609	4.01E-12	8.50E-08
Trim2	tripartite motif protein 2	2.6455	1.29E-06	0.027284
Mamdc2	MAM domain containing 2	2.6311	1.62E-06	0.034311
Pitpna	phosphatidylinositol transfer protein, alpha	2.6301	1.85E-06	0.039161
Rdh14	retinol dehydrogenase 14 (all-trans and 9-cis)	2.6292	4.16E-10	8.83E-06
Atg12	autophagy-related 12 (yeast)	2.6219	6.11E-07	0.012964
Gadd45a	growth arrest and DNA-damage-inducible 45 alpha	2.6026	1.60E-09	3.39E-05
Pkd2	polycystic kidney disease 2	2.6001	5.79E-09	0.0001228
Tnfrsf13c	tumor necrosis factor receptor superfamily, member 13c	2.5981	5.16E-11	1.09E-06
Oaz2	ornithine decarboxylase antizyme 2	2.5969	1.71E-09	3.63E-05
Atp6v0e	ATPase, H+ transporting, lysosomal V0 subunit E	2.5959	5.30E-07	0.011248
Tmem50a	transmembrane protein 50A	2.5953	1.73E-06	0.03665
Abca3	ATP-binding cassette, sub-family A (ABC1), member 3	2.589	3.40E-07	0.007206
Pfkfb3	6-phosphofructo-2-kinase/fructose-2,6-biphosphatase 3	2.5883	7.24E-07	0.015355
B230209C24Rik	RIKEN cDNA B230209C24 gene	2.5881	2.97E-07	0.0062979
Fnbp1l	formin binding protein 1-like	2.5746	4.36E-10	9.25E-06
Fryl	furry homolog-like (Drosophila)	2.5652	2.37E-08	0.00050356
2900011O08Rik	RIKEN cDNA 2900011O08 gene	2.5515	4.43E-07	0.0093972
Scg2	secretogranin II	2.5373	5.74E-08	0.0012186
Lynx1	Ly6/neurotoxin 1	2.5366	7.46E-07	0.015822
Tcn2	transcobalamin 2	2.535	1.71E-08	0.00036182
Sema3b	sema domain, immunoglobulin domain (Ig), short basic domain, secreted, (semaphorin) 3B	2.5295	1.49E-08	0.0003165
Nr1d1	nuclear receptor subfamily 1, group D, member 1	2.5295	9.90E-08	0.0021005
Ndrg4	N-myc downstream regulated gene 4	2.5237	5.43E-13	1.15E-08
Add3	adducin 3 (gamma)	2.5183	1.46E-06	0.030996
Btbd1	BTB (POZ) domain containing 1	2.5129	2.03E-06	0.043009
Slc3a2	solute carrier family 3 (activators of dibasic and neutral amino acid transport), member 2	2.5072	2.07E-10	4.39E-06
9030409G11Rik	RIKEN cDNA 9030409G11 gene	2.5055	3.92E-09	8.32E-05
Tmem44	transmembrane protein 44	2.5021	1.36E-06	0.028911
Hibadh	3-hydroxyisobutyrate dehydrogenase	2.4913	1.71E-10	3.64E-06
Fkbp14	FK506 binding protein 14	2.4906	6.91E-11	1.47E-06
Tspan7	tetraspanin 7	2.4846	6.06E-07	0.012857
Tmem50b	transmembrane protein 50B	2.4756	6.64E-08	0.0014091
Iqsec1	IQ motif and Sec7 domain 1	2.4718	1.18E-09	2.50E-05

Rabac1	Rab acceptor 1 (prenylated)	2.458	3.49E-08	0.00074077
Impact	imprinted and ancient	2.4553	1.16E-09	2.46E-05
BC064033	cDNA sequence BC064033	2.4517	4.08E-08	0.0008654
Usp53	ubiquitin specific peptidase 53	2.4485	4.83E-09	0.00010256
Flot1	flotillin 1	2.4479	8.72E-08	0.0018503
Gabarapl1	gamma-aminobutyric acid (GABA(A)) receptor-associated protein-like 1	2.4468	1.51E-08	0.00032072
Pip5k2c	phosphatidylinositol-4-phosphate 5-kinase, type II, gamma	2.428	6.38E-07	0.013537
Manea	mannosidase, endo-alpha	2.4247	1.67E-06	0.035469
1190005I06Rik	RIKEN cDNA 1190005I06 gene	2.4221	2.01E-06	0.042669
Acox2	acyl-Coenzyme A oxidase 2, branched chain	2.4181	1.86E-09	3.94E-05
Xpr1	xenotropic and polytropic retrovirus receptor 1	2.4126	9.23E-07	0.019592
Mtch1	mitochondrial carrier homolog 1 (C. elegans)	2.412	4.73E-08	0.001003
Rab33b	RAB33B, member of RAS oncogene family	2.4072	8.94E-09	0.00018972
Dap	death-associated protein	2.4058	2.41E-07	0.0051146
Hsd3b7	hydroxy-delta-5-steroid dehydrogenase, 3 beta- and steroid delta-isomerase 7	2.4057	1.27E-08	0.00026856
Igsf3	immunoglobulin superfamily, member 3	2.398	2.04E-07	0.0043375
Pnpla8	patatin-like phospholipase domain containing 8	2.3962	9.58E-09	0.00020332
Syt11	synaptotagmin XI	2.388	2.10E-07	0.0044466
AW456874	expressed sequence AW456874	2.38	2.41E-07	0.0051062
Fndc5	fibronectin type III domain containing 5	2.3704	1.47E-07	0.003124
1500005A01Rik	RIKEN cDNA 1500005A01 gene	2.3554	1.41E-07	0.003
Pttg1ip	pituitary tumor-transforming 1 interacting protein	2.3506	1.86E-06	0.039547
Suox	sulfite oxidase	2.3475	4.01E-09	8.50E-05
Clcn3	chloride channel 3	2.342	4.95E-08	0.0010506
Tmem106b	transmembrane protein 106B	2.3406	1.60E-06	0.033986
Atp2a2	ATPase, Ca++ transporting, cardiac muscle, slow twitch 2	2.3402	8.03E-09	0.00017045
Tmco3	transmembrane and coiled-coil domains 3	2.3399	5.02E-09	0.0001066
Eif2ak2	eukaryotic translation initiation factor 2-alpha kinase 2	2.3365	4.62E-07	0.0097919
Slc26a6	solute carrier family 26, member 6	2.3357	3.84E-07	0.0081518
Igsf9b	immunoglobulin superfamily, member 9B	2.3334	1.07E-10	2.27E-06
Lrp1	low density lipoprotein receptor-related protein 1	2.3294	4.06E-07	0.0086127
Slc24a3	solute carrier family 24 (sodium/potassium/calcium exchanger), member 3	2.3284	1.02E-06	0.021738
Fnbp1	formin binding protein 1	2.3057	5.54E-07	0.011755
2500002L14Rik	RIKEN cDNA 2500002L14 gene	2.3041	5.69E-09	0.00012081
Tmem150	transmembrane protein 150	2.3029	6.02E-09	0.00012763
Lcat	lecithin cholesterol acyltransferase	2.2956	2.36E-08	0.00049976
Mpv17l	Mpv17 transgene, kidney disease mutant-like	2.293	3.31E-08	0.00070259
Nrp1	neuropilin 1	2.2889	1.08E-06	0.023003
Cpeb3	cytoplasmic polyadenylation element binding protein 3	2.2859	3.39E-09	7.18E-05
BC013529	cDNA sequence BC013529	2.2849	6.70E-08	0.0014221
Serpine2	serine (or cysteine) peptidase inhibitor, clade E, member 2	2.2807	6.70E-08	0.0014219
Mbnl2	muscleblind-like 2	2.2746	5.53E-09	0.00011739
Lrpap1	low density lipoprotein receptor-related protein associated protein 1	2.2694	2.44E-08	0.00051673
Rps6ka5	ribosomal protein S6 kinase, polypeptide 5	2.257	7.91E-07	0.016781

Amfr	autocrine motility factor receptor	2.2551	3.62E-07	0.0076895
Kif1b	kinesin family member 1B	2.255	3.63E-07	0.0077058
Hsbp1	heat shock factor binding protein 1	2.2503	1.03E-08	0.00021904
B930095G15Rik	RIKEN cDNA B930095G15 gene	2.2491	5.90E-08	0.0012512
Stat3	signal transducer and activator of transcription 3	2.2471	8.17E-07	0.017333
Vamp4	vesicle-associated membrane protein 4	2.2425	4.43E-07	0.0094072
Zhx1	zinc fingers and homeoboxes protein 1	2.2342	9.87E-09	0.00020935
Erlin2	ER lipid raft associated 2	2.2316	3.54E-07	0.0075189
Zfp521	zinc finger protein 521	2.2251	5.16E-07	0.010951
Papss2	3'-phosphoadenosine 5'-phosphosulfate synthase 2	2.2235	3.14E-09	6.65E-05
Vamp2	vesicle-associated membrane protein 2	2.2231	9.78E-07	0.020752
Gnb5	guanine nucleotide binding protein, beta 5	2.2226	8.82E-09	0.00018723
Cxxc5	CXXC finger 5	2.2201	1.80E-06	0.038144
Smpd1	sphingomyelin phosphodiesterase 1, acid lysosomal	2.2162	2.03E-06	0.042984
Abhd5	abhydrolase domain containing 5	2.2075	2.89E-09	6.14E-05
Ngfr	nerve growth factor receptor (TNFR superfamily, member 16)	2.2037	1.31E-06	0.027796
Galt	galactose-1-phosphate uridyl transferase	2.2034	7.02E-08	0.0014901
1200009F10Rik	RIKEN cDNA 1200009F10 gene	2.1877	9.56E-07	0.020284
Ech1	enoyl coenzyme A hydratase 1, peroxisomal	2.1774	2.33E-07	0.0049462
Atp1a2	ATPase, Na+/K+ transporting, alpha 2 polypeptide	2.1741	1.25E-06	0.026492
Phyhipl	phytanoyl-CoA hydroxylase interacting protein-like	2.1702	4.69E-08	0.00099598
Bmper	BMP-binding endothelial regulator	2.169	3.73E-08	0.00079208
Tpd52l1	tumor protein D52-like 1	2.1685	1.35E-09	2.87E-05
Ap3s2	adaptor-related protein complex 3, sigma 2 subunit	2.1573	5.40E-08	0.0011451
Lsamp	limbic system-associated membrane protein	2.1563	5.91E-08	0.0012535
Prdx5	peroxiredoxin 5	2.1546	4.59E-08	0.00097457
BC067047	cDNA sequence BC067047	2.1457	5.27E-08	0.0011183
Mvp	major vault protein	2.1443	1.75E-08	0.00037099
Ebpl	emopamil binding protein-like	2.1421	4.26E-09	9.03E-05
OTTMUSG00000004461	predicted gene, OTTMUSG00000004461	2.1379	2.08E-09	4.42E-05
Scp2	sterol carrier protein 2, liver	2.1357	5.81E-08	0.0012319
Art3	ADP-ribosyltransferase 3	2.1303	8.95E-09	0.00018982
Fez2	fasciculation and elongation protein zeta 2 (zygin II)	2.1231	8.20E-08	0.001739
D10Ertd641e	DNA segment, Chr 10, ERATO Doi 641, expressed	2.121	1.51E-06	0.032086
Mcl1	myeloid cell leukemia sequence 1	2.1167	4.86E-07	0.01031
Vldlr	very low density lipoprotein receptor	2.1095	1.65E-06	0.035004
St3gal2	ST3 beta-galactoside alpha-2,3-sialyltransferase 2	2.1036	2.25E-07	0.0047733
Cib1	calcium and integrin binding 1 (calmyrin)	2.1028	7.69E-09	0.00016326
Mgat5	mannoside acetylglucosaminyltransferase 5	2.1008	9.36E-07	0.019858
P4ha1	procollagen-proline, 2-oxoglutarate 4-dioxygenase, alpha 1 polypeptide	2.0992	6.78E-09	0.00014395
Fkbp9	FK506 binding protein 9	2.0992	1.97E-06	0.041852
Bdh1	3-hydroxybutyrate dehydrogenase, type 1	2.0971	1.02E-06	0.0217
Sdk1	sidekick homolog 1 (chicken)	2.0957	5.17E-07	0.010961
Grhl1	grainyhead-like 1 (Drosophila)	2.0937	3.69E-10	7.82E-06

Ccdc126	coiled-coil domain containing 126	2.0934	1.12E-07	0.0023772
Cyp46a1	cytochrome P450, family 46, subfamily a, polypeptide 1	2.092	6.72E-08	0.001426
Armcx3	armadillo repeat containing, X-linked 3	2.0913	1.15E-07	0.0024346
BC051227	cDNA sequence BC051227	2.0894	1.09E-07	0.0023019
Nxt2	nuclear transport factor 2-like export factor 2	2.0894	1.18E-06	0.02507
Osbpl9	oxysterol binding protein-like 9	2.0879	1.95E-08	0.00041384
Dag1	dystroglycan 1	2.0843	6.56E-07	0.013911
Aifm2	apoptosis-inducing factor, mitochondrion-associated 2	2.0814	8.80E-07	0.018665
Egfl9	EGF-like-domain, multiple 9	2.0807	2.75E-08	0.00058392
Eml3	echinoderm microtubule associated protein like 3	2.0734	1.22E-10	2.59E-06
Col4a5	procollagen, type IV, alpha 5	2.0644	4.85E-08	0.0010283
Fmn2	formin 2	2.0605	2.17E-08	0.00046102
2310005P05Rik	RIKEN cDNA 2310005P05 gene	2.0601	3.51E-07	0.007442
Tjp2	tight junction protein 2	2.0572	1.23E-07	0.0026019
Iscu	IscU iron-sulfur cluster scaffold homolog (E. coli)	2.0555	2.54E-08	0.00053876
Arsb	arylsulfatase B	2.0548	3.76E-08	0.00079714
Caskin1	CASK interacting protein 1	2.0461	6.42E-08	0.0013614
Gpr155	G protein-coupled receptor 155	2.0459	3.41E-08	0.00072432
Kctd6	potassium channel tetramerisation domain containing 6	2.0451	1.59E-08	0.0003383
Aqp9	aquaporin 9	2.0385	1.52E-06	0.032148
Adam23	a disintegrin and metallopeptidase domain 23	2.0249	9.06E-10	1.92E-05
Pxmp3	peroxisomal membrane protein 3	2.0178	3.81E-09	8.09E-05
Entpd5	ectonucleoside triphosphate diphosphohydrolase 5	2.0116	4.53E-10	9.62E-06
Ticam1	toll-like receptor adaptor molecule 1	2.0102	4.63E-07	0.0098221
Ptplad1	protein tyrosine phosphatase-like A domain containing 1	2.0088	9.54E-08	0.002024
Plekhh3	pleckstrin homology domain containing, family H (with MyTH4 domain) member 3	2.0068	2.22E-09	4.70E-05
Ikbkg	inhibitor of kappaB kinase gamma	2.0037	9.63E-07	0.020442
G6pc3	glucose 6 phosphatase, catalytic, 3	2.0037	2.07E-06	0.043873
Uqcr	ubiquinol-cytochrome c reductase (6.4kD) subunit	2.0008	3.40E-07	0.0072155
Pgcp	plasma glutamate carboxypeptidase	2.0002	1.71E-09	3.64E-05

High in Neuro.

Symbol	Description	Fold Change	p.value	FDR
Hist1h2ak	histone cluster 1, H2ak	21.829	5.43E-07	0.011515
Ccnd1	cyclin D1	21.403	1.11E-06	0.023622
Hist1h2ah	histone cluster 1, H2ah	20.87	8.29E-07	0.017592
Mest	mesoderm specific transcript	18.076	8.53E-12	1.81E-07
Hist1h2an	histone cluster 1, H2an	17.507	5.07E-07	0.01075
Cdca8	cell division cycle associated 8	16.488	2.31E-07	0.0048908
Mcm5	minichromosome maintenance deficient 5, cell division cycle 46 (S. cerevisiae)	16.007	5.51E-07	0.01169
Hist1h2ag	histone cluster 1, H2ag	15.589	1.16E-06	0.02461
Plk1	polo-like kinase 1 (Drosophila)	15.4	7.81E-07	0.016575

Cdca3	cell division cycle associated 3	14.925	7.30E-07	0.015496
Prc1	protein regulator of cytokinesis 1	14.919	2.03E-06	0.043125
Uhrf1	ubiquitin-like, containing PHD and RING finger domains, 1	14.452	5.84E-07	0.012386
Fbln2	fibulin 2	13.024	1.13E-08	0.00023923
Hist1h2ai	histone cluster 1, H2ai	12.865	1.10E-06	0.023337
6720460F02Rik	RIKEN cDNA 6720460F02 gene	11.343	7.91E-07	0.016785
Bok	Bcl-2-related ovarian killer protein	10.869	1.93E-10	4.10E-06
Ccnb1	cyclin B1	10.385	3.54E-08	0.00075063
Cdc2a	cell division cycle 2 homolog A (S. pombe)	10.114	9.28E-07	0.019683
Spsb4	splA/ryanodine receptor domain and SOCS box containing 4	10.06	1.46E-10	3.11E-06
Nusap1	nucleolar and spindle associated protein 1	9.5812	6.72E-07	0.014256
Cdc20	cell division cycle 20 homolog (S. cerevisiae)	8.9983	2.94E-07	0.0062321
Spbc24	spindle pole body component 24 homolog (S. cerevisiae)	8.908	9.67E-08	0.0020514
Aurka	aurora kinase A	8.7623	3.28E-07	0.0069612
Rrm2	ribonucleotide reductase M2	8.752	5.58E-07	0.011848
Hist1h2ao	histone cluster 1, H2ao	8.6659	3.16E-07	0.0067006
Hist2h2ac	histone cluster 2, H2ac	8.6076	6.34E-07	0.013455
Kif22	kinesin family member 22	8.491	2.11E-07	0.0044744
Pif1	PIF1 5'-to-3' DNA helicase homolog (S. cerevisiae)	8.153	8.53E-08	0.0018108
Bcas1	breast carcinoma amplified sequence 1	8.0399	2.15E-07	0.0045591
Mcm6	minichromosome maintenance deficient 6 (MIS5 homolog, S. pombe) (S. cerevisiae)	7.8417	3.58E-07	0.0076051
9630019K15Rik	RIKEN cDNA 9630019K15 gene	7.7443	1.03E-09	2.18E-05
Cdca5	cell division cycle associated 5	7.7288	8.19E-07	0.017376
Camk2b	calcium/calmodulin-dependent protein kinase II, beta	7.7107	5.14E-07	0.010897
Cenpe	centromere protein E	7.5456	2.20E-07	0.0046599
Pold1	polymerase (DNA directed), delta 1, catalytic subunit	6.9333	1.63E-06	0.034565
Skp2	S-phase kinase-associated protein 2 (p45)	6.6554	1.27E-09	2.70E-05
Birc5	baculoviral IAP repeat-containing 5	6.5903	1.96E-06	0.041603
Hist1h2af	histone cluster 1, H2af	6.5129	1.76E-07	0.0037303
Tpx2	TPX2, microtubule-associated protein homolog (Xenopus laevis)	6.3922	2.33E-07	0.0049484
Cdca2	cell division cycle associated 2	6.3707	7.72E-07	0.016385
Cdca7	cell division cycle associated 7	6.2411	1.97E-06	0.041857
Hirip3	HIRA interacting protein 3	6.0516	4.19E-08	0.00088831
Hn1	hematological and neurological expressed sequence 1	5.9466	1.55E-11	3.28E-07
Sox11	SRY-box containing gene 11	5.9236	5.73E-14	1.22E-09
2810025M15Rik	RIKEN cDNA 2810025M15 gene	5.8636	2.75E-09	5.83E-05
Rfc4	replication factor C (activator 1) 4	5.8635	3.69E-07	0.0078328
Mcm7	minichromosome maintenance deficient 7 (S. cerevisiae)	5.8473	1.01E-08	0.00021509
Kif2c	kinesin family member 2C	5.8419	1.92E-07	0.0040701
2610036L11Rik	RIKEN cDNA 2610036L11 gene	5.6019	8.64E-07	0.018321
Chaf1b	chromatin assembly factor 1, subunit B (p60)	5.5047	1.83E-06	0.038928
Tacc2	transforming, acidic coiled-coil containing protein 2	5.4991	3.26E-07	0.0069229
Nola1	nucleolar protein family A, member 1 (H/ACA small nucleolar RNPs)	5.4897	9.81E-08	0.0020813

Cdca4	cell division cycle associated 4	5.4609	1.15E-10	2.44E-06
Rpl13a	ribosomal protein L13a	5.4154	3.38E-10	7.17E-06
Mcm2	minichromosome maintenance deficient 2 mitotin (S. cerevisiae)	5.2617	1.34E-06	0.028523
Hist1h2ad	histone cluster 1, H2ad	5.2353	3.38E-07	0.0071652
Ncaph	non-SMC condensin I complex, subunit H	5.1835	1.81E-06	0.038469
Cdc7	cell division cycle 7 (S. cerevisiae)	5.1355	9.10E-07	0.019306
Hip1	huntingtin interacting protein 1	5.0713	1.22E-06	0.025818
Lbr	lamin B receptor	5.0567	4.06E-09	8.62E-05
Lig1	ligase I, DNA, ATP-dependent	5.0526	1.86E-06	0.03946
Hist2h2aa2	histone cluster 2, H2aa2	5.0403	1.68E-07	0.0035697
Thoc4	THO complex 4	4.9925	2.53E-08	0.00053619
RP23-336J1.4	Ras-GTPase-activating protein SH3-domain binding protein	4.9718	1.54E-09	3.27E-05
Basp1	brain abundant, membrane attached signal protein 1	4.903	2.23E-07	0.0047294
Nup210	nucleoporin 210	4.8402	9.95E-07	0.021116
Tmpo	thymopoietin	4.8242	2.50E-07	0.0053141
Mki67	antigen identified by monoclonal antibody Ki 67	4.823	2.07E-06	0.043968
Cdk4	cyclin-dependent kinase 4	4.7566	7.35E-09	0.00015585
Troap	trophinin associated protein	4.6515	2.23E-07	0.0047299
Blm	Bloom syndrome homolog (human)	4.5642	2.56E-07	0.0054273
H2afz	H2A histone family, member Z	4.4559	4.18E-07	0.008865
Dbf4	DBF4 homolog (S. cerevisiae)	4.429	8.80E-07	0.018676
Set	SET translocation	4.422	1.12E-08	0.00023805
Coro1c	coronin, actin binding protein 1C	4.3535	3.99E-08	0.00084599
Ppp1r14b	protein phosphatase 1, regulatory (inhibitor) subunit 14B	4.334	5.90E-09	0.00012526
Psmc3ip	proteasome (prosome, macropain) 26S subunit, ATPase 3, interacting protein	4.3021	2.41E-07	0.0051088
H2afx	H2A histone family, member X	4.1987	2.13E-06	0.045295
Dtymk	deoxythymidylate kinase	4.1694	2.72E-08	0.0005764
Nasp	nuclear autoantigenic sperm protein (histone-binding)	4.1139	2.25E-07	0.0047639
Ybx1	Y box protein 1	4.1043	4.23E-07	0.0089829
LOC241621	NA	4.0858	4.46E-08	0.00094681
Fbl	fibrillarin	4.0848	5.36E-08	0.0011374
Ranbp1	RAN binding protein 1	4.0703	7.24E-07	0.015358
2410015N17Rik	RIKEN cDNA 2410015N17 gene	4.0011	3.17E-07	0.006734
Bub1b	budding uninhibited by benzimidazoles 1 homolog, beta (S. cerevisiae)	3.9988	4.37E-07	0.009282
Tbrg4	transforming growth factor beta regulated gene 4	3.9812	3.08E-08	0.00065301
Galntl1	UDP-N-acetyl-alpha-D-galactosamine:polypeptide N-acetylgalactosaminyltransferase-like 1	3.9024	3.22E-07	0.0068259
Dnmt1	DNA methyltransferase (cytosine-5) 1	3.8227	1.89E-06	0.040085
Rpl10a	ribosomal protein L10A	3.8089	1.84E-09	3.91E-05
EG237361	predicted gene, EG237361	3.7194	5.22E-09	0.00011074
Kif4	kinesin family member 4	3.668	1.35E-06	0.028741
Rpl12	ribosomal protein L12	3.6635	5.98E-11	1.27E-06
Snrpd1	small nuclear ribonucleoprotein D1	3.6631	3.98E-08	0.00084432
Igf2bp3	insulin-like growth factor 2 mRNA binding protein 3	3.6515	8.62E-08	0.0018281

Idh2	isocitrate dehydrogenase 2 (NADP+), mitochondrial	3.6344	2.83E-09	6.01E-05
Hnrpa1	heterogeneous nuclear ribonucleoprotein A1	3.6211	2.38E-09	5.04E-05
Scarb1	scavenger receptor class B, member 1	3.5929	7.64E-07	0.016202
Rad54l	RAD54 like (S. cerevisiae)	3.5917	1.25E-06	0.026495
Mad2l1	MAD2 (mitotic arrest deficient, homolog)-like 1 (yeast)	3.5803	7.98E-07	0.016934
Egfr	epidermal growth factor receptor	3.5576	1.94E-09	4.12E-05
2010317E24Rik	RIKEN cDNA 2010317E24 gene	3.5573	1.67E-07	0.0035397
Exosc8	exosome component 8	3.5554	8.16E-08	0.0017321
Neurl	neuralized-like homolog (Drosophila)	3.5321	8.40E-08	0.0017828
Rassf3	Ras association (RalGDS/AF-6) domain family 3	3.5285	4.46E-07	0.0094567
2600005C20Rik	RIKEN cDNA 2600005C20 gene	3.5227	9.26E-07	0.019657
Rps24	ribosomal protein S24	3.5129	7.60E-09	0.00016131
Nup205	nucleoporin 205	3.479	9.02E-07	0.019137
Ppan	peter pan homolog (Drosophila)	3.4697	1.44E-06	0.030488
Usp1	ubiquitin specific peptdiase 1	3.4528	2.33E-07	0.0049478
5133400G04Rik	RIKEN cDNA 5133400G04 gene	3.4185	1.25E-10	2.64E-06
Rfc5	replication factor C (activator 1) 5	3.4183	2.10E-06	0.044569
Etv1	ets variant gene 1	3.3887	1.97E-06	0.041856
Eif4a1	eukaryotic translation initiation factor 4A1	3.3763	6.72E-09	0.00014252
Sfrs7	splicing factor, arginine/serine-rich 7	3.3757	2.68E-08	0.00056952
Prmt7	protein arginine N-methyltransferase 7	3.3245	6.26E-07	0.013291
Whsc1	Wolf-Hirschhorn syndrome candidate 1 (human)	3.3108	3.62E-09	7.67E-05
2410016O06Rik	RIKEN cDNA 2410016O06 gene	3.275	6.72E-08	0.0014265
Ivns1abp	influenza virus NS1A binding protein	3.2671	1.79E-07	0.0037945
Ezh2	enhancer of zeste homolog 2 (Drosophila)	3.2601	2.76E-07	0.0058621
Rcc1	regulator of chromosome condensation 1	3.2478	6.35E-07	0.013479
Nsbp1	nucleosome binding protein 1	3.2352	3.57E-09	7.58E-05
Rpo1-4	RNA polymerase 1-4	3.2291	1.49E-06	0.031515
Hmgb1	high mobility group box 1	3.2061	8.75E-09	0.00018568
Nes	nestin	3.1777	7.15E-07	0.015174
Vash2	vasohibin 2	3.1749	2.57E-09	5.46E-05
Prr6	proline-rich polypeptide 6	3.1709	2.12E-09	4.49E-05
Nxph1	neurexophilin 1	3.1627	7.32E-07	0.015528
Lmnb2	lamin B2	3.1586	2.52E-10	5.34E-06
Prmt1	protein arginine N-methyltransferase 1	3.1541	4.02E-07	0.008535
Plekha2	pleckstrin homology domain-containing, family A member 2	3.151	6.88E-08	0.0014595
Nrarp	Notch-regulated ankyrin repeat protein	3.1426	1.51E-08	0.00032052
Dgkg	diacylglycerol kinase, gamma	3.1408	1.21E-08	0.00025719
EG382843	predicted gene, EG382843	3.1365	3.97E-09	8.43E-05
Hnrpab	heterogeneous nuclear ribonucleoprotein A/B	3.1235	4.37E-10	9.27E-06
D11Ertd497e	DNA segment, Chr 11, ERATO Doi 497, expressed	3.0886	1.78E-09	3.78E-05
1810014F10Rik	RIKEN cDNA 1810014F10 gene	3.0857	3.55E-08	0.00075388
E2f2	E2F transcription factor 2	3.083	3.87E-09	8.21E-05
Ppid	peptidylprolyl isomerase D (cyclophilin D)	3.0829	5.03E-09	0.00010673

Ptma	prothymosin alpha	3.0828	1.14E-06	0.024144
Gng2	guanine nucleotide binding protein (G protein), gamma 2 subunit	3.0682	5.87E-13	1.25E-08
Rfx4	regulatory factor X, 4 (influences HLA class II expression)	3.0519	3.51E-07	0.0074556
Rpl18	ribosomal protein L18	3.0508	1.16E-09	2.46E-05
Lsm3	LSM3 homolog, U6 small nuclear RNA associated (S. cerevisiae)	3.0224	1.14E-07	0.0024169
Akr1b3	aldo-keto reductase family 1, member B3 (aldose reductase)	3.0101	2.78E-07	0.0058882
Pfn1	profilin 1	3.0098	1.70E-06	0.036001
Psip1	PC4 and SFRS1 interacting protein 1	2.9932	1.05E-07	0.0022324
Cbx3	chromobox homolog 3 (Drosophila HP1 gamma)	2.9855	2.68E-08	0.00056858
Fkbp4	FK506 binding protein 4	2.9499	1.30E-09	2.77E-05
Phf17	PHD finger protein 17	2.9373	8.28E-10	1.76E-05
Rps20	ribosomal protein S20	2.9367	9.05E-09	0.00019199
Plk4	polo-like kinase 4 (Drosophila)	2.9366	1.54E-06	0.032747
Trib2	tribbles homolog 2 (Drosophila)	2.9328	5.53E-09	0.00011726
Nmral1	NmrA-like family domain containing 1	2.8949	1.02E-10	2.16E-06
Ruvbl2	RuvB-like protein 2	2.8874	1.14E-07	0.0024231
Trim27	tripartite motif protein 27	2.8858	3.78E-09	8.01E-05
Traf4	Tnf receptor associated factor 4	2.8704	6.83E-07	0.01449
Zfp334	zinc finger protein 334	2.8626	3.21E-08	0.00068088
Nola2	nucleolar protein family A, member 2	2.8618	1.42E-06	0.030093
Nudt21	nudix (nucleoside diphosphate linked moiety X)-type motif 21	2.8589	4.51E-09	9.58E-05
Emg1	EMG1 nucleolar protein homolog (S. cerevisiae)	2.8583	4.77E-09	0.00010115
Asns	asparagine synthetase	2.857	9.57E-07	0.020302
Rbmx	RNA binding motif protein, X chromosome	2.8531	7.71E-09	0.00016362
Sfrs1	splicing factor, arginine/serine-rich 1 (ASF/SF2)	2.8295	9.07E-10	1.92E-05
Aarsd1	alanyl-tRNA synthetase domain containing 1	2.8255	1.64E-06	0.034753
LOC277692	NA	2.8072	3.97E-08	0.00084283
Ptbp1	polypyrimidine tract binding protein 1	2.8014	3.28E-07	0.0069506
Stmn1	stathmin 1	2.8012	2.81E-08	0.00059529
5930416I19Rik	RIKEN cDNA 5930416I19 gene	2.7962	1.79E-06	0.037959
Adsl	adenylosuccinate lyase 1	2.796	5.70E-08	0.0012092
1700113I22Rik	RIKEN cDNA 1700113I22 gene	2.7923	2.83E-08	0.00059949
Ddx18	DEAD (Asp-Glu-Ala-Asp) box polypeptide 18	2.7869	2.34E-07	0.0049574
Nup62	nucleoporin 62	2.7868	2.41E-07	0.0051211
Depdc1b	DEP domain containing 1B	2.7819	1.83E-06	0.038772
Rpl23a	ribosomal protein L23a	2.7809	2.49E-08	0.0005289
Sf3a3	splicing factor 3a, subunit 3	2.7799	6.23E-09	0.00013217
Rpl7a	ribosomal protein L7a	2.7634	4.67E-07	0.0098982
Vrk1	vaccinia related kinase 1	2.7489	9.05E-09	0.00019192
Banf1	barrier to autointegration factor 1	2.7188	2.11E-06	0.044774
Sfrs2	splicing factor, arginine/serine-rich 2 (SC-35)	2.7163	9.43E-07	0.020016
Rps23	ribosomal protein S23	2.6991	5.28E-09	0.00011193
Shmt1	serine hydroxymethyltransferase 1 (soluble)	2.6982	1.53E-06	0.032433
Rpl10	ribosomal protein 10	2.6981	4.45E-08	0.0009441

Impdh2	inosine 5'-phosphate dehydrogenase 2	2.6964	8.98E-07	0.019053
Rps3	ribosomal protein S3	2.6941	5.30E-09	0.00011247
Ddx20	DEAD (Asp-Glu-Ala-Asp) box polypeptide 20	2.6875	2.85E-07	0.0060529
Lsm7	LSM7 homolog, U6 small nuclear RNA associated (S. cerevisiae)	2.6804	2.99E-07	0.006353
Siva1	SIVA1, apoptosis-inducing factor	2.6792	2.62E-07	0.0055485
Rfc2	replication factor C (activator 1) 2	2.6777	2.70E-07	0.0057282
Nol11	nucleolar protein 11	2.6769	1.03E-08	0.00021898
Zeb1	zinc finger E-box binding homeobox 1	2.6744	5.65E-10	1.20E-05
Cnot6	CCR4-NOT transcription complex, subunit 6	2.6624	2.01E-07	0.0042581
Mns1	meiosis-specific nuclear structural protein 1	2.6614	1.29E-07	0.0027395
Ebna1bp2	EBNA1 binding protein 2	2.6575	3.28E-08	0.00069696
Gpatc4	G patch domain containing 4	2.6565	2.00E-06	0.042447
Ptpre	protein tyrosine phosphatase, receptor type, E	2.6478	9.80E-07	0.020796
Rps26	ribosomal protein S26	2.6445	1.62E-09	3.44E-05
Parp1	poly (ADP-ribose) polymerase family, member 1	2.6439	7.19E-09	0.00015247
Kars	lysyl-tRNA synthetase	2.6403	1.08E-08	0.00022989
Hdac2	histone deacetylase 2	2.6388	1.30E-09	2.76E-05
Gprin1	G protein-regulated inducer of neurite outgrowth 1	2.6385	3.33E-09	7.06E-05
Tcf12	transcription factor 12	2.6364	5.52E-08	0.0011714
Rad51c	Rad51 homolog c (S. cerevisiae)	2.6348	4.23E-08	0.00089769
Aspm	asp (abnormal spindle)-like, microcephaly associated (Drosophila)	2.6292	3.51E-07	0.0074434
Dazap1	DAZ associated protein 1	2.6219	3.34E-08	0.00070962
Snrpg	small nuclear ribonucleoprotein polypeptide G	2.6	1.26E-09	2.67E-05
Gars	glycyl-tRNA synthetase	2.5971	4.45E-07	0.009447
Ard1	N-acetyltransferase ARD1 homolog (S. cerevisiae)	2.5933	8.60E-07	0.018237
Rsl1d1	ribosomal L1 domain containing 1	2.5907	6.47E-07	0.013722
Rpl6	ribosomal protein L6	2.5905	2.65E-07	0.0056304
Lsm8	LSM8 homolog, U6 small nuclear RNA associated (S. cerevisiae)	2.584	2.66E-09	5.65E-05
Rpl36	ribosomal protein L36	2.5834	2.10E-09	4.45E-05
Rad51ap1	RAD51 associated protein 1	2.5744	2.84E-07	0.0060283
Prps1	phosphoribosyl pyrophosphate synthetase 1	2.5723	6.75E-07	0.014318
Arbp	acidic ribosomal phosphoprotein P0	2.5626	3.96E-08	0.0008392
Smn1	survival motor neuron 1	2.545	8.10E-07	0.017192
Bxdc1	brix domain containing 1	2.5424	7.94E-08	0.0016842
Eif3s4	eukaryotic translation initiation factor 3, subunit 4 (delta)	2.5271	7.54E-08	0.001599
Cep78	centrosomal protein 78	2.5246	1.46E-09	3.09E-05
Rpl28	ribosomal protein L28	2.5159	8.44E-09	0.00017905
Top2a	topoisomerase (DNA) II alpha	2.5079	3.46E-08	0.00073476
Lyar	Ly1 antibody reactive clone	2.5072	2.34E-06	0.049598
Rplp2	ribosomal protein, large P2	2.504	2.87E-07	0.0060819
Adam19	a disintegrin and metallopeptidase domain 19 (meltrin beta)	2.4944	5.35E-07	0.011355
Sfrs9	splicing factor, arginine/serine rich 9	2.4897	4.64E-08	0.00098363
Ran	RAN, member RAS oncogene family	2.4852	3.52E-08	0.00074788
6820424L24Rik	RIKEN cDNA 6820424L24 gene	2.4783	8.08E-08	0.0017149

Pabpc4	poly A binding protein, cytoplasmic 4	2.4716	2.04E-07	0.0043335
Ilf2	interleukin enhancer binding factor 2	2.4701	2.83E-07	0.0060054
Igf2bp2	insulin-like growth factor 2 mRNA binding protein 2	2.4681	5.55E-07	0.011784
Rcl1	RNA terminal phosphate cyclase-like 1	2.4628	9.79E-09	0.00020776
Rps10	ribosomal protein S10	2.4593	5.12E-10	1.09E-05
Nedd1	neural precursor cell expressed, developmentally down-regulated gene 1	2.4542	1.09E-07	0.0023025
Ccdc9	coiled-coil domain containing 9	2.4523	2.45E-07	0.0051875
2810417H13Rik	RIKEN cDNA 2810417H13 gene	2.4405	1.21E-06	0.025623
Smad5	MAD homolog 5 (Drosophila)	2.439	1.59E-07	0.0033729
Ddx21	DEAD (Asp-Glu-Ala-Asp) box polypeptide 21	2.4383	5.78E-07	0.012262
Skiv2l2	superkiller viralicidic activity 2-like 2 (S. cerevisiae)	2.4373	6.60E-09	0.00014
Rpl8	ribosomal protein L8	2.4372	3.01E-08	0.00063948
Tyms	thymidylate synthase	2.4348	2.11E-06	0.044865
Rps3a	ribosomal protein S3a	2.4269	5.69E-08	0.0012082
U2af1	U2 small nuclear ribonucleoprotein auxiliary factor (U2AF) 1	2.4226	1.64E-06	0.03474
Rpl35	ribosomal protein L35	2.4154	1.10E-07	0.0023281
Trim28	tripartite motif protein 28	2.4082	3.68E-08	0.00078062
Mum1	melanoma associated antigen (mutated) 1	2.4063	1.94E-06	0.041114
Rps6	ribosomal protein S6	2.4054	1.34E-09	2.84E-05
2610318N02Rik	RIKEN cDNA 2610318N02 gene	2.4051	4.07E-10	8.63E-06
Nutf2	nuclear transport factor 2	2.404	1.56E-07	0.0033126
Rps9	ribosomal protein S9	2.3959	1.97E-08	0.0004184
Mrpl21	mitochondrial ribosomal protein L21	2.3866	1.80E-06	0.038196
Dcbld1	discoidin, CUB and LCCL domain containing 1	2.3831	6.86E-07	0.014558
Snrpd3	small nuclear ribonucleoprotein D3	2.3779	1.62E-06	0.034385
C79407	expressed sequence C79407	2.3627	1.04E-06	0.021979
Rrp15	ribosomal RNA processing 15 homolog (S. cerevisiae)	2.3552	8.05E-07	0.017084
Hnrpdl	heterogeneous nuclear ribonucleoprotein D-like	2.3519	2.35E-06	0.049899
Ick	intestinal cell kinase	2.3518	1.74E-07	0.0036973
BC046331	cDNA sequence BC046331	2.349	1.94E-08	0.00041096
Faah	fatty acid amide hydrolase	2.3489	3.67E-08	0.00077823
Rpl36a	ribosomal protein L36a	2.3481	2.69E-12	5.71E-08
Chchd1	coiled-coil-helix-coiled-coil-helix domain containing 1	2.339	2.95E-07	0.0062649
Eif4a3	eukaryotic translation initiation factor 4A, isoform 3	2.335	1.55E-07	0.0032912
Sssca1	Sjogren's syndrome/scleroderma autoantigen 1 homolog (human)	2.3342	6.80E-09	0.00014421
Ckap2l	cytoskeleton associated protein 2-like	2.3342	1.56E-06	0.03308
Ppih	peptidyl prolyl isomerase H	2.3314	9.61E-07	0.020385
Cct6a	chaperonin subunit 6a (zeta)	2.329	6.13E-07	0.013005
Apex1	apurinic/apyrimidinic endonuclease 1	2.3283	1.29E-07	0.0027429
Sf3a1	splicing factor 3a, subunit 1	2.3281	3.97E-08	0.00084167
Cdc25c	cell division cycle 25 homolog C (S. pombe)	2.3281	8.75E-08	0.0018565
5730427N09Rik	RIKEN cDNA 5730427N09 gene	2.3207	1.29E-10	2.74E-06
Gtpbp4	GTP binding protein 4	2.3185	5.50E-07	0.01167
Pdlim1	PDZ and LIM domain 1 (elfin)	2.3181	2.33E-06	0.049344

Naca	nascent polypeptide-associated complex alpha polypeptide	2.3169	3.64E-09	7.73E-05
Phf5a	PHD finger protein 5A	2.3145	6.54E-08	0.0013872
Exosc1	exosome component 1	2.3095	2.06E-06	0.043709
Foxm1	forkhead box M1	2.3056	5.88E-07	0.012473
Ubl4	ubiquitin-like 4	2.3033	4.16E-08	0.00088185
2610524G07Rik	RIKEN cDNA 2610524G07 gene	2.3009	1.78E-07	0.0037766
Csrp2	cysteine and glycine-rich protein 2	2.2993	6.08E-07	0.01291
Fau	Finkel-Biskis-Reilly murine sarcoma virus (FBR-MuSV) ubiquitously expressed	2.2978	1.05E-06	0.022212
Csnk1d	casein kinase 1, delta	2.2963	1.10E-09	2.34E-05
Casp2	caspase 2	2.2936	7.21E-08	0.0015294
Hmgn2	high mobility group nucleosomal binding domain 2	2.2916	9.34E-08	0.0019807
Rps28	ribosomal protein S28	2.2897	4.54E-09	9.64E-05
Mrpl47	mitochondrial ribosomal protein L47	2.2853	1.09E-08	0.00023146
Rps5	ribosomal protein S5	2.2841	3.30E-10	7.01E-06
Rpl5	ribosomal protein L5	2.2766	2.88E-07	0.0061115
Lsm4	LSM4 homolog, U6 small nuclear RNA associated (S. cerevisiae)	2.2731	1.93E-06	0.040859
Ipo9	importin 9	2.2682	4.20E-09	8.92E-05
Myef2	myelin basic protein expression factor 2, repressor	2.2681	2.78E-07	0.0058992
6720463M24Rik	RIKEN cDNA 6720463M24 gene	2.2661	1.56E-06	0.033081
Rpl13	ribosomal protein L13	2.2538	4.86E-09	0.00010304
Phb2	prohibitin 2	2.2531	1.96E-07	0.0041594
Sfpq	splicing factor proline/glutamine rich (polypyrimidine tract binding protein associated)	2.2518	1.48E-06	0.031503
Rpl32	ribosomal protein L32	2.2509	2.94E-07	0.0062377
Csda	cold shock domain protein A	2.2503	1.96E-06	0.041566
Nid2	nidogen 2	2.2491	1.90E-07	0.0040335
Rps2	ribosomal protein S2	2.247	9.02E-07	0.019138
Rps8	ribosomal protein S8	2.2442	4.95E-09	0.00010509
Rpl35a	ribosomal protein L35a	2.2378	1.02E-07	0.0021654
Nme4	expressed in non-metastatic cells 4, protein	2.2376	4.27E-09	9.06E-05
Polr1e	polymerase (RNA) I polypeptide E	2.2306	3.34E-07	0.0070788
Ccdc95	coiled-coil domain containing 95	2.2233	9.41E-08	0.0019966
Cdc6	cell division cycle 6 homolog (S. cerevisiae)	2.2227	6.83E-07	0.014495
Nlgn3	neuroligin 3	2.2199	1.85E-10	3.93E-06
Chic2	cysteine-rich hydrophobic domain 2	2.2162	1.95E-06	0.041307
Fancl	Fanconi anemia, complementation group L	2.2122	3.79E-08	0.0008045
Pwp2	PWP2 periodic tryptophan protein homolog (yeast)	2.2097	6.42E-07	0.013628
Gbp3	guanylate nucleotide binding protein 3	2.209	5.84E-09	0.00012388
Arhgef3	Rho guanine nucleotide exchange factor (GEF) 3	2.2066	1.82E-09	3.86E-05
Dhx15	DEAH (Asp-Glu-Ala-His) box polypeptide 15	2.1978	5.62E-09	0.00011917
Znrd1	zinc ribbon domain containing, 1	2.1978	2.44E-07	0.0051714
Rpl7	ribosomal protein L7	2.1944	3.34E-08	0.00070812
Gsg2	germ cell-specific gene 2	2.1917	2.66E-08	0.00056382
Saal1	serum amyloid A-like 1	2.1915	6.06E-08	0.0012853

Rpo1-1		RNA polymerase 1-1	2.1874	6.27E-07	0.013302
Mki67ip		Mki67 (FHA domain) interacting nucleolar phosphoprotein	2.1847	4.70E-08	0.00099758
Cenpm		centromere protein M	2.1845	9.35E-07	0.019833
Rbm28		RNA binding motif protein 28	2.18	2.82E-07	0.0059874
Arpp21		cyclic AMP-regulated phosphoprotein, 21	2.1731	3.75E-07	0.007959
Anapc1		anaphase promoting complex subunit 1	2.1698	2.29E-06	0.048509
Phf6		PHD finger protein 6	2.1684	2.26E-08	0.0004796
Pdcd2		programmed cell death 2	2.1571	2.35E-08	0.00049756
Rpl26		ribosomal protein L26	2.1561	6.85E-08	0.0014529
Snrpa		small nuclear ribonucleoprotein polypeptide A	2.1547	7.16E-09	0.00015197
Rps13		ribosomal protein S13	2.1533	1.12E-07	0.0023744
Raver1		ribonucleoprotein, PTB-binding 1	2.1511	2.80E-08	0.00059497
5730528L13Rik		RIKEN cDNA 5730528L13 gene	2.1501	8.03E-07	0.01703
Rpl15		ribosomal protein L15	2.1491	1.65E-08	0.00035052
Uhrf2		ubiquitin-like, containing PHD and RING finger domains 2	2.148	7.11E-08	0.0015082
Cct4		chaperonin subunit 4 (delta)	2.1407	6.74E-07	0.01431
Zc3hc1		zinc finger, C3HC type 1	2.1381	2.06E-07	0.0043662
Gm1907		NA	2.1302	1.86E-07	0.0039436
Rps12		ribosomal protein S12	2.1283	1.23E-06	0.026185
Rpl3		ribosomal protein L3	2.1245	1.33E-08	0.00028316
Tomm70a		translocase of outer mitochondrial membrane 70 homolog A (yeast)	2.1222	5.89E-07	0.012494
	6-Sep	septin 6	2.1218	2.07E-08	0.00043883
Ilf3		interleukin enhancer binding factor 3	2.1144	4.55E-07	0.0096608
Rpl31		ribosomal protein L31	2.1128	9.54E-08	0.002025
Pabpc1		poly A binding protein, cytoplasmic 1	2.1083	1.52E-08	0.0003232
Pola2		polymerase (DNA directed), alpha 2	2.1036	4.74E-07	0.010061
Timm50		translocase of inner mitochondrial membrane 50 homolog (yeast)	2.0963	1.70E-06	0.036157
Uck2		uridine-cytidine kinase 2	2.0935	2.18E-07	0.0046188
Rplp1		ribosomal protein, large, P1	2.091	3.48E-08	0.00073871
Cstf1		cleavage stimulation factor, 3' pre-RNA, subunit 1	2.0907	1.06E-07	0.0022471
Srpk1		serine/arginine-rich protein specific kinase 1	2.0871	1.59E-08	0.00033836
Mrpl53		mitochondrial ribosomal protein L53	2.0854	6.05E-07	0.01283
Glt25d1		glycosyltransferase 25 domain containing 1	2.0851	2.68E-09	5.68E-05
Ssb		Sjogren syndrome antigen B	2.0833	1.69E-08	0.00035904
2010012C16Rik		RIKEN cDNA 2010012C16 gene	2.0801	5.89E-07	0.012506
Dck		deoxycytidine kinase	2.0766	3.26E-08	0.00069151
D4Ertd22e		DNA segment, Chr 4, ERATO Doi 22, expressed	2.0712	1.04E-06	0.022169
Rars		arginyl-tRNA synthetase	2.0683	6.85E-08	0.0014524
Exosc2		exosome component 2	2.068	1.81E-06	0.038468
Zfp106		zinc finger protein 106	2.0656	3.52E-08	0.00074783
Noc2l		nucleolar complex associated 2 homolog (S. cerevisiae)	2.0628	2.51E-08	0.00053246
Nat11		N-acetyltransferase 11	2.0603	1.48E-07	0.0031446
Gins4		GINS complex subunit 4 (Sld5 homolog)	2.0525	5.29E-07	0.011234
Trp53		transformation related protein 53	2.0486	5.63E-09	0.00011936

Rnps1	ribonucleic acid binding protein S1	2.0438	1.18E-07	0.00251
Wdr74	WD repeat domain 74	2.0372	9.93E-09	0.00021071
Cops2	COP9 (constitutive photomorphogenic) homolog, subunit 2 (Arabidopsis thaliana)	2.0359	3.08E-08	0.00065333
Hyal2	hyaluronoglucosaminidase 2	2.0356	1.66E-06	0.035174
Sf3b2	splicing factor 3b, subunit 2	2.0324	4.56E-09	9.67E-05
Dcps	decapping enzyme, scavenger	2.0304	6.16E-07	0.013062
Fmnl3	formin-like 3	2.0277	6.71E-07	0.014241
Klhl3	NA	2.0276	3.71E-07	0.0078794
Cog8	component of oligomeric golgi complex 8	2.0255	4.45E-07	0.0094352
Scye1	small inducible cytokine subfamily E, member 1	2.0123	4.89E-08	0.0010376
Acot7	acyl-CoA thioesterase 7	2.0118	1.65E-07	0.0035009
Gtf2h4	general transcription factor II H, polypeptide 4	2.0104	1.49E-06	0.0316
Pmf1	polyamine-modulated factor 1	2.0103	9.99E-08	0.0021188
Nudt5	nudix (nucleoside diphosphate linked moiety X)-type motif 5	2.0082	8.42E-07	0.01786
Tgfbr1	transforming growth factor, beta receptor I	2.0071	2.27E-06	0.048127
Mrps5	mitochondrial ribosomal protein S5	2.0052	4.58E-08	0.00097094
Sgol1	shugoshin-like 1 (S. pombe)	2.0034	2.13E-06	0.045135

Table 2-4. A list of differentially expressed genes identified by the comparison of BMP- and LIF-induced astrocytes. Genes are ordered based on largest to smallest fold difference. Genes that show less than two-fold change are excluded. A total of 383 genes are differentially expressed. 257 genes are expressed more highly in BMP-induced astrocytes compared to LIF-induced astrocytes. Conversely, 124 genes are expressed more highly in LIF-induced astrocytes compared to BMP-induced astrocytes.

High in BMP				
Symbol	**Description**	**Fold Change**	**p.value**	**FDR**
Serpinf1	serine (or cysteine) peptidase inhibitor, clade F, member 1	158.42	2.29E-17	4.86E-13
Cidea	cell death-inducing DNA fragmentation factor, alpha subunit-like effector A	41.865	3.73E-16	7.92E-12
Tmem158	transmembrane protein 158	33.301	2.08E-09	4.40E-05
Rgs9	regulator of G-protein signaling 9	20.909	3.92E-12	8.32E-08
Ndg2	Nur77 downstream gene 2	19.963	6.19E-11	1.31E-06
Fbxo2	F-box protein 2	18.808	2.56E-12	5.42E-08
Kcnk13	potassium channel, subfamily K, member 13	17.971	5.38E-13	1.14E-08
Ctgf	connective tissue growth factor	16.707	4.85E-08	0.0010298
Hopx	homeobox only domain	15.21	3.90E-08	0.00082717
Man1c1	mannosidase, alpha, class 1C, member 1	14.74	3.88E-10	8.23E-06
Ncan	neurocan	14.547	1.09E-13	2.31E-09
Slc7a5	solute carrier family 7 (cationic amino acid transporter, y+ system), member 5	13.57	2.77E-11	5.88E-07
Fxyd6	FXYD domain-containing ion transport regulator 6	13.068	2.39E-09	5.07E-05
Hspb8	heat shock protein 8	12.376	4.12E-09	8.74E-05
Hspb1	heat shock protein 1	12.133	2.66E-07	0.0056357
Kcne1l	potassium voltage-gated channel, Isk-related family, member 1-like	12.055	5.08E-10	1.08E-05
Fgf1	fibroblast growth factor 1	11.819	6.04E-08	0.0012818
Timp4	tissue inhibitor of metalloproteinase 4	10.944	1.46E-08	0.00030901
ENSMUSG00000056615	predicted gene, ENSMUSG00000056615	10.644	9.83E-13	2.08E-08
Sphk1	sphingosine kinase 1	10.536	1.68E-07	0.0035703
Cryab	crystallin, alpha B	10.176	7.73E-07	0.016393
Id2	inhibitor of DNA binding 2	10.121	6.17E-10	1.31E-05
Scg5	secretogranin V	9.7941	6.52E-08	0.0013836
Slc6a8	solute carrier family 6 (neurotransmitter transporter, creatine), member 8	9.2509	2.27E-09	4.81E-05
Aqp4	aquaporin 4	9.2406	7.07E-10	1.50E-05
Padi2	peptidyl arginine deiminase, type II	8.8989	6.32E-08	0.0013402
AI593442	expressed sequence AI593442	8.6109	5.73E-10	1.22E-05
Id1	inhibitor of DNA binding 1	8.4898	2.92E-11	6.19E-07
Kcnc4	potassium voltage gated channel, Shaw-related subfamily, member 4	8.4146	2.01E-10	4.27E-06
Hrsp12	heat-responsive protein 12	7.7676	1.70E-08	0.00036153
Gbx2	gastrulation brain homeobox 2	7.6672	9.85E-10	2.09E-05
Kif26b	kinesin family member 26B	7.6311	4.11E-10	8.73E-06
Rcsd1	RCSD domain containing 1	7.3013	5.32E-13	1.13E-08

Tmem166	transmembrane protein 166	7.1583	1.71E-08	0.00036366
Cd59a	CD59a antigen	6.698	8.65E-08	0.0018344
Adra2a	adrenergic receptor, alpha 2a	6.685	2.30E-10	4.88E-06
Pdgfrl	platelet-derived growth factor receptor-like	6.4011	1.72E-09	3.64E-05
Ankrd15	ankyrin repeat domain 15	6.3705	6.59E-10	1.40E-05
Mt3	metallothionein 3	6.2941	7.20E-07	0.015276
Tmem100	transmembrane protein 100	6.0493	8.94E-10	1.90E-05
Vasn	vasorin	6.0132	5.19E-08	0.0011008
Chgb	chromogranin B	5.9103	4.50E-15	9.54E-11
Eef1a2	eukaryotic translation elongation factor 1 alpha 2	5.8914	6.82E-08	0.0014478
Pfkm	phosphofructokinase, muscle	5.8351	3.55E-10	7.53E-06
Nog	noggin	5.7756	2.27E-10	4.81E-06
Reln	reelin	5.6982	6.03E-08	0.0012795
Stk32a	serine/threonine kinase 32A	5.6849	2.74E-09	5.81E-05
Pib5pa	phosphatidylinositol (4,5) bisphosphate 5-phosphatase, A	5.5707	2.73E-10	5.79E-06
AW125753	expressed sequence AW125753	5.4561	1.30E-08	0.00027585
C1qtnf5	C1q and tumor necrosis factor related protein 5	5.3357	2.15E-09	4.57E-05
Aox1	aldehyde oxidase 1	5.3334	1.63E-06	0.034681
Smad6	MAD homolog 6 (Drosophila)	5.2831	9.79E-15	2.08E-10
C130076O07Rik	RIKEN cDNA C130076O07 gene	5.2141	3.06E-08	0.00064877
Hmox1	heme oxygenase (decycling) 1	5.1335	9.20E-09	0.0001951
Slc2a1	solute carrier family 2 (facilitated glucose transporter), member 1	5.0795	1.57E-06	0.033271
Ldb2	LIM domain binding 2	5.0598	1.72E-08	0.00036491
Chst8	carbohydrate (N-acetylgalactosamine 4-0) sulfotransferase 8	5.0116	8.15E-11	1.73E-06
Caln1	calneuron 1	4.9311	5.22E-07	0.011067
Sparcl1	SPARC-like 1 (mast9, hevin)	4.8315	3.38E-08	0.00071754
Slc8a1	solute carrier family 8 (sodium/calcium exchanger), member 1	4.7879	2.25E-09	4.78E-05
Ramp2	receptor (calcitonin) activity modifying protein 2	4.7119	5.04E-08	0.0010687
Slc6a6	solute carrier family 6 (neurotransmitter transporter, taurine), member 6	4.704	4.45E-07	0.0094406
Itpk1	inositol 1,3,4-triphosphate 5/6 kinase	4.6783	6.52E-08	0.0013833
Gstm6	glutathione S-transferase, mu 6	4.61	2.16E-09	4.59E-05
2900062L11Rik	RIKEN cDNA 2900062L11 gene	4.5999	2.49E-10	5.28E-06
Scrg1	scrapie responsive gene 1	4.5913	8.21E-07	0.017427
Htra1	HtrA serine peptidase 1	4.5744	8.35E-11	1.77E-06
Adcy8	adenylate cyclase 8	4.5677	2.08E-08	0.00044035
Pea15	phosphoprotein enriched in astrocytes 15	4.5511	9.41E-07	0.019958
Lgals8	lectin, galactose binding, soluble 8	4.4273	1.82E-09	3.86E-05
Ddit4l	DNA-damage-inducible transcript 4-like	4.3615	3.22E-07	0.0068303
1190002H23Rik	RIKEN cDNA 1190002H23 gene	4.3545	4.34E-07	0.0092146
Slc20a1	solute carrier family 20, member 1	4.354	1.01E-06	0.021337
Snta1	syntrophin, acidic 1	4.3031	9.86E-07	0.020923
Cdh22	cadherin 22	4.2941	7.07E-07	0.015005

Agl	amylo-1,6-glucosidase, 4-alpha-glucanotransferase	4.2932	2.70E-11	5.73E-07
Slc1a2	solute carrier family 1 (glial high affinity glutamate transporter), member 2	4.2133	1.68E-10	3.56E-06
Wwc2	WW, C2 and coiled-coil domain containing 2	4.2072	1.02E-09	2.16E-05
Id3	inhibitor of DNA binding 3	4.2034	5.57E-09	0.00011807
AI646023	expressed sequence AI646023	4.194	3.59E-08	0.00076206
Ablim2	actin-binding LIM protein 2	4.1858	6.35E-09	0.00013478
Ephx1	epoxide hydrolase 1, microsomal	4.1335	3.49E-08	0.00073944
Emb	embigin	4.1044	1.08E-12	2.28E-08
Rarres1	retinoic acid receptor responder (tazarotene induced) 1	4.0845	1.83E-08	0.00038798
Gas6	growth arrest specific 6	4.0812	9.60E-08	0.0020361
Fcgrt	Fc receptor, IgG, alpha chain transporter	4.0128	3.53E-07	0.0074891
Tapt1	transmembrane anterior posterior transformation 1	3.987	1.38E-11	2.93E-07
Nedd9	neural precursor cell expressed, developmentally down-regulated gene 9	3.9525	1.39E-08	0.00029545
Cyp2j9	cytochrome P450, family 2, subfamily j, polypeptide 9	3.9153	2.42E-08	0.00051248
Ank	progressive ankylosis	3.8089	4.24E-08	0.00090032
Il11ra2	interleukin 11 receptor, alpha chain 2	3.8043	1.73E-06	0.036793
Evi5	ecotropic viral integration site 5	3.7969	4.43E-09	9.39E-05
Pde4b	phosphodiesterase 4B, cAMP specific	3.7905	9.68E-08	0.0020542
Cd9	CD9 antigen	3.7284	1.22E-09	2.60E-05
Cadps	Ca<2+>dependent activator protein for secretion	3.7262	1.75E-06	0.03708
Selm	selenoprotein M	3.7139	9.63E-07	0.020442
Tceal3	transcription elongation factor A (SII)-like 3	3.6835	5.06E-10	1.07E-05
Gstm1	glutathione S-transferase, mu 1	3.637	6.60E-07	0.014008
App	amyloid beta (A4) precursor protein	3.6304	6.79E-09	0.00014412
Atp1a1	ATPase, Na+/K+ transporting, alpha 1 polypeptide	3.6219	4.15E-09	8.80E-05
Aatk	apoptosis-associated tyrosine kinase	3.6049	7.79E-07	0.016536
Rasl11b	RAS-like, family 11, member B	3.5606	5.64E-08	0.0011963
Ramp1	receptor (calcitonin) activity modifying protein 1	3.557	2.00E-06	0.042523
Bag3	Bcl2-associated athanogene 3	3.5286	7.18E-07	0.015225
Tmem108	transmembrane protein 108	3.5071	2.21E-07	0.0046955
Lhfpl2	lipoma HMGIC fusion partner-like 2	3.4781	8.78E-09	0.00018621
Fstl1	follistatin-like 1	3.4726	1.63E-06	0.03452
Ctnnbip1	catenin beta interacting protein 1	3.4556	3.55E-08	0.00075229
Plekhb2	pleckstrin homology domain containing, family B (evectins) member 2	3.3983	1.32E-08	0.00028043
Gprc5b	G protein-coupled receptor, family C, group 5, member B	3.3789	6.28E-09	0.00013315
P2ry1	purinergic receptor P2Y, G-protein coupled 1	3.3634	2.46E-08	0.00052284
Arntl	aryl hydrocarbon receptor nuclear translocator-like	3.3583	5.71E-07	0.012122
Ctnnal1	catenin (cadherin associated protein), alpha-like 1	3.3565	1.22E-07	0.0025856
Pcsk1n	proprotein convertase subtilisin/kexin type 1 inhibitor	3.3436	5.55E-08	0.0011784
Sdsl	serine dehydratase-like	3.3266	5.09E-10	1.08E-05
Ppp1r3c	protein phosphatase 1, regulatory (inhibitor) subunit 3C	3.3122	7.28E-07	0.015437
Tceal5	transcription elongation factor A (SII)-like 5	3.3106	3.94E-07	0.0083509

Pstpip1	proline-serine-threonine phosphatase-interacting protein 1	3.3083	2.52E-08	0.00053399
Cited2	Cbp/p300-interacting transactivator, with Glu/Asp-rich carboxy-terminal domain, 2	3.3081	4.50E-07	0.0095538
Aqp11	aquaporin 11	3.3057	3.51E-12	7.45E-08
Ppargc1a	peroxisome proliferative activated receptor, gamma, coactivator 1 alpha	3.2765	2.52E-07	0.0053386
Osbpl1a	oxysterol binding protein-like 1A	3.2688	9.59E-07	0.02035
Spon2	spondin 2, extracellular matrix protein	3.2264	6.54E-07	0.013884
AI427515	expressed sequence AI427515	3.1633	9.02E-07	0.019147
AW049604	expressed sequence AW049604	3.1288	2.65E-08	0.0005626
Pim3	proviral integration site 3	3.1196	9.45E-09	0.00020042
Adora2b	adenosine A2b receptor	3.094	5.56E-07	0.01179
Mtch1	mitochondrial carrier homolog 1 (C. elegans)	3.0892	9.70E-07	0.020581
Zbtb7c	zinc finger and BTB domain containing 7C	3.0868	4.23E-08	0.00089794
Ncam1	neural cell adhesion molecule 1	3.0789	1.11E-08	0.0002361
Slc36a2	solute carrier family 36 (proton/amino acid symporter), member 2	3.0761	1.80E-10	3.82E-06
Ctsh	cathepsin H	3.0713	2.47E-08	0.00052373
Il17rb	interleukin 17 receptor B	3.0657	5.36E-07	0.011363
BC046404	cDNA sequence BC046404	3.0649	9.13E-08	0.0019361
Serpine2	serine (or cysteine) peptidase inhibitor, clade E, member 2	3.052	3.07E-09	6.50E-05
Rab7l1	RAB7, member RAS oncogene family-like 1	3.0346	2.40E-08	0.00050856
Aktip	thymoma viral proto-oncogene 1 interacting protein	3.0278	9.80E-11	2.08E-06
Dner	delta/notch-like EGF-related receptor	3.0166	2.59E-08	0.0005491
Susd4	sushi domain containing 4	2.9848	1.14E-07	0.0024102
Lyzs	lysozyme	2.9607	1.79E-09	3.80E-05
Pcdh7	protocadherin 7	2.9597	1.26E-07	0.0026731
Glud1	glutamate dehydrogenase 1	2.9554	2.39E-07	0.0050621
Rora	RAR-related orphan receptor alpha	2.9338	4.36E-08	0.00092609
Capzb	capping protein (actin filament) muscle Z-line, beta	2.9336	7.55E-08	0.0016018
Pls3	plastin 3 (T-isoform)	2.9199	7.36E-07	0.015615
Fzd5	frizzled homolog 5 (Drosophila)	2.9054	3.55E-08	0.0007535
BC065085	cDNA sequence BC065085	2.8979	2.98E-08	0.00063303
2410166I05Rik	RIKEN cDNA 2410166I05 gene	2.8978	5.71E-11	1.21E-06
Ubl3	ubiquitin-like 3	2.883	3.63E-08	0.00077015
Cpxm1	carboxypeptidase X 1 (M14 family)	2.877	1.50E-08	0.00031859
D12Ertd647e	DNA segment, Chr 12, ERATO Doi 647, expressed	2.8764	3.38E-08	0.00071645
Pfkl	phosphofructokinase, liver, B-type	2.8705	5.86E-08	0.0012437
Omd	osteomodulin	2.8664	7.71E-12	1.64E-07
Elovl1	elongation of very long chain fatty acids (FEN1/Elo2, SUR4/Elo3, yeast)-like 1	2.8648	4.31E-08	0.00091525
Setd7	SET domain containing (lysine methyltransferase) 7	2.8585	8.77E-07	0.0186
S100a13	S100 calcium binding protein A13	2.8333	1.22E-09	2.58E-05
1810014F10Rik	RIKEN cDNA 1810014F10 gene	2.827	1.60E-09	3.40E-05
Tspan3	tetraspanin 3	2.7837	6.39E-07	0.013547
Pitpnc1	phosphatidylinositol transfer protein, cytoplasmic 1	2.7837	7.51E-07	0.015926

Bbox1	butyrobetaine (gamma), 2-oxoglutarate dioxygenase 1 (gamma-butyrobetaine hydroxylase)	2.7832	1.83E-08	0.00038823
9130213B05Rik	RIKEN cDNA 9130213B05 gene	2.7829	1.48E-06	0.031454
Slc38a3	solute carrier family 38, member 3	2.756	7.92E-10	1.68E-05
Ghitm	growth hormone inducible transmembrane protein	2.7549	1.22E-06	0.025903
Dlgap1	discs, large (Drosophila) homolog-associated protein 1	2.69	6.61E-07	0.014032
Ugp2	UDP-glucose pyrophosphorylase 2	2.681	3.89E-08	0.0008253
Hmgcs2	3-hydroxy-3-methylglutaryl-Coenzyme A synthase 2	2.6702	1.43E-08	0.00030295
Fnbp1l	formin binding protein 1-like	2.6602	3.06E-10	6.50E-06
Prpsap1	phosphoribosyl pyrophosphate synthetase-associated protein 1	2.6395	1.89E-07	0.0040182
Txndc5	thioredoxin domain containing 5	2.6236	4.93E-07	0.010463
Tmem86a	transmembrane protein 86A	2.618	1.17E-07	0.002476
Rnf182	ring finger protein 182	2.611	2.15E-09	4.56E-05
Bmpr1a	bone morphogenetic protein receptor, type 1A	2.5947	5.32E-10	1.13E-05
B230209C24Rik	RIKEN cDNA B230209C24 gene	2.5744	3.14E-07	0.0066538
Tnfrsf13c	tumor necrosis factor receptor superfamily, member 13c	2.5625	6.01E-11	1.27E-06
Slc44a1	solute carrier family 44, member 1	2.5542	3.52E-07	0.007477
Nfat5	nuclear factor of activated T-cells 5	2.5538	1.19E-08	0.00025224
Skp1a	S-phase kinase-associated protein 1A	2.5536	1.09E-08	0.00023117
5730472N09Rik	RIKEN cDNA 5730472N09 gene	2.5512	1.68E-08	0.00035741
Myl4	myosin, light polypeptide 4	2.5445	1.39E-07	0.002945
1200015A19Rik	RIKEN cDNA 1200015A19 gene	2.5302	4.45E-07	0.009446
Zfp423	zinc finger protein 423	2.5238	7.20E-12	1.53E-07
Sgcb	sarcoglycan, beta (dystrophin-associated glycoprotein)	2.5169	2.21E-07	0.0046965
Fkbp14	FK506 binding protein 14	2.4747	7.44E-11	1.58E-06
Ndrg4	N-myc downstream regulated gene 4	2.4736	6.85E-13	1.45E-08
Tpd52l1	tumor protein D52-like 1	2.4651	2.75E-10	5.83E-06
Tmem117	transmembrane protein 117	2.4625	1.61E-06	0.034077
2500002L14Rik	RIKEN cDNA 2500002L14 gene	2.4552	2.68E-09	5.68E-05
BC064033	cDNA sequence BC064033	2.451	4.09E-08	0.00086847
Ddo	D-aspartate oxidase	2.4354	1.30E-06	0.027664
Hs3st3a1	heparan sulfate (glucosamine) 3-O-sulfotransferase 3A1	2.43	1.61E-08	0.00034071
Acox2	acyl-Coenzyme A oxidase 2, branched chain	2.4264	1.78E-09	3.78E-05
Slc3a2	solute carrier family 3 (activators of dibasic and neutral amino acid transport), member 2	2.4235	3.06E-10	6.50E-06
Sema3b	sema domain, immunoglobulin domain (Ig), short basic domain, secreted, 3B	2.4064	2.62E-08	0.00055554
Nav1	neuron navigator 1	2.3805	2.58E-08	0.00054777
Hist1h2bm	histone cluster 1, H2bm	2.3797	1.45E-06	0.030782
Scg2	secretogranin II	2.3567	1.31E-07	0.0027899
Tmem106b	transmembrane protein 106B	2.3559	1.49E-06	0.031593
Vldlr	very low density lipoprotein receptor	2.3527	4.39E-07	0.0093067
Entpd5	ectonucleoside triphosphate diphosphohydrolase 5	2.3375	5.94E-11	1.26E-06

Tbcel	tubulin folding cofactor E-like	2.3344	1.50E-06	0.031776
Reep5	receptor accessory protein 5	2.331	1.69E-06	0.035758
Dap	death-associated protein	2.3298	3.48E-07	0.0073899
Igsf9b	immunoglobulin superfamily, member 9B	2.3121	1.20E-10	2.54E-06
Cbfb	core binding factor beta	2.3034	3.70E-07	0.0078541
Hist1h2bp	histone cluster 1, H2bp	2.2965	1.36E-06	0.028806
9030409G11Rik	RIKEN cDNA 9030409G11 gene	2.295	1.10E-08	0.00023323
Ngfr	nerve growth factor receptor (TNFR superfamily, member 16)	2.2899	8.28E-07	0.017569
Nrp1	neuropilin 1	2.2882	1.09E-06	0.023085
Enpp5	ectonucleotide pyrophosphatase/phosphodiesterase 5	2.2718	5.42E-07	0.011494
Egfl9	EGF-like-domain, multiple 9	2.2666	8.93E-09	0.00018943
Tmco3	transmembrane and coiled-coil domains 3	2.2663	7.45E-09	0.00015798
Slc24a6	solute carrier family 24 (sodium/potassium/calcium exchanger), member 6	2.2625	1.40E-08	0.00029696
Gpr85	G protein-coupled receptor 85	2.259	2.85E-08	0.00060509
Ak3l1	adenylate kinase 3 alpha-like 1	2.2485	1.17E-07	0.0024794
Lcat	lecithin cholesterol acyltransferase	2.2325	3.33E-08	0.0007064
Cxxc5	CXXC finger 5	2.2322	1.69E-06	0.035755
B930095G15Rik	RIKEN cDNA B930095G15 gene	2.2112	7.30E-08	0.0015484
Atp2a2	ATPase, Ca++ transporting, cardiac muscle, slow twitch 2	2.2008	1.73E-08	0.00036674
Gpx4	glutathione peroxidase 4	2.1999	4.11E-09	8.73E-05
Zfpm1	zinc finger protein, multitype 1	2.198	1.03E-06	0.021782
Bdh1	3-hydroxybutyrate dehydrogenase, type 1	2.1951	5.71E-07	0.012123
Degs1	degenerative spermatocyte homolog 1 (Drosophila)	2.1888	1.18E-06	0.025105
Rab33b	RAB33B, member of RAS oncogene family	2.1883	2.88E-08	0.00061175
H2afy	H2A histone family, member Y	2.1875	1.97E-07	0.004186
Asb8	ankyrin repeat and SOCS box-containing protein 8	2.1849	3.48E-09	7.39E-05
2310005E10Rik	RIKEN cDNA 2310005E10 gene	2.1796	5.17E-07	0.010972
Paqr8	progestin and adipoQ receptor family member VIII	2.1793	8.00E-07	0.016973
Usp53	ubiquitin specific peptidase 53	2.1763	2.05E-08	0.00043433
Nxt2	nuclear transport factor 2-like export factor 2	2.1752	7.05E-07	0.014965
Tmem150	transmembrane protein 150	2.171	1.27E-08	0.00027034
Papss2	3'-phosphoadenosine 5'-phosphosulfate synthase 2	2.1648	4.45E-09	9.45E-05
Nrxn3	neurexin III	2.1565	5.98E-08	0.0012685
Ptpro	protein tyrosine phosphatase, receptor type, O	2.1548	1.10E-07	0.0023233
Mgat5	mannoside acetylglucosaminyltransferase 5	2.1545	6.76E-07	0.014347
Art3	ADP-ribosyltransferase 3	2.1508	7.86E-09	0.00016681
Mbnl2	muscleblind-like 2	2.1494	1.15E-08	0.00024402
Rdh14	retinol dehydrogenase 14 (all-trans and 9-cis)	2.1169	5.76E-09	0.00012212
Gm22	gene model 22, (NCBI)	2.1145	6.77E-07	0.014367
Ormdl3	ORM1-like 3 (S. cerevisiae)	2.1043	1.83E-06	0.038862
Hibadh	3-hydroxyisobutyrate dehydrogenase	2.1041	1.44E-09	3.06E-05
Phyhipl	phytanoyl-CoA hydroxylase interacting protein-like	2.0975	7.39E-08	0.0015671

Galt	galactose-1-phosphate uridyl transferase	2.0936	1.37E-07	0.0029118
Pmm1	phosphomannomutase 1	2.091	8.96E-07	0.019005
Id4	inhibitor of DNA binding 4	2.0909	6.46E-07	0.013714
1110020P15Rik	RIKEN cDNA 1110020P15 gene	2.0825	8.48E-08	0.0017987
Slc26a6	solute carrier family 26, member 6	2.0796	1.61E-06	0.034101
P4ha1	procollagen-proline, 2-oxoglutarate 4-dioxygenase (proline 4-hydroxylase), alpha 1	2.0774	7.85E-09	0.00016652
Etfa	electron transferring flavoprotein, alpha polypeptide	2.0661	3.77E-07	0.0079929
Scrn1	secernin 1	2.0545	5.24E-11	1.11E-06
St3gal2	ST3 beta-galactoside alpha-2,3-sialyltransferase 2	2.0523	3.14E-07	0.0066685
Pkd2	polycystic kidney disease 2	2.052	1.04E-07	0.002209
Aco2	aconitase 2, mitochondrial	2.0519	1.17E-06	0.024838
BC051227	cDNA sequence BC051227	2.0254	1.67E-07	0.0035398
Fndc5	fibronectin type III domain containing 5	2.0242	1.07E-06	0.022751
D930001I22Rik	RIKEN cDNA D930001I22 gene	2.0147	1.23E-07	0.0026147
Pnpla8	patatin-like phospholipase domain containing 8	2.0079	9.47E-08	0.002009
Grhl1	grainyhead-like 1 (Drosophila)	2.005	6.91E-10	1.47E-05
Endod1	endonuclease domain containing 1	2.0037	3.32E-07	0.0070467
High in LIF.NOG				
Symbol	**Description**	**Fold Change**	**p.value**	**FDR**
Cldn11	claudin 11	19.641	1.65E-08	0.00035048
Rbp1	retinol binding protein 1, cellular	19.318	3.41E-07	0.007231
Egr4	early growth response 4	15.449	8.41E-07	0.017852
Fbln2	fibulin 2	13.15	1.09E-08	0.00023022
Egr3	early growth response 3	11.458	1.63E-07	0.0034561
Bcas1	breast carcinoma amplified sequence 1	10.825	5.66E-08	0.0012009
Cenpa	centromere protein A	9.2201	3.54E-07	0.0075111
Col18a1	procollagen, type XVIII, alpha 1	7.4217	1.37E-07	0.0029049
Mest	mesoderm specific transcript	7.3456	4.22E-10	8.96E-06
Galntl1	UDP-N-acetyl-alpha-D-galactosamine:polypeptide N-acetylgalactosaminyltransferase-like 1	7.2731	7.23E-09	0.00015331
Gpd1	glycerol-3-phosphate dehydrogenase 1 (soluble)	7.1528	5.19E-07	0.011014
Igf2bp2	insulin-like growth factor 2 mRNA binding protein 2	7.0947	2.09E-10	4.44E-06
Basp1	brain abundant, membrane attached signal protein 1	6.8895	3.19E-08	0.00067647
Adamts4	a disintegrin-like and metallopeptidase with thrombospondin type 1 motif, 4	6.4957	1.65E-06	0.035072
Bok	Bcl-2-related ovarian killer protein	6.3338	2.77E-09	5.88E-05
Spsb4	splA/ryanodine receptor domain and SOCS box containing 4	6.0629	1.92E-09	4.08E-05
Sulf1	sulfatase 1	5.1388	6.25E-08	0.0013271
Coro1c	coronin, actin binding protein 1C	4.7005	2.38E-08	0.00050541
9630019K15Rik	RIKEN cDNA 9630019K15 gene	4.3967	2.86E-08	0.00060635
Cdk4	cyclin-dependent kinase 4	4.3436	1.36E-08	0.00028797

Hn1	hematological and neurological expressed sequence 1	4.3342	1.20E-10	2.54E-06
2810003C17Rik	RIKEN cDNA 2810003C17 gene	4.2383	2.45E-07	0.0051934
Plekha2	pleckstrin homology domain-containing, family A member 2	4.2039	7.06E-09	0.00014969
Rpl13a	ribosomal protein L13a	4.0916	2.22E-09	4.71E-05
Neurl	neuralized-like homolog (Drosophila)	3.9266	3.73E-08	0.00079146
Igf2bp3	insulin-like growth factor 2 mRNA binding protein 3	3.9244	5.00E-08	0.0010601
Rgs16	regulator of G-protein signaling 16	3.7396	2.77E-07	0.0058868
Rpl10a	ribosomal protein L10A	3.6828	2.40E-09	5.09E-05
Nes	nestin	3.6735	2.24E-07	0.0047496
Nrarp	Notch-regulated ankyrin repeat protein	3.6413	4.37E-09	9.28E-05
Sox11	SRY-box containing gene 11	3.6158	1.78E-12	3.78E-08
Egfr	epidermal growth factor receptor	3.5722	1.88E-09	3.99E-05
Adcyap1r1	adenylate cyclase activating polypeptide 1 receptor 1	3.4886	1.68E-06	0.03574
Gbp3	guanylate nucleotide binding protein 3	3.4282	5.97E-11	1.27E-06
Ehd2	EH-domain containing 2	3.3459	3.61E-07	0.0076629
2810025M15Rik	RIKEN cDNA 2810025M15 gene	3.2928	1.52E-07	0.003224
Csnk1e	casein kinase 1, epsilon	3.2329	6.68E-07	0.014174
Tcf12	transcription factor 12	3.2155	8.30E-09	0.00017617
Hnrpa1	heterogeneous nuclear ribonucleoprotein A1	3.2059	6.61E-09	0.00014026
Nxph1	neurexophilin 1	3.1484	7.61E-07	0.016136
Cdca4	cell division cycle associated 4	3.1015	7.68E-09	0.00016293
Midn	midnolin	3.0904	2.24E-07	0.0047449
Hnrpdl	heterogeneous nuclear ribonucleoprotein D-like	3.066	1.69E-07	0.0035834
LOC241621	NA	3.0578	4.44E-07	0.0094273
Rpl12	ribosomal protein L12	3.0428	3.00E-10	6.36E-06
Mcm7	minichromosome maintenance deficient 7 (S. cerevisiae)	2.9304	1.43E-06	0.030254
Pdgfra	platelet derived growth factor receptor, alpha polypeptide	2.8366	8.23E-07	0.017456
Idh2	isocitrate dehydrogenase 2 (NADP+), mitochondrial	2.7635	3.25E-08	0.00069025
Vash2	vasohibin 2	2.7575	9.80E-09	0.00020789
Pros1	protein S (alpha)	2.7556	2.33E-06	0.049532
EG237361	predicted gene, EG237361	2.7422	7.65E-08	0.0016232
Chic2	cysteine-rich hydrophobic domain 2	2.7409	1.93E-07	0.004102
Gprin1	G protein-regulated inducer of neurite outgrowth 1	2.6819	2.80E-09	5.94E-05
Ppp1r14b	protein phosphatase 1, regulatory (inhibitor) subunit 14B	2.6679	3.40E-07	0.0072062
Rpl18	ribosomal protein L18	2.6622	4.45E-09	9.44E-05
RP23-336J1.4	Ras-GTPase-activating protein SH3-domain binding protein	2.6185	2.74E-07	0.0058179
Eif4a1	eukaryotic translation initiation factor 4A1	2.6104	7.51E-08	0.0015926
Rps20	ribosomal protein S20	2.5981	3.10E-08	0.00065686
Ptpre	protein tyrosine phosphatase, receptor type, E	2.596	1.20E-06	0.02536
Lbr	lamin B receptor	2.5642	9.47E-07	0.0201
Rps9	ribosomal protein S9	2.5355	1.04E-08	0.00022043
Mns1	meiosis-specific nuclear structural protein 1	2.5165	2.32E-07	0.0049223

Rps26	ribosomal protein S26	2.5153	2.80E-09	5.93E-05
Lypla2	lysophospholipase 2	2.5115	4.18E-08	0.00088724
Set	SET translocation	2.4986	1.40E-06	0.029731
Nfkbiz	nuclear factor of kappa light polypeptide gene enhancer in B-cells inhibitor, zeta	2.4836	1.40E-06	0.029774
Rpl3	ribosomal protein L3	2.4523	2.23E-09	4.72E-05
Maml1	mastermind like 1 (Drosophila)	2.4514	1.12E-06	0.023733
Rps24	ribosomal protein S24	2.4452	2.36E-07	0.005005
Rps10	ribosomal protein S10	2.4154	6.31E-10	1.34E-05
Nid2	nidogen 2	2.4009	8.77E-08	0.0018608
Rps5	ribosomal protein S5	2.392	1.87E-10	3.97E-06
Pard6g	par-6 partitioning defective 6 homolog gamma (C. elegans)	2.3887	6.99E-07	0.014832
Ick	intestinal cell kinase	2.3877	1.46E-07	0.003103
Rpl23a	ribosomal protein L23a	2.3804	1.31E-07	0.0027853
Rpl10	ribosomal protein 10	2.3735	1.78E-07	0.0037768
Rps3	ribosomal protein S3	2.3676	2.21E-08	0.00046893
Tagln3	transgelin 3	2.3595	2.55E-08	0.00054142
EG382843	predicted gene, EG382843	2.3593	7.34E-08	0.0015578
Eif1a	eukaryotic translation initiation factor 1A	2.3451	6.03E-07	0.012788
Hnrpab	heterogeneous nuclear ribonucleoprotein A/B	2.3445	8.76E-09	0.00018593
Prr6	proline-rich polypeptide 6	2.3391	4.84E-08	0.0010259
Rps28	ribosomal protein S28	2.3301	3.67E-09	7.78E-05
LOC277692	NA	2.3242	3.00E-07	0.0063561
Rpl28	ribosomal protein L28	2.3104	2.27E-08	0.00048136
5133400G04Rik	RIKEN cDNA 5133400G04 gene	2.3031	6.93E-09	0.00014702
Rassf2	Ras association (RalGDS/AF-6) domain family 2	2.2949	7.76E-08	0.001646
Cnot6	CCR4-NOT transcription complex, subunit 6	2.2857	1.06E-06	0.022413
Ddx25	DEAD (Asp-Glu-Ala-Asp) box polypeptide 25	2.2807	2.28E-07	0.0048318
Rps8	ribosomal protein S8	2.2694	4.30E-09	9.12E-05
Arbp	acidic ribosomal phosphoprotein P0	2.2626	1.64E-07	0.0034878
Ephb1	Eph receptor B1	2.2553	1.71E-06	0.036371
Rps3a	ribosomal protein S3a	2.2414	1.46E-07	0.0030985
Rps23	ribosomal protein S23	2.241	4.37E-08	0.00092764
Fau	Finkel-Biskis-Reilly murine sarcoma virus (FBR-MuSV) ubiquitously expressed	2.2366	1.44E-06	0.030533
Nmral1	NmrA-like family domain containing 1	2.2341	1.87E-09	3.96E-05
Rpl31	ribosomal protein L31	2.225	4.87E-08	0.0010336
Adam19	a disintegrin and metallopeptidase domain 19 (meltrin beta)	2.2168	2.04E-06	0.043213
Zfp334	zinc finger protein 334	2.2094	5.38E-07	0.011423
Rps2	ribosomal protein S2	2.1955	1.19E-06	0.025346
Litaf	LPS-induced TN factor	2.1684	1.84E-06	0.038963
Snrpg	small nuclear ribonucleoprotein polypeptide G	2.166	1.12E-08	0.00023716
Rpl35	ribosomal protein L35	2.1569	4.28E-07	0.0090907
D11Ertd497e	DNA segment, Chr 11, ERATO Doi 497, expressed	2.1555	8.97E-08	0.0019032

Rprm	reprimo, TP53 dependent G2 arrest mediator candidate	2.1538	1.58E-06	0.033534
Rpl36a	ribosomal protein L36a	2.1496	8.51E-12	1.81E-07
Csnk1d	casein kinase 1, delta	2.1378	2.80E-09	5.94E-05
Dazap1	DAZ associated protein 1	2.1336	3.70E-07	0.007858
Faah	fatty acid amide hydrolase	2.1324	1.23E-07	0.0026052
Tgfbr1	transforming growth factor, beta receptor I	2.1291	1.04E-06	0.022048
Rpl36	ribosomal protein L36	2.1149	2.38E-08	0.00050408
Rpl32	ribosomal protein L32	2.1116	6.58E-07	0.01396
Whsc1	Wolf-Hirschhorn syndrome candidate 1 (human)	2.1025	4.45E-07	0.009439
Klf4	Kruppel-like factor 4 (gut)	2.0964	1.09E-07	0.0023036
Casp2	caspase 2	2.0707	2.67E-07	0.0056713
Nudt21	nudix (nucleoside diphosphate linked moiety X)-type motif 21	2.0553	2.06E-07	0.0043628
Hmgb1	high mobility group box 1	2.0485	1.12E-06	0.023693
Rpl7	ribosomal protein L7	2.0434	8.71E-08	0.0018477
Rplp1	ribosomal protein, large, P1	2.0414	4.86E-08	0.001032
Rpl26	ribosomal protein L26	2.0358	1.49E-07	0.0031611
2700060E02Rik	RIKEN cDNA 2700060E02 gene	2.035	8.11E-10	1.72E-05
Erdr1	erythroid differentiation regulator 1	2.0295	7.95E-07	0.016869
5730427N09Rik	RIKEN cDNA 5730427N09 gene	2.027	8.01E-10	1.70E-05
Gabrb3	gamma-aminobutyric acid (GABA-A) receptor, subunit beta 3	2.0269	9.57E-08	0.0020314
Sfrs1	splicing factor, arginine/serine-rich 1 (ASF/SF2)	2.0259	4.81E-08	0.0010205

Table 2-5 A list of differentially expressed genes identified by the comparison of LIF-induced astrocytes and neurospheres.

Genes are ordered based on largest to smallest fold difference. Genes that show less than two-fold change are excluded. A total of 69 genes are differentially expressed. 57 genes are expressed more highly in LIF-induced astrocytes compared to neurospheres. Conversely, 12 genes are expressed more highly in neurospheres compared to LIF-induced astrocytes

High in LIF.NOG				
Symbol	**Description**	**Fold Change**	**p.value**	**FDR**
Fos	FBJ osteosarcoma oncogene	34.543	7.26E-11	1.54E-06
Rbp1	retinol binding protein 1, cellular	30.43	8.23E-08	0.0017469
Apoe	apolipoprotein E	23.053	2.82E-08	0.00059815
Clu	clusterin	16.02	6.02E-08	0.0012774
Serpina3n	serine (or cysteine) peptidase inhibitor, clade A, member 3N	13.509	1.46E-06	0.031058
Cldn11	claudin 11	11.09	1.42E-07	0.0030094
Aqp4	aquaporin 4	11.017	3.51E-09	7.44E-05
Lrp4	low density lipoprotein receptor-related protein 4	8.5392	1.59E-06	0.033752
Col16a1	procollagen, type XVI, alpha 1	6.7499	3.91E-07	0.0082998
Kcna6	potassium voltage-gated channel, shaker-related, subfamily, member 6	6.7238	2.31E-06	0.048922
Nfkbiz	nuclear factor of kappa light polypeptide gene enhancer in B-cells inhibitor, zeta	5.3919	2.90E-09	6.16E-05
Plec1	plectin 1	5.3414	2.41E-07	0.0051167
Dusp1	dual specificity phosphatase 1	5.2348	2.59E-08	0.00054986
Sulf1	sulfatase 1	5.0911	6.63E-08	0.0014056
Hspb8	heat shock protein 8	4.3883	8.56E-07	0.01817
Dbp	D site albumin promoter binding protein	4.2853	3.38E-08	0.00071737
Klf6	Kruppel-like factor 6	4.25	2.36E-07	0.0050052
Ltbp3	latent transforming growth factor beta binding protein 3	4.077	1.89E-06	0.040194
Cml1	camello-like 1	3.8983	1.53E-06	0.032547
Cpe	carboxypeptidase E	3.8406	1.71E-07	0.0036179
Junb	Jun-B oncogene	3.8242	4.04E-07	0.0085715
Pros1	protein S (alpha)	3.8026	1.58E-07	0.0033557
Itih3	inter-alpha trypsin inhibitor, heavy chain 3	3.8026	1.30E-06	0.027565
Stat3	signal transducer and activator of transcription 3	3.728	6.26E-09	0.00013287
Cd63	Cd63 antigen	3.7115	4.23E-09	8.97E-05
9130404D14Rik	RIKEN cDNA 9130404D14 gene	3.3855	1.67E-09	3.54E-05
Ctsb	cathepsin B	3.3413	2.36E-08	0.00049979
Srf	serum response factor	3.3158	7.28E-07	0.015443
Cyr61	cysteine rich protein 61	3.314	4.38E-07	0.0092883
Lgals3	lectin, galactose binding, soluble 3	3.313	4.52E-07	0.0095884
Arhgef4	Rho guanine nucleotide exchange factor (GEF) 4	3.2421	9.15E-07	0.019405

Hist1h2bc	histone cluster 1, H2bc	3.2036	1.31E-06	0.027839
Ugt1a6b	UDP glucuronosyltransferase 1 family, polypeptide A6B	3.0046	1.79E-09	3.80E-05
Paqr8	progestin and adipoQ receptor family member VIII	2.9887	2.70E-08	0.00057299
Gfra1	glial cell line derived neurotrophic factor family receptor alpha 1	2.9759	1.00E-09	2.12E-05
Flot1	flotillin 1	2.905	1.48E-08	0.00031489
Glud1	glutamate dehydrogenase 1	2.8856	2.97E-07	0.0063113
Itm2c	integral membrane protein 2C	2.8822	3.69E-07	0.0078315
Gdf1	growth differentiation factor 1	2.8748	9.70E-07	0.020572
Igf2bp2	insulin-like growth factor 2 mRNA binding protein 2	2.8746	1.19E-07	0.0025192
Ugt1a7c	UDP glucuronosyltransferase 1 family, polypeptide A7C	2.7626	3.86E-10	8.19E-06
Tmem108	transmembrane protein 108	2.7098	2.08E-06	0.044174
Klf4	Kruppel-like factor 4 (gut)	2.6328	7.15E-09	0.00015167
2810459M11Rik	RIKEN cDNA 2810459M11 gene	2.6013	5.33E-07	0.011311
Prnp	prion protein	2.5473	2.72E-07	0.005776
Hsd3b7	hydroxy-delta-5-steroid dehydrogenase, 3 beta- and steroid delta-isomerase 7	2.5288	7.19E-09	0.00015252
Cd151	CD151 antigen	2.4861	1.30E-07	0.0027483
Gabrb3	gamma-aminobutyric acid (GABA-A) receptor, subunit beta 3	2.4852	7.31E-09	0.00015511
Lynx1	Ly6/neurotoxin 1	2.3736	1.53E-06	0.032378
Col4a5	procollagen, type IV, alpha 5	2.3695	8.25E-09	0.00017494
Aifm2	apoptosis-inducing factor, mitochondrion-associated 2	2.3213	2.26E-07	0.0047845
Tagln3	transgelin 3	2.1537	7.94E-08	0.0016851
Anxa5	annexin A5	2.1324	1.75E-06	0.037082
Ndph	Norrie disease homolog	2.0916	7.16E-07	0.015192
Bzrap1	benzodiazapine receptor associated protein 1	2.072	6.59E-07	0.013973
Nr1d1	nuclear receptor subfamily 1, group D, member 1	2.0535	1.21E-06	0.02571
Eno2	enolase 2, gamma neuronal	2.0255	6.84E-08	0.0014518
High in Neuro.				
Symbol	**Description**	**Fold Change**	**p.value**	**FDR**
Gng2	guanine nucleotide binding protein (G protein), gamma 2 subunit	2.4069	7.70E-12	1.63E-07
Arhgef3	Rho guanine nucleotide exchange factor (GEF) 3	2.2655	1.30E-09	2.75E-05
Kcnc4	potassium voltage gated channel, Shaw-related subfamily, member 4	4.0361	1.59E-08	0.00033773
Skp2	S-phase kinase-associated protein 2 (p45)	3.7582	5.01E-08	0.0010638
Efs	embryonal Fyn-associated substrate	3.798	1.40E-07	0.0029617
Arpp21	cyclic AMP-regulated phosphoprotein, 21	2.2241	2.81E-07	0.0059536
Zfp365	zinc finger protein 365	2.1544	3.38E-07	0.007164
Nsbp1	nucleosome binding protein 1	2.0864	4.02E-07	0.0085302
Sfrs7	splicing factor, arginine/serine-rich 7	2.4904	4.76E-07	0.01009
Tnnt1	troponin T1, skeletal, slow	2.7843	4.95E-07	0.010513
Tmem158	transmembrane protein 158	7.2373	6.64E-07	0.014095
Mest	mesoderm specific transcript	2.4607	1.31E-06	0.027759

2010317E24Rik	RIKEN cDNA 2010317E24 gene	2.6996	1.83E-06	0.038874

BMP4-regulated microarray candidates revealed known and novel astrocyte enriched genes.

Our interest in the diversity among differentiated astrocytes in the cerebral cortex prompted us to focus first on genes that were upregulated in the BMP4 treated group. To identify astrocyte-enriched genes in this group, we compared 121 genes that were greater than five-fold higher in the BMP4 group relative to the neurosphere group and cross-referenced them with genes that were identified as ten-fold enriched in astrocytes compared to neurons and oligodendrocytes (Cahoy et al., 2008). Fourteen genes that fit these criteria were selected (Figure 2.1D), and quantitative real-time PCR (qPCR) was performed to independently verify gene expression changes observed by the microarray (Figure 2.1E and data not shown). mRNA expression *in vivo* was first inspected using the Allen Brain Atlas (ABA) mouse brain expression database (Lein et al., 2007) and validated by in house *in situ* hybridization (ISH) (Figure 2.1F, 2.1G). Three candidates, Homeodomain only protein (Hopx), High temperature requirement A1 (HtrA1), and F3, show expression patterns that resemble the distribution of astrocytes in the cerebral cortex or in the hippocampus (Fig. 2.1F and 2.1G). These findings suggest that select genes expressed by BMP4-induced astrocytes may identify sub populations of astrocytes or distinguish astrocytes from NSCs in the adult mouse forebrain.

HtrA1 is expressed in mouse and human astrocytes.

We chose to focus on the serine protease HtrA1 for further analysis due to its known roles in Transforming Growth Factor-β (TGF-β) family signaling and extracellular matrix protein organization (Chamberland et al., 2009; Hadfield et al., 2008; Oka et al., 2004). To better determine whether HtrA1 mRNA is localized to astrocytes, we investigated HtrA1 expression *in vivo* by mRNA *in situ* hybridization (ISH). HtrA1 mRNA in the adult mouse forebrain is

strongly expressed in astrocytes located in the cerebral cortex and the hippocampus, and present but less strongly in thalamus and the hypothalamus (Fig. 2.2A-2.2F). Co-localization with GFAP by immunohistochemistry (IHC) found that the majority of HtrA1^{+} cells in cortical layer 1 express GFAP (86.34±5.42%, Fig. 2.2H), and that none of the HtrA1^{+} cells express the neuronal cell marker NeuN (0/1961, Fig. 2.2I). We also did not detect HtrA1 mRNA in oligodendrocytes or their precursors marked by Olig2 expression in the same cortical region during the period of cortical oligodendroglial differentiation (0/537, Fig. 2.2J). In deeper cortical layers, where the majority of the astrocytes lack GFAP expression but still express S100β and Aldehyde Dehydrogenase 1L1 (Aldh1L1), HtrA1 expression is limited to cells with stellate morphology (Fig. 2.2K, arrowheads) and does not overlap with NeuN or Olig2 (Fig. 2.2L, 2.2M arrowheads). ISH also revealed a small difference in the level of HtrA1 mRNA expressed in the upper cortex (cortical layers 1-3) versus deeper cortex (cortical layers 4-6) (Fig. 2.2C). This difference in HtrA1 transcript is also observed when compared mRNA isolated from upper and deeper cortical tissue by qPCR, which concurrently detected differential expression in GFAP but not in Tuj1 as expected (Fig. 2.2G). However, HtrA1 mRNA is rarely detected in GFAP-expressing white matter astrocytes in the corpus callosum (Fig. 2.2C dotted lines, 2.2N arrowheads, 2.2N'), nor is it highly expressed in the medial thalamus or hypothalamus (Fig. 2.2E, 2.2F). These findings suggest that HtrA1 mRNA is differentially expressed by astrocytes in multiple forebrain regions.

More interestingly, we found that HtrA1 mRNA is not expressed in adult mouse brain NSCs of the anterior subventricular zone (SVZ) (Fig. 2.2O, O' arrowheads), making HtrA1 a rare astrocyte marker that distinguishes between post-mitotic astrocytes and adult NSCs. It is sparsely distributed in the subgranular zone (SGZ) of the hippocampus (Fig. 2.2P, 2.2P'), unlike

transcripts that are enriched in hippocampal NSCs such as Hopx (Fig. 2.1G). Examination of HtrA1 mRNA with GFAP IHC revealed that the great majority of the $HtrA1^+$ cells (92.3±5.4%) in the SGZ do not display radial morphology, a hallmark of hippocampal NSCs. Taken together, mRNA expression analyses by ISH suggest HtrA1 may be a potential marker of specific populations of differentiated astrocytes in the adult mouse forebrain.

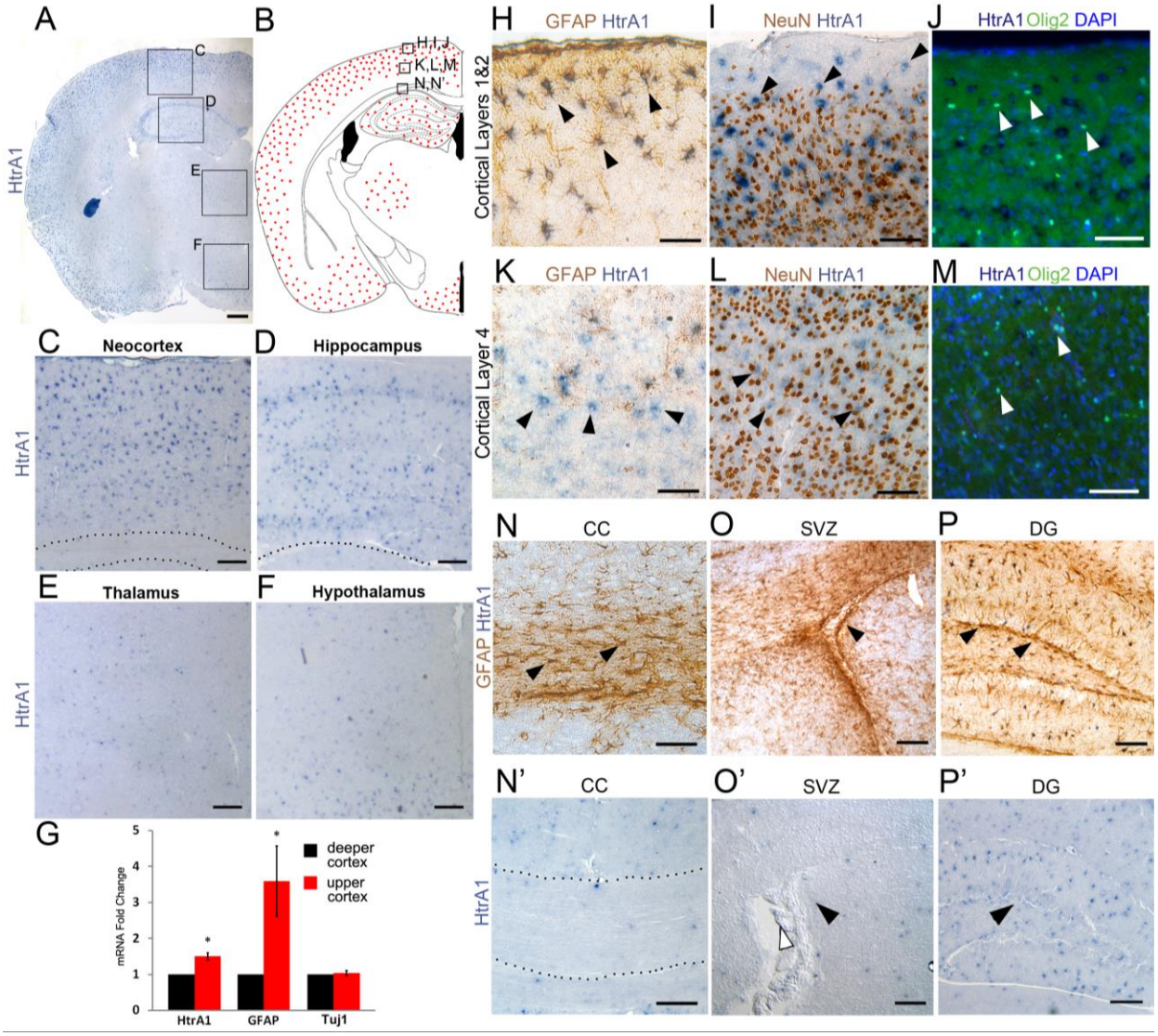

Figure 2.2 HtrA1 mRNA *in situ* hybridization reveals region and cell type-specific expression.

(A) Representative expression pattern of HtrA1 mRNA (blue) in P60 adult mouse forebrain (n= 8). Boxes indicate areas of interest in panels C-F. (B) Schematic diagram of HtrA1-expressing cells in the adult mouse forebrain. Red dots represent areas where HtrA1 mRNA is detected. Boxes indicate areas of interest as shown in panels H-N'. (C-F) Higher magnification views of HtrA1 mRNA expression in dorsal neocortex (C), hippocampus (D), medial thalamus (E), and medial hypothalamus (F). Dotted lines demarcate boundaries between cortex and corpus callosum in panel C and hippocampus and thalamus in panel D. (G) HtrA1 expression comparison between upper and deeper cortex by qPCR shows a small (1.5 fold) but significant difference (p=0.005, n=6). GFAP and Tuj1 were used as positive and negative controls for differential expression respectively. (H, I) HtrA1 mRNA with GFAP (H) or NeuN (I) immunostaining in cortical layers 1 and 2 of adult mouse cortex demonstrates that HtrA1 is specifically expressed in astrocytes but not neurons (arrowheads). (J) HtrA1 mRNA (dark blue)

with immunofluorescent staining of Olig2 (green) in postnatal day 14 mouse cerebral cortex. No HtrA1 expression was observed in Olig2-expressing oligodendrocyte progenitors and oligodendrocytes (white arrowheads) in the upper layers of dorsal cortex where HtrA1 is strongly expressed. (K, L) HtrA1 mRNA with GFAP (K) or NeuN (L) IHC in cortical layer 4 where HtrA1 mRNA is detected in GFAP-negative cells with stellate morphology (K, arrowheads) and does not colocalize with NeuN (L, arrowheads). Similarly, $Olig2^{+}$ cells also lack HtrA1 expression in deeper cortical layers (M, white arrowsheads). (N, N') HtrA1 mRNA is rarely detected in the corpus callosum (CC) where GFAP is strongly expressed (N, arrowheads). Dotted line demarcates the boundaries for CC in N'. (O, O') HtrA1 mRNA is not detected around the lateral ventricle (O', white arrowhead), where GFAP-expressing adult neural stem cells reside in the subventricular zone (SVZ, arrowheads). (P, P') HtrA1 mRNA is highly expressed in the dentate gyrus (DG) of the hippocampus. However, expression is sparse in the subgranular zone where GFAP-expressing NSCs reside (P, arrowheads). Scale bar: panel A, 400μm; C-F, 100μm, H-N', 50μm; panels O-P',100μm.

We also examined HtrA1 protein distribution by performing immunocytochemistry (ICC) in GFAP$^+$ cells derived from NSCs differentiated for 7 days in BMP4 or LIF with Noggin. Corroborating the qPCR data, we observed markedly higher levels of HtrA1 protein in BMP4-induced GFAP$^+$ cells compared to LIF with Noggin induced GFAP$^+$ cells. (Fig. 2.3A). HtrA1 protein is detected in both cytosol and nuclei of cultured astrocytes, consistent with previous reports of HtrA1 subcellular localization in other cell types (N. Wang et al., 2012). This expression pattern is eliminated when the antibody was preabsorbed with a HtrA1 peptide (Fig. 2.3A). Similar protein expression is also detected in fetal bovine serum (FBS)-derived primary mouse astrocytes (Fig. 2.3B), where HtrA1 immunofluorescent signal diminishes when transitioned into a serum-free (SF) media and is upregulated with BMP4 treatment. (Fig. 2.3B, 3C). Western blot analysis of HtrA1 protein in these conditions also reveals similar expression changes (Fig. 2.3D). These findings suggest that HtrA1 protein expression is regulated by BMP4 signaling in postnatal astrocytes.

To determine whether HtrA1 is also expressed in human astrocytes, we generated astrocytes from human embryonic stem cells and induced-pluripotent stem cells using a previously reported differentiation protocol with some modifications (Duan, Peng, Pan, & Kessler, 2015). Briefly, LIF and BMP4 treatments were used promote astroglial lineage commitment and cell cycle exit, and further maturation of astrocytes was induced with the addition of FGF1 (Roybon et al., 2013). We did not detect HtrA1 in vimentin-expressing neural progenitor cells prior to astrocyte differentiation (Fig. 2.3E). In both BMP4 alone and BMP4/FGF1 conditions, HtrA1 expression is detected in GFAP and S100β expressing astrocytes, where it shares similar protein distribution with its mouse ortholog (Fig. 2.3F, 2.3G). qPCR analysis of HtrA1 mRNA in BMP4/FGF1 induced astrocytes and untreated NSC controls

also supports the ICC observations (data not shown). These findings provide additional evidence that astrocytic expression of HtrA1 is BMP signaling responsive and evolutionarily conserved.

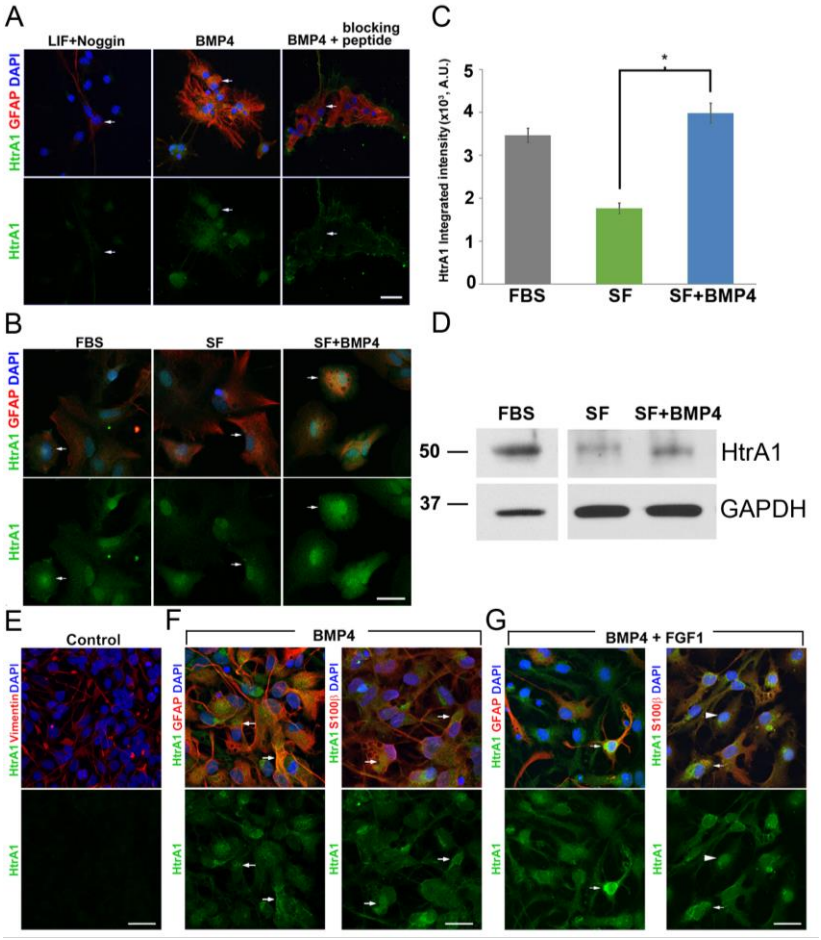

Figure 2.3 Characterization of HtrA1 expression in cultured mouse and human astrocytes. (A) Representative immunofluoresecent images of postnatal day 1 NSCs differentiated for 7 days *in vitro* in either LIF plus Noggin or BMP4. HtrA1 antibody (green) detected both cytosolic and nuclear signals in both LIF plus Noggin and BMP4 differentiated GFAP-expressing cells (red). However, staining signal is significantly stronger in BMP4-induced astrocytes. Elevated HtrA1 immunoreactivity in BMP4-induced astrocytes is eliminated when a HtrA1 peptide is used for blocking the antibody prior to primary incubation. (B) Representative immunofluorescent images of HtrA1 protein (green) and GFAP (red) detected in primary astrocytes isolated from postnatal day 2 mouse cortex using standard culturing protocol with 10% Fetal Bovine Serum (FBS, left panels). Serum withdrawal for 24hrs (middle panels) followed by the addition of BMP4 for 24hrs (right panels) increases the expression level of HtrA1. (C) Quantification of HtrA1 immunofluorescence revealed a significant difference in HtrA1 protein levels between serum-free and BMP4 treated primary astrocytes (n=3, p=0.008). (D) Representative micrograph of western blots showing HtrA1 protein expression in astrocytes cultured in fetal bovine serum containing media (FBS), serum free media (SF), or serum free media with 20ng/ml BMP4 (SF+BMP4). GAPDH is used as a loading control. (D, F, G) Representative immunofluorescent images of human HtrA1 protein (green, arrows) in NSCs marked by Vimentin (D, red), and BMP4 or BMP4/FGF1 induced astrocytes marked by GFAP or S100β (F, G, red). Scale bar, 25μm; * = P<0.05. Figure created with Stephanie Van Gulden.

HtrA1-LacZ reporter confirms astrocyte-specific expression of HtrA1 in mouse forebrain.

To further investigate cell type specificity of HtrA1 expression in the mouse brain, we acquired and examined a mouse reporter line that expresses β-Galactosidase (β-Gal) under the control of endogenous HtrA1 regulatory elements (Brown & Moore, 2012). We found that in the cerebral cortex of adult mice, nearly all (98.7±0.9%) β-Gal-expressing cells also express the pan-astrocytic marker Aldh1L1 (Fig. 2.4A-2.4A"). Conversely, nearly all (97.8±1.14%) Aldh1L1+ cells express β-Gal in adult dorsal cortex, supporting the notion that HtrA1 is astrocyte expressed. In addition to Aldh1L1, β-Gal is also detected in 94.3±3.1% of S100β$^+$ cells (Fig. 2.4B-2.4B") and 88.6±4.4% of layer 1 GFAP$^+$ astrocytes (Fig. 2.4C-2.4C"). Co-immunostaining with antibodies against NeuN (Fig. 2.4D-2.4D") and adenomatous polyposis coli (APC, Fig. 2.4E-2.4E") shows no β-Gal expression in neurons (0/4640 NeuN$^+$ cells) and oligodendrocytes (0/608 APC$^+$ cells). Examination of β-Gal expression in endothelial cells, pericytes, and microglia by co-immunostaining with CD31 (0/523 CD31$^+$ cells, Fig. 2.4F-2.4F"), PDGFRβ (0/403 PDGFRβ$^+$ cells, Fig. 2.4G-2.4G"), and Iba1 (0/420 Iba1$^+$ cells, Fig. 2.4H-2.4H") antibodies respectively also show no overlapping expression in the cerebral cortex. In addition, examination of β-Gal in areas of adult neurogenesis with Nestin co-staining confirmed the absence of HtrA1 expression in neural stem cells, both in the SVZ (Fig. 2.4I-2.4I") and the SGZ (Fig. 2.4J-2.4J"). Taken together, these findings support our mRNA expression analysis and provide further evidence for HtrA1 as an astrocyte specific marker in the adult mouse cerebral cortex.

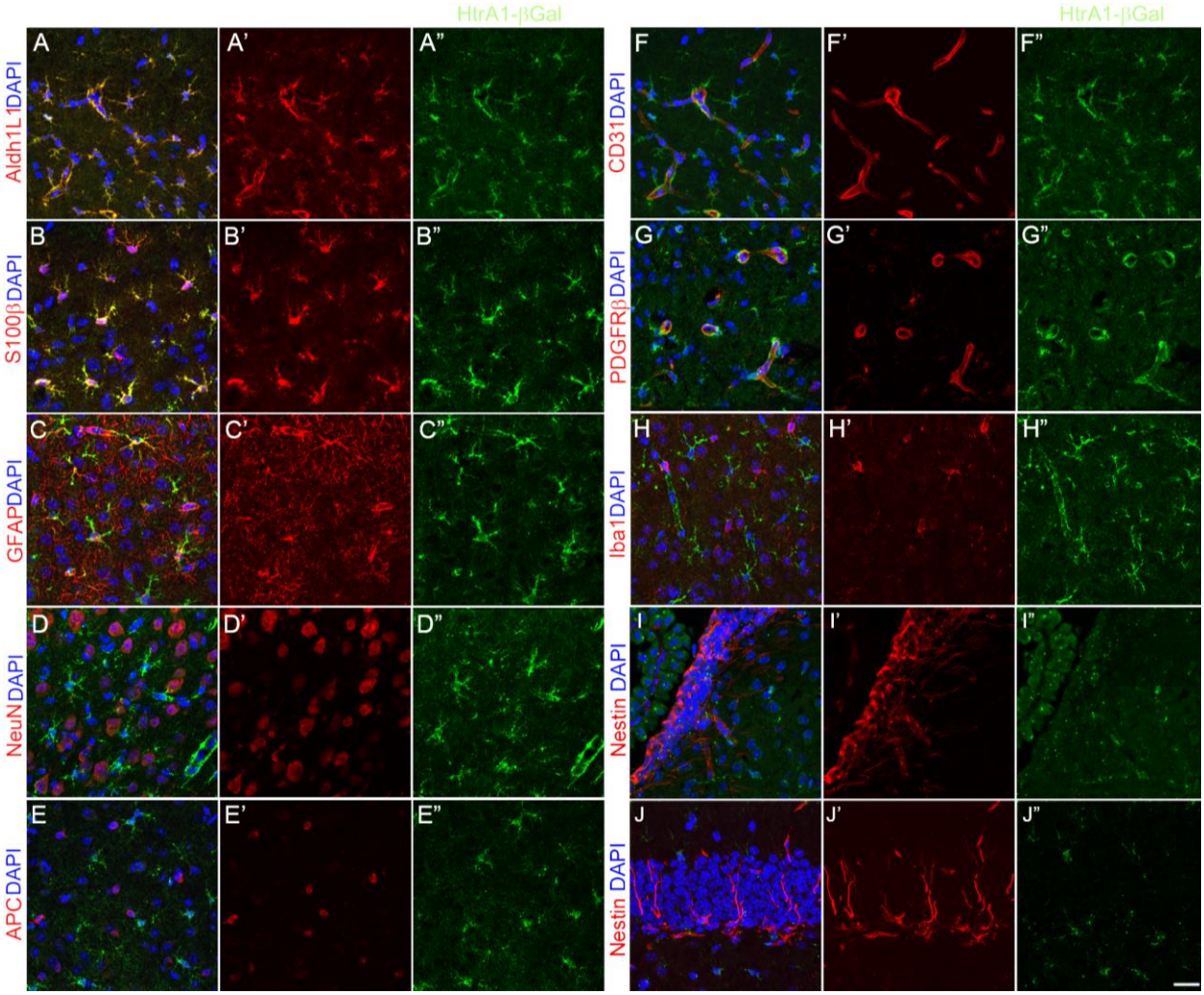

Figure 2.4 HtrA1 expression is astrocyte specific.

(A-H") Representative micrographs showing expression of HtrA1 β-Gal reporter (green) with molecular markers of different neural and non-neural cell types in the dorsal cortex of adult mouse (n=6, red). β-Gal is found to colocalize with known astrocyte markers including Aldh1L1 (A-A"), S100β (B-B"), and GFAP (C-C") where these markers are expressed. β-Gal expression does not colocalize with neuronal marker NeuN (D-D"), oligodendrocyte marker APC (E-E"), endothelial cell marker CD31 (F-F"), Pericyte marker PDGFRβ (G-G"), or microglia marker Iba1 (H-H"). (I-J") Immunofluorescent imaging of β-Gal (green) in germinal zones of the adult mouse brain did not show any colocalization with neural stem cell marker Nestin (red) in anterior SVZ (SVZ, I-I"), subgranular zone of the hippocampus (SGZ, J-J"). DAPI is shown in blue in all panels. Scale bar, 20μm

We next sought to determine whether β-Gal expression in HtrA1-LacZ mice reflects differential expression of HtrA1 observed at the mRNA level. We examined the level of β-Gal expression in different forebrain regions of adult mice, including cerebral cortex, hippocampus, corpus callosum, and thalamus, and found that not all astrocytes express β-Gal at the same levels. Quantification of β-Gal immunofluorescence (IF) in cortical layers 1-3 (IF=2344.57±150.59) versus layers 4-6 (IF=1659.54±99.3) shows a significant difference in the integrated signal intensity (Fig. 2.5A, 2.5B, 2.5G; p=0.003), suggesting that HtrA1 expression is differentially regulated in upper and deeper layers of the dorsal neocortex. In contrast, no difference in S100β IF (layers 1-3=1780.38±69.16; layers 4-6 =1662.23±95.39; p=0.223) was detected in the same regions (Fig. 2.5A', 2.5B', 2.5G). GFAP IF is known to be stronger in the upper cortex, and our integrated intensity quantification confirms this finding (layers 1-3 IF=1825.74±105.76, layers 4-6 IF=1103.85± 39.41, p=8e-04; Fig. 2.5A", 2.5B", 2.5G). In addition to the neocortex, all three astrocyte markers were strongly expressed in the lateral dentate gyrus of the hippocampus (Fig 2.5C-2.5C", 2.5G). However, β-Gal IF was greatly reduced in the corpus callosum (832.99±107.96) where as GFAP, but not S100β, is strongly expressed (Fig. 2.5D-2.5D", 2.5G). In the diencephalon, only S100β is consistently expressed in the dorsal thalamus (Fig. 2.5E', 2.5G) and the hypothalamus (Fig. 2.5F', 2.5G), where GFAP is strongly expressed in select populations (Fig. 2.5E", 2.5F", 2.5G) and HtrA1-βGal is expressed at low levels (dorsal thalamus 1063.4±42.27; hypothalamus 1232.77±57.83) (Fig. 2.5E and 2.5F, 2.5G).

To further analyze regional differences in HtrA1 expression, we quantified the percentage of Aldh1L1-expressing astrocytes that co-express HtrA1 in the above-mentioned brain regions independent of expression levels. Consistent with the signal intensity analysis, we found that dorsal brain regions including the hippocampus (99.35±0.65%), cortical layers 1-3

(97.51±0.86%), and cortical layers 4-6 (94.09±3.24%) show a higher percentage of Aldh1L1^{+} cells expressing HtrA1 compared to ventral brain regions including the thalamus (42.92±6.58%) and hypothalamus (28.71±2.67%, Fig. 2.5H). Similarly, cell counts in the corpus callosum also revealed low numbers of Aldh1L1+ astrocytes expressing HtrA1 (6.63±3.19%, Fig 2.5H). Similar results were obtained for the percentage of S100β cells that express HtrA1 in different forebrain regions (data not shown). Although there are some minor discrepancies between β-Gal expression and ISH findings, possibly due to differences in β-Gal protein and HtrA1 mRNA stability, the HtrA1-LacZ reporter analyses support our previous conclusion that HtrA1 is differentially expressed by astrocytes in different regions of the adult mouse forebrain. Furthermore, HtrA1 expression does not mirror expression of known astrocyte markers GFAP and S100β, and the combinatorial expression of the three markers may be used to identify sub populations of forebrain astrocytes.

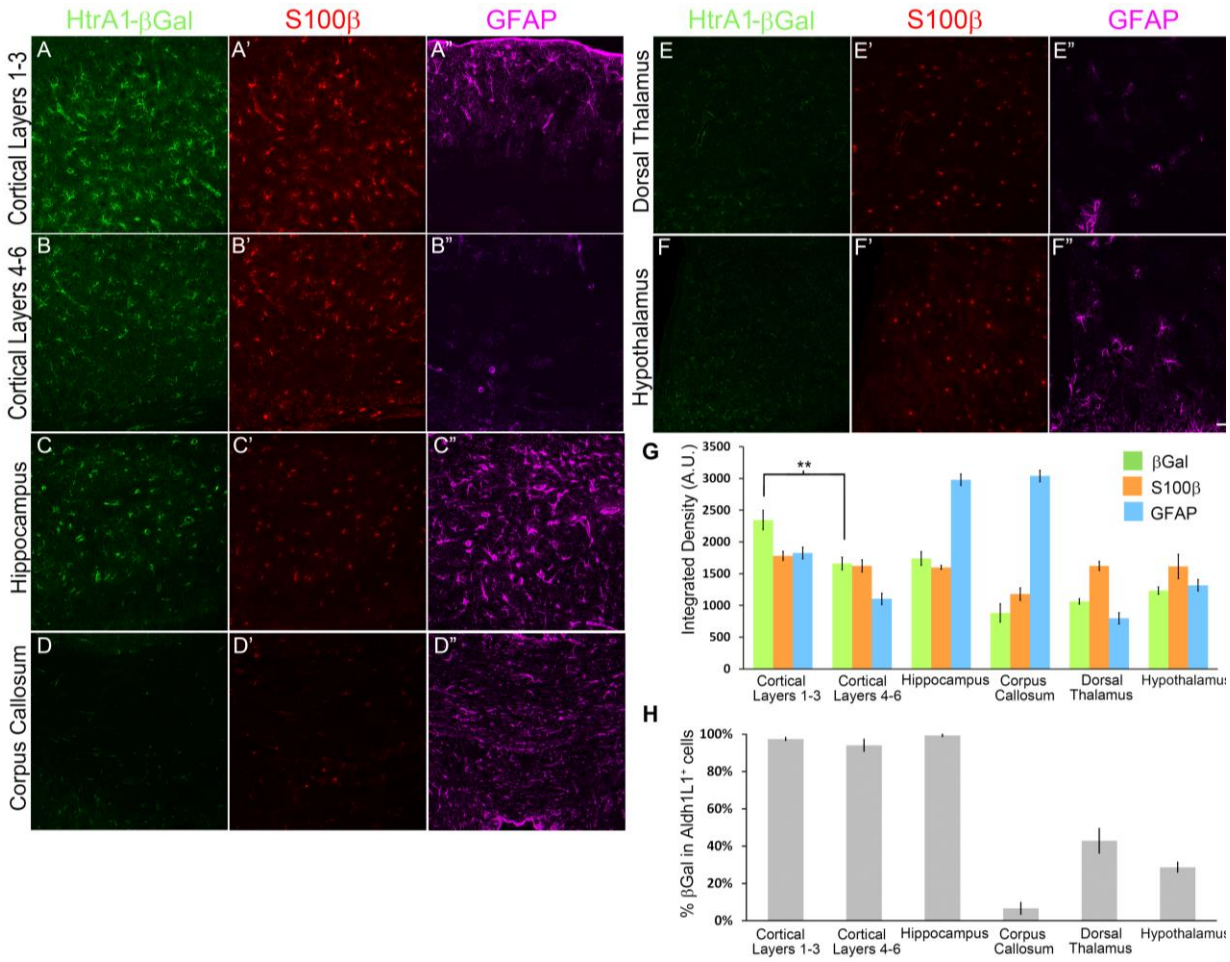

Figure 2.5 HtrA1 is differentially expressed by astrocytes in different forebrain regions.

(A-F") Immunofluorescent images of β-Gal (green), S100β (red), and GFAP (magenta) expression in the forebrain of adult HtrA1-LacZ reporter mice (n=3). Examination of multiple brain regions including upper (layers 1-3, A-A") and deeper (layers 4-6, B-B") neocortex, corpus callosum (C-C"), dentate gyrus of the hippocampus (D-D"), dorsal thalamus (E-E"), and ventral hippothalamus (F-F") revealed varying level of immunofluorescence in multiple brain regions. (G) Quantification of integrated signal density of immunofluorescence for each protein in each brain region. Comparison of upper and deeper cortical layers reveal a significant difference ($p=0.003$) in β-Gal expression level. (H) Quantification of the percentage of Aldh1L1-expressing cells that also express β-Gal in different brain regions of adult HtrA1-LacZ reporter mice (n=3). ** = $p < 0.01$, Scale bar, 50μm.

HtrA1 expression in NSCs inhibits postnatal astrogliogenesis.

Developmentally, we observed HtrA1 mRNA first at embryonic day 14 (E14) enriched at the cortical hem (Fig. 2.6A), the most dorsal neurogenic region that receives high levels of BMP signaling (Furuta et al., 1997). Weaker signal is also detected in the ventral forebrain, which may be neuronal in origin (Launay et al., 2008). At postnatal day zero (P0), HtrA1 expression is found most strongly in the dorsolateral SVZ and weakly in the dorsal cortex (Fig. 2.6B). As more astrocytes populate the neocortex, the number of cortical $HtrA1^+$ cells increases from P7 to P14 and the expression in the SVZ is lost (Fig. 2.6C and 2.6D). The evolving expression profile of HtrA1 during the perinatal period correlates well with the timeline of astrogliogenesis, leading us to ask whether HtrA1 has a role in astrocyte differentiation. We harvested and cultured postnatal NSCs from HtrA1 deleted mice and littermate controls, and differentiated the cells for 3 and 7 days *in vitro* (DIV) in the presence or the absence of BMP4 or noggin. We first quantified the number of GFAP, Nestin, or EdU expressing cells in NSCs differentiated for 3DIV without any cytokines and found a significant increase in the number of GFAP expressing cells (Fig. 6E, 6E' and 6H; control: 14.3±2.15%; mutant: 28.39±1.97%; p=0.0038) and a reduction in Nestin expressing cells when HtrA1 is ablated (Fig. 2.6E, 2.6E' and 2.6I; control: 69.64±3.55%; mutant: 42.04±8.16%; p=0.037). In addition, the numbers of total EdU^+ (control: 19.79±3.9%; mutant: 4.99±3%; p=0.02) and $Nestin^+EdU^+$ (control: 19.41±3.89%; mutant: 4.28±2.41%; p=0.038) proliferating cells were also significantly reduced (Fig. 2.6J). Addition of BMP4 abolished the differences between control and mutant samples (Fig. 2.6F, 2.6F', 2.6H-2.6J), suggesting that sufficiently high levels of BMP4 overcome the inhibitory effects of HtrA1 on astrocyte differentiation. Conversely, blocking BMP signaling with noggin prevented the increase of $GFAP^+$ cells and the decrease of $Nestin^+$ stem cells observed in HtrA1 mutants (Fig.

2.6G, 2.6G', 2.6H-2.6J), suggesting that HtrA1 mediates astrocyte specification at least partly through inhibition of BMP signaling. Taken together, these findings suggest that HtrA1 expression in perinatal NSCs negatively regulates NSC differentiation into GFAP$^+$ astrocytes.

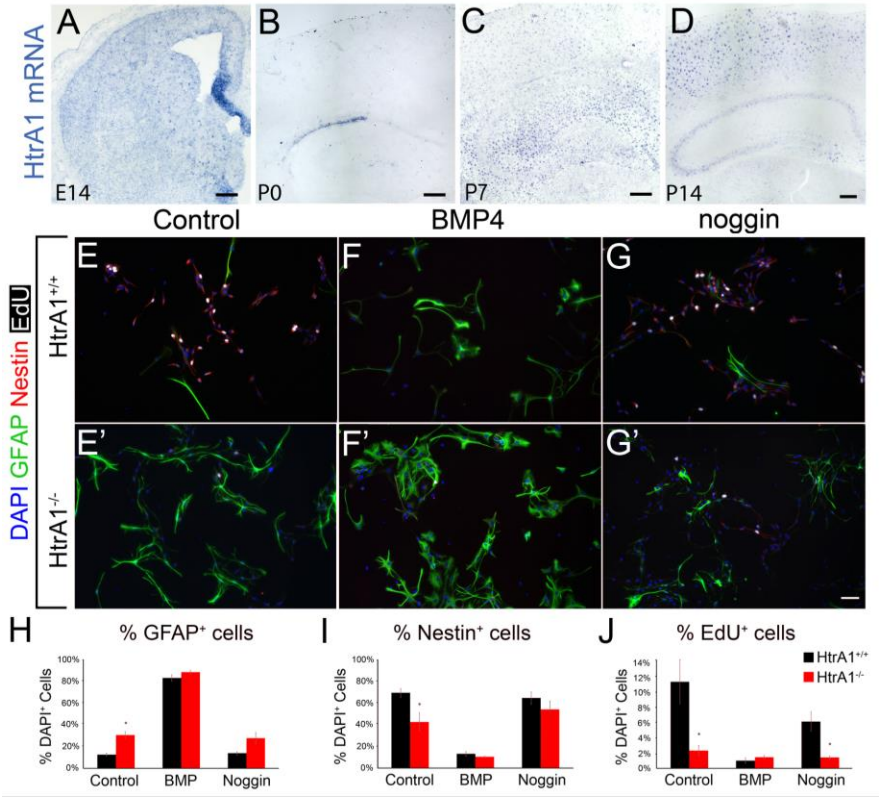

Figure 2.6 Deletion of HtrA1 in postnatal NSCs promotes astrocytic differentiation and maturation.

(A-D) Representative micrograph of HtrA1 mRNA expression by *in situ* hybridization during mouse forebrain development at embryonic day 14 (A) and postnatal days 0, 7, 14 (B, C, and D; n=4 per age). (E-G') Representative micrographs of HtrA1 intact (HtrA1$^{+/+}$; E, F, G; n=5) or deleted (HtrA1$^{-/-}$; E', F', G'; n=4) NSCs after 3 days in vitro (DIV) differentiation. Immunofluorescent stainings of GFAP (green), Nestin (red) and EdU (white) illustrate that GFAP$^+$ astrocytes are significantly increased while Nestin$^+$ NSCs and EdU$^+$ cells are significantly reduced in HtrA1$^{-/-}$ mice. (H-J) Quantification of the number of GFAP$^+$ (H), Nestin$^+$ (I), and EdU$^+$ (J) cells as a percentage of total DAPI$^+$ cells at 3DIV in NSC cultures from HtrA1$^{+/+}$ and HtrA1$^{-/-}$ mice. Scale bar: panels A-D, 200µm; E-G', 50µm. * = p <0.05. Figure created with Stephanie Van Gulden.

To further validate these findings *in vivo*, we investigated whether HtrA1 deletion also alters astrogliogenesis in postnatal mouse brain. Since GFAP only labels a subpopulation of astrocytes in the developing and adult mouse brain, we examined the number of Aldh1L1-expressing ($Aldh1L1^+$) astrocytes in both the dorsal neocortex and the CA1 region of hippocampal primordium at postnatal day 1. To identify dividing astrocyte progenitors, EdU was administered 4 hours prior to sacrifice and the number of $Aldh1L1^+EdU^+$ cells was quantified. In both brain regions, more Aldh1L1+ astrocytes were found in HtrA1 mutants compared to the wild type controls (Fig. 2.7A-2.7B' arrows, 7C). Interestingly, we also observed a significant increase in the number of $Aldh1L1^+EdU^+$ cells in the same brain regions (Fig. 2.7A-2.7B' arrowheads, 2.7D), supporting the idea that HtrA1 may regulate astrocyte differentiation through astrocyte precursor expansion that occurs away from germinal zones (Ge, Miyawaki, Gage, Jan, & Jan, 2012). However, no significant differences were observed at postnatal day 7 in the total number of $Aldh1L1^+$ astrocytes between HtrA1 null mice and the wild type controls in either the cortex or the hippocampus (Fig. 2.7E-2.7F', 2.7G), suggesting that loss of HtrA1 does not lead to long term changes in the total number of astrocytes. Quantification of $Aldh1L1^+EdU^+$ at P7 revealed significant reduction in cortical astrocyte precursors in HtrA1 mutants (Fig. 2.7E-2.7F' arrowheads, 2.7H), suggesting that earlier increases in precursor divisions may result in premature termination of cortical astrocyte generation. Taken together, these findings suggest HtrA1 may regulate the tempo of cortical astrocyte differentiation in the postnatal forebrain.

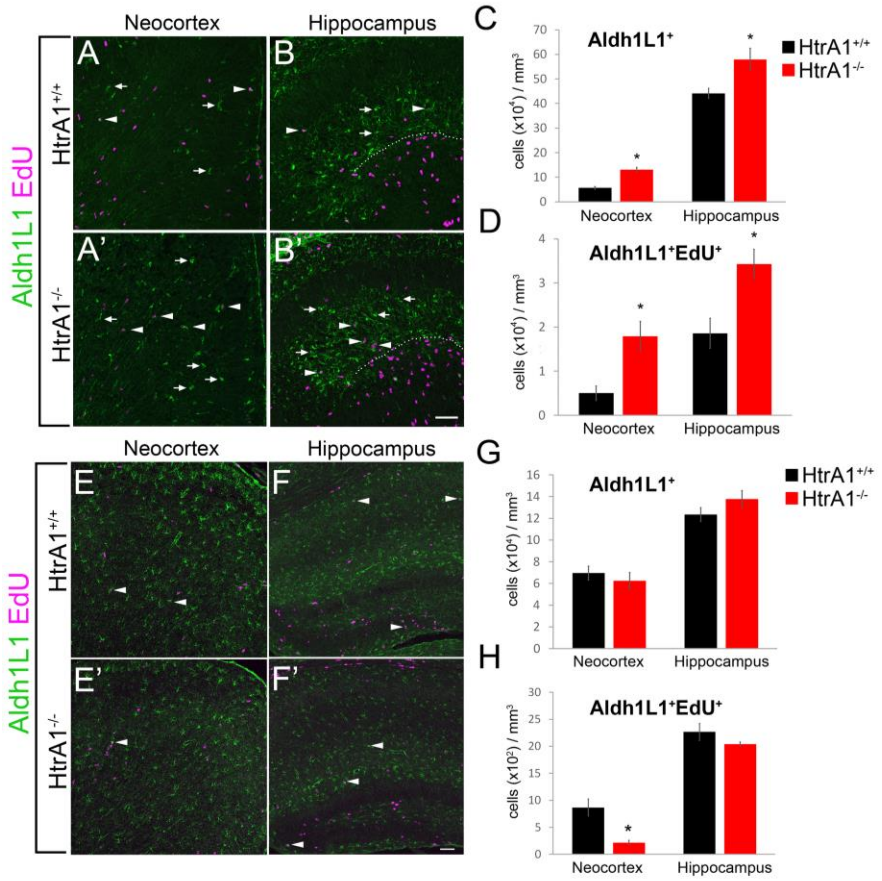

Figure 2.7 *In vivo* analysis of astrocyte differentiation in HtrA1 deleted mice reveal increase in astrogliogenesis at postnatal day 1.

(A-B') Representative immunofluorescent staining of Aldh1L1 (green) and EdU (magenta) in postnatal day 1 (P1) brains of HtrA1$^{+/+}$ (n=3) and HtrA1$^{-/-}$ (n=5) mice. Areas of analysis include dorsomedial neocortex (A, A') and the CA1 region of the hippocampal primordium (B, B'; dotted line demarcates CA1 and dentate gyrus). Aldh1L1^{+} cells (arrows) and Aldh1L1^{+}EdU^{+} precursors (arrowheads) are both significantly increased in both regions in HtrA1$^{-/-}$ mice. (C) Quantification of Aldh1L1^{+} cells in the neocortex and the CA1 region of hippocampus at P1. (D) Quantification of Aldh1L1^{+}EdU^{+} in the neocortex and the CA1 region of Hippocampus. A significant increase in both dividing and non-dividing Aldh1L1^{+} cells were detected in HtrA1$^{-/-}$ mice. (E-F') images of neocortex (E, E') and hippocampus (F, F') stained with Aldh1L1 (green) and EdU (magenta) at postnatal day 7 (P7) in HtrA1$^{+/+}$ (n=3) and HtrA1$^{-/-}$ (n=3) mice. (G, H) Quantification of Aldh1L1^{+} and Aldh1L1^{+}EdU^{+} cells in P7 neocortex and hippocampus. A reduction in Aldh1L1^{+}EdU^{+} cells (arrowheads) in the neocortex of P7 HtrA1$^{-/-}$ mice was observed. All data presented as mean±SEM. Statistical significance was measured by unpaired Student's t-test. Scale bar: 50µm. * = p <0.05. Figure created with Stephanie Van Gulden.

HtrA1 alters astrocyte morphology and extracellular matrix protein expression.

Since the expression of HtrA1 is heterogeneous among astrocytes in different brain regions, we next asked whether HtrA1 plays any role in astrocyte physiology and function using an established cultured astrocyte model (Sahni et al., 2010). We first generated a GFP-tagged lentivirus expressing a short-hairpin RNA (shRNA) to specifically knockdown HtrA1, and validated the reduction of protein production by western blots (Fig. 2.8A). We found that HtrA1 expression is clearly detected in cultured astrocytes derived and maintained in media containing FBS, and the level of expression is reduced significantly when transduced with shRNA expressing lentivirus (Fig. 2.8A). We transduced cultured mouse cortical astrocytes with shRNA-expressing lentivirus and examined their morphology at 7 days and the effects on neurite outgrowth in cortical neuron cocultures at 14 days. Morphologically, we found that astrocytes with reduced HtrA1 exhibited more stellate GFAP-expressing processes compared to control astrocytes, which acquired a more fibroblast-like morphology as expected from serum-containing astrocyte growth conditions (Fig. 2.8B). Quantification of cell size, shape variance, and process number validated this observation (Fig. 2.8C). When HtrA1 knockdown astrocytes were cultured with cortical neurons, reduced neurite length (40.1±4.1μm) was observed compared to neurons cultured with control astrocytes (59.5±4.7μm, $p=0.0145$; Fig. 2.8B and 2.8D). These findings suggest that HtrA1 in astrocytes regulates cellular morphology and modulates neuronal-glial interactions.

Previous studies on the function of HtrA1 as a protease have reported the cleavage of multiple extracellular matrix proteins by HtrA1, including members of the chondroitin sulfate proteoglycan (CSPG) family (Chamberland et al., 2009). Elevated expression of CSPGs post injury is known to inhibit neurite outgrowth in the CNS (Inatani et al., 2001; L. L. Jones,

Margolis, & Tuszynski, 2003), which led us to investigate whether changes in CSPG expression contribute to the reduced cortical neurite length observed in co-cultures with HtrA1 reduced astrocytes. We examined the protein expression of the CNS enriched CSPG, neurocan, in cultured astrocytes with and without HtrA1 knockdown, and found that the level of neurocan protein is significantly increased in astrocytes with reduced HtrA1 (251.67±8.01% compared to control, p=0.00013, Fig. 2.8E). Conversely, incubating cultured wildtype astrocytes with recombinant HtrA1 protein leads to a reduction in the level of CSPGs, detectable by either pan-CSPG or Neurocan specific antibodies (data not shown). These findings support the idea that altered extracellular matrix, including increased levels of CSPGs such as neurocan, may contribute to inhibition of neurite outgrowth observed in coculture with HtrA1 deficient astrocytes.

We next sought to validate our *in vitro* findings by examining astrocytes in adult HtrA1 mutant mice, focusing on the $GFAP^{+}$ cells in layer 1 of the dorsomedial cortex. At 6 months, HtrA1 mutant mice show increased GFAP intensity (control: 754.3±91.79; mutant: 1124.05±77.2) and an enlarged, hypertrophic cellular morphology (Fig. 2.8F and 2.8G). However, quantification of GFAP-expressing cells in layer 1 revealed similar numbers in HtrA1 mutants and control mice (Fig. 2.8G). To distinguish the role of HtrA1 in astrocyte differentiation from its role in regulation of GFAP expression, we examined the same brain region for changes in the expression of the pan-astrocytic marker Aldh1L1 and found no significant difference between HtrA1 mutant and control mice (Fig. 2.8F and 2.8G). Similar to our findings *in vitro*, examination of CSPG expression in $HtrA1^{-/-}$ cortical layer 1 revealed an increase in signal intensity (Fig. 2.8G and 2.8H; control:989.32±60.9; mutant:1290.04±54.45), while the basement membrane enriched collagen IV expression surrounding the vasculature

appeared unaffected (Fig. 2.8H). Finally, since HtrA1 has been shown to regulate expression of TGFβ family proteins in other organs (Oka et al., 2004), we asked whether astrocytes lacking HtrA1 exhibit changes in both BMP4 and TGFβ protein expression. Western blot analyses using protein harvested from HtrA1 null cultured astrocytes revealed significant increases in both BMP4 and TGFβ precursor proteins (Fig. 2.8I, pro-BMP4 and pro-TGFβ), suggesting that HtrA1 participates in the cleavage of the immature forms of BMP4 and TGFβ proteins. Interestingly, we observed a marked reduction in the mature TGFβ but a trend toward increased levels of mature BMP4 in HtrA1 deleted astrocytes (Fig. 2.8I), suggesting that HtrA1 may differentially regulate the levels of mature BMP and TGFβ family members. These observations suggest that HtrA1 may be functionally important for the regulation of extracellular matrix and TGFβ family proteins in astrocytes.

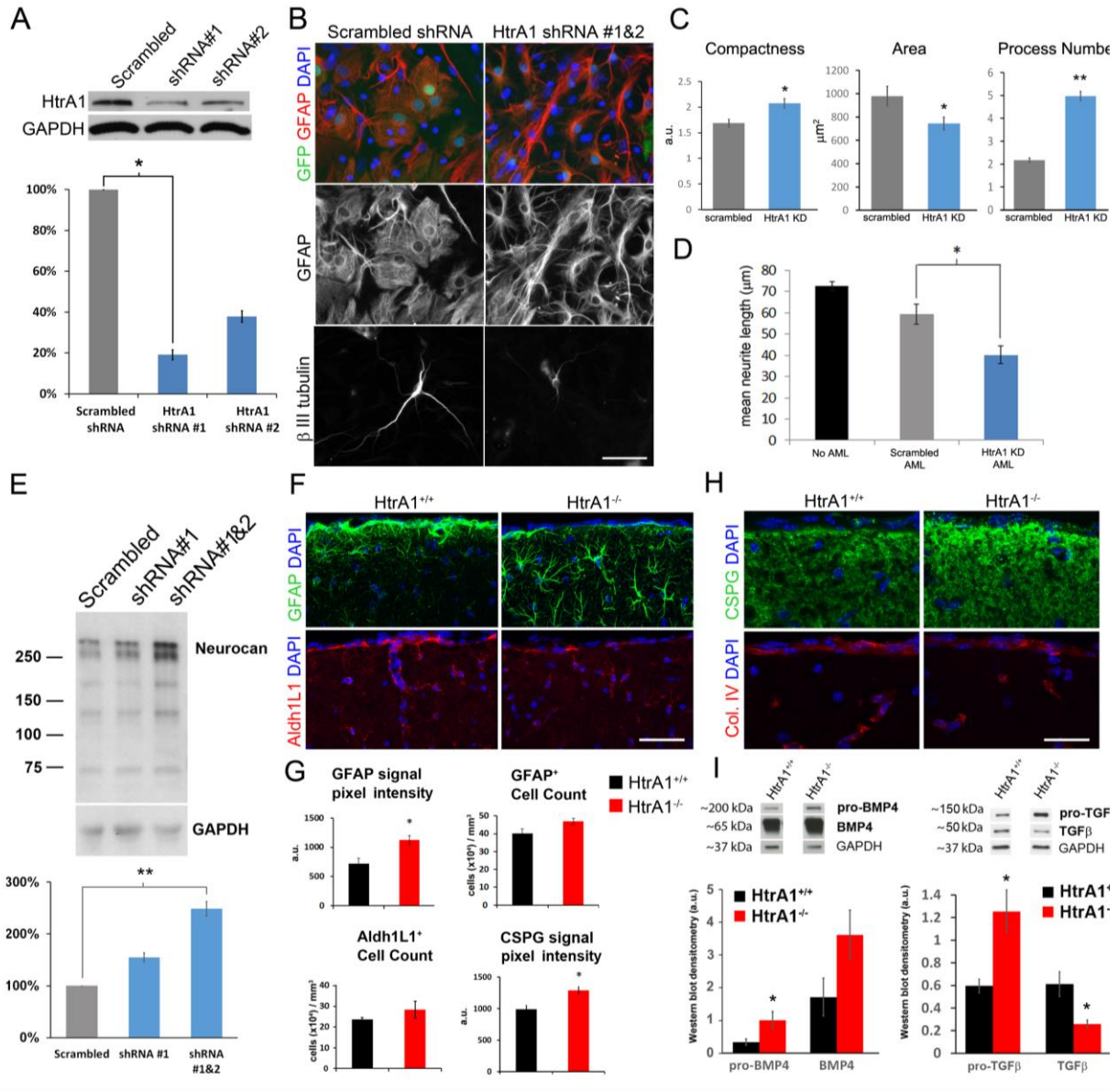

Figure 2.8 Loss of HtrA1 leads to morphological, biochemical, and functional changes in astrocytes.

(A) Validation of HtrA1 shRNA lentivirus efficiency by western blot analysis. (B) Representative micrograph of astrocyte (GFAP, red in top panel) and cortical neuron (βIII tubulin, bottom panels) co-culture studies with GFP-tagged scrambled or HtrA1 shRNAs (green in top panel). (C) Quantification of morphological changes of HtrA1 knockdown (HtrA1 KD, n=179) and control (scrambled, n=78) cultured astrocytes. Significant changes were observed in compactness (p=0.008), cell area (p=0.042), and process number (p=3.4E-6) (D) Quantification of cortical neurite length under culture conditions without an astrocyte monolayer (No AML) or with astrocytes transduced with scrambled (Control AML) or HtrA1 shRNA (HtrA1 KD AML). Significant reduction of neurite outgrowth (p=0.0145) was observed when HtrA1 expression is reduced in astrocytes (n=4). (E) Western blot for Neurocan in cultured astrocytes transduced

with either scrambled control, HtrA1 shRNA #1, or HtrA1 shRNA #1 and #2 (n=3). Lower panel graph represents quantification of relative signal intensity to the scrambled shRNA control condition, demonstrating HtrA1 deficient astrocytes express significant higher Neurocan ($p=0.003$). (F) Immunofluorescent staining of GFAP expressing (green) and Aldh1L1 (red) expressing astrocytes in cortical layer 1 of 6-month-old wild type control (n=4) and HtrA1 null mutant (n=5) mice. (G) Quantifications of GFAP and CSPG signal intensity, GFAP expressing cells, and Aldh1L1 expressing cells in cortical layer 1 of HtrA1 control and mutant mice. (H) Immunofluorescent staining of CSPG (green, CS-56 antibody) and Collagen IV (red) in HtrA1 mutant mice shows an increase in CSPG expression while Collagen IV expression remains unchanged. (I) Western blots of BMP4 and TGF-β from $HtrA1^{+/+}$ and $HtrA1^{-/-}$ astrocytes after 7 days of differentiation. Two bands were detected that correspond to the pre-processing form (~200kDa for BMP4 and 150kDa for TGF-β) and the mature dimer (~65kDa for BMP4 and 50kD for TGF-β). Deletion of HtrA1 led to a near two-fold but not statistically significant increase in pro-BMP4 and mature BMP4, while pro-TGF-β and mature TGF-β are significantly increased and reduced respectively. All data presented as mean±SEM. Statistical significance measured by 1-way ANOVA with Tukey's *post hoc* test for Figs 8A, 8D, and 8E, and student t-test for Fig. 8C, 8G, and 8H. Scale bar: panel B, 25μm; panels F and H, 50μm; * = $p < 0.05$; ** = $p < 0.01$. Figure created with Stephanie Van Gulden.

Since mutation in HtrA1 in human is linked to cerebral vascular disease CARASIL, we asked whether loss of HtrA1 changes the overall morphology and distribution of the cerebral vasculature in 6-month-old adult mouse brains. Despite a significant increase in GFAP immunoreactivity in HtrA1 mutant cortex (Fig. 2.9A and 2.9B), no change in the overall expression pattern and signal density of CD31, an endothelial cell marker, was observed in the dorsal cortex (Fig. 2.9A, 2.9C). There were no changes in distribution or density of the pericyte marker PDGFR-β (Fig. 2.9A, 2.9D). Based on CD31 expression, we next performed a series quantitative analyses of cerebral vasculature properties that included vessel density (Fig. 2.9E, vessel percentage area), vessel branching frequency (Fig. 2.9E, junctions per area), number of vessel endpoints (Fig. 2.9E, endpoints per area), total and average vessel length, as well as vessel pattern uniformity (Fig. 2.9E, lacunarity). We did not observe significant differences between controls and HtrA1 mutants in any of these measures. Lastly, to address whether increased GFAP immunoreactivity in HtrA1 mutant cortex is the result of altered neuroinflammatory responses, we examined the morphology and number of microglia by CD11b and Iba1 IHC. Again, no differences were detected between HtrA1 mutants and controls (Fig. 2.9F). These findings suggest that the overall distribution and morphology of the neurovascular and neuroimmune cells were not significantly affected by the loss of HtrA1 in young adult mice.

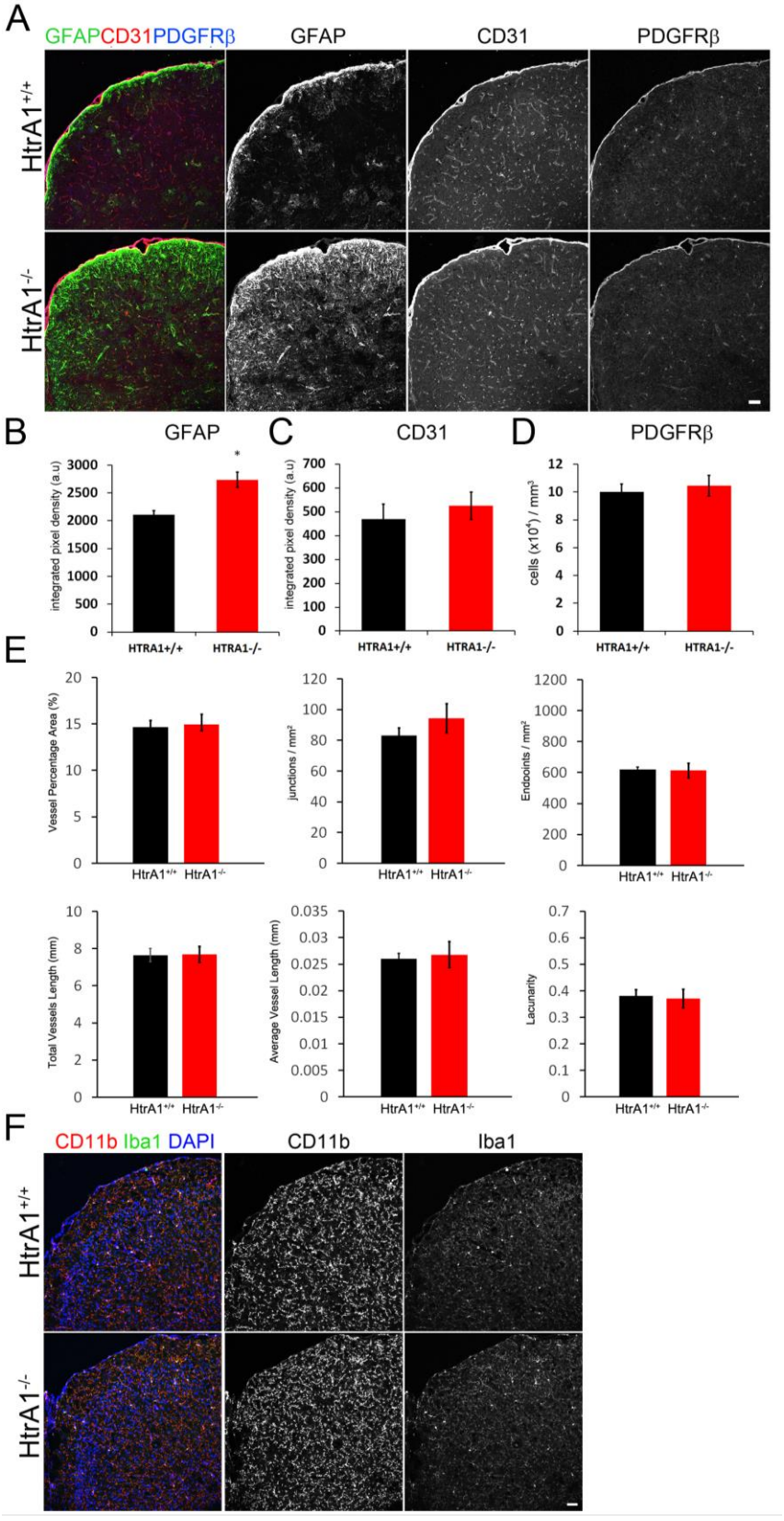
A
GFAPCD31PDGFRβ
GFAP
CD31
PDGFRβ
HtrA1+/+
HtrA1-/-
B
GFAP
integrated pixel density (a.u)
HTRA1+/+
HTRA1-/-
C
CD31
integrated pixel density (a.u)
HTRA1+/+
HTRA1-/-
D
PDGFRβ
cells (x10⁴) / mm³
HTRA1+/+
HTRA1-/-
E
Vessel Percentage Area (%)
junctions / mm²
Endpoints / mm²
Total Vessels Length (mm)
Average Vessel Length (mm)
Lacunarity
HtrA1+/+ HtrA1-/-
F
CD11b Iba1 DAPI
CD11b
Iba1
HtrA1+/+
HtrA1-/-

Figure 2.9 Deletion of HtrA1 does not alter vascular or immune cell morphology or distribution in young adult mouse neocortex.

(A) Representative micrographs illustrating the overall distribution and density of neurovascular unit components marked by GFAP (green), CD31 (red), and PDGFRβ (blue) in 6-month-old HtrA1 control (n=6) and null mutant cortex (n=4). (B-D) Graphs showing the integrated density quantification of astrocytes (B, $GFAP^+$ cells) and endothelial cells (C, $CD31^+$ cells), as well as pericyte numbers (D, $PDGFR\beta^+$ cells in HtrA1 control and null mutant cortex. (E) Quantification of blood vessel properties in the cerebral cortex of 6-month-old adult $HtrA1^{+/+}$ and $HtrA1^{-/-}$ mice. CD31 IHC signal was used for measure vessel properties listed on the Y-axis of each graph. No significant differences were detected for between HtrA1 mutant (n=6) and control (n=4) mice. (F) Representative images of microglia markers CD11b (red) and Iba1 (green) in HtrA1 control and mutant mouse cortex. No significant differences were observed, suggesting HtrA1 deletion does not induce inflammatory responses in uninjured adult mouse forebrain. Scale bar, 50□m. * = < 0.05.

HtrA1 in reactive astrogliosis regulates lesion area size and proliferation after injury

The morphology of HtrA1 deficient astrocytes is reminiscent of reactive astrocytes that surround lesions post injury, leading us to investigate whether HtrA1 is involved in the astrocytic response to injury. We first performed cortical stab wound injury (SWI) in the dorsal-medial cortex of wild-type mice, and examined the expression of HtrA1 by mRNA *in situ* hybridization at 3 days post injury (3DPI). We found that reactive astrocytes surrounding the lesion area expressed high levels of HtrA1 (Fig. 2.10A), including deeper layer astrocytes that normally have low GFAP and HtrA1 expression (Fig. 2.10A inset). The change in HtrA1 expression was accompanied by elevated BMP4 expression, which was strongly expressed by cells surrounding the lesion after injury, in contrast to the gradient in uninjured controls (Fig. 2.10B). Western blot analysis of injured cultured astrocytes also confirmed increased levels of HtrA1 protein, along with increased levels of neurocan protein (Fig. 2.10C).

We next asked whether BMP signaling is necessary for HtrA1 expression in normal and injured astrocytes *in vivo*. We examined HtrA1 expression in mice lacking BMP receptor 1a (BMPR1a) in GFAP expressing cells (GFAP-Cre; BMPR1a$^{fx/-}$), and observed a loss of HtrA1 expression in GFAP expressing astrocytes in cortical layer 1 (Fig. 2.10D, inset). However, deletion of BMPR1a did not alter HtrA1 upregulation in reactive astrocytes (Fig. 2.10D, inset), suggesting that molecular signals other than BMPs contribute to increased HtrA1 expression post injury.

Since astrocytic responses after injury are critical for BBB repair and lesion reduction, we next asked whether HtrA1 ablation affects the lesion area size or vascular repair at 3DPI (Fig. 2.10E-2.10G). Measurement of the lesion area surrounded by GFAP immunostaining revealed a significant increase in HtrA1 mutants compared to the controls (Fig. 2.10E, 2.10F;

control=118943±1895μm^3; mutant=260831±13745μm^3; p=8.7E-7). The number of EdU$^+$ dividing cells near the lesion area was also significantly increased (Fig. 2.10E, 2.10G**;** control=30.46±6.62; mutant=224.95±30.9; p=2.4E-7). Co-labeling with EdU, CD31 and GFAP revealed that proliferation was increased in endothelial cells (Fig. 2.10G; control= 18.19±4.79; mutant=69.22±9.04; p=0.02) but not in GFAP$^+$ astrocytes (Fig. 2.10G**;** control=0.40±0.47; mutant=6.61±2.26; p=0.08). Further analysis of EdU incorporating cells surrounding the lesion revealed that Iba1 expressing microglia constitute the majority of the EdU$^+$ cells, indicating that HtrA1 deletion leads to elevated inflammatory responses (Fig. 2.10H and 2.10I). These findings suggest that HtrA1 expression in astrocytes regulates brain injury recovery by limiting vascular and immune cell proliferation as well as controlling lesion size.

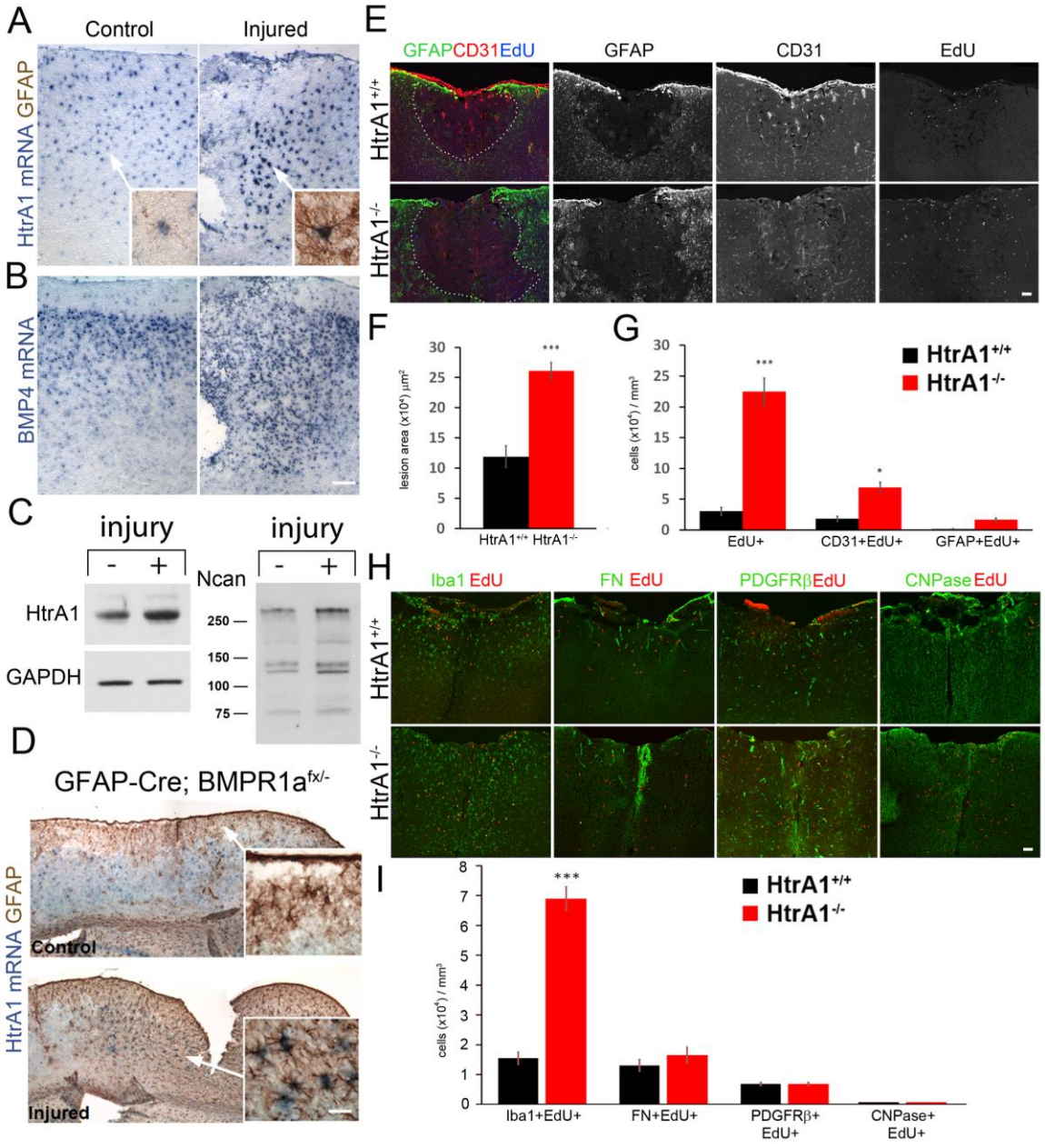

Figure 2.10 HtrA1 expression in reactive astrocytes regulates lesion size and proliferation post injury.

(A) Main panels illustrate ISH detection of HtrA1 mRNA (without GFAP IHC) in P60 wild type control (left panel, n=6) and injured (right panel, n=6) mice, which revealed an increase in HtrA1 expression surrounding the injury site 3 days after cortical stab wound injury. Insets shows HtrA1 mRNA in cortical layer 4 where it is detected in low GFAP-expressing astrocytes in the control but becomes strongly expressed in high GFAP-expressing reactive astrocytes in the injured brain. (B) ISH of BMP4 mRNA in adjacent sections to panels in 10A. The increase in HtrA1 in reactive astrocytes correlates with an increase in BMP4 surrounding the lesion. (C) Western blot of HtrA1 and Neurocan (Ncan) protein in cultured cortical astrocytes with (+, n=3)

and without injury (-, n=3). An increase in both HtrA1 and Neurocan was found in injured astrocytes relative to the control astrocytes. (D) Representative micrographs of HtrA1 mRNA and GFAP protein expression in GFAP-Cre; BMPR1a1$^{fx/-}$ mutant mice without (n=5) and with (n=4) cortical stab wound injury. Deletion of BMP receptor 1a in astrocytes diminishes layer 1 HtrA1 expression but fails to reduce HtrA1 expression in reactive astrocytes post injury. (E) Immunofluorescent co-labeling of GFAP (green), CD31 (red), and EdU (blue) in the lesion area of HtrA1 wild type (n=4) and null mutant mice (n=3). Uninjured brains do not show significant differences in cerebral vasculature between wild type and HtrA1 deleted neocortex. (F) Quantification of lesion area size in HtrA1 wild type and null mutant mice. (G) Quantification of total proliferating cells (EdU^{+}), proliferating endothelial cells (CD31^{+}EdU^{+}), and proliferating astrocytes (GFAP^{+}EdU^{+}) in the lesion area of HtrA1 wild type and null mutant mice. (H) Representative images of EdU-incorporating microglia (Iba1), fibroblasts (FN), pericytes (PDGFR-β) and oligodendrocytes (CNPase) in injured HtrA1$^{+/+}$ and HtrA1$^{-/-}$ mice. (I) Quantification of EdU+ cell types presented in panel J. All data presented as mean±SEM. Statistical significance was measured by unpaired Student's t-test. Scale bar = 50μm. * = $p < 0.05$; *** = $p < 0.001$. Figure created with Stephanie Van Gulden and Chian-Yu Peng.

IV. DISCUSSION

One of the goals for this study was to identify novel molecular markers of differentiated astrocytes. A common complication associated with studying astrocyte differentiation and diversity is that classic astroglial markers such as GFAP and astrocyte-specific glutamate transporter (GLAST) are also expressed by adult NSCs. S100β and glutamate synthetase, two well-accepted astrocyte markers that are not found in NSCs, are expressed in ependymal cells, neurons and oligodendrocytes in the CNS (Bernstein et al., 2014; Carlén et al., 2009; Vives, Alonso, Solal, Joubert, & Legraverend, 2003). Even Aldh1L1, a more recent addition to the list of pan-astrocytic markers, is also found in both differentiated astrocytes and postnatal NSCs (Foo & Dougherty, 2013). In short, the identification of differentiated astrocytes requires a combination of currently existing markers. We have demonstrated here that HtrA1 is expressed by mature astrocytes but not by adult NSCs. This unique property will allow future investigations to distinguish two functionally distinct cell types that share significant molecular similarities in the adult mouse brain.

We have also demonstrated that HtrA1 mRNA is not found in neurons or cells in the oligodendroglial lineage, and co-expression analysis of additional cell type markers in HtrA1-LacZ mice validated this finding and confirms astrocyte specificity of HtrA1 expression. Two recent RNAseq studies that examined neural and non-neural cell types in the mouse brain identified HtrA1 as astrocyte enriched (Zeisel et al., 2015; Y. Zhang et al., 2014). However, one of the studies suggested that HtrA1 may also be expressed at low levels in oligodendrocyte precursors (OPCs) and endothelial cells during postnatal development (Y. Zhang et al., 2014). Our HtrA1 mRNA *in situ* with OPC marker Olig2 at postnatal day 14 did not show any $Olig2^{+}$ cells expressing HtrA1, and we did not detect β-Gal expression in endothelial cells in the adult

neocortex. This discrepancy may be due to detectability of expression in our method or limitations in cell type isolation in the published report. Regardless, the ability to identify select astrocyte populations will be beneficial in studying astrocyte diversity, particularly when combined with a pan astrocyte specific marker such as Aldh1L1 or other existing astrocyte subtype markers like GFAP.

Based on combinatorial expression of HtrA1, S100β, and GFAP, we observed astrocytes that are $HtrA1^{hi}GFAP^{hi}S100\beta^{hi}$ (cortical layers 1 to 3 and hippocampus); $HtrA1^{low}GFAP^{low}S100\beta^{hi}$ (cortical layers 4 to 6); $HtrA1^{low}GFAP^{hi}S100\beta^{low}$ (corpus callosum); and $HtrA1^{low}GFAP^{low}S100\beta^{hi}$(dorsal thalamus). Whether these molecularly distinct astrocytes have unique developmental origin is an intriguing question. Transgenic and adenovirus-based fate-mapping of perinatal NSCs from different forebrain regions has demonstrated contributions of astrocytes from regionally specific progenitors in a radial fashion (Tsai et al., 2012). The broad nature of HtrA1 expression suggests that multiple regional progenitors can give rise to $HtrA1^{+}$ astrocytes, and that heterogeneity of HtrA1 expression may reflect differences in local signals. The increase in expression in deeper layer astrocytes after injury suggests that HtrA1 can be modulated by changes in the local environment. Another example of such a phenomenon is the expression of Gli1 in astrocytes of the deeper cortical layers. Ablation of Sonic hedgehog (Shh) signaling from neighboring neurons significantly reduces Gli1 expression in deep layer astrocytes without affecting total astrocyte numbers (Garcia, Petrova, Eng, & Joyner, 2010). In view of the antagonistic roles of Shh and BMP during neuronal specification (Jessell, 2000), it is also intriguing that there is a reciprocal pattern of expression between BMP-regulated HtrA1 and Shh-regulated Gli1 in cortical astrocytes. Future studies that examine how Shh signaling affects HtrA1 expression may provide new insights into the establishment of cortical astrocyte diversity.

HtrA1 was also selected for further analysis because of its known inhibitory role in TGF-β family protein signaling (Oka et al., 2004). Our microarray and qPCR results demonstrated that HtrA1 expression is a target of BMP4 activation, suggesting that increases in HtrA1 expression in astrocytes may act as an auto-regulatory response to modulate the levels of BMP and/or TGF-β ligands through proteolysis. The increase of BMP4 in HtrA1 null astrocytes, as well as the loss of HtrA1 in BMPR1a deleted layer 1 astrocytes, support this hypothesis. The intriguing loss of HtrA1 expression in cortical layer 1 after BMPR1a deletion likely reflects loss of a region-specific source of BMP ligand expression; for example, meningeal fibroblasts express high levels of BMP ligands including BMP7 (Y. Choe, Huynh, & Pleasure, 2014). However, the maintenance of HtrA1 expression in deeper cortical layer reactive astrocytes in BMPR1a deficient mice suggests that BMPs are not the sole regulator of HtrA1 expression. TGF-β proteins are also known cleavage targets of HtrA1, and were shown to be elevated in HtrA1 null astrocytes in our study. In many systems, BMP4 and TGF-β signaling are often viewed as antagonistic in nature (Oshimori & Fuchs, 2012; Zeisberg et al., 2003; Zode, Clark, & Wordinger, 2009). How HtrA1 is regulated by these cytokines and vice versa in different cellular context is central to elucidating the role of HtrA1 in astrocytes.

HtrA1 also is known for its cleavage of extracellular matrix proteins (Chamberland et al., 2009; A. Jones et al., 2011). This is consistent with our observation of increased Neurocan expression in HtrA1 knockdown astrocytes, suggesting that astrocytic expression of HtrA1 inhibits Neurocan accumulation in astrocytes. Neurocan is also a known target of TGF-β family signaling (Asher et al., 2000; Fuller et al., 2007), making it unclear whether the increase in Neurocan levels in HtrA1 deficient astrocytes is a direct effect from reduced ECM protein cleavage or the result of increased BMP signaling. Regardless, co-culture studies suggest that

astrocyte expression of HtrA1 is permissive for cortical neuron outgrowth, consistent with influences of astrocytic HtrA1 on neighboring cells through ECM modification. This finding also suggests that increased HtrA1 in reactive astrocytes after injury may play a positive role in the regeneration of neuronal processes.

In the context of brain injury, we found that loss of HtrA1 leads to an increase in lesion area size and higher proliferation in $CD31^+$ and $Iba1^+$ cells. As we only detected increased HtrA1 in reactive astrocytes post injury, these findings suggest astrocytic HtrA1 non-cell-autonomously modulates the injury milieu. Our ISH of BMP4 and HtrA1 show concomitant increases in mRNA levels 3 days post injury, raising the possibility of astrocytic HtrA1 acting as a negative feedback regulator of elevated TGF-β family proteins associated with the early inflammatory response (Schachtrup et al., 2010; Simon et al., 2017). We hypothesize that in the absence of HtrA1, unchecked levels of TGF-β family proteins in the injury milieu further simulates the immune response and angiogenesis, resulting in increased proliferation of microglia and endothelial cells in injured HtrA1 null mice. Alternatively, ECM modifications necessary for proper neurovascular unit remodeling may be defective in the absence of HtrA1. Due to the feedback-inhibitory relationship between TGF-β/BMP with HtrA1, deletion of HtrA1 likely results prolonged elevation of TGF-β/BMP signaling in the injury site, which may have beneficial or detrimental effects on the recovery process in the long term. Further analyses of injury responses at additional time points following brain injury will be critical in understanding how astrocytic HtrA1 modulates cytokine and ECM mediated recovery responses post injury.

Mutation in HtrA1 is linked to CARASIL, a rare small blood vessel disease that is characterized by endothelial cell mineralization and associated with high risks of stroke and cognitive impairments (Hara et al., 2009). Several studies have hypothesized that the pathology

of CARASIL is the result of dysregulation of TGF-β signaling (Beaufort et al., 2014; Hara et al., 2009; Shiga et al., 2011), although a consensus on how HtrA1 modulates TGF-β signaling has yet to be reached. Our study demonstrated that HtrA1 in the adult mouse brain is only expressed by astrocytes, and is not detected in endothelial cells or pericytes surrounding the vasculature. We also showed that HtrA1 deletion increases the expression of astrocyte-produced TGF-β family proteins, consistent with changes observed in CARASIL patients (Hara et al., 2009). Dysfunction of astrocytic proteins has been previously linked to neurodegenerative diseases with oligodendroglial and neuronal pathology (Haidet-Phillips et al., 2011; Marignier et al., 2010). Our findings raise the possibility that CARASIL may be astrocytic in origin. Our findings suggest deletion of HtrA1 in astrocytes may increase TGF-β levels and altered the ECM environment at the BBB, which in turn leads to the vascular pathology. In addition, heterogeneity of HtrA1 expression among forebrain astrocytes may reflect, or result in, differential TGF-β/BMP signaling in different regions. A recent report demonstrated molecularly distinct astrocyte subtypes respond differently to inflammatory stimuli from microglia, and this differential response can be modulated by TGF-β signaling (Liddelow et al., 2017). Future studies that isolate and examine the interactions of HtrA1-expressing and non-expressing astrocytes with microglia or vascular endothelial cells will provide insights into functional astrocyte diversity, and may contribute to the treatment of brain injury and cerebral vascular diseases.

Chapter 3

BMP Receptor Subunits BMPR1a and BMPR1b Have Different Transcriptional Effects in Neural Progenitor Cells

I. Introduction

Bone morphogenetic protein signaling (BMP) is a key pathway involved in regulating embryonic development and multiple cell processes. As a moderator of cell cycle dynamics and differentiation of neural progenitor cells (NPCs), the BMP family has numerous ligands and multiple receptors in order to fine-tune its ability to regulate a wide variety of cellular functions. Of particular interest are the receptor subunits, as there is a large body of evidence that suggests the diversity of BMP effects may be due to signaling through the different BMP type 1 receptors (Dijke, Yamashita, Sampath, et al., 1994b), and the same ligand bound to different receptors may result in disparate cellular outcomes.

BMP signaling occurs through heterotetrameric receptors comprised of two type 2 receptor subunits, and two type 1 receptor subunits. In the central nervous system, there are three different type 1 receptor subunits that have been identified, BMPR1a (Activin receptor 3 or ALK3), BMPR1b (Activin receptor 6 or ALK6), and Activin receptor 2 (ALK2). Of primary interest are BMPR1a and BMPR1b, which are expressed throughout the brain at various stages of development and have high affinities for the BMP4 ligand. Some studies have shown them to have overlapping functions, such as in ovarian tumor suppression (Edson et al., 2010) and embryonic dorsal cell fate determination (Wine-Lee et al., 2004). However, evidence has emerged to support their divergent and frequently opposing functions. Developmentally,

BMPR1a and BMPR1b play different roles in cartilage formation, with BMPR1a regulating differentiation of chondrocytes and BMPR1b promoting cellular apoptosis (Zou, Wieser, Massagué, & Niswander, 1997b). A viral vector form of constitutively activated BMPR1a induces expression of BMPR1b mRNA during embryonic chondrogenesis. The diverse effects of BMPR1a versus BMPR1b signaling can also be seen in the spinal cord (Bhalala et al., 2012; Sahni et al., 2010). BMP type 1 receptors likely act at different stages of the neural stem cell cycle and differentiation pathway, with BMPR1a being implicated in the induction of BMPR1b embryonically (Panchision et al., 2001). BMPR1a promotes embryonic NSC proliferation, while BMPR1b, due to its later expression pattern, may be involved in NSC differentiation (Panchision et al., 2001). Constitutive activation of either type I BMP receptor promotes dorsal cell fate specification in chick embryos (Yamauchi et al., 2008). BMPR1b, unlike BMPR1a, is involved in neuronal axon path determination during development (Yamauchi et al., 2013). However, the differences between the two receptor subunits have not been examined in detail during other stages of development, and it is well-known that while BMP may have pro-proliferative effects during embryonic development (Panchision et al., 2001), it has pro-differentiation and anti-proliferative effects on NPCs postnatally and during adulthood (Bond et al., 2014).

Of the few studies that have looked at the cell fate effects of type I BMP receptors, many have used constitutively active and dominant negative constructs of the receptors, which often have off-target and biologically irrelevant effects (Brederlau et al., 2004). Given the lack of understanding of the downstream mechanisms that mediate the diverse effects of BMPR1a and BMPR1b, we chose to examine the downstream transcriptional effects of type I BMP receptor in NSCs through ablation of individual receptor subunits. We found that while there are numerous targets that overlap due to either BMPR1a and BMPR1b activation, ablation of receptor subunits

has revealed hundreds of uniquely regulated targets. In addition, we have uncovered numerous BMP target genes that have not been previously identified in the literature. Through our pathway analyses, we have identified many BMP-regulated biological processes, some of which have been examined in previous studies, such as suppression of oligodendrocyte development, but others of which are relatively poorly understood, such as broader regulation of transcriptional processes or construction of cilia. These biological processes that have not been previously studied in the context of BMP signaling provide new potential targets for future studies.

II. Materials and Methods

Animals All mice were housed in groups and maintained on a 12-hour light/dark cycle with *ad libitum* access food and water. All experiments were performed with both male and female mice in each condition and analyzed without sex separation. Handling and treatment of animals were in accordance with Northwestern University IACUC regulations and policies. $BMPR1a^{fx/fx}$ mice (Mishina, Hanks, Miura, Tallquist, & Behringer, 2002), $BMPR1a^{+/+}$ mice, and $BMPR2^{fx/fx}$ mice (Beppu, Lei, Bloch, & Li, 2005) were each crossed with mice harboring a Rosa-CAG-LSL-ZsGreen1 transgene (Jackson Laboratory) and maintained on a homozygous background. $BMPR1b^{-/-}$ transgenic mice (Yi, Daluiski, Pederson, Rosen, & Lyons, 2000) were maintained on a heterozygous background and mated to produce +/+, +/-, and -/- offspring due to homozygous progeny being infertile.

Neural Stem Cell Dissection and culture Dissection for subventricular zone (SVZ) neural stem cells was performed on postnatal day 1 animals by using forceps to mechanically remove the lateral ganglionic eminence, followed by chemical dissociation using 0.05% trypsin with EDTA. Cells were maintained and passaged in a floating culture with DMEM/F12 media

(Gibco/Invitrogen) with N2, B27, and 20ng/mL EGF (Millipore). Cells used for RNA sequencing were additionally cultured in 250ng/mL Noggin (R&D). For cells to be harvested for RNA to be used in RNA sequencing, cultures dissected from transgenic mice had Adeno-Cre-GFP virus (Vector Biolabs) added at a concentration of 1:2000 from stock to induce Cre-mediated recombination the day after passage 2. Virus was removed after 48 hours. For $BMPR1a^{+/+}$, $BMPR1a^{fx/fx}$, and $BMPR2^{fx/fx}$ cells, fluorescence-activated cell sorting (FACS) was used 7 days after infection to purify only cells that had undergone recombination. Cells without virus added were used as a gating control for FACS. $BMPR1b^{-/-}$ cells also had Ad-Cre-GFP virus added and were prepared in parallel, but did not undergo FACS. Cells harvested for RNA for qPCR validation did not undergo FACS, and were not cultured in Noggin.

RNA isolation and Quantitative RT-PCR For cells to be used in RNA sequencing, cell culture media was replaced and either Noggin (250ng/mL, R&D) or BMP4 ligand (50ng/mL, R&D) added at for 4 hours before RNA collection. During this time, EGF (Millipore) concentration was reduced to 2ng/mL. For cells used for qPCR validation, 50ng/mL BMP4 ligand was simply added to experimental cultures for 6 hours before RNA collection, as these cells were not previously maintained in Noggin. RNA was isolated using the RNeasy Micro RNA extraction kit according to manufacturer's instructions (Qiagen). Reverse transcription of total RNA for qPCR analysis was performed by using the SuperScript IV kit (ThermoFisher). Real-time PCR was conducted with the system using SYBR Green Master Mix (Applied Biosystems, Foster City, CA, USA). Reactions were performed in triplicate and reached threshold amplification within 40 cycles. Levels of transcripts were determined relative to GAPDH using the $2^{-\Delta\Delta Ct}$ method. Primers were sourced from Primerbank, verified by NCBI Blast, and validated in house. *Gapdh:* (F: GTCGTGGATCTGACGTGCC, R:

TGCCTGCTTCACCACCTTC). *Gpr17:* (F: CACCCTGTCAAGTCCCTCAAG, R: GTGGGCTGACTAGCAGTGG), *Limk1* (F: ATGAGGTTGACGCTACTTTGTTG, R: CTACACTCGCAGCACCTGAA), *Fibcd1* (F: CAAGGCTGACCTTCAGAGGG, R: GGGGAAGATAGAGTAGACACCAT), Fzd9 (F: CGCACGCACTCTGTATGGAG, R: GCCGAGACCAGAACACCTC), GFAP (F: CGGAGACGCATCACCTCTG, R: AGGGAGTGGAGGAGTCATTCG), Sox10 (F: ACACCTTGGGACACGGTTTTC, R: TAGGTCTTGTTCCTCGGCCAT), Adra1b (F: GCAGCGGTTGATGTCCTGT, R: AGTATCGCACCCCAATGTAGC).

RNA Sequencing and Analysis RNA was measured for RNA integrity number (RIN) by the NU Sequencing Core, and only samples with an RIN score above 9.5 were used. Each experimental group was sequenced in triplicate. cDNA libraries were generated by the NU Sequencing Core using the Ribo-Zero method to remove ribosomal RNA. Samples were sequenced on the Illumina HiSeq 2500 platform using paired-end sequencing at the University of Chicago Sequencing Core. Transcript alignment was conducted with STAR, gene counting with HTSeq, and differential expression analysis with DESeq2. BMP4-treated groups were compared directly to their Noggin-treated counterparts in a pairwise comparison.

Pathway Analyses Ingenuity Pathway Analysis was conducted by the NU Sequencing Core, using IPA software. For Metascape analysis, a list of statistically significantly regulated genes was identified for each genotype, and submitted for analysis without accounting for size of transcript regulation. Express analysis was used, with the *mus musculis* reference genome. For MetaCore (version 19.4.69900) analysis, lists of statistically significantly regulated genes with the size of up- or down-regulation due to BMP4 ligand addition were included in analysis.

III. Results

Overview

In order to gain a detailed understanding of downstream BMP signaling mechanisms, we used postnatal day 1 SVZ NPCs dissected and maintained in a floating neurosphere culture. SVZ NPCs have been shown to maintain the ability to differentiate into neurons, astrocytes, and oligodendrocytes in vitro and in vivo (Craig et al., 1996; Gross et al., 1996; Levison & Goldman, 1993; Lois & Alvarez-Buylla, 1993), and BMPR1a, BMPR1b, and BMPR2 are all expressed in the SVZ at this stage of murine development (D. Zhang et al., 1998). We chose to use BMP4 as our stimulus ligand as it has previously demonstrated the ability to induce a robust astrocyte differentiation phenotype in SVZ NPCs, and it is expressed by these same cultures (Gross et al., 1996). NPCs were cultured in Noggin due to its ability to bind directly to BMP4 (Zimmerman et al., 1996) and inhibit its activity.

We dissected SVZ NPCs from four different genetic backgrounds: wild-type, $BMPR1a^{fx/fx}$ (conditional knockout), $BMPR1b^{-/-}$ (constitutive knockout), and $BMPR2^{fx/fx}$ (conditional knockout) mice. Following dissection of SVZ NPCs, we cultured them in EGF in a floating neurosphere model to promote proliferation, and a high dose of Noggin to suppress endogenous BMP signaling. After NPC expansion, all cells were treated with adeno-Cre virus to induce recombination and delete BMPR1a and BMPR2 from the relevant cultures, as well as to maintain consistency across cultures. Following 48 hours of viral treatment, WT, $BMPR1a^{fx/fx}$, and $BMPR2^{fx/fx}$ culture, which had fluorescent reporters to indicate recombination efficiency, underwent fluorescence-activated cell sorting (FACS) to purify populations. 7 days after initial viral treatment, cultures were treated with either 50ng/mL BMP4 or 250ng/mL Noggin for 4 hours, and RNA was collected and transcriptomes analyzed by the Northwestern sequencing core (NUSeq).

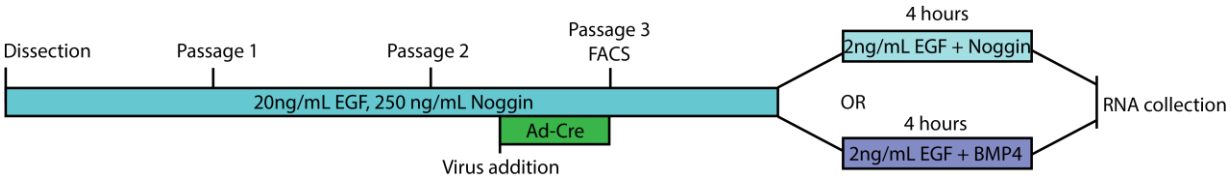

Figure 3.1 Diagram of timeline for RNA sequencing cell culture

Postnatal SVZ NPCs were cultured in Noggin to the effects of BMP signaling that might be generated from NPC-generated BMP ligand binding.

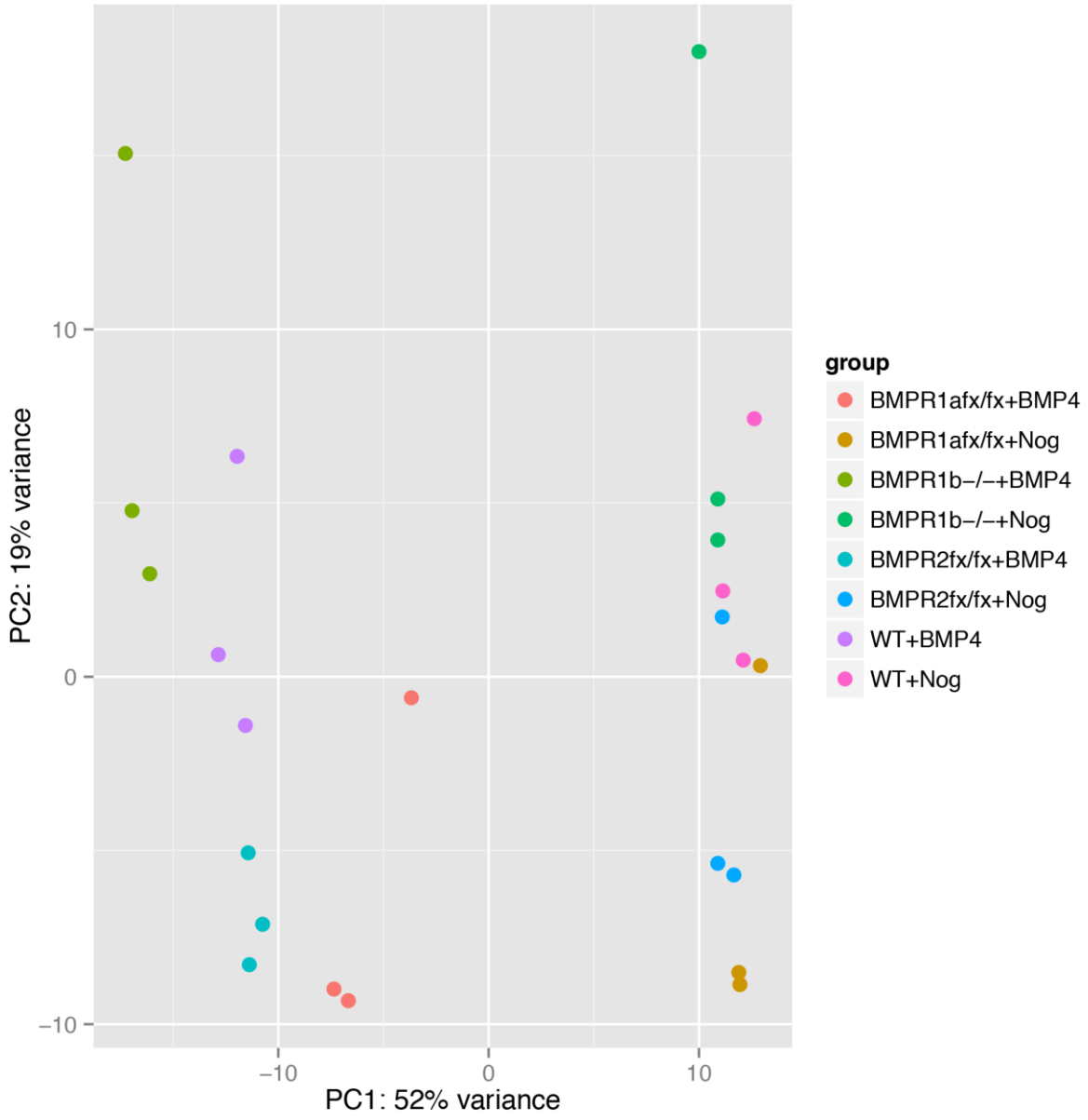

Figure 3.2 Principal component analysis of all groups sequenced
There is a large amount of variance between Noggin versus BMP-treated groups, as expected, and some variance between genotypes within the same treatment groups.

In our principal component analysis (PCA) plot, the largest amount of variance seen was between Noggin-treated and BMP4-treated groups, mostly differentiated by PC1. As the sequenced cultures differed primarily by the presence of BMP4 or the absence of an individual receptor subunit, this was expected. Noggin-treated groups clustered closely together along the PC1-axis. Between BMP-treated groups, $BMPR1b^{-/-}$+BMP4 and $BMPR1a^{fx/fx}$+BMP4 show the greatest variance, both on the PC1 as well as the PC2 axis. $BMPR1a^{fx/fx}$+BMP4 and $BMPR2^{fx/fx}$+BMP4 cluster relatively closely together, as do $BMPR1a^{fx/fx}$+Noggin and $BMPR2^{fx/fx}$+Noggin, indicating that the BMPR1a and BMPR2 receptors may have overlapping functions, or may be required to act together for some of their transcriptional activities.

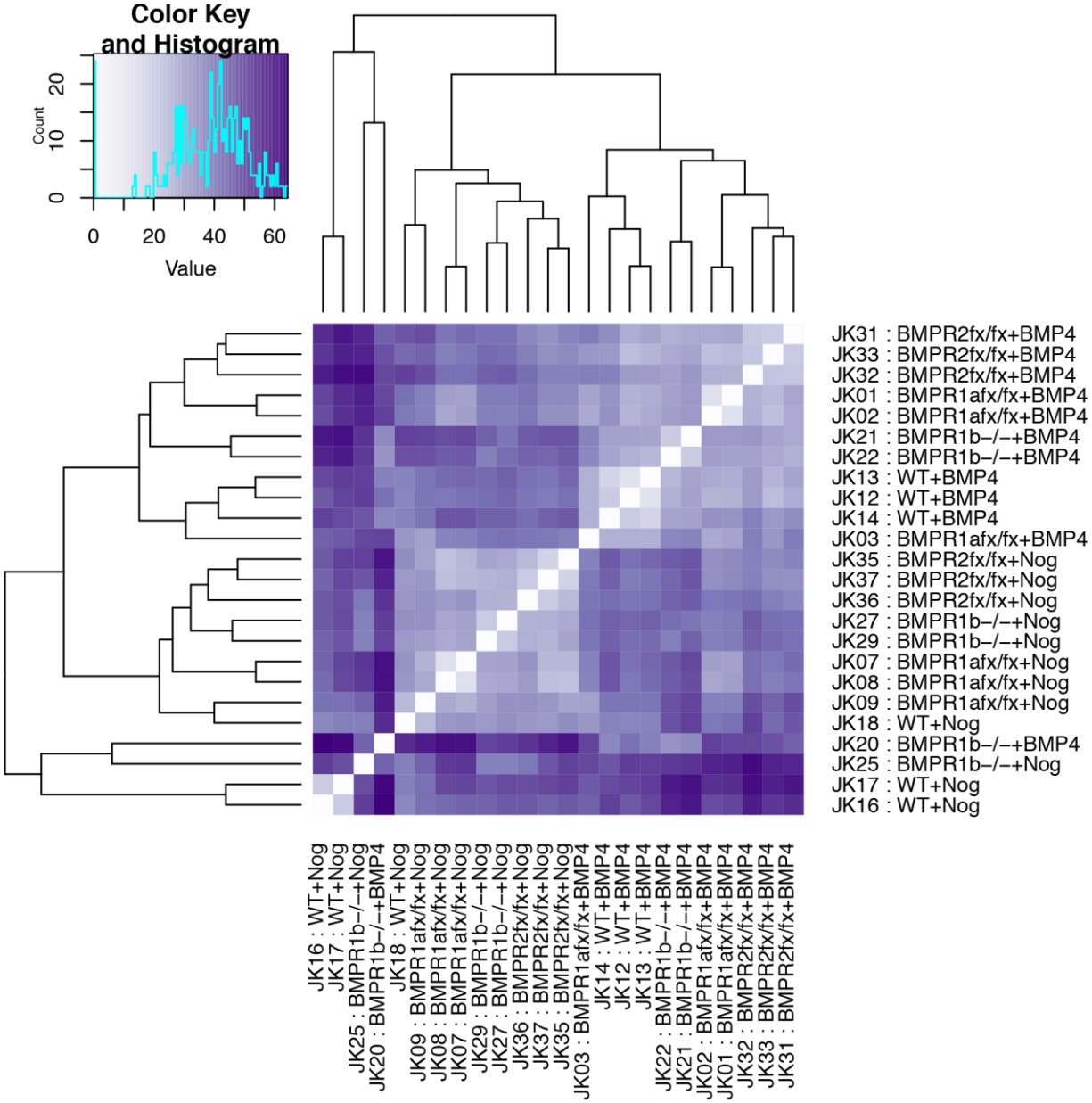

Figure 3.3 Dendrogram of sequenced groups.

Genotypes and treatment groups tend to largely self-segregate in a dendrogram, with the exception of the BMPR1b- genotype.

Meta-Analyses

With the assistance of the NU Sequencing Core, we compared transcription levels of BMP4-stimulated groups with their Noggin-cultured control genotype counterparts to generate four comparison datasets, one for each genetic background (wild-type, BMPR1a$^{fx/fx}$, BMPR1b$^{-/-}$, and BMPR2$^{fx/fx}$). We identified thousands of statistically significantly regulated genes. Wild-type cultures produced the largest number of identified genes, including the largest number of unique genes that did not occur in the other 3 datasets. Interestingly, 931 genes were identified as statistically changed across all four datasets, which may indicate that BMP4 ligand presence in such high doses stimulates receptors other than the ones examined here.

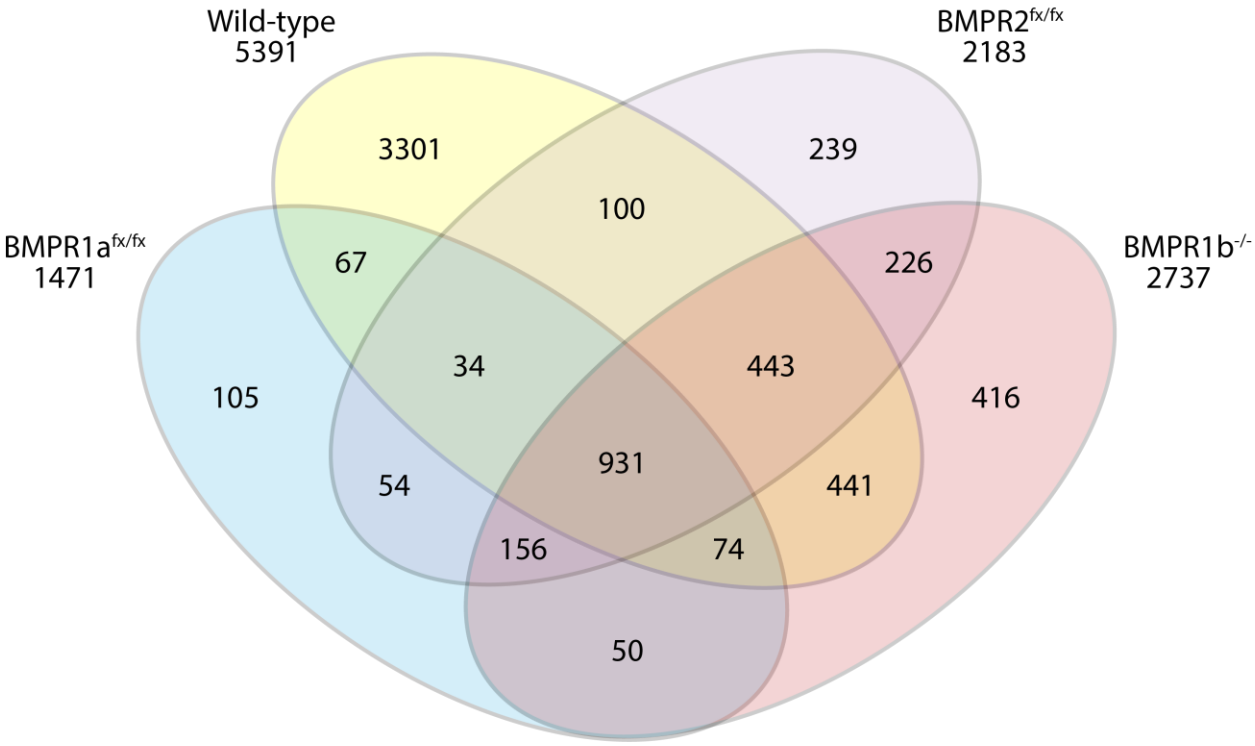

Figure 3.4 Venn Diagram of BMP4-regulated genes.

Following FDR correction, BMP4-regulated genes numbered 5391 in wild-type NPCs, 2183 in BMPR2$^{fx/fx}$ NPCs, 2737 in BMPR1b$^{-/-}$ NPCs, and 1471 in BMPR1a$^{fx/fx}$ NPCs. 931 genes were regulated across all four genetic groups.

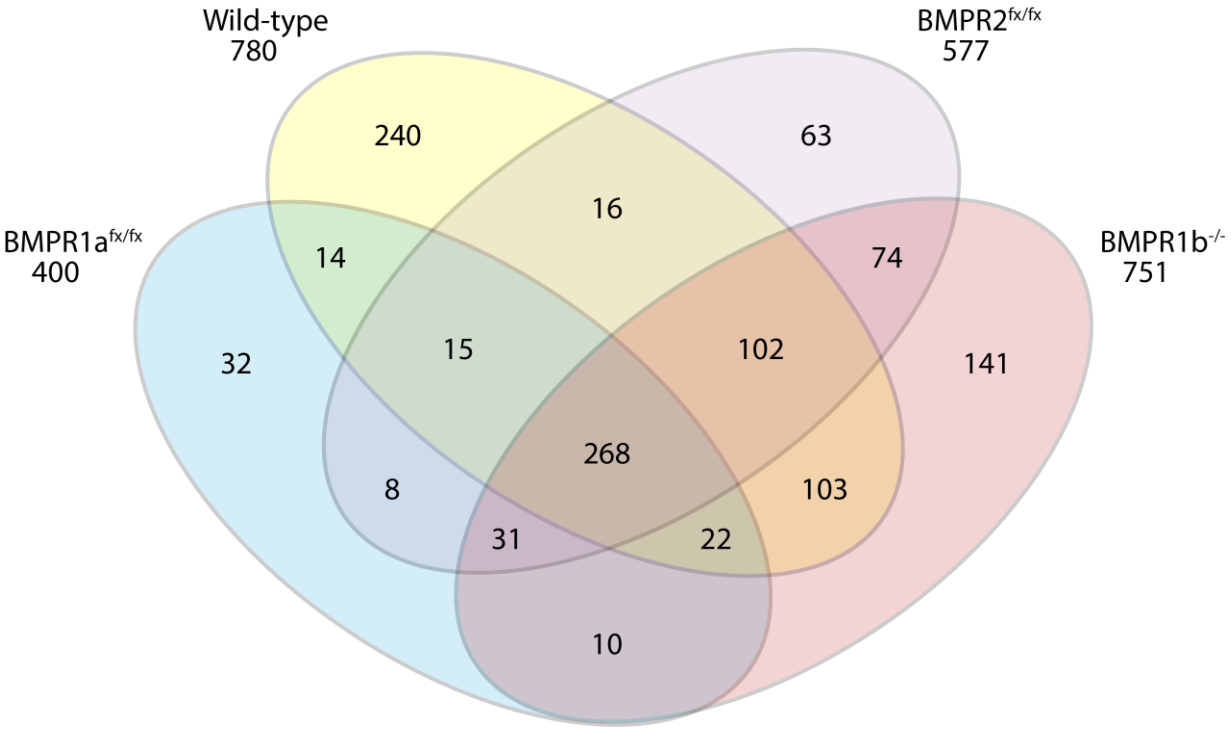

Figure 3.5 Genes regulated by BMP4 over 2-fold.

When genes were filtered for both statistical significance (FDR-corrected $p<0.05$) as well as at least a 2-fold change in either direction, the number of significantly regulated genes was greatly reduced: 780 for wild-type, 577 for BMPR2$^{fx/fx}$, 751 for BMPR1b$^{-/-}$, and 400 for BMPR1a$^{fx/fx}$. 268 genes were regulated by more than 2-fold across all four groups.

In order to fully explore BMP-regulated pathways, we included all statistically significantly regulated genes in our meta-analyses. However, because the wild-type group had over 3000 statistically significantly regulated BMP4 gene targets, we necessarily split up our analysis between upregulated and downregulated genes. We first conducted Metascape analyses of all four comparison datasets generated to identify the degree to which genes overlap or are similar between datasets. All genes identified as differentially regulated (FDR $p<0.05$) were included. As seen in Figure 3.6, among both upregulated and downregulated datasets, there is a large degree of overlap among all datasets for not only identical genes, but also genes sharing common ontology terms, re-emphasizing what we saw previously in Figure 3.4 and Figure 3.5.

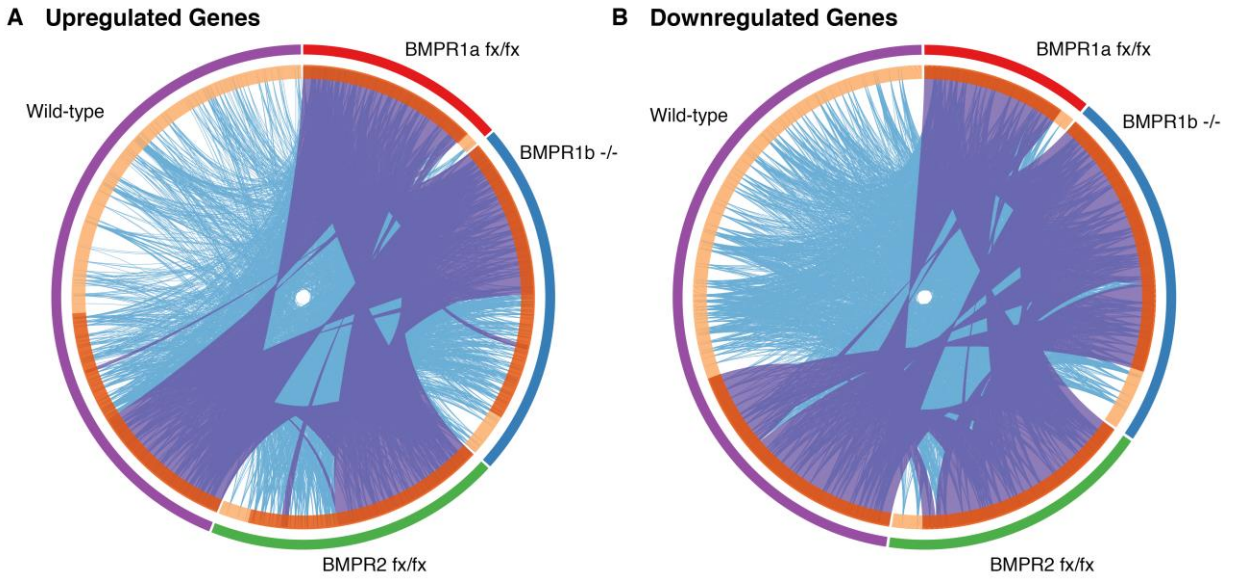

Figure 3.6 Circos Overlay Analysis from Metascape, demonstrating overlap between transcriptional targets for WT, BMPR1a$^{fx/fx}$, BMPR1b$^{-/-}$, and BMPR2$^{fx/fx}$ NPCs.

Significantly upregulated and significantly downregulated genes lists were analyzed using GeneGo to determine commonalities and differences. The outermost ring of each graph is colored according to genotype. The inner ring of each graph is shaded dark orange to indicate genes in common with other genotype lists, while light orange indicates unique targets for that genotype. Blue lines link genes under common ontology terms, which are required to be statistically enriched. Purple lines link genes shared between lists**.**

We next analyzed top pathways, process networks, and processes regulated by BMP treatment, again by splitting lists into upregulated and downregulated genes. We submitted the lists of gene identifiers to Metascape, which then identified the top 20 biological processes regulated across all four upregulated gene lists and the top 20 biological processes across all four downregulated gene lists. In both sets of lists, there are a number of identified processes that align with previous BMP research, such as ossification (GO:0001503), pathways in cancer (mmu05200), and regulation of neuron differentiation (GO:0045664) (Fig 3.7).

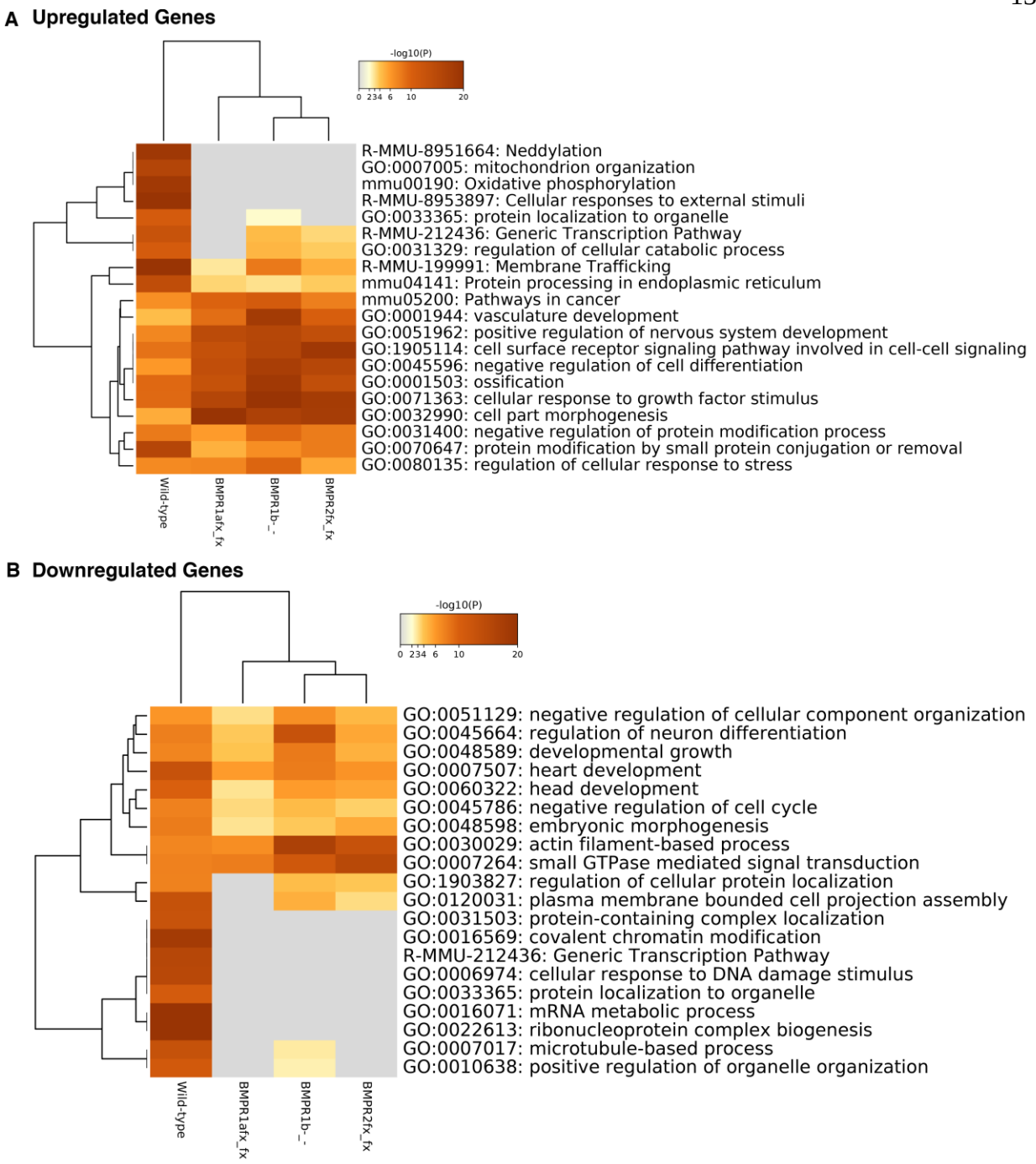

Figure 3.7 Metascape Analysis demonstrating the top 20 biological processes activated by up- and down-regulated genes upon BMP stimulus of wild-type NPCs.

BMP receptors have numerous common processes activated by BMP4 ligand stimulation. The top 20 biological processes identified within upregulated and downregulated genes by Metascape Analysis differ in degree of regulation for WT, BMPR1a$^{fx/fx}$, BMPR1b$^{-/-}$, and BMPR2$^{fx/fx}$ NPCs. Many processes identified in WT NPCs are not identified in the other three groups.

We next wanted to briefly examine the BMP targets that were most strongly up or downregulated, and examine whether they were similarly regulated across groups, even in the absence of individual receptor subunits. After filtering for only statistically significantly regulated genes, and sorting for fold change in transcription, we found the 30 genes most changed in each direction, as listed in Figure 3.8. As can be seen, if a gene was regulated in wild-type NPCs, it was usually also regulated in the same direction across the other three groups, although the fold change observed was frequently smaller. In downregulated genes, some genes were suppressed in wild-type NPCs, but not statistically changed in the other three groups, indicating that perhaps the effect of any one receptor subunit on the identified gene is relatively weak, requiring the cooperative action of all receptor subunits.

Among the genes identified as upregulated, a number are BMP inhibitory genes, such as the i-SMADs SMAD6 and SMAD7, as well as Noggin and Follistatin. Others known to be involved in canonical BMP signaling, such as Id1 and SMAD9, are among the top upregulated genes as well. Among the genes identified as most downregulated, some are involved in oligodendrocyte differentiation (Zfp488), and others with actin cytoskeletal regulation (Pstpip2). Most downregulated genes have not been well-linked to BMP in published studies (Table 3-1). However, despite these genes being the top-most significantly upregulated or downregulated by short-term BMP4 ligand stimulation, several are relatively unknown, particularly their relationship to BMP signaling. Given their responsiveness to BMP4, these relationships may be worth further pursuit.

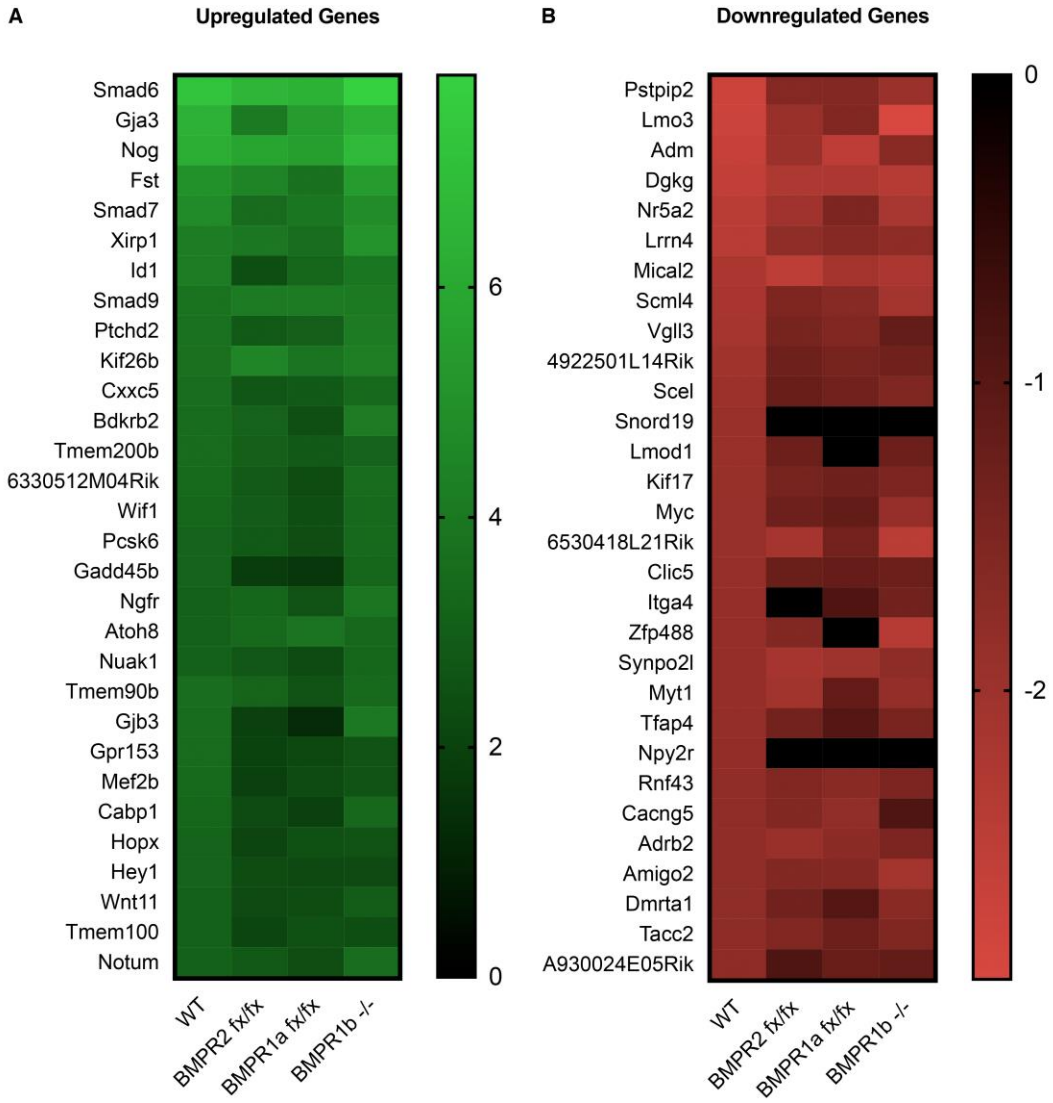

Figure 3.8 Heatmap of the top 30 upregulated and downregulated genes in BMP-treated wild-type NPCs, compared across BMP-treated BMPR2$^{fx/fx}$, BMPR1a$^{fx/fx}$, and BMPR1b$^{-/-}$ groups.

Scaled according to Log_2Fold change. Genes were excluded from the list if the FDR-corrected p-value was insignificant, or read quality unsuitable, for the WT+BMP group. Log_2Fold value was input as 0 if the FDR-corrected p-value was insignificant, or read quality unsuitable, for all other groups. Many familiar genes BMP-target are identified, such as SMAD6 and Id1, but many others are not well understood in the context of BMP signaling. Several unnamed genes were also identified.

Table 3-1: Pubmed Results Identified for BMP-Regulated Genes

Gene abbreviations were input into the Pubmed search. It should be noted that in some cases, a full gene name search (ie "Noggin" instead of "Nog," and "BMP Noggin", instead of "BMP Nog") returned more results than the abbreviation. For Tmem90b, the alternate name Syndig1 was found and used. For Adm, the full gene name was used due to Adm returning results on a journal name. Results were accurate as of time of writing, but may change on a daily basis.

Gene	# of Pubmed results for "[Gene]"	# of Pubmed results for "BMP [Gene]"	Gene	# of Pubmed results for "[Gene]"	# of Pubmed results for "BMP [Gene]"
Smad6	521	238	Pstpip2	47	0
Gja3	105	0	Lmo3	61	2
Nog	1148	68	Adm (adrenomedullin)	3627	3
Fst	8608	34	Dgkg	17	0
Smad7	2341	188	Nr5a2	466	1
Xirp1	29	0	Lrm4	0	0
Id1	1692	278	Mical2	24	0
Smad9	130	62	Scml4	6	0
Ptchd2	10	0	Vgll3	38	1
Kif26b	38	0	4922501L14Rik	0	0
Cxxc5	66	3	Scel	42	0
Bdkrb2	113	0	Snord19	0	0
Tmem200b	0	0	Lmod1	41	0
6300512M04Rik	0	0	Kif17	104	0
Wif1	504	9	Myc	40230	103
Pcsk6	190	4	6530418L21Rik	0	0
Gadd45b	388	2	Clic5	53	0
Ngfr	1166	8	Itga4	170	2
Atoh8	39	3	Zfp488	6	0
Nuak1	103	0	Synpo2l	10	1
Tmem90b (Syndig1)	14	0	Myt1	300	1
Gjb3	284	0	Tfap4	30	0
Gpr153	9	0	Npy2r	92	0
Mef2b	109	0	Rnf43	209	1
Cabp1	130	0	Cacng5	10	0
Hopx	126	1	Adrb2	9126	1
Hey1	578	36	Amigo2	31	1
Wnt11	521	26	Dmrta1	14	0
Tmem100	32	6	Tacc1	67	0
Notum	262	4	A930024E05Rik	0	0

Ingenuity Pathway Analysis

To better understand the pathways activated or suppressed by individual BMP receptor subunits, we conducted pathway analysis on each comparison dataset for each genetic background with the assistance of the NUSeq Core. Across all groups, a number of pathways and upstream regulators commonly appeared in our analysis, including Wnt/β-catenin signaling, BMP, and TGFβ (Tables 3-2 to 3-13). This seems to indicate a large degree of overlap in BMP4 transcriptional targets, despite the absence of individual BMP receptor subunits in some groups.

Strikingly, although BMP ligands 2 and 4 came up as some of the top predicted upstream regulators of activated pathways, they were not the most statistically significant predicted regulator in any group. Across all four groups, Growth Differentiation Factor 2 (GDF2), also known as BMP9, was the most statistically significantly predicted regulator. The prediction of upstream regulator Tumor Necrosis Factor (TNF) in multiple groups (with the exception of BMPR1a$^{fx/fx}$) indicates that BMP signaling does regulate inflammation-related genes. TGFβ was also a predictor upstream regulator, perhaps unsurprising given that BMP and TGFβ frequently have opposing roles and BMP itself strongly upregulates many of its own antagonists, including Noggin and Follistatin.

Table 3-2 Top Canonical Pathways predicted by IPA analysis of wild-type NPCs activated by BMP4 compared to Noggin-treated NPCs.

Top Canonical Pathways		
Name	p-value	Overlap
Wnt/-catenin Signaling	7.91E-12	16.0% 27/169
Human Embryonic Stem Cell Pluripotency	9.50E-12	17.9% 24/134
Role of Macrophages, Fibroblasts and Endothelial Cells in Rheumatoid Arthritis	3.09E-09	10.8% 32/296
Role of Osteoblasts, Osteoclasts and Chondrocytes in Rheumatoid Arthritis	3.16E-09	12.3% 27/219
TGF- Signaling	1.86E-08	18.4% 16/87

Table 3-3 Top Upstream Regulators predicted by IPA analysis of wild-type NPCs activated by BMP4 compared to Noggin-treated NPCs

Top Upstream Regulators		
Upstream Regulator	p-value of overlap	Predicted Activation
GDF2	2.74E-24	Activated
TGFB1	1.46E-20	Activated
TNF	3.21E-17	
NOTCH1	1.37E-16	
BMP2	3.83E-16	Activated

Table 3-4 Top Networks predicted by IPA analysis of wild-type NPCs activated by BMP4 compared to Noggin-treated NPCs

Top Networks

ID Associated Network Functions	Score
Cellular Development, Nervous System Development and Function, Tissue Development	48
Cell-To-Cell Signaling and Interaction, Nervous System Development and Function, Skeletal and Muscular System Development and Function	36
Cancer, Organismal Injury and Abnormalities, Cell Death and Survival	36
Cell Cycle, Reproductive System Development and Function, Cell Death and Survival	34
Developmental Disorder, Hereditary Disorder, Organismal Injury and Abnormalities	33

Table 3-5 Top Canonical Pathways predicted by IPA analysis of BMPR2$^{fx/fx}$ NPCs activated by BMP4 compared to Noggin-treated NPCs

Top Canonical Pathways		
Name	p-value	Overlap
Human Embryonic Stem Cell Pluripotency	2.04E-12	16.4% 22/134
Factors Promoting Cardiogenesis in Vertebrates	9.91E-12	19.6% 18/92
Wnt/-catenin Signaling	3.47E-11	13.6% 23/169
Role of Osteoblasts, Osteoclasts and Chondrocytes in Rheumatoid Arthritis	2.31E-10	11.4% 25/219
Axonal Guidance Signaling	1.03E-09	8.1% 35/434

Table 3-6 Top Upstream Regulators predicted by IPA analysis of BMPR2$^{fx/fx}$ NPCs activated by BMP4 compared to Noggin-treated NPCs

Top Upstream Regulators		
Upstream Regulator	p-value of	Predicted Activation

	overlap	
GDF2	4.76E-21	Activated
Beta-estradiol	4.68E-15	
SOX2	7.98E-15	Inhibited
TGFB1	1.06E-14	
TNF	1.47E-14	

Table 3-7 Top Networks predicted by IPA analysis of BMPR2$^{fx/fx}$ NPCs activated by BMP4 compared to Noggin-treated NPCs

Top Networks	
ID Associated Network Functions	Score
Cancer, Organismal Injury and Abnormalities, Gastrointestinal Disease	39
Connective Tissue Development and Function, Skeletal and Muscular System Development and Function	35
Cancer, Organismal Injury and Abnormalities,, Dermatological Diseases and Conditions	31
Gene Expression, Cell Cycle, Connective Tissue Development and Function	31
Inflammatory Response, Infectious Diseases, Cellular Development	31

Table 3-8 Top Canonical Pathways predicted by IPA analysis of BMPR1a$^{fx/fx}$ NPCs activated by BMP4 compared to Noggin-treated NPCs

Top Canonical Pathways		
Name	p-value	Overlap
Human Embryonic Stem Cell Pluripotency	1.88E-15	16.4% 22/134
Basal Cell Carcinoma Signaling	2.44E-11	19.4% 14/72
Mouse Embryonic Stem Cell Pluripotency	1.07E-10	15.8% 15/95
Wnt/-catenin Signaling	1.53E-10	11.2% 19/169
Role of Osteoblasts, Osteoclasts and Chondrocytes in Rheumatoid Arthritis	3.29E-10	9.6% 21/219

Table 3-9 Top Upstream Regulators predicted by IPA analysis of BMPR1a$^{fx/fx}$ NPCs activated by BMP4 compared to Noggin-treated NPCs

Top Upstream Regulators		
Upstream Regulator	p-value of overlap	Predicted Activation
GDF2	5.37E-18	Activated
BMP4	2.76E-17	Activated
TGFB1	7.63E-15	Activated
BMP2	7.91E-15	Activated
NOTCH1	2.76E-14	

Table 3-10 Top Networks predicted by IPA analysis of BMPR1a$^{fx/fx}$ NPCs activated by BMP4 compared to Noggin-treated NPCs

Top Networks	
ID Associated Network Functions	Score
Cancer, Organismal Injury and Abnormalities, Cell Death and Survival	37

Cardiovascular System Development and Function, Organismal Development, Nervous System Development and Function	32
Cardiovascular Disease, DNA Replication, Recombination, and Repair, Nucleic Acid Metabolism	32
Cancer, Organismal Injury and Abnormalities, Gastrointestinal Disease	32
Cancer, Hematological Disease, Immunological Disease	30

Table 3-11 Top Canonical Pathways predicted by IPA analysis of BMPR1b$^{-/-}$ NPCs activated by BMP4 compared to Noggin-treated NPCs

Top Canonical Pathways		
Name	p-value	Overlap
Human Embryonic Stem Cell Pluripotency	1.93E-15	20.9% 28/134
Wnt/-catenin Signaling	1.98E-14	17.8% 30/169
Factors Promoting Cardiogenesis in Vertebrates	9.45E-12	21.7% 20/92
Role of Osteoblasts, Osteoclasts and Chondrocytes in Rheumatoid Arthritis	2.02E-11	13.7% 30/219
TGF- Signaling	2.47E-10	20.7% 18/87

Table 3-12 Top Upstream Regulators predicted by IPA analysis of BMPR1b$^{-/-}$ NPCs activated by BMP4 compared to Noggin-treated NPCs

Top Upstream Regulators		
Upstream Regulator	p-value of overlap	Predicted Activation
GDF2	9.83E-26	Activated
TNF	2.86E-23	
TGFB1	1.60E-21	Activated
Beta-estradiol	5.52E-19	
Tretinoin	9.52E-17	

Table 3-13 Top Networks predicted by IPA analysis of BMPR1b$^{-/-}$ NPCs activated by BMP4 compared to Noggin-treated NPCs

Top Networks	
ID Associated Network Functions	Score
Digestive System Development and Function, Organismal Development, Organ	39

Morphology	
Cell-To-Cell Signaling and Interaction, Nervous System Development and Function, Neurological Disease	38
Cellular Development, Nervous System Development and Function, Tissue Development	38
Embryonic Development, Organismal Development, Cardiovascular System Development and Function	36
Cancer, Organismal Injury and Abnormalities, Gastrointestinal Disease	32

To understand particular pathways regulated by BMP4 stimulation across all 4 groups, and see if we could uncover more specific regulated processes, we conducted pathway analysis using the software MetaCore as well. As seen in Table 3-14, we were able to identify a number of specific pathways that were identified as regulated across all four groups. Again, many of these pathways were unsurprising, such as regulation of WNT/Beta-catenin signaling and oligodendrocyte differentiation, but genes identified as BMP-regulated in these pathways may be of interest to future studies on these biological processes.

Table 3-14 Pathway Maps statistically significant across all four groups, sorted by statistical significance in MetaCore

#	Maps	Total	Min (pValue)	Min FDR
1	Development Negative regulation of WNT/Beta-catenin signaling in the cytoplasm	80	4.451E-17	4.625E-14
2	Chemotaxis Lysophosphatidic acid signaling via GPCRs	129	6.331E-17	4.625E-14
3	Apoptosis and survival NGF/TrkA PI3K-mediated signaling	77	1.875E-15	9.133E-13
4	Oxidative stress ROS-induced cellular signaling	108	1.449E-14	4.287E-12

5	Aberrant B-Raf signaling in melanoma proression	55	1.467E-14	4.287E-12
6	Mitogenic action of ErbB2 in breast cancer	56	3.274E-14	7.972E-12
7	Development Negative regulation of WNT/Beta-catenin signaling in the nucleus	89	6.940E-14	1.448E-11
8	Signal transduction CXCR4 signaling via MAPKs cascades	53	2.085E-13	3.808E-11
9	Development Epigenetic and transcriptional regulation of oligodendrocyte precursor cell differentiation and myelination	34	5.874E-13	8.535E-10
10	Signal transduction Activation of PKC via G-Protein coupled receptor	52	7.729E-13	1.255E-10
11	Development The role of GDNF ligand family/ RET receptor in cell survival, growth and proliferation	95	1.644E-12	2.402E-10
12	Deregulation of canonical WNT signaling in major depressive disorder	31	3.032E-12	4.977E-10
13	Development Oligodendrocyte differentiation from adult stem cells	51	4.592E-12	2.224E-09
14	Signal transduction Additional pathways of NF-kB activation (in the cytoplasm)	52	5.870E-12	7.147E-10
15	Cytoskeleton remodeling Regulation of actin cytoskeleton organization by the kinase effectors of Rho GTPases	58	7.389E-12	8.304E-10
16	Ligand-independent activation of Androgen receptor in Prostate Cancer	67	8.191E-12	8.547E-10
17	Inhibition of oligodendrocyte precursor cells differentiation by Wnt signaling in multiple sclerosis	25	8.900E-12	8.668E-10
18	Apoptosis and survival BAD phosphorylation	42	1.095E-11	9.999E-10
19	Stem cells Oligodendrocyte differentiation (general schema)	38	1.203E-11	3.495E-09
20	Role of activation of WNT signaling in the progression of lung cancer	77	1.263E-11	1.086E-09
21	Development BMP signaling	33	1.294E-11	4.238E-09
22	Development Positive regulation of STK3/4 (Hippo) pathway and negative regulation of YAP/TAZ function	71	1.412E-11	1.120E-09
23	Development Early embryonal hypaxial myogenesis	37	1.431E-11	4.238E-09
24	Signal transduction mTORC2 downstream signaling	68	1.457E-11	1.120E-09

25	Development Thromboxane A2 signaling pathway	50	1.793E-11	4.254E-09
26	WNT signaling in HCC	40	1.827E-11	1.335E-09
27	Immune response IFN-alpha/beta signaling via PI3K and NF-kB pathways	94	1.925E-11	1.340E-09
28	NRF2 regulation of oxidative stress response	54	2.328E-11	1.479E-09
29	ERBB family and HGF signaling in gastric cancer	54	2.328E-11	1.479E-09
30	Signal transduction Angiotensin II signaling via Beta-arrestin	57	2.505E-11	1.525E-09

Novel BMP Targets

It is clear from the large number of unique targets identified in the wild-type NPC comparison dataset that there are a number of genes regulated by BMP require the presence of one or both type 1 receptors BMPR1a and BMPR1b. Given the high depth read of our sequencing, we also have the ability to flag a number of networks that may not previously have been identified as BMP-regulated. To do so, we separated genes identified as statistically significantly upregulated versus downregulated by BMP4 ligand stimulation, then input each separate list of genes into Metascape to identify the gene ontology terms and biological processes that were statistically enriched (Figures 3.9 and 3.10). Within the upregulated gene list, a large number of familiar processes appeared within the top 100 terms. Even processes that have been well-studied and are known to be BMP-regulated, such as rostrocaudal neural tube patterning (GO: 0021903) and negative regulation of cell proliferation (GO: 0008285), while enriched, were not near the top of the list. Some pathways identified among upregulated genes that may be of interest, such as generic transcription pathway (R-MMU-212436) and Translation (R-MMU-72766), may be worth further exploration due to broader implications on cellular regulation. The presence of multiple terms related to RNA processing and transcription among pathways

enriched in the downregulated genes list lends further strength to the idea that BMP4 signaling may regulate a broad program of transcription and translational control. Because BMP4 is known to promote neural stem and progenitor cell quiescence (Bond et al., 2014), it is possible that this is one mechanism by which BMP regulates NPC quiescence and activation.

Very striking is the potential involvement of BMP signaling in cilium assembly (R-MMU-5617833, enriched in downregulated genes). Both neurons and astrocytes develop primary cilia (Moser, Fritzler, & Rattner, 2009; Sterpka & Chen, 2018), and cilia act as regulators of multiple signaling pathways, although little is known about how primary cilia may regulate NPC fate specification. While TGFβ receptors are trafficked to the ciliary tip (Clement et al., 2013), how BMP ligands and receptors may influence ciliary construction has not been well explored. The identification of the GO term protein localization to cilium (GO: 0061512) among terms enriched in the downregulated gene list may indicate that BMP signaling, or perhaps its antagonists, are involved in important ciliary processes.

Given that the processes identified were not limited to those of the CNS, there are a number of terms that may be worth exploring BMP signaling in other biological systems, such as Oocyte meiosis (mmu04114) and Factors involved in megakaryocyte development and platelet production (R-MMU-983231).

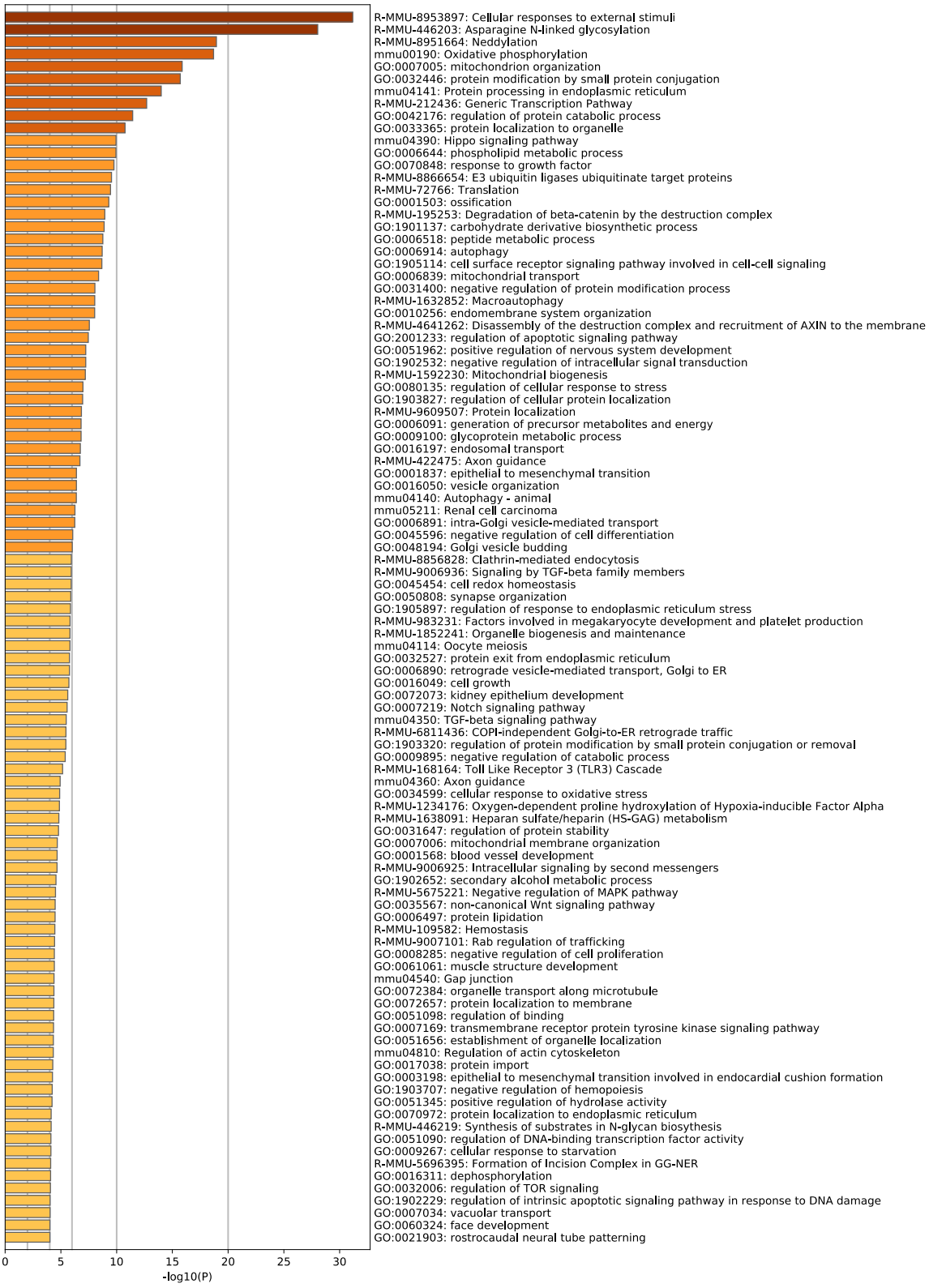

Figure 3.9 Top 100 gene ontology terms enriched from genes identified as upregulated by BMP4 in wild-type NPCs.

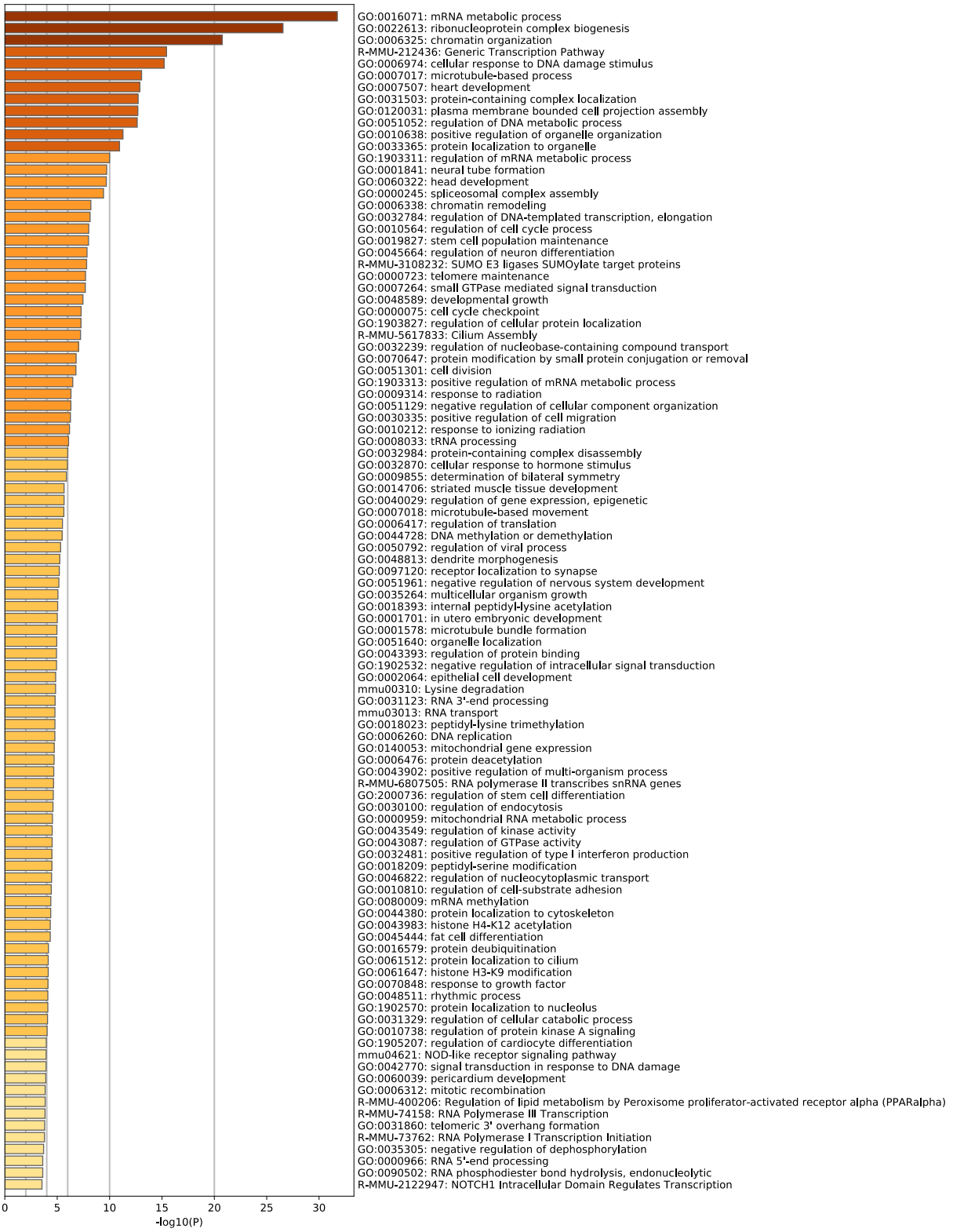

Figure 3.10 Top 100 GO terms enriched in genes identified as downregulated in response to BMP4 stimulus of wild-type NPCs

Comparison of BMPR1a$^{fx/fx}$ and BMPR1b$^{-/-}$ Datasets

One of the primary goals of our study was to compare the gene targets of the two BMP type 1 receptor subunits, BMPR1a and BMPR1b. We therefore next used Metascape analysis to identify gene networks maximally differentially regulated within the BMPR1a$^{fx/fx}$ and BMPR1b $^{-/-}$ datasets. To gain an overview of the number and scale of similarly and dissimilarly regulated targets, we identified all significantly up or downregulated genes in each genotype and mapped them using Metascape's Circos function.

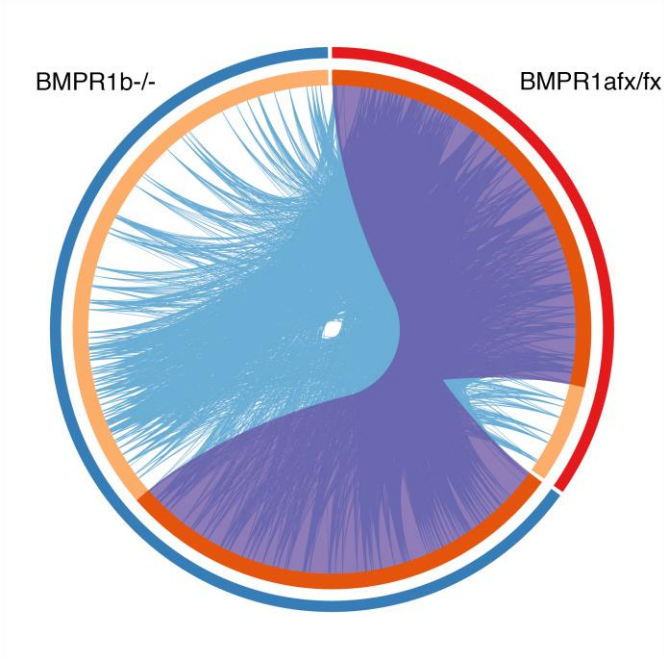

Figure 3.11 A comparison of all genes regulated by BMP4 in BMPR1b$^{-/-}$ (blue portion of circle outline) and BMPR1a$^{fx/fx}$ (red portion of circle outline) NPCs.

Genes regulated by both are connected by the purple overlay and comprise the dark orange circle outline, while genes with the same or similar gene ontology (GO) terms are connected by blue lines. Uniquely regulated genes comprise the light orange sections of the inner circle. Blue lines link genes under common ontology terms, which are required to be statistically enriched. Purple lines link genes shared between lists.

BMP stimulation of BMPR1a$^{fx/fx}$ and BMPR1b$^{-/-}$ NPCs results in a large number of commonly regulated genes, as well as genes with similar gene ontology terms. In the absence of BMPR1b receptor subunits, BMP4 still has the ability to regulate numerous genes, indicating that BMPR1a maintains unique transcriptional control of those genes. In the absence of BMPR1a receptor subunits, hundreds of genes are still transcriptionally regulated by BMPR1b, although not nearly as many as by BMPR1a. This may speak to the relative importance and abundance of BMPR1a in neural progenitor populations, as compared to BMPR1b (Mira et al., 2010).

We identified several genes that were identified as regulated by BMP4 stimulation in either BMPR1a$^{fx/fx}$ or BMPR1b$^{-/-}$ cells, but not both. Of these, several have not been previously identified in the context of BMP, or there is a relative dearth of knowledge on the relationship between the gene and BMP signaling, such as with Fibcd1, gliomedin, and Adra1b. When these terms are searched with “BMP” in the Pubmed database, only 1 or 0 published studies were found as of the time of writing.

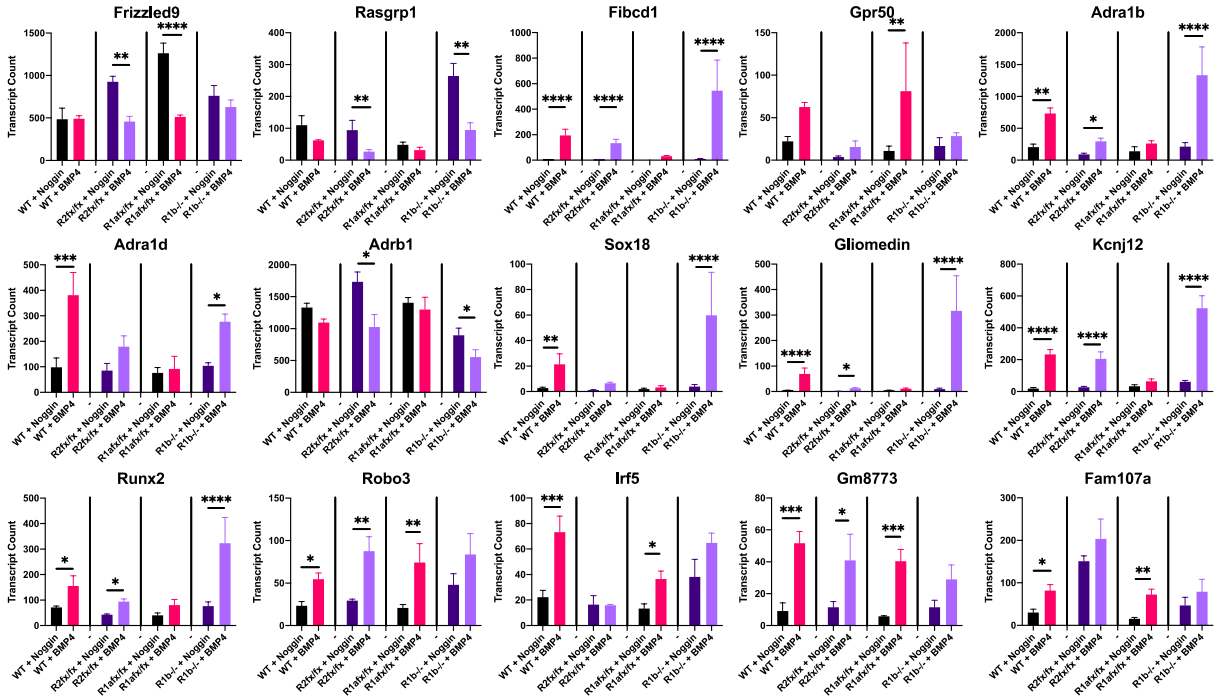

Figure 3.12 Some genes differentially regulated in BMPR1a$^{fx/fx}$ and BMPR1b$^{-/-}$ NPCs.

Transcript levels for multiple genes differentially regulated in the absence of BMPR1a and BMPR1b, taken from RNA sequencing reads. Transcript levels across genotypes are not directly comparable. *p<0.05, **p<0.01, ***p<0.001, ****p<0.0001. All p-values are corrected for false discovery rate.

We conducted qPCR analysis on a few of these genes to validate our RNA sequencing results. For RNA sequencing we had cultured our cells in Noggin from dissection through RNA collection, but we chose to conduct our validation using cells cultured in our standard EGF without Noggin, and with a longer (6 hours, 50ng/mL) BMP4 treatment before collection. Even with this changed paradigm, we still identified numerous genes that were differentially regulated in BMPR1a$^{fx/fx}$ and BMPR1b$^{-/-}$ NPCs by BMP4 addition (Fig 3.13, 3.15, 3.18).

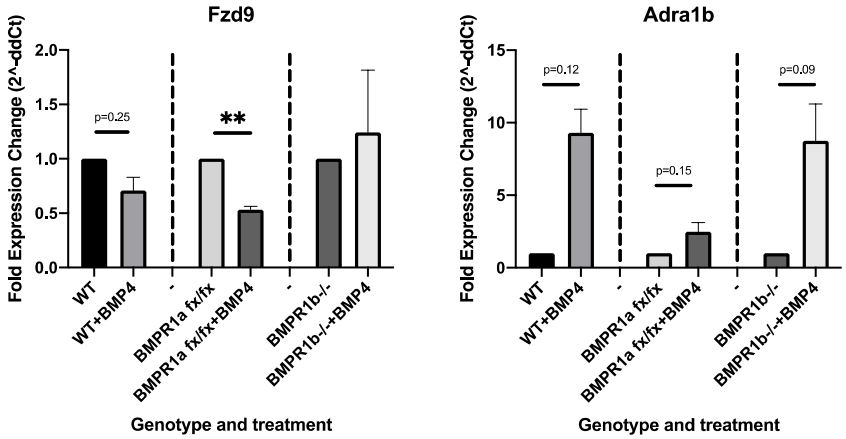

Figure 3.13 qPCR validation of genes identified as differentially regulated by BMPR1a and BMPR1b.

Validation of Fzd9 and Adra1b differential regulation in BMPR1a$^{fx/fx}$ and BMPR1b$^{-/-}$ NPCs, by qPCR. Cells were measured after being treated for 6 hours with BMP4. Fzd9 expression appears to be suppressed by BMP4 in BMPR1a$^{fx/fx}$ but not BMPR1b$^{-/-}$ NPCs, suggesting BMPR1b ordinarily regulates Fzd9 mRNA. Adra1b is slightly increased in both BMPR1a$^{fx/fx}$ and BMPR1b$^{-/-}$ NPCs, but the difference appears to be far greater in BMPR1b$^{-/-}$ NPCs, indicating BMPR1a is the primary mediator of Adra1b mRNA expression. n=3.

Cytoskeletal Regulation

Another mechanism by which BMP receptors are known to exert different effects is through LIM domain containing protein kinase 1 (LIMK1) and its downstream effector cofilin (Arber et al., 1998; Yang et al., 1998). LIMK1 regulates the actin cytoskeleton by phosphorylation of cofilin, an agent in actin depolymerization (Arber et al., 1998; Yang et al., 1998) and interacts with the C-terminal region of the BMPR2 subunit (Foletta et al., 2003; Lee-Hoeflich et al., 2004). BMP signaling induces the activation of LIMK1 in neuronal process extension (Eaton & Davis, 2005; Gamell et al., 2008; Hocking et al., 2009; Lee-Hoeflich et al., 2004; Podkowa, Christova, Zhao, Jian, & Attisano, 2013), and BMPR1b but not BMPR1a regulates LIMK1 phosphorylation activity (Podkowa et al., 2013; Yamauchi et al., 2013). Regulation of LIMK1 and cofilin may be one method by which BMP type 1 receptors exert

different effects in NSC division and differentiation. Upon examination of mRNA transcript reads in our comparison datasets, we found that BMP4 stimulation induces LIMK1 mRNA transcript increases. Ablation of BMPR1b or BMPR2, but not of BMPR1a, blocks this effect.

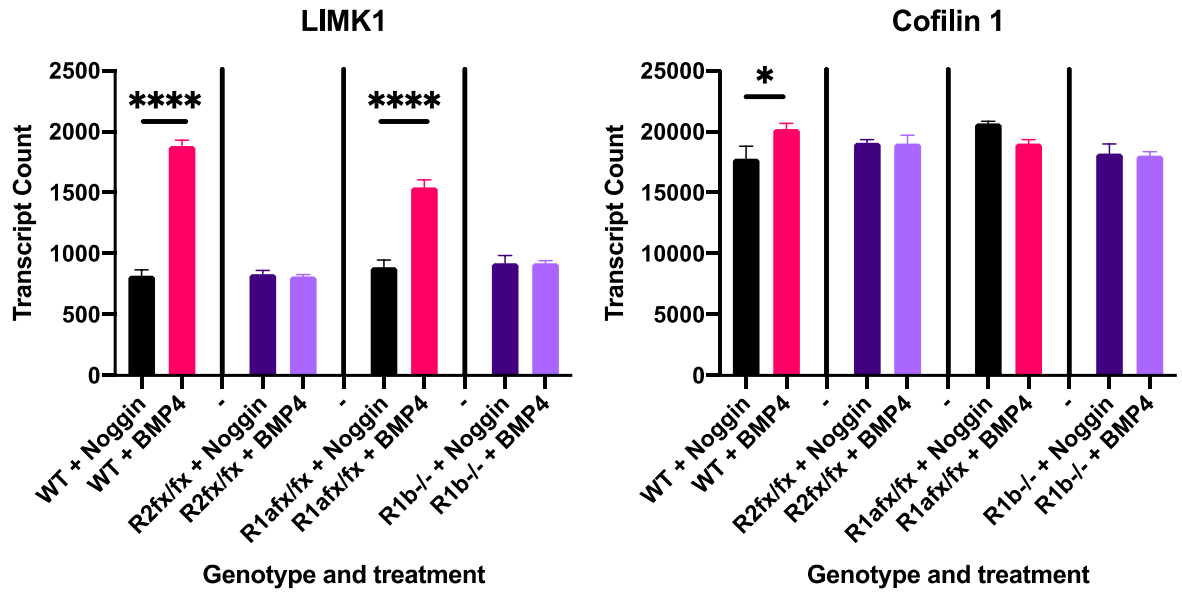

Figure 3.14 Transcript counts of LIMK1 and Cofilin 1 in response to BMP4 stimulus across genotypes.

LIMK1 shows a BMP4-responsive effect that is abolished when either BMPR2 or BMPR1b is ablated. Cofilin shows a slight BMP4 response in wild-type cells, but that does not hold up across other genotypes. *FDR-corrected $p<0.05$ ****FDR-corrected $p<0.0001$.

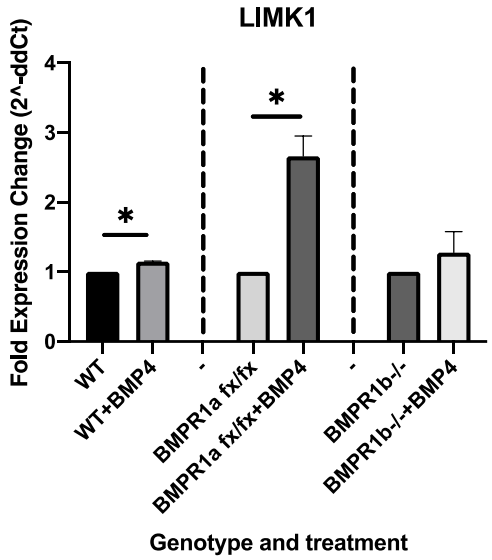

Figure 3.15 qPCR validation of LIMK1.

BMP4 treatment of NPCs shows an increase in LIMK1 transcript levels after 6 hours in WT and BMPR1a$^{fx/fx}$ NPCs, but not BMPR1b$^{-/-}$ NPCs. *p<0.05. n=3.

This led us to believe that BMP signaling has broader effects on cytoskeletal regulation. BMP signaling has been linked to neurite and axon extension during development. For example, in Olig1-derived neurons of the arcuate nucleus of the hypothalamus, BMP signaling through BMPR1a is required for neurite extension in response to leptin (Peng et al., 2012). BMPR1b is required for commissural axon extension during development (Yamauchi et al., 2013). Further examination of BMP regulation of the cytoskeleton, particularly as it may have effects on cell fate specification and function, may be useful. For example, BMP-generated astrocytes differ dramatically in morphology and other properties from LIF/Noggin-induced GFAP-positive astrocytes (Bonaguidi et al., 2005), but whether BMP-induced cytoskeletal changes are at least partially responsible is unclear.

To examine BMP effects on cell architecture, we referred to the RNA sequencing data to identify BMP-regulated cytoskeletal genes. When we examined pathways regulated across all

four comparison datasets, “Cytoskeleton remodeling Regulation of actin cytoskeleton organization by the kinase effectors of Rho GTPases” was identified as one of the top statistically significantly enriched pathways (see Table 3-14). In wild-type NPCs, numerous pathways relating to the cytoskeleton and cell morphology were identified as enriched in Metascape.

Table 3-15: Cytoskeletal related processes identified from wild-type genes in Metascape

Direction of gene regulation used for identification	Identifier	Process term
Upregulated	R-MMU-422475	Axon guidance
Upregulated	mmu04360	Axon guidance
Downregulated	GO: 0007017	Microtubule-based process
Downregulated	GO: 0120031	Plasma membrane bounded cell projection assembly
Downregulated	R-MMU-5617833	Cilium assembly
Downregulated	GO: 0048813	Dendrite morphogenesis
Downregulated	GO: 0001578	Microtubule bundle formation
Downregulated	GO: 0044380	Protein localization to cytoskeleton

In addition to our identification of specific cytoskeletal-related genes by BMP4 stimulus, the Hippo pathway, whose effectors Yes-associated protein (YAP) and Ww-domain containing transcription regulator 1 (TAZ) are known as cytoskeletal regulators, was flagged as an enriched pathway in both our MetaCore analysis across all four datasets (“Development Positive regulation of STK3/4 (Hippo) pathway and negative regulation of YAP/TAZ function”) as well as in our Metascape analysis of the pathways enriched in upregulated genes (mmu 04390: Hippo signaling pathway). Further examination of BMP regulation of YAP and TAZ, and their effects on NPC fate specification, can be found in Chapter 4.

BMP Transcriptional Regulation of Oligodendrocyte Differentiation

BMP signaling has been implicated in regulation of oligodendrocyte differentiation. We found further confirmation of this when we analyzed all BMP-regulated genes from all four of our comparison datasets in MetaCore using the standard compare experiments workflow. In our enrichment analysis in this workflow, the pathway map with the most significant FDR-corrected p-value for enrichment was “inhibition of oligodendrocyte precursor cells differentiation by Wnt signaling in multiple sclerosis.” As shown in Figure 3.16, transcription of genes related to oligodendrocyte differentiation are regulated by BMP ligand stimulation. Although studies have largely focused on the role of BMPR1a in oligodendrocyte differentiation (Govier-Cole et al., 2019; Samanta et al., 2007), both BMPR1a and BMPR1b appear to have effects on the BMP-Wnt mediation of oligodendrocyte specification (Feigenson, Reid, See, Crenshaw, & Grinspan, 2011). Even in the absence of BMPR2, strong stimulation with BMP4 ligand results in regulation of oligodendrocyte-related genes, indicating that other type 2 receptor subunits may be involved if BMPR2 is unavailable.

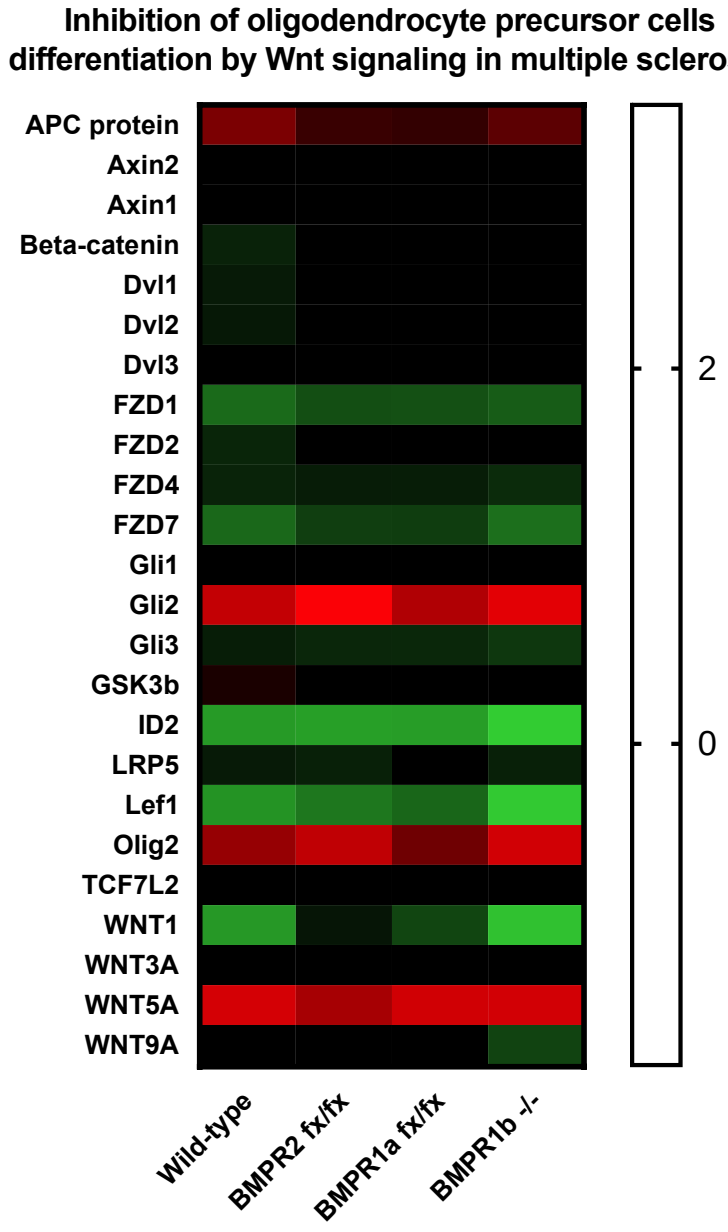

Figure 3.16 Regulation of oligodendrocyte differentiation genes by different BMP receptors.

Genes listed are part of the "inhibition of oligodendrocyte precursor cells differentiation by Wnt signaling in multiple sclerosis" pathway in MetaCore. Values of BMP-regulated genes were drawn from our RNA sequencing datasets, with values with an FDR-corrected $p>0.05$ listed as a value of 0. Scale of values is $\log_2$fold change.

In our examination of genes differentially regulated by BMPR1a and BMPR1b, we identified Sox10 and Gpr17 mRNA as oligodendrocyte-related genes that were downregulated by BMPR1a, but not BMPR1b (Fig 3.17). This gives further credence to previous studies that have identified BMPR1a as an oligodendrocyte differentiation regulator (Samanta et al., 2007).

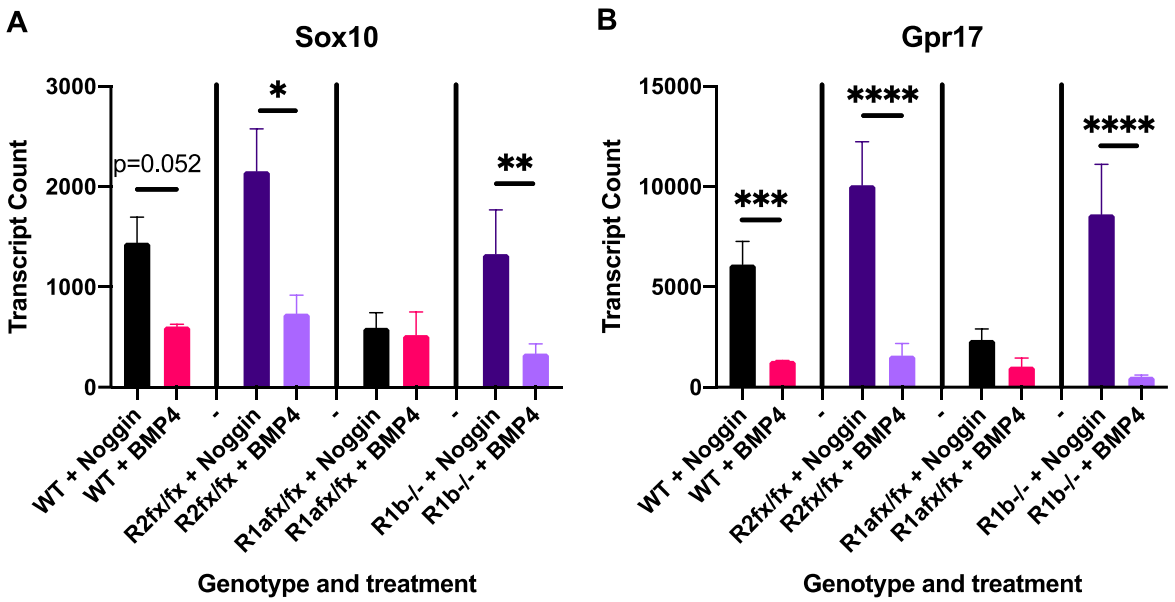

Figure 3.17 Differential regulation of the oligodendrocyte-related genes Sox10 and Gpr17 by BMPR1a and BMPR1b in RNA sequencing data.

A) Sox10 is suppressed by BMP4 ligand stimulation in the absence of BMPR2 or BMPR1b, but not in the absence of BMPR1a. B) Gpr17 is suppressed by BMP4 ligand stimulation in the wild-type, BMPR2$^{fx/fx}$, and BMPR1b$^{-/-}$ NPCs, but not in BMPR1a$^{fx/fx}$ NPCs, indicating that BMPR1a is necessary for the suppression of Gpr17 transcription.

We were able to validate differential expression of Sox10 by BMPR1a and BMPR1b via qPCR (Fig 3.18). In wild-type cells, BMP4 stimulation reduces mRNA levels of both Gpr17 and Sox10, as expected and in accordance with the RNA sequencing data. Sox10 is also reduced by BMP4 addition in BMPR1b$^{-/-}$ NPCs. While it is very slightly reduced in BMPR1a$^{fx/fx}$ NPCs, the

effect is less than that in BMPR1b$^{-/-}$ NPCs, indicating that Sox10 is primarily regulated by BMPR1a. The slight effect seen in the BMPR1a$^{fx/fx}$ cohort may be because FACS was not conducted on these cells, and some non-recombined cells may have been included. Gpr17 is also reduced by BMP4 ligand, in all groups, although again the effect appears to be lesser in BMPR1a-ablated cells. These results support the hypothesis that BMPR1a, but not BMPR1b, is the primary BMP type 1 receptor that regulates oligodendrocyte gene expression and differentiation.

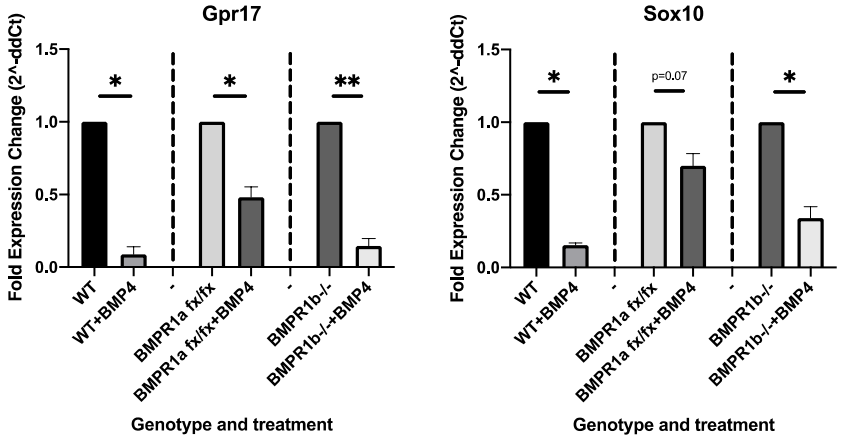

Figure 3.18 qPCR validation of Gpr17 and Sox10 regulation by BMP4.
qPCR analysis was conducted on BMP4-stimulated wild-type, BMPR1a$^{fx/fx}$, and BMPR1b$^{-/-}$ NPCs. Cells were treated for 6 hours and grown in EGF without Noggin, and were not sorted for recombination by FACS due to machine availability limitations. BMP-treated conditions were normalized to their non-treated counterparts. WT n=2, BMPR1a$^{fx/fx}$ n=3, BMPR1b$^{-/-}$ n=3. Within each genotype, each control was a biological match to each treatment group.

IV. Discussion

This study has produced a rich dataset of short-term BMP4 transcriptional targets in NPCs. Moreover, through deletion of specific BMP receptor subunits, we have identified genes that are upregulated by BMP4 even in specific receptor subunit absence, which will lead us to an

enriched understanding of why BMP signaling has such a diverse array of functions, and why different BMP receptors appear to have different roles in certain contexts, as with early embryonic development, gliosis following spinal cord injury, and oligodendrogliosis. Strikingly, given that many canonical BMP signaling targets are upregulated even in the absence of BMPR2, this indicates that there may be another BMP type 2 receptor subunit that plays a significant role in NPCs, at least when exposed to high exogenous levels of BMP4 ligand. This may be more important when cells are being exposed to increased ligand availability during inflammation, cell quiescence, or aging.

Through examination of specific genes, we have identified transcriptional differences regulated by the BMP receptor subunits BMPR1a and BMPR1b. Interestingly, many of these genes identified as differentially regulated have not been previously established to be BMP4 signaling targets. While further analysis should be conducted on these datasets to tease apart BMPR1a versus BMPR1b effects, the pathway analysis we conducted here provides a starting point for future studies on differential targets and divergent effects of BMPR1a and BMPR1b, particularly in neural stem cell fate specification and cellular morphology.

Chapter 4

TAZ Regulates Astrocytic Differentiation of Postnatal Neural Stem and Progenitor Cells

I. Introduction

Yes-associated protein (YAP) and WW domain-containing transcription regulator 1 (TAZ) are evolutionarily conserved transcriptional co-activators found in multiple cell types. Initially identified as binding partners of Yes and 14-3-3, respectively (Kanai et al., 2000; Sudol, 1994), YAP and TAZ cannot directly bind DNA, but instead recruit and interact with other transcription factors to regulate both cell proliferation and organ size during development (Dong et al., 2007; Gill et al., 2018; J. Huang, Wu, Barrera, Matthews, & Pan, 2005). Due to their large degree of homology, YAP and TAZ are commonly assumed to have overlapping functions. However, recent studies have indicated that they may in fact play divergent roles, depending on the biological system and timing during development. For example, YAP expressed in HEK293T cells has larger effects on cell physiology than TAZ, and the two have different transcriptional effects under lipoprotein A (LPA) stimulation (Plouffe et al., 2018). Within skeletal muscle stem cells, YAP and TAZ both initially promote proliferation, but during later stages YAP inhibits differentiation whereas TAZ promotes generation of muscle cells and the expression of certain muscle-related genes (C. Sun et al., 2017). Regulation of YAP and TAZ also may differ, with TAZ having additional phosphorylation sites for degradation (W. Huang et al., 2012).

The roles of YAP and TAZ within neural stem and progenitor cells (NPCs), the way they are regulated, and whether they have overlapping or unique functions are unclear. YAP and TAZ have been found to promote NPC proliferation *in vivo* through action with TEA domain family transcription factors (TEADs) (Cao, Pfaff, & Gage, 2008; Han et al., 2015), but studies *in vitro*

have conflicting results on YAP's role in NPC proliferation (Z. Huang, Sun, et al., 2016b; Yao et al., 2014). TAZ has not been independently well studied in the CNS, particularly not in NPCs.

While YAP and TAZ are canonical effectors of Hippo signaling and are regulated by LATS phosphorylation, emerging evidence supports a role for YAP and TAZ in other signaling pathways. One candidate regulatory pathway is bone morphogenetic protein (BMP) signaling. During early development, BMP signaling directs neurogenesis and is involved in dorsal-ventral axis patterning. However, postnatally it promotes exit of NPCs from cell cycle (Bond et al., 2014) and astrocyte lineage commitment (Bonaguidi et al., 2005; 2008). The intracellular mechanisms mediating effects of BMP signaling on NPC fate specification have not been fully elucidated. Prior studies have suggested that YAP may mediate effects of BMP signaling on both embryonic NPC proliferation (Yao et al., 2014) and on astrogliogenesis (Z. Huang, Sun, et al., 2016b). However, in view of the pro-proliferative effects of YAP in other stem cells (Kostic et al., 2019), this seemed at odds with the effects of BMP signaling in promoting exit of postnatal NPCs from cell cycle (Bonaguidi et al., 2008; Bond et al., 2014).

YAP and TAZ are mechanosensing proteins (Dupont et al., 2011; Shimizu et al., 2017) that likely also integrate mechanical cues into NPC fate decisions. There are a number of transmembrane receptors that detect the extracellular matrix and that are potential candidates for YAP/TAZ regulators, including β1-integrin. β1-integrin signaling regulates NPC maintenance and suppresses NPC astrocytic lineage commitment (Brooker et al., 2016; Leone et al., 2005; North et al., 2015; L. Pan et al., 2014). Since components of β1-integrin signaling have been identified as Hippo regulators in other cell systems (Elbediwy et al., 2016; Serrano, McDonald, Lock, Muller, & Dedhar, 2013), it is a prime candidate for regulation of YAP and TAZ in NPCs.

Thus the available evidence suggested that YAP and TAZ might be points of convergence for multiple signaling cues that regulate NPCs, but how YAP and TAZ respond to these inputs in NPCs was unclear. In this study, we examined if YAP and TAZ are effectors of the BMP and β1-integrin signaling pathways in NPCs, and whether YAP and TAZ are responsible for the effects of these signaling cues on NPC proliferation and fate specification. We found that the effects of BMP signaling on astrocyte lineage commitment involve TAZ but not YAP, contradicting previous studies (Z. Huang, Hu, et al., 2016a; Yao et al., 2014). Further, while both YAP and TAZ are targets of β1-integrin/integrin-linked kinase (ILK), YAP promotes proliferation whereas TAZ promotes differentiation into glial fibrillary acidic protein (GFAP)-expressing astrocytes. Our ability in this study to separate YAP and TAZ has enabled us determine that YAP and TAZ are distinct entities with unique roles in NPC proliferation and fate determination.

II. Materials and Methods

Mouse Lines Yap^{tm1Hmc};Taz^{tm1Hmc} mice were obtained from Jackson Laboratories (strain 030532). To obtain TAZ conditional knockout mice, Yap^{tm1Hmc};Taz^{tm1Hmc} mice were crossed to a Bl6C57 mouse, and progeny crossed until the YAP mutant allele was lost. Yap^{dupa} mice were obtained from Jackson Laboratories (strain 027929). Rosa26:ZsGreen (strain 007906) mice on a BL6C57 background were crossed with Yap^{tm1Hmc};Taz^{tm1Hmc} mice. Wild-type BL6C57 mice were ordered as timed pregnancies from Jackson Laboratories.

The following primers were used for mouse genotyping: YAP(dupa)-F: AGGACAGCCAGGACTACACAG, YAP(dupa)-R: CACCAGCCTTTAAATTGAGAAC, YAP(hmc)-F: GTCTTTCTCTAGGCACAAAAAGG, YAP(hmc)-R:

AGTGGTAAAGAATAATGCTCATCC, TAZ-F: CTTCCAAGGTGCTTCAGAGA, TAZ-R: GGAGAGGTAAAGCCCACCAG, ZsGreen-9103: GGCATTAAAGCAGCGTATCC, ZsGreen-9104: AACCAGAAGTGGCACCTGAC, ZsGreen-9020: AAGGGAGCTGCAGTGGAGTA, ZsGreen-9021: CCGAAAATCTGTGGGAAGTC

All experiments involving animals were conducted under IACUC guidelines at Northwestern University.

Cell Culture Neural stem cells were dissected at postnatal day 1 mice from the subventricular zone (SVZ) by using forceps to mechanically remove the lateral ganglionic eminence, followed by chemical dissociation using 0.05% trypsin with EDTA. Cells were maintained and passaged in a floating culture with DMEM/F12 media (Gibco/Invitrogen) with N2, B27, and 20ng/mL EGF (Millipore). For differentiation, cells were plated on either PDL (Corning 08-774-384) or PDL/Laminin (BD 354087) coated glass coverslips in 0.2ng/mL EGF at a concentration of 50,000 cells per well. Cells from wild-type mice were used between passage 2 and passage 5.

NPCs dissected from transgenic mice were treated with Adeno-Cre (Vector Biolabs 1700) or Adeno-GFP (Vector Biolabs 1060) at a concentration of 1:2000 at 18 hours after passage 2 to ablate the relevant gene of interest. Virus was removed 48 hours after addition. Cells were not used for experiments until at least 7 days after virus addition.

Cell Treatments Floating cultures treated with BMP4 (R&D) had 20ng/mL added for 6 hours, after which either protein or RNA was collected. Adherent cultures for staining were treated during plating with 10ng/mL BMP4. For ILK inhibition, cpd22 (Millipore) was administered to floating cultures at 1uM for 6 hours. Adherent cultures were treated during plating with 0.25uM cpd22. MG-132 (Sigma) was added to floating cultures at 100uM to inhibit

proteasome-mediated degradation immediately prior to cpd22 treatment, so that cells were treated with both drugs simultaneously. Cycloheximide (CHX) (Sigma) was added to floating cultures at 100ng/mL to inhibit translation immediately prior to BMP4 treatment, so that cells were treated with both drugs simultaneously. β1-integrin blocking antibodies (BD Bisciences 555003) were added to cultures for 24 hours at a concentration of 1:100.

Nucleofection of NPCs The plasmid for TAZ(S89A) overexpression (Addgene 19026) was nucleofected using program A-033 using the Lonza Amaxa I nucleofector and the Lonza Mouse NSC kit.

Western blots Protein samples were collected in either M-PER (Thermo Fisher 78501) with HALT protease and phosphatase inhibitor (Thermo Fisher 78440) for whole cell lysates, or using a nuclear/cytoplasmic extraction kit (Thermo Scientific 78835) to separate compartments. Protein was boiled in reducing buffer for 20 minutes, then run on SDS-Page gradient gels, transferred to PVDF membrane, blocked for one hour with either 5% Blotto in TBS-Tween or 5% BSA in TBS-Tween, then probed with antibodies in blocking buffer at 4°C overnight. Secondary antibody detection was done on the following morning. Antibodies used for immunoblots included TAZ (BD Pharmigen 560235, 1:500), TAZ (Cell Signaling 83669S, 1:500), pTAZ (CS 59971, 1:500), GFAP (Dako Z0334, 1:1000), GAPDH (Millipore, 1:4000), YAP/TAZ (Sigma WH0010413M1, 1:1000), pSerYAP (CS 4911S, 1:1000), pLATS1 (Cell Signaling, 1:1000), LATS1 (Cell Signaling, 1:1000), pGSK3b (Cell Signaling 9336, 1:500), GSK3b (Cell Signaling 9315, 1:500). Secondary antibodies were used at 1:2000: anti-mouse IgG-HRP (CS 7076), anti-rabbit IgG-HRP (CS 7074). Pierce ECL or Pierce Femto ECL was added for 5 minutes, and blots were imaged either using Amersham Hyperfilm ECL (GE) or the Azure c600 and quantified in NIH ImageJ.

Immunocytochemistry Cells on glass coverslips were washed with cold 1X PBS, then fixed for 20 minutes at 4°C in 4% paraformaldehyde. Cells were washed three times with 1X PBS, then stored at 4°C until staining. Cells stained for proliferation were fixed at 1 day post-plating, while cells stained for differentiation were fixed at 3 days post-plating. Coverslips were blocked with 10% normal goat serum in PBS with 0.025% Triton-X for one hour at room temperature. Primary antibodies were diluted in this blocking solution and cell incubated overnight at 4°C. Cells were washed 4 times with PBS with 0.025% Triton-X at room temperature after primary incubation. AlexaFluor secondary antibodies were diluted in blocking buffer at 1:500 with Hoescht nuclear stain at 1:2000, and cell incubated for one hour at room temperature. After washing 4 times with PBS-Triton-X, coverslips were mounted with Prolong Gold. Primary antibodies used include YAP/TAZ (Sigma WH0010413M1, 1:250), S100β (Proteintech 14146-1-AP, 1:500), GFAP (abcam 4674, 1:1000), Nestin (BD 556309, 1:2000), TAZ (Cell Signaling 83669, 1:500), Aldh1L1 (abcam 87117, 1:500). Cells stained with TAZ were subjected to a 10-minute antigen retrieval treatment in 0.1% SDS at 37˚C prior to blocking.

EdU treatment and staining For cells, 10□M EdU was administered to cultures four hours before fixation. Staining was done through use of the Click-iT EdU Cell Proliferation Kit, Alexa Fluor 594 dye (Invitrogen C10339).

qRT-PCR RNA was collected from cultured NPCs with the Qiagen RNeasy micro kit (Qiagen 74004) according to the manufacturer's protocol. cDNA was synthesized using the SuperScript IV kit (Thermo Fischer 18090010), and qPCR conducted using the SYBR Green system (Thermo Fisher 4385612). Primers used: YAP1-F: CAGAATGCTGCGAGGTCATA, YAP1-R: ATGGCCTCAAATGACTGACC , TAZ-F: GAAGGTGATGAATCAGCCTCTG, TAZ- R: GTTCTGAGTCGGGTGGTTCTG, CTGF- F: GGGCCTCTTCTGCGATTTC, CTGF-

R: ATCCAGGCAAGTGCATTGGTA, GAPDH-F: GTC GTG GAT CTG ACG TGC C, GAPDH-R: TGC CTG CTT CAC CAC CTT C.

Imaging Images for differentiation experiments were taken on a confocal microscope (Leica SP5) at 40x and exported to NIH Image J for cell counting. Image stacks used for counting contained 4 slices taken 2.5um apart, flattened using max projection. Images for proliferation experiments were taken on a fluorescent microscope (Zeiss Axiovert 200m) at 20x and exported to NIH Image J for cell counting.

Cell area quantification Images taken for differentiation experiments were also used for cell area quantification. Images were converted to 16-bit grayscale, threshold for the GFAP channel set to 5, and area in micron^2 automatically measured. Cells touching the border of an image and areas of GFAP-positivity under 10um^2 and over 2000um^2 were excluded in order to maximize the number of cells captured and exclude multiple-cell aggregates.

Sholl analysis Images used for differentiation cell counts were also used for Sholl analysis. GFAP+ astrocytic processes semi-manually traced and analyzed following protocols previously established using Fiji (Ferreira et al., 2014). A radius step size of 4um from the center of DAPI-stained nuclei was used.

Data analysis and statistics Data analysis and graph generation was conducted using Prism 8 using the statistical tests specified by experiment. When relevant, paired t-tests were used for experiments in which cells treated with Adeno-GFP and Adeno-Cre come from the same individual mouse. Data are all presented as means ± standard error of the mean (s.e.m.).

III. Results

Effects of BMP signaling on TAZ and YAP

Given that YAP and TAZ have a large amount of sequence homology, and that many antibodies recognize both, we first validated the antibodies we would use for our studies. To accomplish this, we first utilized mutant mice with Cre/LoxP mediated conditional ablation of TAZ and examined TAZ expression in postnatal NPCs. Cultured NPCs from homozygous TAZ mutant ($TAZ^{fx/fx}$) were treated with either an adeno GFP or an adeno Cre virus for 7 days, followed by protein analysis via Western blot using a monoclonal TAZ antibody (Fig. 4.1A). We identified a 50 kD TAZ band in the adeno GFP treated cultures that was absent in the $TAZ^{fx/fx}$ cells. We then added the adeno Cre virus to cultures of $Yap^{+/fx}$ and $YAP^{fx/fx}$ cells and identified a band at about 65kD as YAP (Fig 4.1B). Another band at 50kD was also detected that was partially reduced in $YAP^{fx/fx}$ cultures. Since TAZ is detected at 50kD, we asked whether YAP antibody also detects TAZ. Importantly, when probed with a monoclonal TAZ antibody, no reduction in the 50kD band was observed in $YAP^{fx/fx}$ cells (Fig 4.2A-C). This finding suggests that the 50kD band detected by the YAP antibody likely represents a different YAP isoform and not TAZ, and that ablation of YAP does not regulate TAZ. To determine if the converse was also true, we probed for YAP in $TAZ^{fx/fx}$ cells, and found no alteration in protein levels (Fig 4.2D-F). This result suggests that YAP protein expression is not affected by TAZ ablation in postnatal NPCs.

Once we validated the specificity of our antibodies, we examined the effects of BMP signaling on TAZ and YAP levels in NPCs. Wildtype (WT) NPC cultures were treated with BMP4 for 6 hours, and YAP and TAZ protein levels were examined via immunoblotting. BMP regulated TAZ protein in a dose-dependent manner, but YAP protein did not respond to

treatment (Fig 4.1C,D). Given that traditional Hippo signaling regulates TAZ and YAP protein stability through LATS phosphorylation, we probed for pLATS1 and total LATS1, but found no significant change in the relevant time frame (Fig 4.1D-F), suggesting that BMP-mediated upregulation of TAZ is independent of Hippo signaling. GSK3b, another potential kinase that has been shown to regulate TAZ phosphorylation and degradation in other systems (W. Huang et al., 2012) similarly showed no change (Fig 4.1E,F) in the presence of BMP.

Since YAP and TAZ did not seem to be regulated by traditional LATS phosphorylation and degradation, we next checked mRNA levels by quantitative PCR (qPCR) to see if transcription was affected. No change in YAP mRNA was detected with or without BMP4 treatment (Fig. 4.1G). On the other hand, TAZ mRNA was more abundant after 6 hours of BMP4 treatment, although the increase seen smaller than what would be expected from the observed protein changes (Fig 4.1G). We therefore examined if translation was instead the most important regulatory step, and found that inhibition of translation through addition of 100ng/mL cycloheximide (CHX) prevented BMP-induced TAZ protein increases. Additionally, CHX alone led to a decrease in TAZ protein, indicating that TAZ has a relatively short half-life. In contrast, no significant change in YAP protein levels was observed after CHX treatment (Fig 4.1G,I). Taken together, these results indicate that short-term BMP signaling regulates TAZ protein levels by modulating TAZ protein translation in NPCs.

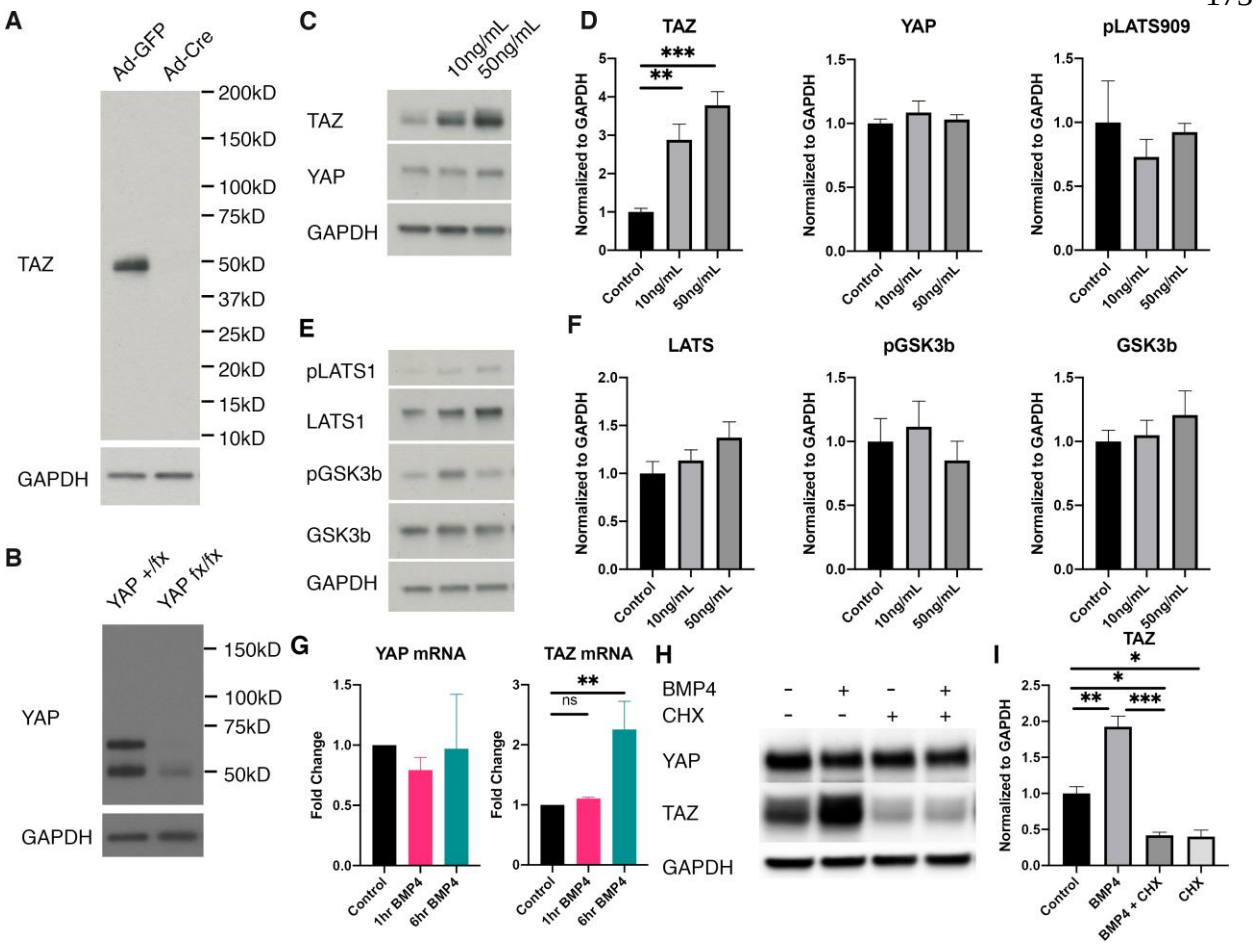

Figure 4.1 Short-term BMP signaling regulates TAZ, but not YAP, at the post-transcriptional level.

A) antibody validation by TAZ knockout in NPCs. B) antibody validation by YAP knockout in NPCs. C,D) TAZ but not YAP responds to BMP treatment in a dose-dependent manner (TAZ by RM one-way ANOVA, n =4: $F_{2,6} = 29.15$, ***p=0.0008; Tukey's multiple comparisons test: control vs 10ng/mL **p=0.0055, control vs 50ng/mL ***p=0.0007, YAP by RM one-way ANOVA, n = 4: $F_{2,6} = 1.143$, p=0.3798). E,F) Short-term BMP treatment does not impact pLATS(S909) (RM one-way ANOVA: $F_{2,6} = 0.4638$, p=0.6497), LATS1 (RM one-way ANOVA: $F_{2,6} = 2.563$, p=0.1568), pGSK3b (RM one-way ANOVA: $F_{2,6} = 0.5537$, p=0.6016), or GSK3b (RM one-way ANOVA: $F_{2,6} = 0.8271$, p=0.4817) protein levels. All n = 4. G) BMP increases TAZ but not YAP mRNA levels. (TAZ by ordinary one-way ANOVA: $F_{2,8} = 9.552$, **p=0.0076; Dunnett's multiple comparisons test: control vs 1 hr BMP4 p=0.9088, control vs 6 hrs BMP4 **p=0.0070, YAP by ordinary one-way ANOVA: $F_{2,8} = 0.2908$, p=0.7552). All n = 4. H,I) CHX treatment impairs BMP-mediated TAZ protein increases (RM one-way ANOVA: $F_{3,6} = 54.31$, ****p<0.0001; Tukey's multiple comparisons test: control vs BMP4 **p=0.0021, control vs BMP4+CHX *p=0.0214, control vs CHX *p=0.0186, BMP4 vs BMP4+CHX ***p=0.0001, BMP4 vs CHX ***p=0.0001, BMP4+CHX vs CHX p=0.9990). All n = 3. Data are presented as means ± s.e.m.

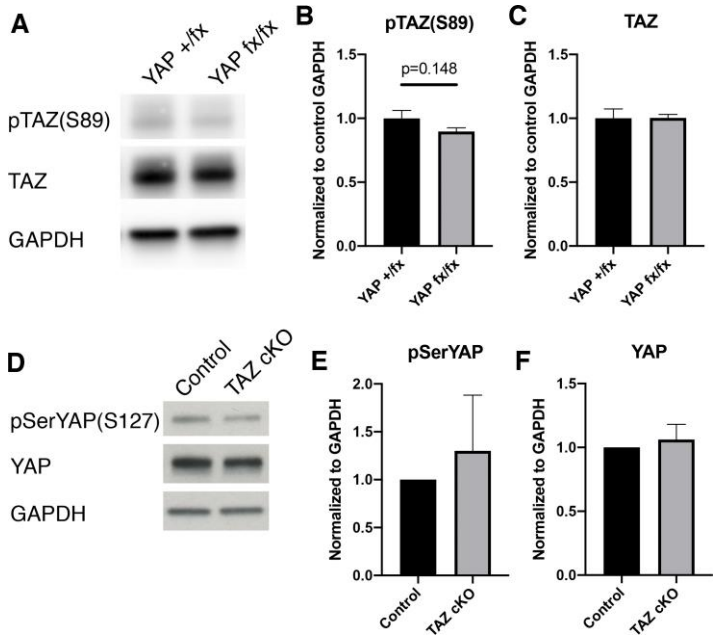

Figure 4.2 Ablation of TAZ and YAP does not affect protein levels of each other.

A) $YAP^{+/fx}$ and $YAP^{fx/fx}$ NPCs are probed for TAZ and pTAZ(S89) via western. Scale bar = 20□□□□B) pTAZ protein levels (unpaired t-test p=0.1480 *n*=4 and 5). C) TAZ protein levels (unpaired t-test p=0.9608 *n*=4 and 5). D) $TAZ^{fx/fx}$ + Adeno-GFP and $TAZ^{fx/fx}$ + Adeno-Cre NPCs are probed for pYAP (S127) and YAP via western. E) pSerYAP protein levels (paired t-test p=0.6403 *n*=4). F) YAP protein levels (paired t-test p=0.6392 *n*=4).

Since YAP and TAZ must translocate to the nucleus to exert their transcriptional effects, we next examined the effects of BMP signaling on their nuclear presence. A 6-hour BMP4 treatment of NPC cultures resulted in increased levels of TAZ in both the nuclear and the cytoplasmic protein fractions (Fig 4.3A,B,F,G). No effect of BMP on total YAP or pSerYAP marked for degradation was observed in this timeframe (Fig 4.3A,C,F,H). Immunocytochemical analysis of TAZ protein in NPCs cultured in the presence or absence of BMP4 for 2hrs also demonstrate an increase in TAZ protein expression with BMP4 treatment (Fig 4.3J-L). To examine if the BMP-induced increase in nuclear TAZ was transcriptionally active, we measured mRNA levels of connective tissue growth factor (CTGF), a TAZ transcriptional target, by qPCR in TAZ knockout NPCs with and without BMP4 treatment. CTGF mRNA decreased in TAZ knockout cells, and a BMP4-induced increase in CTGF mRNA CTGF was partially abrogated by TAZ knockout (Fig 4.3E), suggesting that TAZ mediates some of the effects of BMP signaling on transcriptional targets.

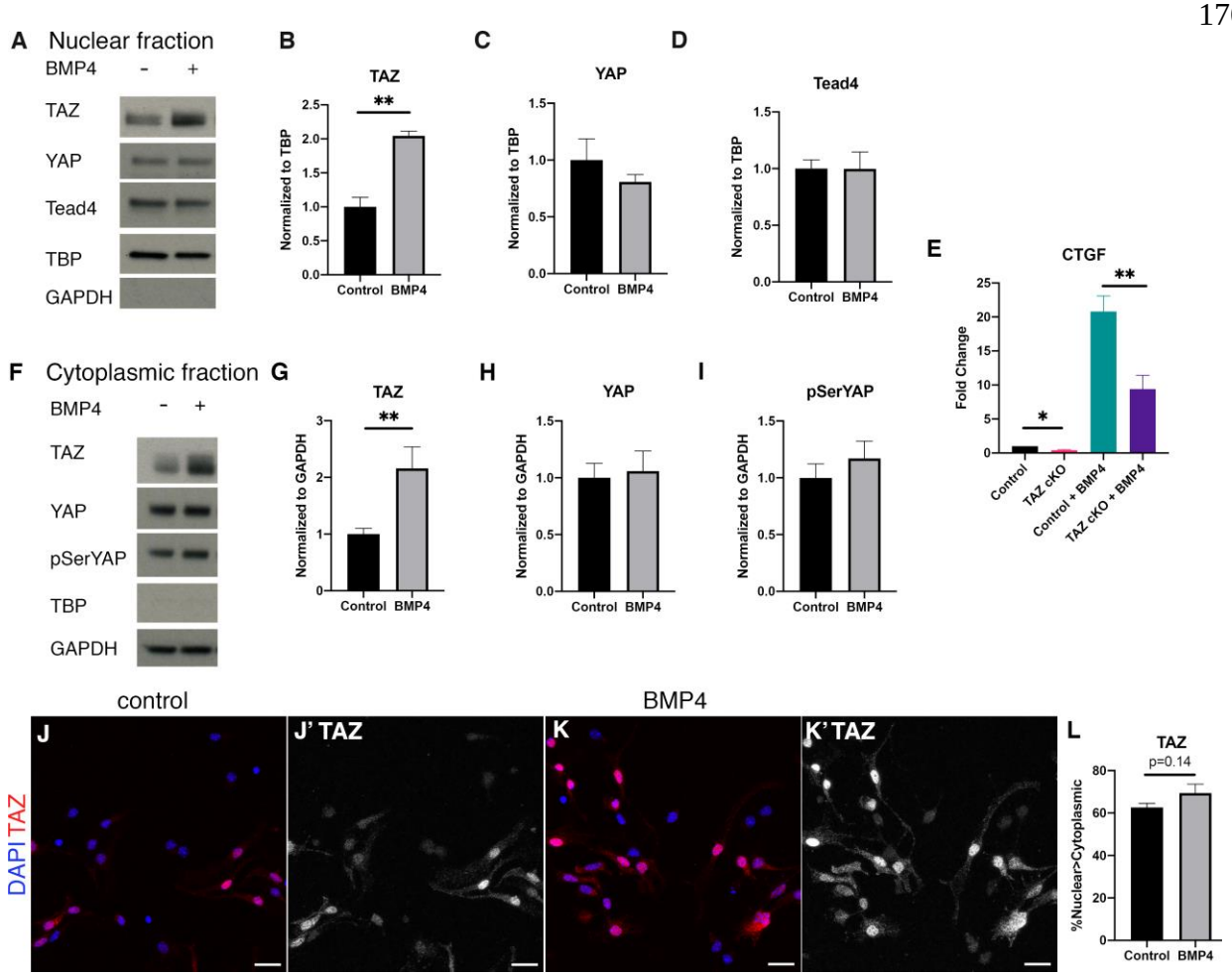

Figure 4.3 BMP increases TAZ protein levels in both the nuclear and cytoplasmic fractions of NPCs, but does not impact YAP sub cellular localization.

A-D) The nuclear fraction of neurospheres treated with BMP4 shows an increase in TAZ, but not YAP (TAZ ratio paired t-test **p=0.0047, YAP ratio paired t-test p=0.2290, TEAD4 ratio paired t-test p=0.7628). All *n* = 5. E) CTGF mRNA is increased in response to BMP4 signaling in neurospheres, and that response is partially abrogated by deletion of TAZ (by RM one-way ANOVA: $F_{3,6}$ = 57.74, ****p<0.0001; paired t-test control vs TAZ cKO *p=0.0260; paired t-test control+BMP4 vs TAZ cKO + BMP4 **p=0.0057). *n* = 3. F-I) The cytoplasmic fraction of BMP4-treated neurospheres shows an increase in TAZ, but no change in total YAP or YAP phosphorylated for degradation (TAZ ratio paired t-test **p=0.0058, YAP ratio paired t-test p=0.8858, pSerYAP ratio paired t-test p=0.2263). All *n* = 6. J-L) Wild-type NPCs plated on PDL/laminin, treated for 2 hours with 20ng/mL BMP4. A trend towards increased nuclear TAZ can be observed in NPCs plated on PDL/laminin (n=3, paired t-test, p=0.14). Scale bar = 20μm. Data are presented as means ± s.e.m.

YAP/TAZ affect NPC astrocytic differentiation

The observation that BMP signaling increases TAZ levels suggested that TAZ might mediate some of the effects of BMP signaling in NPC, such as cell cycle exit and astrocytic differentiation. However, YAP and TAZ have traditionally been ascribed pro-proliferative roles (J. Huang et al., 2005; Q.-Y. Lei et al., 2008; Yu, Zhao, & Guan, 2015). To resolve this seeming contradiction we first examined the effects of knockout of YAP and TAZ in NPC proliferation and differentiation. YAP and TAZ were both ablated through the use of an adeno-Cre virus in $YAP^{fx/fx}/TAZ^{fx/fx}$ cells to generate double conditional knockout (dcKO) NPCs, and EdU incorporation was examined one day post-plating on PDL/laminin coated coverslips in differentiation conditions. Surprisingly, ablation of YAP and TAZ together did not significantly alter EdU incorporation by nestin-expressing NPCs (Figure 4.4A,B,I). Since prior studies have suggested that YAP mediates the anti-proliferative effects of BMP signaling in NPCs (Yao et al., 2014), we examined the responses of YAP and TAZ dcKO NPCs to BMP4 treatment. Treatment of NPCs with BMP4 for 24 hours in differentiation conditions dramatically reduced EdU incorporation in both control and YAP/TAZ dcKO cultures compared to their non-treated counterparts (Fig 4.4C,D,J). These findings indicate that YAP and TAZ are not necessary for the BMP-mediated effects on cell cycle exit. However, the low number of EdU+ cells in BMP4-treated controls was further reduced in YAP/TAZ dcKO cells treated with BMP4 suggesting that YAP and TAZ may have a very slight pro-proliferative effect.

We next investigated whether YAP/TAZ affect astrocytic lineage commitment and differentiation. Cells were plated on PDL/laminin-coated coverslips in order to promote cell survival. Under these conditions, YAP/TAZ dcKO reduced the number of GFAP+ astrocytes after three days in vitro (Fig 4.4E,F,K). There was no change in the percentage of MAP2+ cells

(Fig 4.4M), indicating that YAP and TAZ do not impact neuronal differentiation. Interestingly, when control and YAP/TAZ dcKO NPCs were plated on PDL-only coverslips for differentiation, there was no significant difference in numbers of either GFAP+ astrocytes or MAP2+ neurons (Fig 4.5), indicating that the presence of laminin is necessary for YAP and TAZ to impact astrocyte specification.

Although YAP/TAZ dcKO did not alter the percentage of cells on PDL/laminin coverslips that differentiated into GFAP+ astrocytes after BMP4 treatment (Fig 4.4G,H,L), the morphology of the astrocytes generated was strikingly different. BMP4-induced YAP/TAZ dcKO astrocytes were much more spindly with narrower processes than BMP4-generated control astrocytes, and the GFAP+ astrocytes in the dcKO condition had a much smaller cytoplasmic volume (Fig 4.4O). Sholl analysis of GFAP+ cells generated by BMP treatment also showed a significant increase in the number of processes in dcKO compared to control cells (Fig 4.4P).

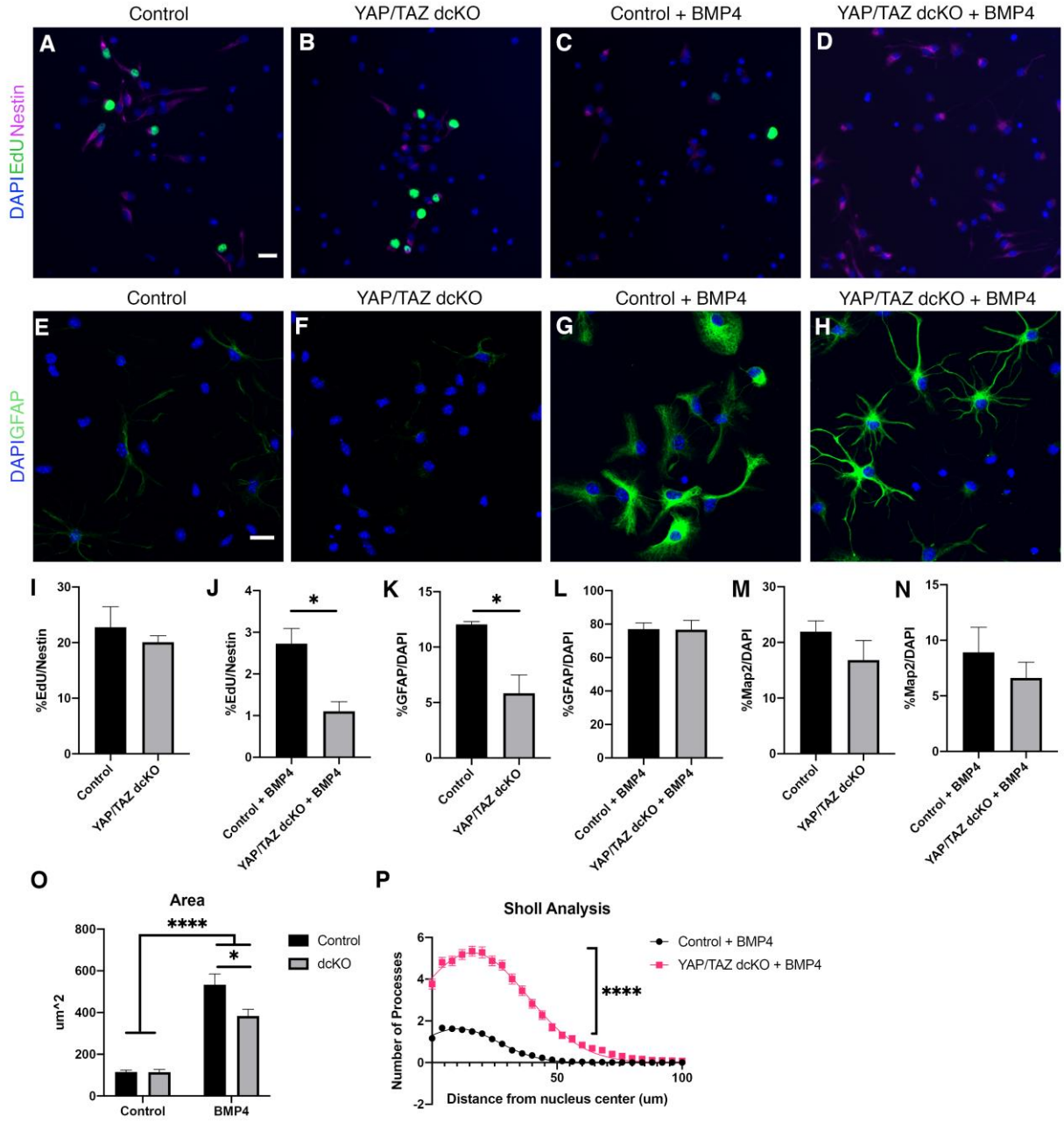

Figure 4.4 YAP and TAZ do not impact NPC proliferation, but do affect NPC astrocytic differentiation.

A,B,I) EdU incorporation in control versus YAP/TAZ double knockout NPCs, plated on PDL (paired t-test p=0.5387, *n* = 5). C,D,J) EdU incorporation in control and YAP/TAZ dcKO NPCs treated with 10ng/mL BMP4 for 24 hours on PDL (paired t-test *p=0.0328, *n* = 5). E,F,K) GFAP+ astrocytes differentiated from control versus YAP/TAZ double knockout NPCs after 3DIV on PDL/laminin (paired t-test *p=0.0134 *n* = 5). G,H,L) GFAP+ astrocytes generated from BMP4-treated control and YAP/TAZ dcKO cells on PDL/laminin (paired t-test p=0.9595 *n* = 5). M) Quantification of MAP2+ cells generated from control and YAP/TAZ double knockout NPCs on PDL/laminin (paired t-test p=0.3881 *n* = 5). N) Quantification of MAP2+ cells

generated from control and YAP/TAZ double knockout NPCs treated with BMP4 on PDL/laminin (paired t-test p=0.4833 *n* = 5). O) Quantification of cell area for GFAP+ astrocytes. (by two-way ANOVA: BMP4 $F_{1,5}$ = 227.7, ****p<0.0001; YAP/TAZ dcKO $F_{1,5}$ = 4.033, p=1.009; BMP4*YAP/TAZ dcKO $F_{1,5}$ = 5.311, p=0.0694; Sidak post-hoc test *YAP/TAZdcKO+BMP4* versus *Control+BMP4* *p<0.05). P) Sholl analysis conducted on control and YAP/TAZ dcKO GFAP+ astrocytes generated in BMP4 on PDL/laminin with a Gaussian fit (unpaired t test of nonlinear fit ****p<0.0001, N=4 or 5, n=20). Data are presented as means ± s.e.m. Scale bars = 20μm.

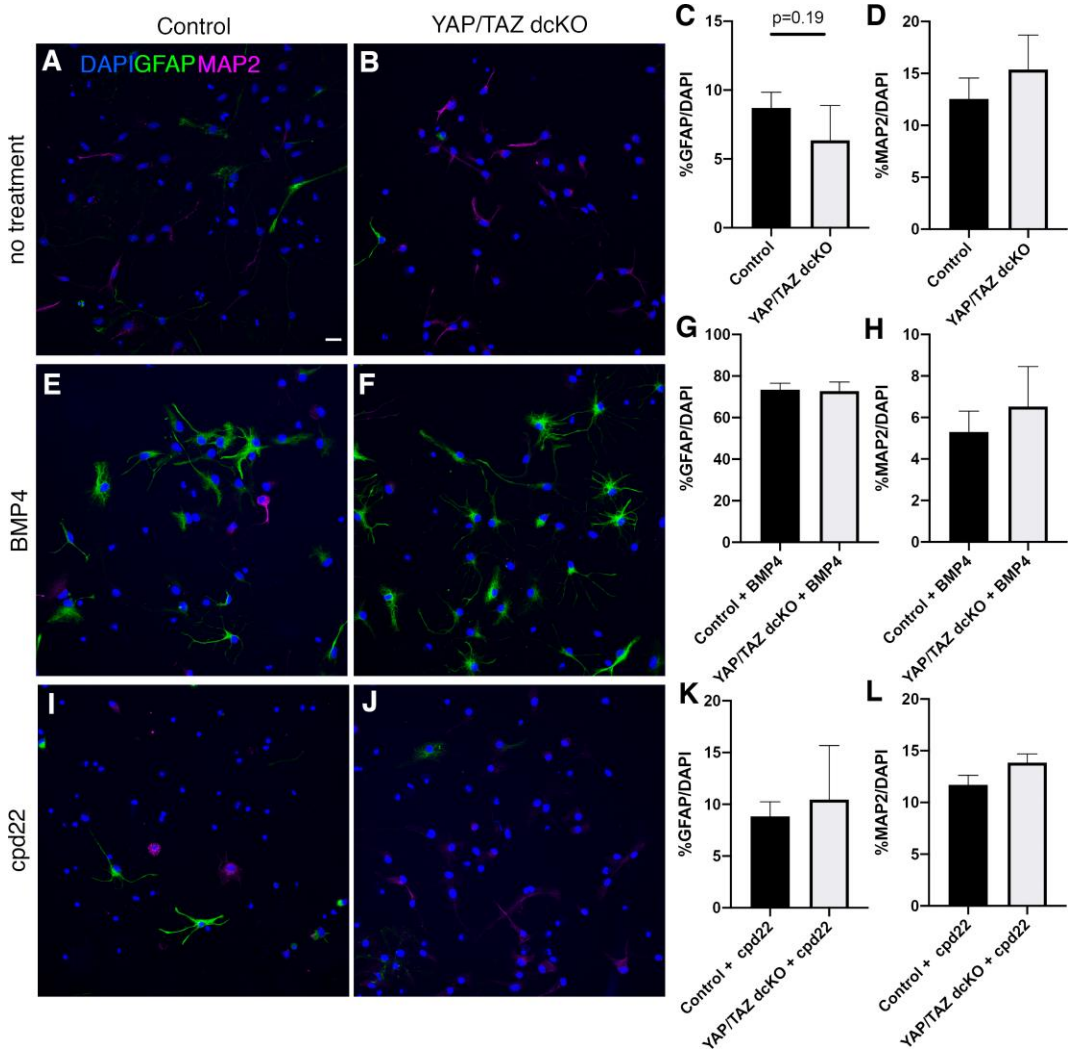

Figure 4.5 Ablation of both YAP and TAZ from NPCs differentiated on PDL-only coverslips does not affect GFAP+ astrocyte differentiation.

A,B) control and YAP/TAZ dcKO NPCs differentiated for 3 days on PDL coverslips, stained for GFAP and MAP2. C) quantification of GFAP+ cells in control and YAP/TAZ dcKO cells (paired t-test p=0.4813 *n*=6). D) Quantification of MAP2+ cells (paired t-test p=0.3905 *n*=6). E,F) control and YAP/TAZ dcKO NPCs differentiated in BMP4 for 3 days on PDL. G) quantification of GFAP+ cells in e-f (paired t-test p=0.9079 *n*=6). H) quantification of MAP2+ cells in e-f (paired t-test p=0.6567 *n*=6). I,J) control and YAP/TAZ dcKO NPCs differentiated in cpd22 for 3 days on PDL. K) quantification of GFAP+ cells in i-j (paired t-test p=0.7774 *n*=6). L) quantification of MAP2+ cells in I-J (paired t-test p=0.2209 *n*=6).

TAZ promotes astrocytic differentiation

YAP and TAZ have been reported to have divergent roles in other cell lines (Kristal Kaan et al., 2017; Plouffe et al., 2018; Tang, Takahashi-Kanemitsu, Kikuchi, Ben, & Hatakeyama, 2018). To determine if TAZ itself can regulate NPC proliferation and astrocyte differentiation, we examined NPCs dissected from a TAZ cKO mouse line. One day post-plating in differentiation conditions, EdU incorporation did not differ significantly between control and TAZ cKO cells (Fig 4.6A,B,I). Since Hippo pathway components may interact with EGF signaling to exert effects on proliferation (Fan, Kim, & Gumbiner, 2013; H. Xia et al., 2018; Yang et al., 2012), we increased levels of EGF 10-fold to determine whether this would help to elicit effects of TAZ, but this did not change proliferation between the two groups (data not shown). We then tested whether overexpression of TAZ would alter proliferation using nucleofection of a constitutively active version of TAZ, TAZ(S89A), which prevents phosphorylation necessary for TAZ protein degradation and increases nuclear TAZ-mediated transcription (Q.-Y. Lei et al., 2008). TAZ(S89A) overexpression did not significantly alter EdU incorporation in NPCs (Fig 4.6C,D,J) despite an over 12-fold increase in TAZ expression without any accompanying increase in the phospho-tagged version (Fig 4.6O).

Since knockout of YAP and TAZ together reduced the number of GFAP+ cells generated from NPCs in culture, we studied them separately to determine their effects on NPC astrocytic differentiation. Ablation of YAP did not significantly alter the number of GFAP+ cells (Fig 4.7). Further, control and YAP NPCs showed no difference in the number of GFAP+ astrocytes after 3 days of BMP4 treatment, nor did they show any obvious differences in morphology. We also observed no difference in the number of cells expressing Aldehyde Dehydrogenase 1L1 (Aldh1L1), a pan-astrocytic marker (Cahoy et al., 2008), between control and YAP cKO

conditions. YAP is therefore not responsible for the differences in GFAP+ astrocytes generated in YAP/TAZ double knockout cells.

We next examined the effects of a knockout of TAZ. The number of GFAP+ astrocytes was decreased in TAZ knockout cells compared to control cells on PDL/laminin, although the number of Aldh1L1 cells was not different (Fig 4.8), indicating that TAZ regulates differentiation of astrocyte subtype (Fig 4E,F,K). The number of GFAP-positive cells did not differ between BMP-treated control and BMP-treated TAZ cKO cultures. This suggests that TAZ is not necessary for BMP signaling to exert its pro-astrocytic effects in spite of the upregulation of TAZ by BMP (Fig 4.6G,H,L). Additionally, GFAP+ astrocyte morphology did not significantly differ in the absence of TAZ when cells were differentiated with BMP (Fig 4.6G,H).

Even though TAZ is not necessary for BMP-induced astrogliogenesis, we found that overexpression of TAZ(S89A) increased the percentage of GFAP+ cells after 3 days in culture (Fig 4.6M,P,Q), although the number of Aldh1L1-expressing astrocytes did not change (Fig 4.6N,P,Q). This suggests that TAZ specifically regulates GFAP+ astrocytes but not all astrocytes.

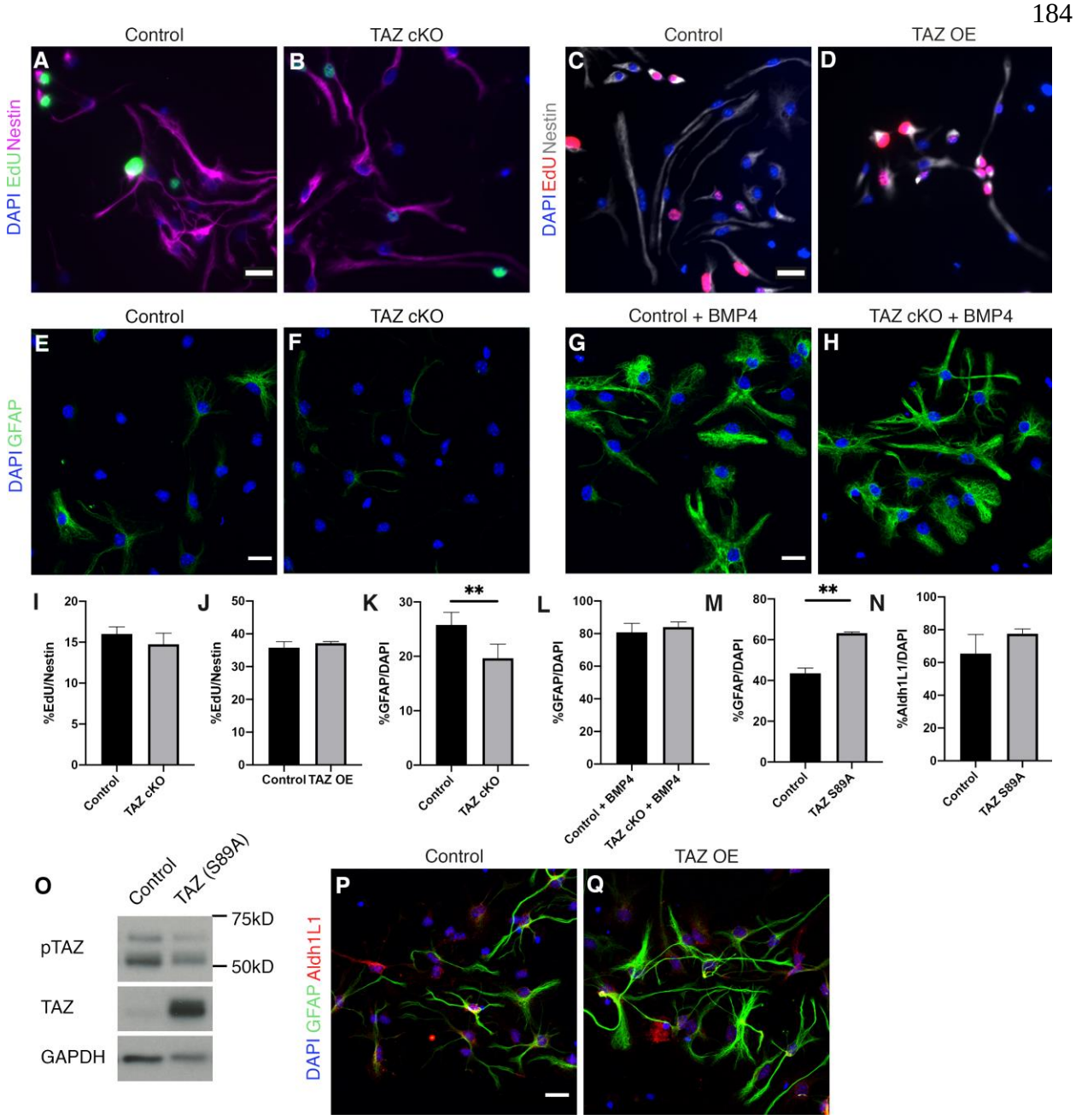

Figure 4.6 TAZ promotes NPC differentiation into GFAP+ astrocytes.

A,B,I) EdU incorporation in control and TAZ knockout cells plated on PDL does not differ (paired t-test p=0.2236 *n* = 4). C,D,J) EdU incorporation in control and TAZ(S89A) overexpression cells plated on PDL does not differ (unpaired t-test p=0.4966 *n* = 3). E,F,K) TAZ knockout cells differentiate into fewer GFAP+ astrocytes on PDL/laminin coverslips after 3DIV (paired t-test **p=0.0078 *n* = 8). G,H,L) GFAP+ astrocytes differentiated from control and TAZ cKO cells in BMP4 treatment on PDL/laminin (paired t-test p=0.5182 *n* = 8). M,P,Q) TAZ overexpression (TAZ OE) results in an increased number of GFAP+ astrocytes after 3DIV on PDL (unpaired t-test **p=0.0017 *n* = 3). N) Aldh1L1 cell counts of control and TAZ overexpressed cells differentiated on PDL (unpaired t-test p=0.3664 *n* = 3). O) Immunoblot

showing overexpression of TAZ(S89A) does not result in increases to the phosphorylated version of TAZ (band around 55kD). Data are presented as means ± s.e.m. Scale bars = 20μm.

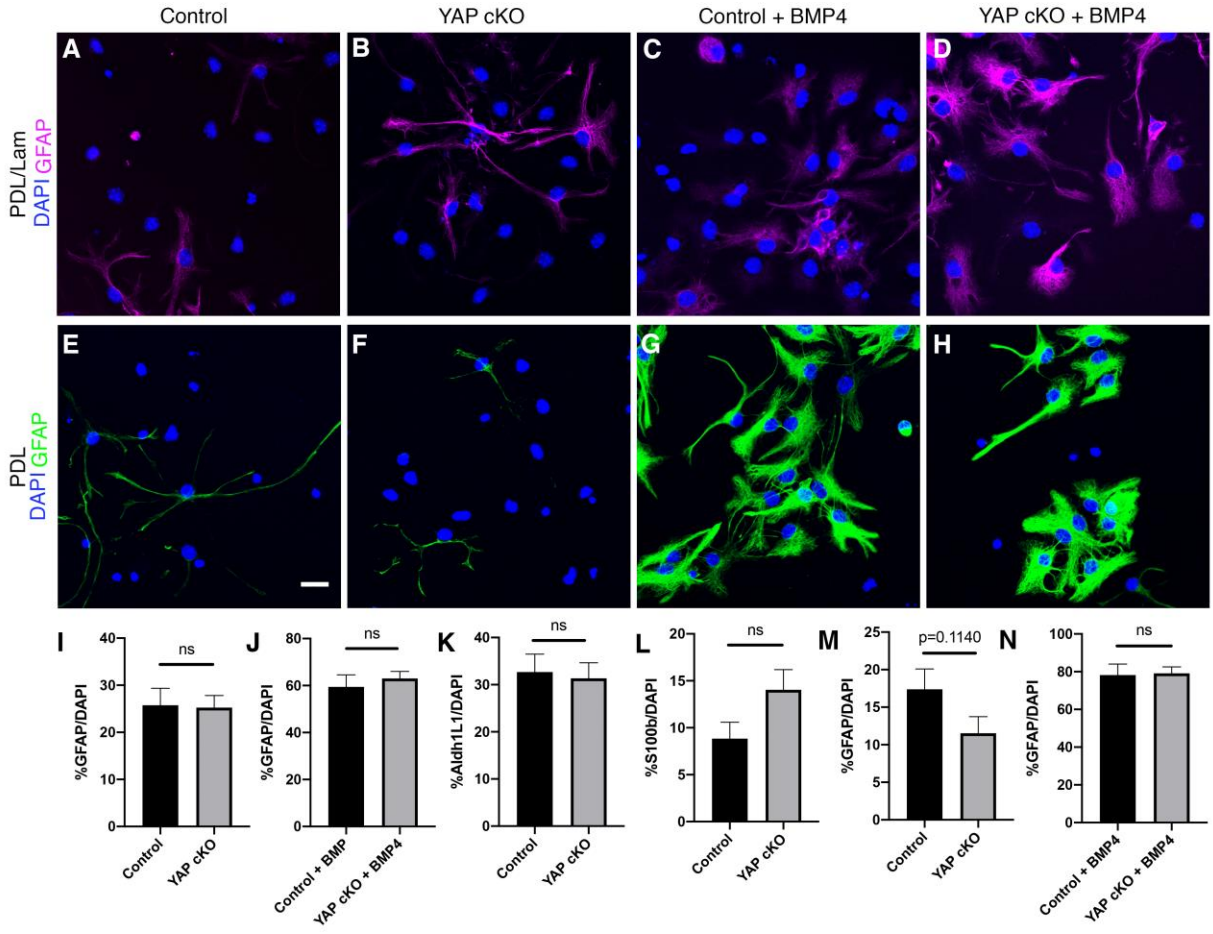

Figure 4.7 Ablation of YAP does not affect differentiation of GFAP+ astrocytes.

A,B) GFAP+ astrocytes in control and YAP cKO cells differentiated on PDL/laminin for 3 days. (paired t-test p=0.9036 ***n*** = 5). C,D) GFAP+ astrocytes in control and YAP cKO cells differentiated in BMP4 on PDL/laminin for 3 days. E,F) GFAP+ astrocytes in control and YAP cKO cells differentiated on PDL for 3 days. G,H) GFAP+ astrocytes in control and YAP cKO cells differentiated in BMP4 on PDL for 3 days. I) quantification of A-B (paired t-test p=0.9036 ***n***=5). J) quantification of C-D (paired t-test p=0.6576 ***n***=5). K) quantification of Aldh1L1+ astrocytes generated in control and YAP cKO NPCs after 3 days differentiation on PDL/laminin (unpaired t-test p=0.8008 ***n***=4,5). L) quantification of S100β+ astrocytes in control and YAP cKO cells differentiated on PDL/laminin (unpaired t-test p=0.1131 ***n***=4,5). M) quantification of GFAP+ astrocytes from E-F (unpaired t-test p=0.1140 ***n***=7,8). N) quantification of GFAP+ astrocytes from G- H (unpaired t-test p=0.8958 ***n***=7.8). Scale bar = 20μm. Data are presented as means ± s.e.m.

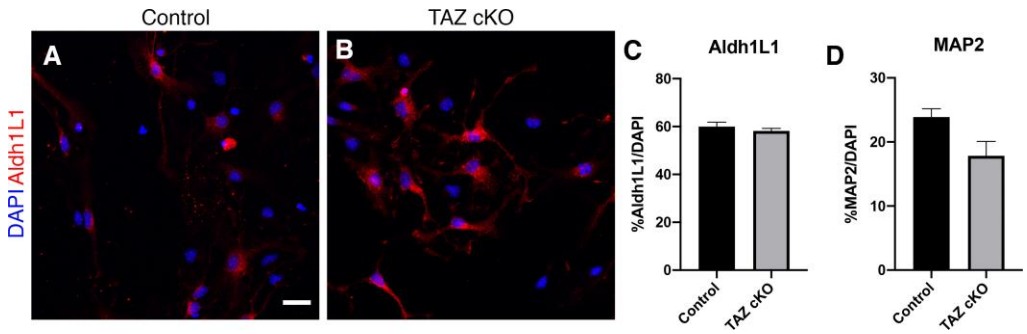

Figure 4.8 Ablation of TAZ from NPCs does not affect expression of the pan-astrocytic marker Aldh1L1

A,B) control and TAZ cKO NPCs differentiated on PDL/laminin for 3 days and stained with pan-astrocytic marker Aldh1L1. Scale bar = 20μm. C) quantification of Aldh1L1+ astrocytes of A-B (paired t-test p=0.4947, *n*=5). D) quantification of MAP2+ neurons of control and TAZ cKO differentiated cells (paired t-test p=0.1139, *n*=5).

The effects of ILK signaling on TAZ and YAP

β1-integrin promotes stem cell survival and regulates NPC proliferation and lineage commitment (Brooker et al., 2016; Leone et al., 2005; L. Pan et al., 2014). In other systems, β1-integrin and its downstream signaling components are known to regulate TAZ and YAP through suppression of the Hippo pathway. β1-integrin regulation of YAP has been demonstrated in mammary epithelial cells (J. Y. Lee et al., 2019), myofibroblasts (Martin et al., 2016), osteoblasts, and mouse embryonic fibroblasts (Sabra et al., 2017). Downstream effectors of integrins regulate TAZ nuclear localization as well (P. Xia, Gütl, Zheden, & Heisenberg, 2019), but extracellular matrix (ECM) effects on TAZ have not been as well examined as those of its paralogue YAP.

To examine the effect of β1-integrin signaling on YAP and TAZ expression, we added a β1-integrin blocking antibody to NPC cultures for 24 hours before harvesting the cells for western blot analyses. TAZ protein levels were reduced in cultures treated with the blocking antibody, whereas YAP and its phosphorylated version were not as significantly affected (Figure 5A,C,D,E). YAP and TAZ expression are regulated by a number of kinases including LATS1 and GSK3β, but levels of phospho-LATS1 (Fig 4.9A,B), phospho-GSK3β, and total GSK3β were not altered (Fig 4.10). Similar effects were seen when cells were treated for 6 hours with cpd22, a pharmacologic inhibitor that targets integrin-linked kinase (ILK), a downstream effector of β1-integrin (Fig 4.10). To determine if cellular localization of TAZ and YAP is affected by disruption of β1-integrin signaling, we next fractionated cells and examined the nuclear and cytoplasmic compartments separately. Both nuclear and cytoplasmic fractions of TAZ were significantly decreased in cpd22-treated NPCs, while only nuclear YAP was decreased in the

presence of cpd22 (Figure 4.9F-H,J-L). These findings suggest that ILK signaling regulates nuclear shuttling of transcriptional active YAP.

We sought to examine if transcriptional changes were responsible for the decrease in protein levels. However, cpd22 treatment did not significantly change YAP mRNA, and actually slightly increased levels of TAZ mRNA (Fig 4.9I). Staining of cells using a YAP antibody also confirmed that cpd22 treatment for 4 hours was sufficient to reduce YAP levels in the nuclear compartment compared to the cytoplasm (Fig 4.9O-Q). To determine if protein turnover was instead responsible, we treated NPCs with MG-132, a proteasome inhibitor, and found that MG-132 treatment abrogated cpd22-mediated degradation of TAZ, but not YAP protein (Fig 4.9M,N). Together, these data indicate that ILK signaling promotes TAZ protein stability but does not alter nuclear vs cytoplasmic localization of TAZ.

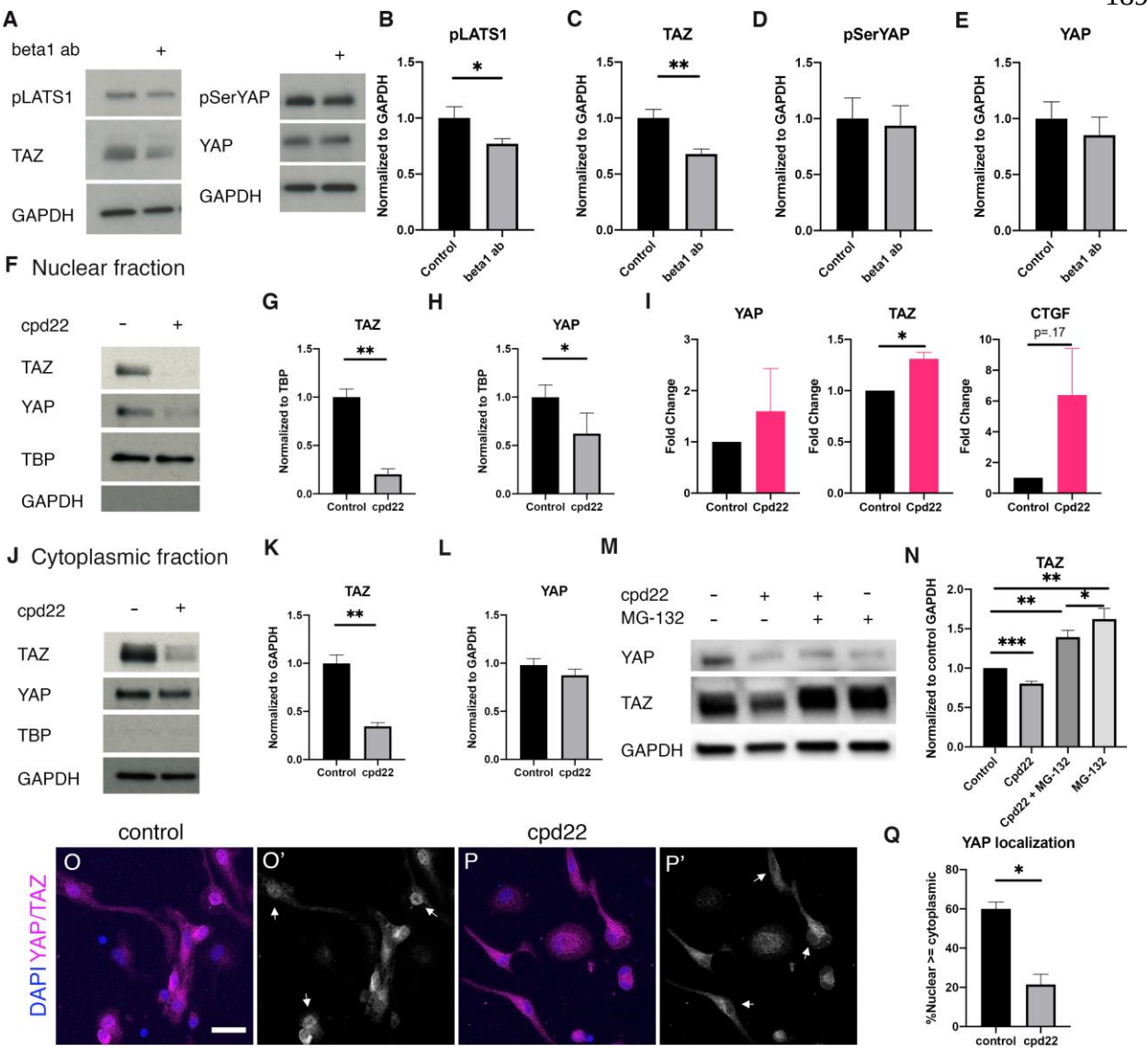

Figure 4.9 ILK signaling promotes YAP and TAZ protein stability.

A-E) 24 hour addition of β1-integrin blocking antibody to NPCs measured by immunoblotting. B) pLATS1 protein levels (paired t-test *p=0.0299 *n*=5). C) TAZ protein levels are reduced by β1-integrin blocking antibodies (paired t-test **p=0.0057 *n*=5). D) pSerYAP protein levels (paired t-test p=0.5974 *n*=5). E) YAP protein levels (paired t-test p=0.1108). F) 6 hour treatment with cpd22 reduces YAP and TAZ protein levels in the nuclear fraction of NPCs. G) TAZ nuclear protein levels (paired t-test **p=0.0021 *n*=5). H) YAP nuclear protein levels (paired t-test *p=0.0409 *n*=5). I) mRNA levels of YAP, TAZ, and CTGF in response to 6 hours of cpd22 treatment (paired t-test; YAP p=0.5251, TAZ *p=0.0163, CTGF p=0.1742. All *n*=4). J) immunoblotting of cytoplasmic fraction of NPCs treated with cpd22 for 6 hours. K) TAZ cytoplasmic protein levels (paired t-test **p=0.0028 *n*=5). L) YAP cytoplasmic protein levels (paired t-test p=0.1047 *n*=5). M) NPCs treated with cpd22, MG-132, or both for 6 hours and probed for TAZ and YAP via immunoblotting. N) TAZ protein levels (via paired t-test; control vs cpd22 ***p=0.0005, control vs cpd22+MG-132 **0.0034, control vs MG-132 **p=0.0036,

MG-132 vs cpd22+MG-132 *p=0.0378, *n*=7). O-O') YAP staining of wild-type NPCs plated on PDL in 2ng/mL EGF. Arrows indicate nuclear localization of YAP in individual cells. Scale bar = 20μm. P-P') YAP staining of wild-type NPCs treated with 1uM cpd22 for 4 hours on PDL in 2ng/mL EGF. Arrows indicate cells with lower nuclear YAP compared to cytoplasmic YAP. Q) YAP demonstrates decreased nuclear localization in cpd22-treated NPCs after 4 hours (paired t-test *p=0.027, *n*=3). Data are presented as means ± s.e.m.

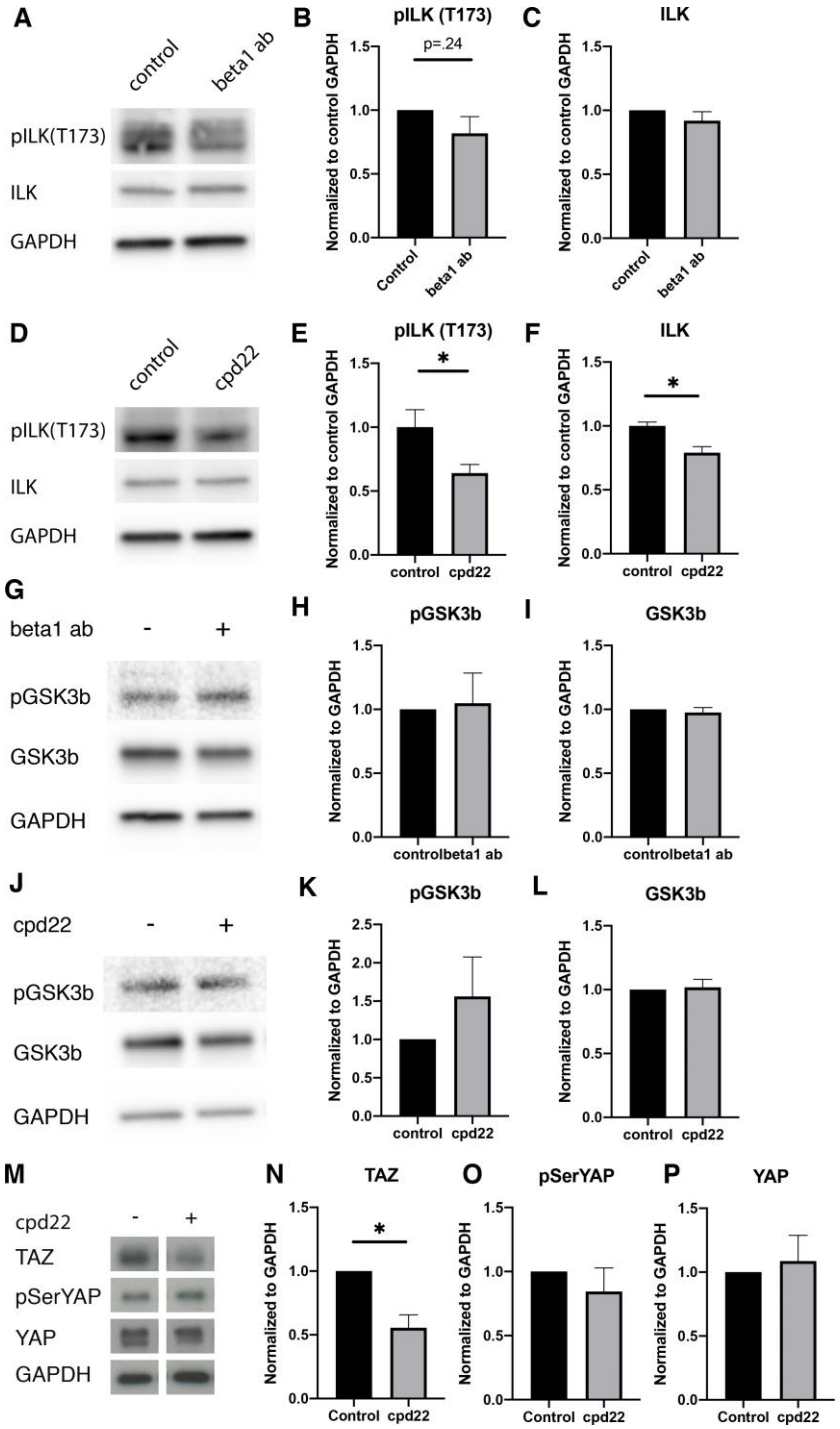

Figure 4.10 Use of either of a β1-blocking antibody or the ILK-inhibitor cpd22 lowers levels of phospho-ILK in NPCs.

A) immunoblotting of NPCs treated with β1-blocking antibody for 24 hours. B) pILK(T173) in β1-inhibited NPCs (paired t-test p=0.2374 *n*=5). C) ILK in β1-inhibited NPCs (paired t-test p=0.3122 *n*=5). D) immunoblotting of NPCs treated with cpd22 for 6 hours. E) pILK(T173) in

cpd22-treated NPCs (unpaired t-test *p=0.0498 *n*=3 and 4). F) ILK in cpd22-treated NPCs (unpaired t-test *p=0.0198 *n*=3 and 4). G) immunoblotting of NPCs treated with β1-blocking antibody for 24 hours. H) pGSK3b measurements from part G (paired t-test p=0.8470 *n*=5). I) GSK3b measurements from part G (paired t-test p=0.5663 *n*=5). J) immunoblotting of NPCs treated with cpd22 for 6 hours. K) pGSK3b measurements from part J (paired t-test p=0.3373 *n*=5). L) GSK3b measurements from part J (paired t-test p=0.7902 *n*=5). M) immunoblotting of NPCs treated with cpd22 for 6 hours. N) TAZ in cpd22-treated NPCs (paired t-test *p=0.0117 *n*=5). O) pSerYAP in cpd22-treated NPCs (paired t-test p=0.4453 *n*=5). P) YAP in cpd22-treated NPCs (paired t-test p=0.6907 *n*=5). Data are presented as means ± s.e.m.

β1-integrin promotes NPC proliferation and inhibits astrocytic differentiation through YAP/TAZ

We next asked whether β1-integrin -mediated changes in nuclear/cytoplasmic shuttling of YAP have functional consequences on NPC proliferation or fate specification. Since laminin is a ligand for 1-integrin (Belkin & Stepp, 2000; Chernousov, Kaufman, Stahl, Rothblum, & Carey, 2007; Colognato, MacCarrick, O'Rear, & Yurchenco, 1997), we compared NPCs plated for 24hrs on PDL versus PDL/laminin. As expected, we found that YAP nuclear levels in PDL/laminin plated cells were slightly more elevated compared to cytoplasmic levels (Fig 4.11A,C). Additionally, the percentage of Ki67+ cells was increased in the PDL/laminin condition, indicating an increase of cells in cell cycle, consistent with β1-integrin's role in maintaining stemness of NPCs (Fig 4.11B) (Campos et al., 2004; Leone et al., 2005). Strikingly, when YAP knockout NPCs were plated on PDL/laminin coated coverslips, they demonstrated reduced EdU incorporation compared to control cells (Fig 4.11D). This difference in proliferation was not observed when we compared control cells to YAP cKO cells plated on PDL (Fig 4.11E), suggesting that activation of extracellular matrix-sensing cellular components may be necessary for YAP action, in line with the known roles of YAP and TAZ in mechanosensing. Ablation of TAZ on PDL/laminin did not demonstrate a similar effect on proliferation (Fig 4.11F), indicating this is a YAP-specific effect.

We also examined if β1-integrin signaling has a role in mediating YAP/TAZ action during NPC astrocytic differentiation. When control NPCs on PDL/laminin were treated with cpd22 to abrogate ILK signaling, the number of GFAP+ astrocytes increased (Fig 4.11G-K), in line with previous studies of the role of -integrin and ILK signaling in suppressing astrocyte differentiation. However, there was no increase in GFAP+ astrocyte numbers after cpd22

treatment of YAP/TAZ double cKO NPCs on PDL/laminin, although this was not seen in YAP cKO only NPCs (Fig 4.11L). Neuronal differentiation marked by MAP2+ cells was not affected in YAP/TAZ dcKO NPCs (Fig 4.12A). This difference in GFAP expression in response to cpd22 was not seen in NPCs plated on PDL alone (Fig 4.12B). Thus the presence of extracellular laminin promotes YAP/TAZ-mediated inhibition of astrocyte differentiation, but ablation of ILK signaling prevents these effects.

Taken together, these findings suggest that TAZ and YAP perform distinct functions in the context of postnatal astrogliogenesis. Our data support a model where TAZ responds to instructive cues from pro-differentiation signals such as BMPs, which needs to be coordinated with the inhibition of pro-proliferative YAP and integrin signaling to permit a release from cell cycle and astrocyte lineage commitment.

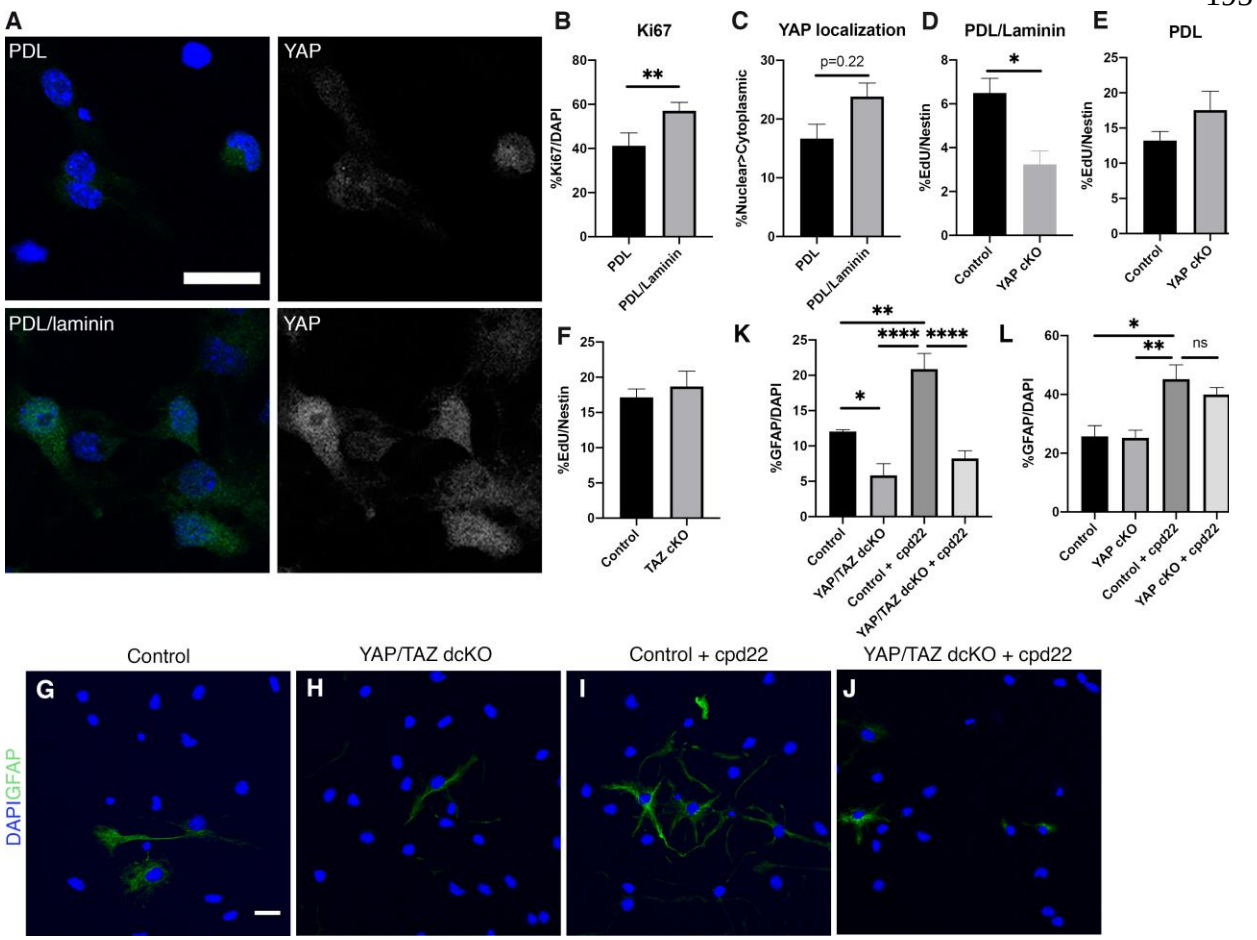

Figure 4.11 β1-integrin signaling promotes YAP to regulate NPC proliferation and TAZ for astrocytic differentiation.

A) NPCs plated on PDL and PDL/laminin stained for YAP. Scale bar = 20μm. B) Ki67+ cells were increased in PDL/laminin plated NPCs compared to PDL-only cells (paired t-test **p=0.0088 *n*=4). C) YAP localizes more to the nucleus of PDL/laminin NPCs compared to PDL-only plated NPCs (paired t-test p=0.2202 *n*=4). D) EdU incorporation is reduced in YAP cKO NPCs plated on PDL/laminin compared to control NPCs (paired t-test *p=0.0406 *n*=5). E) EdU incorporation in control and YAP cKO NPCs on PDL does not differ (paired t-test p=0.0908 *n* = 5). F) EdU incorporation does not differ between control and TAZ cKO NPCs plated on PDL/laminin (paired t-test p=0.5088 *n*=5). G-J) GFAP+ cells generated from control and YAP/TAZ dcKO cells differentiated on PDL/laminin in the presence of cpd22. Scale bar = 20μm. K) quantification of GFAP+ cells in G-J (RM one-way ANOVA $F_{3,12}$=25.42 ****p<0.0001; Tukey's post-hoc test control vs YAP/TAZ dcKO *p=0.0256, control vs control+cpd22 **p=0.0022, YAP/TAZ dcKO vs control+cpd22 ****p<0.0001, control+cpd22 vs YAP/TAZ dcKO+cpd22 ****p<0.0001, *n*=5). L) quantification of GFAP+ cells generated from cpd22-treated control and YAP cKO cells on PDL/laminin (RM one-way ANOVA $F_{3,12}$=7.786 **p=0.0038; Tukey's post-hoc test control vs control+cpd22 *p=0.0117, YAP cKO vs control+cpd22 **p=0.0099, *n*=5). Data are presented as means ± s.e.m.

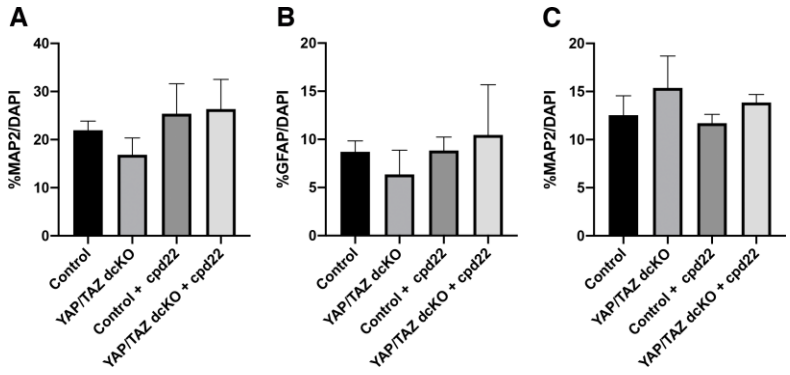

Figure 4.12 Effects of cpd22 treatment on control and YAP/TAZ dcKO NPC differentiation.

A) Quantification of MAP2+ neurons in control and YAP/TAZ dcKO NPCs differentiated for 3 days on PDL/laminin with and without ILK inhibitor cpd22 (by ordinary one-way ANOVA $F_{3,16}$=0.7983 p=0.5127). B) quantification of GFAP+ astrocytes in control and YAP/TAZ dcKO NPCs differentiated for 3 days on PDL with and without ILK inhibitor cpd22 (by RM one-way ANOVA $F_{3,15}$=0.3650 p=0.7793). C) quantification of MAP2+ neurons in control and YAP/TAZ dcKO NPCs differentiated for 3 days on PDL with and without ILK inhibitor cpd22 (by RM one-way ANOVA $F_{3,15}$=0.5982 p=0.6260). Data are presented as means ± s.e.m.

IV. Discussion

YAP and TAZ are well known to have pro-proliferative effects in multiple systems, but TAZ in particular has not previously been well characterized in neural stem cells, and rarely have YAP and TAZ been examined separately. In this study, we examined the role of YAP and TAZ in NPCs, as well as their interactions with two other signaling pathways, BMP and β1-integrin, to form a model for how all of these cues intersect (Fig 7). We found that BMP signaling promotes TAZ but not YAP expression in NPCs, underlining the need to treat these two transcriptional coactivators as distinct molecular entities. This also stands in contrast to previous studies that report BMP regulation of YAP activity through phosphorylation. This discrepancy may reflect difficulties in separating YAP from TAZ using the limited antibodies that were available previously. Although less likely, it is also possible that this reflects our use of BMP4 rather than BMP2 that was used in the prior studies and/or differences in dosing and time points. Crucially, we found using double null mutant cells that neither YAP or TAZ are necessary for the pro-astrocytic effects of BMP signaling, although astrocyte morphology was altered in the joint absence of YAP and TAZ. This is consistent with past studies on the effect of YAP and TAZ on regulation of cell morphology through cytoskeletal elements, and the lack of striking morphological changes observed with deletion of either one alone suggests that they have overlapping functions in this regard.

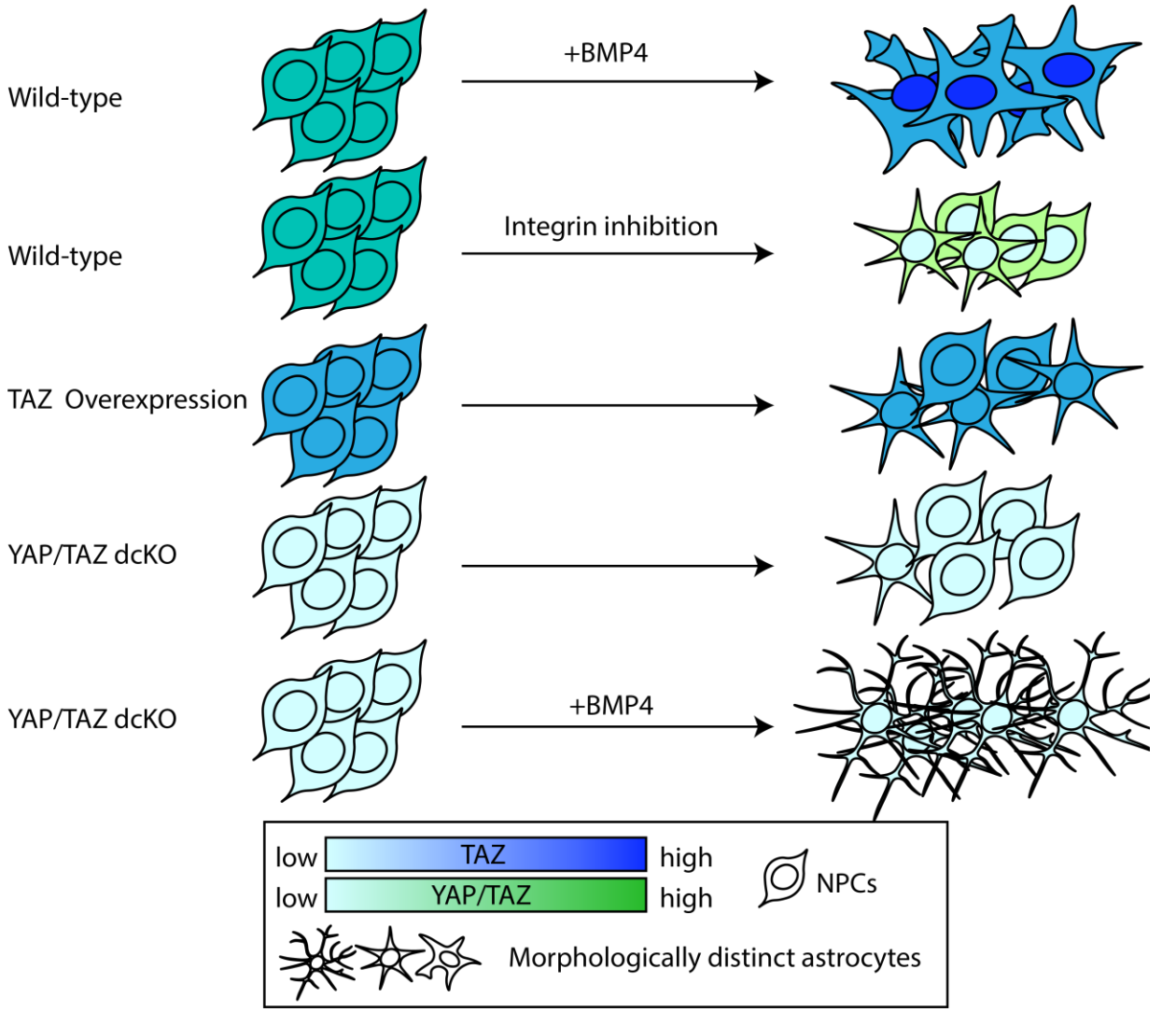

Figure 4.13 A model for BMP4 and β1-integrin regulation of YAP and TAZ in neural stem and progenitor cells.

Wild-type NPCs treated with BMP have increased levels of TAZ and differentiate into large GFAP+ astrocytes. Overexpression of TAZ also results in an increased number of GFAP+ astrocytes. From YAP/TAZ dcKO NPCs, fewer GFAP+ astrocytes are generated, but in the presence of BMP4, a large number of spindly GFAP+ astrocytes are observed. When integrin signaling is inhibited through use of cpd22, YAP and TAZ levels are decreased and the number of GFAP+ astrocytes increases.

We also found that ablation of TAZ but not YAP inhibits GFAP+ astrocyte differentiation, and that overexpression of TAZ conversely is sufficient to promote astrocyte differentiation. However, these effects on astrocyte subtype differentiation were only observed in NPCs plated on PDL/laminin-coated coverslips for differentiation, rather than PDL-only coverslips. Combined with our results on EdU incorporation and astrocyte differentiation in YAP/TAZ deleted cells in the presence of ILK inhibitor cpd22, this indicates that YAP and TAZ only have effects on cell proliferation and astrocyte subtype specification in the presence of extracellular matrix cues such as □-integrin and ILK. This highlights the importance of carefully controlling culture conditions when examining these signaling pathways in vitro.

Our ability to separate YAP and TAZ in this study has enabled us identify that YAP and TAZ are distinct entities with unique roles in NPC fate determination. When downstream of integrin signaling, YAP promotes proliferation, while TAZ promotes differentiation into GFAP-expressing astrocytes. Additionally, regulation of these transcriptional coactivators differs. While both are downstream of β1-integrin/ILK signaling, BMP signaling regulates TAZ but not YAP, contradicting previous studies. Nevertheless, although BMP signaling targets TAZ into the nucleus with the potential to subserve an instructive role for transcriptional activation and fate determination, TAZ is not required for BMP-mediated promotion of astrocyte lineage commitment.

Our findings suggest that TAZ instead modifies the morphology and other characteristics of astrocytes after they are born. Thus future studies may consider examining Rho GTPases, or other actin cytoskeletal regulatory elements that may have connections to both YAP/TAZ and β1-integrin.

Chapter 5

General Discussion

I. Summary

Bone morphogenetic protein signaling (BMP) plays a major role during embryonic development, injury and inflammation, and numerous diseases, and yet the downstream mechanisms of BMP are largely unknown. Previous studies from our lab have shown that BMP signaling promotes astrogliogenesis, and inhibition of BMP signaling through administration of an antagonist results in protection from CNS injury (Samanta et al., 2010). The studies described in previous chapters examined BMP signaling targets, both transcriptional and otherwise, in neural stem/progenitor cells and astrocytes, as well as their impact on cell fate and morphology. The following sections discuss our primary conclusions and limitations, as well as potential future directions that may be pursued as a result of these studies.

II. BMP-responsive HtrA1 is a novel astrocyte-specific marker

Through our microarray to examine genes upregulated in BMP-differentiated astrocytes and enriched in astrocytes compared to mRNA levels in neurospheres, oligodendrocytes, and neurons, we identified several candidate genes that have increased expression in astrocytes and might serve as astrocytic markers, either alone or in combination with other established genes. In particular, we identified high temperature requirement A1 serine protease (HtrA1). We characterized HtrA1 mRNA expression across multiple brain regions, showing that *in vivo* it is not present in non-astrocyte cell types, thereby identifying an astrocyte marker that is not also present in neural stem cells. We also identified HtrA1 as upregulated by BMP treatment in

astrocytes derived from human embryonic stem cells, indicating HtrA1 presence and regulation in astrocytes is evolutionarily conserved.

We showed expression of HtrA1 mRNA over the course of development, starting from embryonic day 14 in the cortical hem, through increases seen during gliogenesis from P7 to P14. We demonstrated that in HtrA1-deficient NPCs differentiated *in vitro*, Nestin expression is downregulated as GFAP expression is increased. Additionally, the absence of HtrA1 results in decreased cell proliferation *in vitro*. *In vivo*, Aldh1L1 expression is increased in HtrA1 deleted mice, indicating increased early astrogliogenesis, although by P7 the difference in Aldh1L1 expression has disappeared. Increased EdU incorporation seen *in vivo* at P1 in HtrA1-/- mutants is gone by P7, and indeed, EdU incorporation is decreased in mutant neocortex by P7 compared to controls. These findings indicate that not only is HtrA1 a novel astrocyte marker, but it may also play a role in astrocyte division and maturation tempo.

HtrA1 mutations are linked to cerebral autosomal recessive arteriopathy with subcortical infarcts and leukoecephalopathy (CARASIL). Therefore, understanding how HtrA1 functions is important to potentially addressing this disease. We found that HtrA1 impacts astrocyte morphology by regulating area and process number, as well as upregulates neurite length in co-cultured cortical neurons. Additionally, HtrA1 may modulate the extracellular environment through its protease activities, including cleavage of CSPGs such as neurocan.

HtrA1 additionally modulates reactive gliosis following cortical stab wound injury. Following injury, both BMP signaling and HtrA1 are upregulated, although deletion of BMPR1a does not appear to impact HtrA1 levels in this situation, indicating that HtrA1 is upregulated by other signaling mechanisms during inflammation. Moreover, lesion size following injury is larger in HtrA1 deficient mice compared to controls, with proliferating endothelial and

microglial cells increased as well, indicating that HtrA1 modulates cortical injury recovery through repressing proliferation of immune and vascular cells.

Given that in the mouse brain, we have only found HtrA1 to be present in astrocytes, these results indicate that HtrA1 in astrocytes functions to regulate aspects of injury response, astrocyte morphology, ECM modulation, and neuronal dendrites. However, CARASIL, which is a disease linked to HtrA1 mutation, is a genetic, adult-onset disease. It is therefore possible that our experiments on HtrA1 function may not fully expose the underlying molecular mechanisms due to our use of primarily postnatal and young adult mice. Future studies should examine HtrA1 function in an aging model, particularly since the blood brain barrier becomes leakier with age (Montagne et al., 2015), and proper astrocytic regulation of the blood-brain barrier becomes more critical. Future directions may also include additional co-culture studies, where $HtrA1^{-/-}$ astrocytes are cultured with endothelial cells, and the properties of those endothelial cells are examined. As the field of organoid 3D culture advances, once vasculature and vascular flow can be reliably replicated in an organoid model, generation of cortical organoids with $HtrA1^{-/-}$ astrocytes will allow for more detailed analysis and understanding of HtrA1 function.

Future studies may also focus on F3 and Hopx, which our microarray also identified as upregulated in BMP-induced astrocytes. While there have been some recent studies on Hopx as a potential neural stem cell marker (D. A. Berg et al., 2019), there have been few studies on its function and relation to BMP signaling. Although HtrA1 was originally identified as upregulated in BMP-induced astrocytes, in our RNA sequencing study of Chapter 3, it was not identified in wild-type NPCs as transcriptionally regulated by short-term BMP stimulus. Similarly, F3 was not identified as transcriptionally responsive to BMP, but Hopx was. How BMP regulates these proteins in NPCs and astrocytes is unclear, as well as what their function might be in the CNS.

Future studies undertaking a closer examination of F3 and Hopx may reveal more insights into astrocyte specification mechanisms.

III. BMP signaling short-term transcriptional targets in NPCs

Our RNA sequencing has identified thousands of direct, short-term BMP transcriptional targets in neural stem and progenitor cells. Through pathway analysis, we have identified numerous biological processes and pathways that are regulated by short-term BMP4-stimulated transcription. Additionally, we have identified a number of genes that are regulated differentially by BMPR1a and BMPR1b. Further analysis of these targets will help with understanding why BMPR1a and BMPR1b govern different developmental processes, such as oligodendrocyte development, embryonic development, limb chondrogenesis, neurite outgrowth, as well as various diseases and disorders such as excessive gliosis following spinal cord injury. While we have only conducted a preliminary examination of the transcriptomic data here, we have clearly shown that BMPR1b and BMPR1a have different transcriptional effects in NPCs. BMPR1a regulates a larger number of genes for transcription than BMPR1b, as evidenced through the number of genes changed in the absence of these individual receptors. Additionally, we have shown that there are a number of BMP target genes that require the presence of both BMPR1a and BMPR1b for regulation by BMP4 ligand (as demonstrated by the large number of genes solely identified as changed in wild-type NPCs).

The next immediate step of studies to follow up on the creation of this database is to examine genes that are uniquely regulated in either BMPR1a or BMPR1b ablated cultures, but not both. Following identification of these genes, pathway analysis should be conducted to pick out specific biological process that may be differentially regulated. Additionally, future studies may seek to compare the Noggin baseline cultures to each other, to examine whether ablation of

a receptor itself in the absence of ligand stimulation results in differences in gene expression. Similarly, the BMP4-treated transcriptomes may be compared to each other.

BMP signaling clearly has more than transcriptional effects, as is clear by the phosphorylation activity of BMP receptors and SMADs. Further studies may include an examination of proteomics or metabolomics. However, in the absence of such data to better understand this pathway, the identification of multiple biological processes from BMP-regulated genes may provide specific targets for further study of non-transcriptional regulation.

IV. Regulation of YAP and TAZ in NPCs

In Chapter 3's examination of the NPC transcriptome in response to short-term BMP4 stimulus, the Hippo pathway was identified as BMP-regulated in multiple analyses. In our examination of YAP and TAZ in NPCs in Chapter 4, we found that BMP regulates TAZ protein levels through translation regulation, but does not regulate YAP, which is in contrast to previously published studies (Z. Huang, Hu, et al., 2016a; Yao et al., 2014). We additionally identified a novel role for TAZ in facilitating astrocyte differentiation that was not observed for YAP, thereby clearly identifying YAP and TAZ as distinct molecular entities with divergent functions in neural stem and progenitor cells. Despite YAP and TAZ commonly being treated as one target, and despite the use of verteporfin as a YAP/TAZ inhibitor in potential cancer treatment (Lui et al., 2019), this clearly speaks to the need for individually targeted drugs and small molecules, as this may indicate that YAP and TAZ play disparate roles in disease models as well. However, in NPCs YAP and TAZ do still play some overlapping role in cell morphology, as the ablation of both in BMP-generated astrocytes resulted in cells with a greater number of long processes, which is not observed with individual gene knockouts. Both are regulated by extracellular cues including laminin and integrin signaling, and TAZ requires the

presence of laminin substrate to exert its effects on astrocyte fate specification, while YAP requires laminin to promote NPC proliferation.

Although we have shown that BMP regulates TAZ, the downstream molecular mechanisms by which BMP exerts its effects on downstream cellular phenotypes are not clear. There are number of potential signaling components to explore. Further studies would include immunoprecipitation of TAZ in wild-type versus BMP-treated NPCs, then probing for likely binding partners, including SMADs, as well as factors such as Runx2, which has been implicated in BMP's pro-differentiation effects in other systems (Okawa, Nicklas, Zickenrott, Schwamborn, & Del Sol, 2016; Park et al., 2019). Further molecular studies should also include examination of cell cycle regulators, particularly cyclin dependent kinases regulators such as Cyclin D1 (ccnd1) and p21, which are known to act downstream of BMP or TGFβ signaling and have been linked to YAP/TAZ in a few studies (Dai et al., 2013; Muramatsu et al., 2011; Podkowa et al., 2013; Yao et al., 2014). For a broader understanding of how YAP and TAZ act downstream of BMP, $YAP^{fx/fx}$, $TAZ^{fx/fx}$, and $YAP^{fx/fx}TAZ^{fx/fx}$ NPCs should be generated, treated with BMP4 ligands, and the RNA transcriptomes compared.

Detailed functional studies of control versus TAZ-ablated astrocytes may be a future direction to better understand how TAZ-mediated morphological changes in BMP-generated astrocytes are functionally relevant, and if TAZ deletion merely lowers the rate of GFAP+ astrocyte maturation, or changes other properties as well. Differentiation of $TAZ^{fx/fx}$ and $YAP^{fx/fx}$ NPCs on different substrates will provide insights into how TAZ and YAP regulate input from different ECM components. It has previously been reported that YAP responds to fibronectin substrate more robustly in comparison to laminin (N.-G. Kim & Gumbiner, 2015), so it is

possible that BMP stimulation of $YAP^{fx/fx}$ NPCs on laminin and PDL alone was not able to elicit certain YAP activities.

Further *in vivo* studies to identify TAZ and YAP functions should be conducted, particularly in the context of BMP signaling, as different layers of astrocytes in the cortex are subject to different BMP ligands and levels of pathway activation. Moreover, a recent study has shown a role for YAP in spinal cord injury (Xie, 2020). Unpublished observations from our own lab indicate that not only YAP, but also TAZ is increased following spinal cord injury. When taken in context with our group's previous studies examining the role of different BMP receptors in gliosis following injury (Sahni et al., 2010), it seems possible that YAP and TAZ are downstream players in BMP-mediated reactive gliosis. *In vivo* studies may seek to examine this relationship, as effective treatments for spinal cord injury are still scarce.

V. Conclusion

Altogether, this body of work contributes to our deeper understanding of BMP signaling, its immediate targets, and the physiological effects that some of those targets have on neural stem cell fate specification and astrogliogenesis. These findings contribute to the field of astrocyte research by identifying a marker, HtrA1, that identifies astrocytes but not NPCs, a problem that has plagued the stem cell research field for many years. Our research on the transcriptional targets of different BMP receptors has enhanced our understanding of a signaling pathway that is ubiquitous through development, and plays a major role in many disease models. We have identified TAZ as a downstream effector of aspects of BMP signaling, and as a promoter of astrocyte differentiation. Since BMPs have already been approved for clinical use in some settings, and yet have demonstrated numerous side effects, this research will pave the way for more refined clinical therapeutics that can address clinical needs with fewer negative side

effects on patients. Given the array of diseases in which BMP signaling and its downstream targets play a major role, even outside of CNS disorders, a better understanding of the range of diverse BMP transcriptional targets will assist in understanding off-target effects of BMP-related therapeutic manipulations.

As age-related cognitive diseases are likely to be an increasing health burden as the general population ages, and since BMP increases have been implicated in age-related cognitive decline as well as multiple age-related neurodegenative diseases, an examination of BMP signaling's targets and downstream mechanisms with age will have high clinical relevance. It is currently unclear if BMP signaling and transcriptional targets change with aging, but this is not unlikely, given the dramatically different roles that various BMPs play from early embryonic development through adulthood. A comparison of BMP effects, both transcriptional and otherwise, on neural stem cells from early postnatal development through old age may be key to understand how biological processes change with age to produce the learning and cognitive effects observed. A better understanding of how BMP signaling interacts with other critical signaling pathways is important for properly understanding underlying cellular fate determination mechanisms, and how modulation of BMP may have cascading effects.

REFERENCES

Agius, E., Decker, Y., Soukkarieh, C., Soula, C., & Cochard, P. (2010). Role of BMPs in controlling the spatial and temporal origin of GFAP astrocytes in the embryonic spinal cord. *Developmental Biology*, *344*(2), 611–620. http://doi.org/10.1016/j.ydbio.2010.05.017

Ahn, K., Mishina, Y., Hanks, M. C., Behringer, R. R., & Crenshaw, E. B. (2001). BMPR-IA signaling is required for the formation of the apical ectodermal ridge and dorsal-ventral patterning of the limb. *Development (Cambridge, England)*, *128*(22), 4449–4461.

Angley, C., Kumar, M., Dinsio, K. J., Hall, A. K., & Siegel, R. E. (2003). Signaling by bone morphogenetic proteins and Smad1 modulates the postnatal differentiation of cerebellar cells. *The Journal of Neuroscience : the Official Journal of the Society for Neuroscience*, *23*(1), 260–268. http://doi.org/10.1523/JNEUROSCI.23-01-00260.2003

Aragona, M., Panciera, T., Manfrin, A., Giulitti, S., Michielin, F., Elvassore, N., et al. (2013). A Mechanical Checkpoint Controls Multicellular Growth through YAP/TAZ Regulation by Actin-Processing Factors. *Cell*, *154*(5), 1047–1059. http://doi.org/10.1016/j.cell.2013.07.042

Arber, S., Barbayannis, F. A., Hanser, H., Schneider, C., Stanyon, C. A., Bernard, O., & Caroni, P. (1998). Regulation of actin dynamics through phosphorylation of cofilin by LIM-kinase. *Nature*, *393*(6687), 805–809. http://doi.org/10.1038/31729

Asher, R. A., Morgenstern, D. A., Fidler, P. S., Adcock, K. H., Oohira, A., Braistead, J. E., et al. (2000). Neurocan is upregulated in injured brain and in cytokine-treated astrocytes. *The Journal of Neuroscience : the Official Journal of the Society for Neuroscience*, *20*(7), 2427–2438. http://doi.org/10.1523/JNEUROSCI.20-07-02427.2000

Attisano, L., Wrana, J. L., Montalvo, E., & Massagué, J. (1996). Activation of signalling by the activin receptor complex. *Molecular and Cellular Biology*, *16*(3), 1066–1073. http://doi.org/10.1128/mcb.16.3.1066

Augsburger, A., Schuchardt, A., Hoskins, S., Dodd, J., & Butler, S. (1999). BMPs as mediators of roof plate repulsion of commissural neurons. *Neuron*, *24*(1), 127–141. http://doi.org/10.1016/s0896-6273(00)80827-2

Bachoo, R. M., Kim, R. S., Ligon, K. L., Maher, E. A., Brennan, C., Billings, N., et al. (2004). Molecular diversity of astrocytes with implications for neurological disorders. *Proceedings of the National Academy of Sciences*, *101*(22), 8384–8389. http://doi.org/10.1073/pnas.0402140101

Baker, J. C., Beddington, R. S., & Harland, R. M. (1999). Wnt signaling in Xenopus embryos inhibits bmp4 expression and activates neural development. *Genes & Development*, *13*(23), 3149–3159. http://doi.org/10.1101/gad.13.23.3149

Bandyopadhyay, A., Yadav, P. S., & Prashar, P. (2013). BMP signaling in development and diseases: a pharmacological perspective. *Biochemical Pharmacology*, *85*(7), 857–864. http://doi.org/10.1016/j.bcp.2013.01.004

Barth, K. A., Kishimoto, Y., Rohr, K. B., Seydler, C., Schulte-Merker, S., & Wilson, S. W. (1999). Bmp activity establishes a gradient of positional information throughout the entire neural plate. *Development (Cambridge, England)*, *126*(22), 4977–4987.

Batter, D. K., & Kessler, J. A. (1991). Region-specific regulation of preproenkephalin mRNA in cultured astrocytes. *Molecular Brain Research*, *11*(1), 65–69. http://doi.org/10.1016/0169-328X(91)90022-P

Beaufort, N., Scharrer, E., Kremmer, E., Lux, V., Ehrmann, M., Huber, R., et al. (2014).

Cerebral small vessel disease-related protease HtrA1 processes latent TGF-β binding protein 1 and facilitates TGF-β signaling. *Proceedings of the National Academy of Sciences of the United States of America*, *111*(46), 16496–16501. http://doi.org/10.1073/pnas.1418087111

Belkin, A. M., & Stepp, M. A. (2000). Integrins as receptors for laminins. *Microscopy Research and Technique*, *51*(3), 280–301. http://doi.org/10.1002/1097-0029(20001101)51:3<280::AID-JEMT7>3.0.CO;2-O

Ben Haim, L., & Rowitch, D. H. (2017). Functional diversity of astrocytes in neural circuit regulation. *Nature Reviews. Neuroscience*, *18*(1), 31–41. http://doi.org/10.1038/nrn.2016.159

Beppu, H., Kawabata, M., Hamamoto, T., Chytil, A., Minowa, O., Noda, T., & Miyazono, K. (2000). BMP type II receptor is required for gastrulation and early development of mouse embryos. *Developmental Biology*, *221*(1), 249–258. http://doi.org/10.1006/dbio.2000.9670

Beppu, H., Lei, H., Bloch, K. D., & Li, E. (2005). Generation of a floxed allele of the mouse BMP type II receptor gene. *Genesis (New York, N.Y. : 2000)*, *41*(3), 133–137. http://doi.org/10.1002/gene.20099

Berg, D. A., Su, Y., Jimenez-Cyrus, D., Patel, A., Huang, N., Morizet, D., et al. (2019). A Common Embryonic Origin of Stem Cells Drives Developmental and Adult Neurogenesis. *Cell*, *177*(3), 654–668.e15. http://doi.org/10.1016/j.cell.2019.02.010

Bernstein, H.-G., Bannier, J., Meyer-Lotz, G., Steiner, J., Keilhoff, G., Dobrowolny, H., et al. (2014). Distribution of immunoreactive glutamine synthetase in the adult human and mouse brain. Qualitative and quantitative observations with special emphasis on extra-astroglial protein localization. *Journal of Chemical Neuroanatomy*, *61-62*, 33–50. http://doi.org/10.1016/j.jchemneu.2014.07.003

Bhalala, O. G., Pan, L., Sahni, V., McGuire, T. L., Gruner, K., Tourtellotte, W. G., & Kessler, J. A. (2012). microRNA-21 regulates astrocytic response following spinal cord injury. *The Journal of Neuroscience : the Official Journal of the Society for Neuroscience*, *32*(50), 17935–17947. http://doi.org/10.1523/JNEUROSCI.3860-12.2012

Blomfield, I. M., Rocamonde, B., del Mar Masdeu, M., Mulugeta, E., Vaga, S., van den Berg, D. L. C., et al. (2019). Id4 promotes the elimination of the pro-activation factor ascl1 to maintain quiescence of adult hippocampal stem cells. *eLife*, *8*, 271. http://doi.org/10.7554/eLife.48561

Bohrer, C., Pfurr, S., Mammadzada, K., Schildge, S., Plappert, L., Hils, M., et al. (2015). The balance of Id3 and E47 determines neural stem/precursor cell differentiation into astrocytes. *The EMBO Journal*, *34*(22), 2804–2819. http://doi.org/10.15252/embj.201591118

Bonaguidi, M. A., McGuire, T., Hu, M., Kan, L., Samanta, J., & Kessler, J. A. (2005). LIF and BMP signaling generate separate and discrete types of GFAP-expressing cells. *Development (Cambridge, England)*, *132*(24), 5503–5514. http://doi.org/10.1242/dev.02166

Bonaguidi, M. A., Peng, C.-Y., McGuire, T., Falciglia, G., Gobeske, K. T., Czeisler, C., & Kessler, J. A. (2008). Noggin expands neural stem cells in the adult hippocampus. *The Journal of Neuroscience : the Official Journal of the Society for Neuroscience*, *28*(37), 9194–9204. http://doi.org/10.1523/JNEUROSCI.3314-07.2008

Bond, A. M., Bhalala, O. G., & Kessler, J. A. (2012). The dynamic role of bone morphogenetic proteins in neural stem cell fate and maturation. *Developmental Neurobiology*, *72*(7), 1068–1084. http://doi.org/10.1002/dneu.22022

Bond, A. M., Peng, C.-Y., Meyers, E. A., McGuire, T., Ewaleifoh, O., & Kessler, J. A. (2014). BMP signaling regulates the tempo of adult hippocampal progenitor maturation at multiple stages of the lineage. *Stem Cells (Dayton, Ohio)*, *32*(8), 2201–2214. http://doi.org/10.1002/stem.1688

Brederlau, A., Faigle, R., Elmi, M., Zarebski, A., Sjöberg, S., Fujii, M., et al. (2004). The bone morphogenetic protein type Ib receptor is a major mediator of glial differentiation and cell survival in adult hippocampal progenitor cell culture. *Molecular Biology of the Cell*, *15*(8), 3863–3875. http://doi.org/10.1091/mbc.E03-08-0584

Brooker, S. M., Bond, A. M., Peng, C.-Y., & Kessler, J. A. (2016). β1-integrin restricts astrocytic differentiation of adult hippocampal neural stem cells. *Glia*, *64*(7), 1235–1251. http://doi.org/10.1002/glia.22996

Brooker, S. M., Gobeske, K. T., Chen, J., Peng, C. Y., & Kessler, J. A. (2017). Hippocampal bone morphogenetic protein signaling mediates behavioral effects of antidepressant treatment., *22*(6), 910–919. http://doi.org/10.1038/mp.2016.160

Brown, S. D. M., & Moore, M. W. (2012). The International Mouse Phenotyping Consortium: past and future perspectives on mouse phenotyping. *Mammalian Genome : Official Journal of the International Mammalian Genome Society*, *23*(9-10), 632–640. http://doi.org/10.1007/s00335-012-9427-x

Brunner, M., Mandier, N., Gautier, T., Chevalier, G., Ribba, A.-S., Guardiola, P., et al. (2018). β1 integrins mediate the BMP2 dependent transcriptional control of osteoblast differentiation and osteogenesis. *PloS One*, *13*(4), e0196021. http://doi.org/10.1371/journal.pone.0196021

Butler, S. J., & Dodd, J. (2003). A role for BMP heterodimers in roof plate-mediated repulsion of commissural axons. *Neuron*, *38*(3), 389–401. http://doi.org/10.1016/s0896-6273(03)00254-x

Cahoy, J. D., Emery, B., Kaushal, A., Foo, L. C., Zamanian, J. L., Christopherson, K. S., et al. (2008). A transcriptome database for astrocytes, neurons, and oligodendrocytes: a new resource for understanding brain development and function. *The Journal of Neuroscience : the Official Journal of the Society for Neuroscience*, *28*(1), 264–278. http://doi.org/10.1523/JNEUROSCI.4178-07.2008

Campos, L. S., Leone, D. P., Relvas, J. B., Brakebusch, C., Fässler, R., Suter, U., & Ffrench-Constant, C. (2004). Beta1 integrins activate a MAPK signalling pathway in neural stem cells that contributes to their maintenance. *Development (Cambridge, England)*, *131*(14), 3433–3444. http://doi.org/10.1242/dev.01199

Cao, X., Pfaff, S. L., & Gage, F. H. (2008). YAP regulates neural progenitor cell number via the TEA domain transcription factor. *Genes & Development*, *22*(23), 3320–3334. http://doi.org/10.1101/gad.1726608

Capdevila, J., Vogan, K. J., Tabin, C. J., & Izpisúa Belmonte, J. C. (2000). Mechanisms of left-right determination in vertebrates. *Cell*, *101*(1), 9–21. http://doi.org/10.1016/S0092-8674(00)80619-4

Carlén, M., Meletis, K., Göritz, C., Darsalia, V., Evergren, E., Tanigaki, K., et al. (2009). Forebrain ependymal cells are Notch-dependent and generate neuroblasts and astrocytes after stroke. *Nature Neuroscience*, *12*(3), 259–267. http://doi.org/10.1038/nn.2268

Carpenter, A. E., Jones, T. R., Lamprecht, M. R., Clarke, C., Kang, I. H., Friman, O., et al. (2006). CellProfiler: image analysis software for identifying and quantifying cell phenotypes. *Genome Biology*, *7*(10), R100–11. http://doi.org/10.1186/gb-2006-7-10-r100

Casellas, R., & Brivanlou, A. H. (1998). Xenopus Smad7 inhibits both the activin and BMP

pathways and acts as a neural inducer. *Developmental Biology*, *198*(1), 1–12. http://doi.org/10.1006/dbio.1998.8893
Chamberland, A., Wang, E., Jones, A. R., Collins-Racie, L. A., LaVallie, E. R., Huang, Y., et al. (2009). Identification of a novel HtrA1-susceptible cleavage site in human aggrecan: evidence for the involvement of HtrA1 in aggrecan proteolysis in vivo. *The Journal of Biological Chemistry*, *284*(40), 27352–27359. http://doi.org/10.1074/jbc.M109.037051
Chang, H., Zwijsen, A., Vogel, H., Huylebroeck, D., & Matzuk, M. M. (2000). Smad5 is essential for left-right asymmetry in mice. *Developmental Biology*, *219*(1), 71–78. http://doi.org/10.1006/dbio.1999.9594
Chen, J., Van Gulden, S., McGuire, T. L., Fleming, A. C., Oka, C., Kessler, J. A., & Peng, C.-Y. (2018). BMP-Responsive Protease HtrA1 Is Differentially Expressed in Astrocytes and Regulates Astrocytic Development and Injury Response. *The Journal of Neuroscience : the Official Journal of the Society for Neuroscience*, *38*(15), 3840–3857. http://doi.org/10.1523/JNEUROSCI.2031-17.2018
Chen, Jian, Leong, S.-Y., & Schachner, M. (2005). Differential expression of cell fate determinants in neurons and glial cells of adult mouse spinal cord after compression injury. *The European Journal of Neuroscience*, *22*(8), 1895–1906. http://doi.org/10.1111/j.1460-9568.2005.04348.x
Chenn, A., & Walsh, C. A. (2002). Regulation of cerebral cortical size by control of cell cycle exit in neural precursors. *Science (New York, N.Y.)*, *297*(5580), 365–369. http://doi.org/10.1126/science.1074192
Chernousov, M. A., Kaufman, S. J., Stahl, R. C., Rothblum, K., & Carey, D. J. (2007). Alpha7beta1 integrin is a receptor for laminin-2 on Schwann cells. *Glia*, *55*(11), 1134–1144. http://doi.org/10.1002/glia.20536
Chiang, C., Litingtung, Y., Lee, E., Young, K. E., Corden, J. L., Westphal, H., & Beachy, P. A. (1996). Cyclopia and defective axial patterning in mice lacking Sonic hedgehog gene function. *Nature*, *383*(6599), 407–413. http://doi.org/10.1038/383407a0
Choe, Y., Huynh, T., & Pleasure, S. J. (2014). Migration of oligodendrocyte progenitor cells is controlled by transforming growth factor β family proteins during corticogenesis. *The Journal of Neuroscience : the Official Journal of the Society for Neuroscience*, *34*(45), 14973–14983. http://doi.org/10.1523/JNEUROSCI.1156-14.2014
Choi, S., Yu, J., Park, A., Dubon, M. J., Do, J., Kim, Y., et al. (2019). BMP-4 enhances epithelial mesenchymal transition and cancer stem cell properties of breast cancer cells via Notch signaling. *Scientific Reports*, *9*(1), 11724–14. http://doi.org/10.1038/s41598-019-48190-5
Chvátal, A., Pastor, A., Mauch, M., Syková, E., & Kettenmann, H. (1995). Distinct populations of identified glial cells in the developing rat spinal cord slice: ion channel properties and cell morphology. *The European Journal of Neuroscience*, *7*(1), 129–142. http://doi.org/10.1111/j.1460-9568.1995.tb01027.x
Clarke, L. E., Liddelow, S. A., Chakraborty, C., Münch, A. E., Heiman, M., & Barres, B. A. (2018). Normal aging induces A1-like astrocyte reactivity. *Proceedings of the National Academy of Sciences of the United States of America*, *115*(8), E1896–E1905. http://doi.org/10.1073/pnas.1800165115
Clement, C. A., Ajbro, K. D., Koefoed, K., Vestergaard, M. L., Veland, I. R., Henriques de Jesus, M. P. R., et al. (2013). TGF-β signaling is associated with endocytosis at the pocket region of the primary cilium. *Cell Reports*, *3*(6), 1806–1814.

http://doi.org/10.1016/j.celrep.2013.05.020
Colak, D., Mori, T., Brill, M. S., Pfeifer, A., Falk, S., Deng, C., et al. (2008). Adult neurogenesis requires Smad4-mediated bone morphogenic protein signaling in stem cells. *The Journal of Neuroscience : the Official Journal of the Society for Neuroscience*, *28*(2), 434–446. http://doi.org/10.1523/JNEUROSCI.4374-07.2008
Colognato, H., MacCarrick, M., O'Rear, J. J., & Yurchenco, P. D. (1997). The laminin alpha2-chain short arm mediates cell adhesion through both the alpha1beta1 and alpha2beta1 integrins. *The Journal of Biological Chemistry*, *272*(46), 29330–29336. http://doi.org/10.1074/jbc.272.46.29330
Craig, C. G., Tropepe, V., Morshead, C. M., Reynolds, B. A., Weiss, S., & van der Kooy, D. (1996). In vivo growth factor expansion of endogenous subependymal neural precursor cell populations in the adult mouse brain. *The Journal of Neuroscience : the Official Journal of the Society for Neuroscience*, *16*(8), 2649–2658. http://doi.org/10.1523/JNEUROSCI.16-08-02649.1996
Csiszar, A., Ahmad, M., Smith, K. E., Labinskyy, N., Gao, Q., Kaley, G., et al. (2006). Bone morphogenetic protein-2 induces proinflammatory endothelial phenotype. *The American Journal of Pathology*, *168*(2), 629–638. http://doi.org/10.2353/ajpath.2006.050284
Csiszar, A., Smith, K. E., Koller, A., Kaley, G., Edwards, J. G., & Ungvari, Z. (2005). Regulation of bone morphogenetic protein-2 expression in endothelial cells: role of nuclear factor-kappaB activation by tumor necrosis factor-alpha, H2O2, and high intravascular pressure. *Circulation*, *111*(18), 2364–2372. http://doi.org/10.1161/01.CIR.0000164201.40634.1D
Dai, M., Al-Odaini, A. A., Fils-Aimé, N., Villatoro, M. A., Guo, J., Arakelian, A., et al. (2013). Cyclin D1 cooperates with p21 to regulate TGFβ-mediated breast cancer cell migration and tumor local invasion. *Breast Cancer Research : BCR*, *15*(3), R49–14. http://doi.org/10.1186/bcr3441
Dale, J. K., Vesque, C., Lints, T. J., Sampath, T. K., Furley, A., Dodd, J., & Placzek, M. (1997). Cooperation of BMP7 and SHH in the induction of forebrain ventral midline cells by prechordal mesoderm. *Cell*, *90*(2), 257–269. http://doi.org/10.1016/s0092-8674(00)80334-7
Davies, J. E., Pröschel, C., Zhang, N., Noble, M., Mayer-Pröschel, M., & Davies, S. J. A. (2008). Transplanted astrocytes derived from BMP- or CNTF-treated glial-restricted precursors have opposite effects on recovery and allodynia after spinal cord injury. *Journal of Biology*, *7*(7), 24–20. http://doi.org/10.1186/jbiol85
Davis, S., Miura, S., Hill, C., Mishina, Y., & Klingensmith, J. (2004). BMP receptor IA is required in the mammalian embryo for endodermal morphogenesis and ectodermal patterning. *Developmental Biology*, *270*(1), 47–63. http://doi.org/10.1016/j.ydbio.2004.01.048
Di-Gregorio, A., Sancho, M., Stuckey, D. W., Crompton, L. A., Godwin, J., Mishina, Y., & Rodriguez, T. A. (2007). BMP signalling inhibits premature neural differentiation in the mouse embryo. *Development (Cambridge, England)*, *134*(18), 3359–3369. http://doi.org/10.1242/dev.005967
Dijke, ten, P., Yamashita, H., Ichijo, H., Franzén, P., Laiho, M., Miyazono, K., & Heldin, C. H. (1994a). Characterization of type I receptors for transforming growth factor-beta and activin. *Science (New York, N.Y.)*, *264*(5155), 101–104.
Dijke, ten, P., Yamashita, H., Sampath, T. K., Reddi, A. H., Estevez, M., Riddle, D. L., et al.

(1994b). Identification of type I receptors for osteogenic protein-1 and bone morphogenetic protein-4. *The Journal of Biological Chemistry*, *269*(25), 16985–16988.

Divolis, G., Stavropoulos, A., Brain, M. M., 2019. (n.d.). Activation of both transforming growth factor-β and bone morphogenetic protein signalling pathways upon traumatic brain injury restrains pro-inflammatory and boosts …. *Brain Communications*

.

Dong, J., Feldmann, G., Huang, J., Wu, S., Zhang, N., Comerford, S. A., et al. (2007). Elucidation of a universal size-control mechanism in Drosophila and mammals. *Cell*, *130*(6), 1120–1133. http://doi.org/10.1016/j.cell.2007.07.019

Dosch, R., Gawantka, V., Delius, H., Blumenstock, C., & Niehrs, C. (1997). Bmp-4 acts as a morphogen in dorsoventral mesoderm patterning in Xenopus. *Development (Cambridge, England)*, *124*(12), 2325–2334.

Du, J., Chen, X., Liang, X., Zhang, G., Xu, J., He, L., et al. (2011). Integrin activation and internalization on soft ECM as a mechanism of induction of stem cell differentiation by ECM elasticity. *Proceedings of the National Academy of Sciences of the United States of America*, *108*(23), 9466–9471. http://doi.org/10.1073/pnas.1106467108

Duan, L., Peng, C.-Y., Pan, L., & Kessler, J. A. (2015). Human pluripotent stem cell-derived radial glia recapitulate developmental events and provide real-time access to cortical neurons and astrocytes. *Stem Cells Translational Medicine*, *4*(5), 437–447. http://doi.org/10.5966/sctm.2014-0137

Dupont, S., Morsut, L., Aragona, M., Enzo, E., Giulitti, S., Cordenonsi, M., et al. (2011). Role of YAP/TAZ in mechanotransduction. *Nature*, *474*(7350), 179–183. http://doi.org/10.1038/nature10137

Eaton, B. A., & Davis, G. W. (2005). LIM Kinase1 controls synaptic stability downstream of the type II BMP receptor. *Neuron*, *47*(5), 695–708. http://doi.org/10.1016/j.neuron.2005.08.010

Edson, M. A., Nalam, R. L., Clementi, C., Franco, H. L., Demayo, F. J., Lyons, K. M., et al. (2010). Granulosa cell-expressed BMPR1A and BMPR1B have unique functions in regulating fertility but act redundantly to suppress ovarian tumor development. *Molecular Endocrinology (Baltimore, Md.)*, *24*(6), 1251–1266. http://doi.org/10.1210/me.2009-0461

Elbediwy, A., Vincent-Mistiaen, Z. I., Spencer-Dene, B., Stone, R. K., Boeing, S., Wculek, S. K., et al. (2016). Integrin signalling regulates YAP and TAZ to control skin homeostasis. *Development (Cambridge)*, *143*(10), 1674–1687. http://doi.org/10.1242/dev.133728

Fainsod, A., Steinbeisser, H., & De Robertis, E. M. (1994). On the function of BMP-4 in patterning the marginal zone of the Xenopus embryo. *The EMBO Journal*, *13*(21), 5015–5025.

Fan, R., Kim, N.-G., & Gumbiner, B. M. (2013). Regulation of Hippo pathway by mitogenic growth factors via phosphoinositide 3-kinase and phosphoinositide-dependent kinase-1. *Proceedings of the National Academy of Sciences of the United States of America*, *110*(7), 2569–2574. http://doi.org/10.1073/pnas.1216462110

Feigenson, K., Reid, M., See, J., Crenshaw, E. B., III, & Grinspan, J. B. (2011). Canonical Wnt signalling requires the BMP pathway to inhibit oligodendrocyte maturation. *ASN Neuro*, *3*(3), e00061–158. http://doi.org/10.1042/AN20110004

Ferreira, T. A., Blackman, A. V., Oyrer, J., Jayabal, S., Chung, A. J., Watt, A. J., et al. (2014). Neuronal morphometry directly from bitmap images. *Nature Methods*, *11*(10), 982–984. http://doi.org/10.1038/nmeth.3125

Finley, M. F., Devata, S., & Huettner, J. E. (1999). BMP-4 inhibits neural differentiation of murine embryonic stem cells. *Journal of Neurobiology*, *40*(3), 271–287.

Foletta, V. C., Lim, M. A., Soosairajah, J., Kelly, A. P., Stanley, E. G., Shannon, M., et al. (2003). Direct signaling by the BMP type II receptor via the cytoskeletal regulator LIMK1. *The Journal of Cell Biology*, *162*(6), 1089–1098. http://doi.org/10.1083/jcb.200212060

Foo, L. C., & Dougherty, J. D. (2013). Aldh1L1 is expressed by postnatal neural stem cells in vivo. *Glia*, *61*(9), 1533–1541. http://doi.org/10.1002/glia.22539

Fourel, L., Valat, A., Faurobert, E., Guillot, R., Bourrin-Reynard, I., Ren, K., et al. (2016). β3 integrin-mediated spreading induced by matrix-bound BMP-2 controls Smad signaling in a stiffness-independent manner. *The Journal of Cell Biology*, *212*(6), 693–706. http://doi.org/10.1083/jcb.201508018

Fujiwara, T., Dehart, D. B., Sulik, K. K., & Hogan, B. L. M. (2002). Distinct requirements for extra-embryonic and embryonic bone morphogenetic protein 4 in the formation of the node and primitive streak and coordination of left-right asymmetry in the mouse. *Development (Cambridge, England)*, *129*(20), 4685–4696.

Fuller, M. L., DeChant, A. K., Rothstein, B., Caprariello, A., Wang, R., Hall, A. K., & Miller, R. H. (2007). Bone morphogenetic proteins promote gliosis in demyelinating spinal cord lesions. *Annals of Neurology*, *62*(3), 288–300. http://doi.org/10.1002/ana.21179

Furuta, Y., Piston, D. W., & Hogan, B. L. (1997). Bone morphogenetic proteins (BMPs) as regulators of dorsal forebrain development. *Development (Cambridge, England)*, *124*(11), 2203–2212.

Gamell, C., Osses, N., Bartrons, R., Rückle, T., Camps, M., Rosa, J. L., & Ventura, F. (2008). BMP2 induction of actin cytoskeleton reorganization and cell migration requires PI3-kinase and Cdc42 activity. *Journal of Cell Science*, *121*(Pt 23), 3960–3970. http://doi.org/10.1242/jcs.031286

Garcia, A. D. R., Doan, N. B., Imura, T., Bush, T. G., & Sofroniew, M. V. (2004). GFAP-expressing progenitors are the principal source of constitutive neurogenesis in adult mouse forebrain. *Nature Neuroscience*, *7*(11), 1233–1241. http://doi.org/10.1038/nn1340

Garcia, A. D. R., Petrova, R., Eng, L., & Joyner, A. L. (2010). Sonic hedgehog regulates discrete populations of astrocytes in the adult mouse forebrain. *The Journal of Neuroscience : the Official Journal of the Society for Neuroscience*, *30*(41), 13597–13608. http://doi.org/10.1523/JNEUROSCI.0830-10.2010

Gautschi, O. P., Frey, S. P., & Zellweger, R. (2007). Bone morphogenetic proteins in clinical applications. *ANZ Journal of Surgery*, *77*(8), 626–631. http://doi.org/10.1111/j.1445-2197.2007.04175.x

Ge, W.-P., Miyawaki, A., Gage, F. H., Jan, Y. N., & Jan, L. Y. (2012). Local generation of glia is a major astrocyte source in postnatal cortex. *Nature*, *484*(7394), 376–380. http://doi.org/10.1038/nature10959

Gill, M. K., Christova, T., Zhang, Y. Y., Gregorieff, A., Zhang, L., Narimatsu, M., et al. (2018). A feed forward loop enforces YAP/TAZ signaling during tumorigenesis. *Nature Communications*, *9*(1), 3510. http://doi.org/10.1038/s41467-018-05939-2

Gobeske, K. T., Das, S., Bonaguidi, M. A., Weiss, C., Radulovic, J., Disterhoft, J. F., & Kessler, J. A. (2009). BMP signaling mediates effects of exercise on hippocampal neurogenesis and cognition in mice. *PloS One*, *4*(10), e7506. http://doi.org/10.1371/journal.pone.0007506

Golgi, C. (1886). Sulla fina anatomia degli organi centrali del sistema nervoso.

Gomes, W. A., Mehler, M. F., & Kessler, J. A. (2003). Transgenic overexpression of BMP4 increases astroglial and decreases oligodendroglial lineage commitment. *Developmental Biology*, *255*(1), 164–177.

Govier-Cole, A. E., Wood, R. J., Fletcher, J. L., Gonsalvez, D. G., Merlo, D., Cate, H. S., et al. (2019). Inhibiting Bone Morphogenetic Protein 4 Type I Receptor Signaling Promotes Remyelination by Potentiating Oligodendrocyte Differentiation. *eNeuro*, *6*(2), ENEURO.0399–18.2019. http://doi.org/10.1523/ENEURO.0399-18.2019

Graff, J. M., Thies, R. S., Song, J. J., Celeste, A. J., & Melton, D. A. (1994). Studies with a Xenopus BMP receptor suggest that ventral mesoderm-inducing signals override dorsal signals in vivo. *Cell*, *79*(1), 169–179. http://doi.org/10.1016/0092-8674(94)90409-x

Graham, A., Francis-West, P., Brickell, P., & Lumsden, A. (1994). The signalling molecule BMP4 mediates apoptosis in the rhombencephalic neural crest. *Nature*, *372*(6507), 684–686. http://doi.org/10.1038/372684a0

Gross, R. E., Mehler, M. F., Mabie, P. C., Zang, Z., Santschi, L., & Kessler, J. A. (1996). Bone morphogenetic proteins promote astroglial lineage commitment by mammalian subventricular zone progenitor cells. *Neuron*, *17*(4), 595–606.

Gulacsi, A., & Lillien, L. (2003). Sonic hedgehog and bone morphogenetic protein regulate interneuron development from dorsal telencephalic progenitors in vitro. *The Journal of Neuroscience : the Official Journal of the Society for Neuroscience*, *23*(30), 9862–9872. http://doi.org/10.1523/JNEUROSCI.23-30-09862.2003

Guzman, A., Zelman-Femiak, M., Boergermann, J. H., Paschkowsky, S., Kreuzaler, P. A., Fratzl, P., et al. (2012). SMAD versus non-SMAD signaling is determined by lateral mobility of bone morphogenetic protein (BMP) receptors. *The Journal of Biological Chemistry*, *287*(47), 39492–39504. http://doi.org/10.1074/jbc.M112.387639

Hadfield, K. D., Rock, C. F., Inkson, C. A., Dallas, S. L., Sudre, L., Wallis, G. A., et al. (2008). HtrA1 inhibits mineral deposition by osteoblasts: requirement for the protease and PDZ domains. *The Journal of Biological Chemistry*, *283*(9), 5928–5938. http://doi.org/10.1074/jbc.M709299200

Haidet-Phillips, A. M., Hester, M. E., Miranda, C. J., Meyer, K., Braun, L., Frakes, A., et al. (2011). Astrocytes from familial and sporadic ALS patients are toxic to motor neurons. *Nature Biotechnology*, *29*(9), 824–828. http://doi.org/10.1038/nbt.1957

Han, D., Byun, S.-H., Park, S., Kim, J., Kim, I., Ha, S., et al. (2015). YAP/TAZ enhance mammalian embryonic neural stem cell characteristics in a Tead-dependent manner. *Biochemical and Biophysical Research Communications*, *458*(1), 110–116. http://doi.org/10.1016/j.bbrc.2015.01.077

Hara, K., Shiga, A., Fukutake, T., Nozaki, H., Miyashita, A., Yokoseki, A., et al. (2009). Association of HTRA1 mutations and familial ischemic cerebral small-vessel disease. *The New England Journal of Medicine*, *360*(17), 1729–1739. http://doi.org/10.1056/NEJMoa0801560

Hart, C. G., Dyck, S. M., Kataria, H., Alizadeh, A., Nagakannan, P., Thliveris, J. A., et al. (2020). Acute upregulation of bone morphogenetic protein-4 regulates endogenous cell response and promotes cell death in spinal cord injury. *Experimental Neurology*, *325*, 113163. http://doi.org/10.1016/j.expneurol.2019.113163

Hassel, S., Schmitt, S., Hartung, A., Roth, M., Nohe, A., Petersen, N., et al. (2003). Initiation of Smad-dependent and Smad-independent signaling via distinct BMP-receptor complexes. *The*

Journal of Bone and Joint Surgery. American Volume, *85-A Suppl 3*, 44–51.
Hata, A., Lagna, G., Massagué, J., & Hemmati-Brivanlou, A. (1998). Smad6 inhibits BMP/Smad1 signaling by specifically competing with the Smad4 tumor suppressor. *Genes & Development*, *12*(2), 186–197. http://doi.org/10.1101/gad.12.2.186
Hemmati-Brivanlou, A., Kelly, O. G., & Melton, D. A. (1994). Follistatin, an antagonist of activin, is expressed in the Spemann organizer and displays direct neuralizing activity. *Cell*, *77*(2), 283–295. http://doi.org/10.1016/0092-8674(94)90320-4
Herrera, J., Yang, H., Zhang, S. C., Proschel, C., Tresco, P., Duncan, I. D., et al. (2001). Embryonic-derived glial-restricted precursor cells (GRP cells) can differentiate into astrocytes and oligodendrocytes in vivo. *Experimental Neurology*, *171*(1), 11–21. http://doi.org/10.1006/exnr.2001.7729
Hébert, J. M., Mishina, Y., & McConnell, S. K. (2002). BMP signaling is required locally to pattern the dorsal telencephalic midline. *Neuron*, *35*(6), 1029–1041. http://doi.org/10.1016/s0896-6273(02)00900-5
Hirschhorn, T., Levi-Hofman, M., Danziger, O., Smorodinsky, N. I., & Ehrlich, M. (2017). Differential molecular regulation of processing and membrane expression of Type-I BMP receptors: implications for signaling. *Cellular and Molecular Life Sciences : CMLS*, *74*(14), 2645–2662. http://doi.org/10.1007/s00018-017-2488-y
Hirsinger, E., Duprez, D., Jouve, C., Malapert, P., Cooke, J., & Pourquié, O. (1997). Noggin acts downstream of Wnt and Sonic Hedgehog to antagonize BMP4 in avian somite patterning. *Development (Cambridge, England)*, *124*(22), 4605–4614.
Hocking, J. C., Hehr, C. L., Bertolesi, G., Funakoshi, H., Nakamura, T., & McFarlane, S. (2009). LIMK1 acts downstream of BMP signaling in developing retinal ganglion cell axons but not dendrites. *Developmental Biology*, *330*(2), 273–285. http://doi.org/10.1016/j.ydbio.2009.03.027
Hoodless, P. A., Haerry, T., Abdollah, S., Stapleton, M., O'Connor, M. B., Attisano, L., & Wrana, J. L. (1996). MADR1, a MAD-related protein that functions in BMP2 signaling pathways. *Cell*, *85*(4), 489–500. http://doi.org/10.1016/s0092-8674(00)81250-7
Hu, J.-G., Zhang, Y.-X., Qi, Q., Wang, R., Shen, L., Zhang, C., et al. (2012). Expression of BMP-2 and BMP-4 proteins by type-1 and type-2 astrocytes induced from neural stem cells under different differentiation conditions. *Acta Neurobiologiae Experimentalis*, *72*(1), 95–101.
Huang, J., Wu, S., Barrera, J., Matthews, K., & Pan, D. (2005). The Hippo signaling pathway coordinately regulates cell proliferation and apoptosis by inactivating Yorkie, the Drosophila Homolog of YAP. *Cell*, *122*(3), 421–434. http://doi.org/10.1016/j.cell.2005.06.007
Huang, W., Lv, X., Liu, C., Zha, Z., Zhang, H., Jiang, Y., et al. (2012). The N-terminal phosphodegron targets TAZ/WWTR1 protein for SCFβ-TrCP-dependent degradation in response to phosphatidylinositol 3-kinase inhibition. *The Journal of Biological Chemistry*, *287*(31), 26245–26253. http://doi.org/10.1074/jbc.M112.382036
Huang, Z., Hu, J., Pan, J., Wang, Y., Hu, G., Zhou, J., et al. (2016a). YAP stabilizes SMAD1 and promotes BMP2-induced neocortical astrocytic differentiation. *Development (Cambridge, England)*, *143*(13), 2398–2409. http://doi.org/10.1242/dev.130658
Huang, Z., Sun, D., Hu, J.-X., Tang, F.-L., Lee, D.-H., Wang, Y., et al. (2016b). Neogenin Promotes BMP2 Activation of YAP and Smad1 and Enhances Astrocytic Differentiation in Developing Mouse Neocortex. *The Journal of Neuroscience : the Official Journal of the*

Society for Neuroscience, *36*(21), 5833–5849. http://doi.org/10.1523/JNEUROSCI.4487-15.2016

Imamura, T., Takase, M., Nishihara, A., Oeda, E., Hanai, J., Kawabata, M., & Miyazono, K. (1997). Smad6 inhibits signalling by the TGF-beta superfamily. *Nature*, *389*(6651), 622–626. http://doi.org/10.1038/39355

Inatani, M., Honjo, M., Otori, Y., Oohira, A., Kido, N., Tano, Y., et al. (2001). Inhibitory effects of neurocan and phosphacan on neurite outgrowth from retinal ganglion cells in culture. *Investigative Ophthalmology & Visual Science*, *42*(8), 1930–1938.

Ishisaki, A., Yamato, K., Hashimoto, S., Nakao, A., Tamaki, K., Nonaka, K., et al. (1999). Differential inhibition of Smad6 and Smad7 on bone morphogenetic protein- and activin-mediated growth arrest and apoptosis in B cells. *The Journal of Biological Chemistry*, *274*(19), 13637–13642. http://doi.org/10.1074/jbc.274.19.13637

Ishitani, T., Ninomiya-Tsuji, J., Nagai, S., Nishita, M., Meneghini, M., Barker, N., et al. (1999). The TAK1-NLK-MAPK-related pathway antagonizes signalling between beta-catenin and transcription factor TCF. *Nature*, *399*(6738), 798–802. http://doi.org/10.1038/21674

Iwasaki, S., Iguchi, M., Watanabe, K., Hoshino, R., Tsujimoto, M., & Kohno, M. (1999). Specific activation of the p38 mitogen-activated protein kinase signaling pathway and induction of neurite outgrowth in PC12 cells by bone morphogenetic protein-2. *The Journal of Biological Chemistry*, *274*(37), 26503–26510. http://doi.org/10.1074/jbc.274.37.26503

James, A. W., LaChaud, G., Shen, J., Asatrian, G., Nguyen, V., Zhang, X., et al. (2016). A Review of the Clinical Side Effects of Bone Morphogenetic Protein-2. *Tissue Engineering. Part B, Reviews*, *22*(4), 284–297. http://doi.org/10.1089/ten.TEB.2015.0357

Jessell, T. M. (2000). Neuronal specification in the spinal cord: inductive signals and transcriptional codes. *Nature Reviews. Genetics*, *1*(1), 20–29. http://doi.org/10.1038/35049541

Johe, K. K., Hazel, T. G., Muller, T., Dugich-Djordjevic, M. M., & McKay, R. D. (1996). Single factors direct the differentiation of stem cells from the fetal and adult central nervous system. *Genes & Development*, *10*(24), 3129–3140. http://doi.org/10.1101/gad.10.24.3129

Jones, A., Kumar, S., Zhang, N., Tong, Z., Yang, J.-H., Watt, C., et al. (2011). Increased expression of multifunctional serine protease, HTRA1, in retinal pigment epithelium induces polypoidal choroidal vasculopathy in mice. *Proceedings of the National Academy of Sciences of the United States of America*, *108*(35), 14578–14583. http://doi.org/10.1073/pnas.1102853108

Jones, C. M., Dale, L., Hogan, B. L., Wright, C. V., & Smith, J. C. (1996). Bone morphogenetic protein-4 (BMP-4) acts during gastrula stages to cause ventralization of Xenopus embryos. *Development (Cambridge, England)*, *122*(5), 1545–1554.

Jones, L. L., Margolis, R. U., & Tuszynski, M. H. (2003). The chondroitin sulfate proteoglycans neurocan, brevican, phosphacan, and versican are differentially regulated following spinal cord injury. *Experimental Neurology*, *182*(2), 399–411. http://doi.org/10.1016/s0014-4886(03)00087-6

Jordan, J., Böttner, M., Schluesener, H. J., Unsicker, K., & Krieglstein, K. (1997). Bone morphogenetic proteins: neurotrophic roles for midbrain dopaminergic neurons and implications of astroglial cells. *The European Journal of Neuroscience*, *9*(8), 1699–1709. http://doi.org/10.1111/j.1460-9568.1997.tb01527.x

Kanai, F., Marignani, P. A., Sarbassova, D., Yagi, R., Hall, R. A., Donowitz, M., et al. (2000).

TAZ: a novel transcriptional co-activator regulated by interactions with 14-3-3 and PDZ domain proteins. *The EMBO Journal*, *19*(24), 6778–6791. http://doi.org/10.1093/emboj/19.24.6778

Kaplan, F. S., Xu, M., Seemann, P., Connor, J. M., Glaser, D. L., Carroll, L., et al. (2009). Classic and atypical fibrodysplasia ossificans progressiva (FOP) phenotypes are caused by mutations in the bone morphogenetic protein (BMP) type I receptor ACVR1. *Human Mutation*, *30*(3), 379–390. http://doi.org/10.1002/humu.20868

Kaplan, J., Kaplan, F. S., & Shore, E. M. (2012). Restoration of normal BMP signaling levels and osteogenic differentiation in FOP mesenchymal progenitor cells by mutant allele-specific targeting. *Gene Therapy*, *19*(7), 786–790. http://doi.org/10.1038/gt.2011.152

Kaps, C., Hoffmann, A., Zilberman, Y., Pelled, G., Häupl, T., Sittinger, M., et al. (2004). Distinct roles of BMP receptors Type IA and IB in osteo-/chondrogenic differentiation in mesenchymal progenitors (C3H10T1/2). *BioFactors (Oxford, England)*, *20*(2), 71–84.

Kawaguchi-Niida, M., Shibata, N., & Furuta, Y. (2017). Smad4 is essential for directional progression from committed neural progenitor cells through neuronal differentiation in the postnatal mouse brain. *Molecular and Cellular Neurosciences*. http://doi.org/10.1016/j.mcn.2017.06.008

Kazanis, I., Lathia, J. D., Vadakkan, T. J., Raborn, E., Wan, R., Mughal, M. R., et al. (2010). Quiescence and activation of stem and precursor cell populations in the subependymal zone of the mammalian brain are associated with distinct cellular and extracellular matrix signals. *The Journal of Neuroscience : the Official Journal of the Society for Neuroscience*, *30*(29), 9771–9781. http://doi.org/10.1523/JNEUROSCI.0700-10.2010

Kendall, S. E., Battelli, C., Irwin, S., Mitchell, J. G., Glackin, C. A., & Verdi, J. M. (2005). NRAGE mediates p38 activation and neural progenitor apoptosis via the bone morphogenetic protein signaling cascade. *Molecular and Cellular Biology*, *25*(17), 7711–7724. http://doi.org/10.1128/MCB.25.17.7711-7724.2005

Kim, M., & Choe, S. (2011). BMPs and their clinical potentials. *BMB Reports*, *44*(10), 619–634. http://doi.org/10.5483/BMBRep.2011.44.10.619

Kim, N.-G., & Gumbiner, B. M. (2015). Adhesion to fibronectin regulates Hippo signaling via the FAK-Src-PI3K pathway. *The Journal of Cell Biology*, *210*(3), 503–515. http://doi.org/10.1083/jcb.201501025

Kimelberg, H. K. (2009). Astrocyte Heterogeneity or Homogeneity? In *Astrocytes in (Patho)Physiology of the Nervous System* (Vol. 633, pp. 1–25). Boston, MA: Springer, Boston, MA. http://doi.org/10.1007/978-0-387-79492-1_1

Koenig, B. B., Cook, J. S., Wolsing, D. H., Ting, J., Tiesman, J. P., Correa, P. E., et al. (1994). Characterization and cloning of a receptor for BMP-2 and BMP-4 from NIH 3T3 cells. *Molecular and Cellular Biology*, *14*(9), 5961–5974. http://doi.org/10.1128/mcb.14.9.5961

Kostic, M., Paridaen, J. T. M. L., Long, K. R., Kalebic, N., Langen, B., Grübling, N., et al. (2019). YAP Activity Is Necessary and Sufficient for Basal Progenitor Abundance and Proliferation in the Developing Neocortex. *Cell Reports*, *27*(4), 1103–1118.e6. http://doi.org/10.1016/j.celrep.2019.03.091

Kretzschmar, M., Liu, F., Hata, A., Doody, J., & Massagué, J. (1997). The TGF-beta family mediator Smad1 is phosphorylated directly and activated functionally by the BMP receptor kinase. *Genes & Development*, *11*(8), 984–995. http://doi.org/10.1101/gad.11.8.984

Kristal Kaan, H. Y., Chan, S. W., Tan, S. K. J., Guo, F., Lim, C. J., Hong, W., & Song, H.

(2017). Crystal structure of TAZ-TEAD complex reveals a distinct interaction mode from that of YAP-TEAD complex. *Scientific Reports*, *7*(1), 886. http://doi.org/10.1038/s41598-017-02219-9

Lagna, G., Hata, A., Hemmati-Brivanlou, A., & Massagué, J. (1996). Partnership between DPC4 and SMAD proteins in TGF-beta signalling pathways. *Nature*, *383*(6603), 832–836. http://doi.org/10.1038/383832a0

Lai, C.-F., & Cheng, S.-L. (2005). Alphavbeta integrins play an essential role in BMP-2 induction of osteoblast differentiation. *Journal of Bone and Mineral Research : the Official Journal of the American Society for Bone and Mineral Research*, *20*(2), 330–340. http://doi.org/10.1359/JBMR.041013

Lamb, T. M., Knecht, A. K., Smith, W. C., Stachel, S. E., Economides, A. N., Stahl, N., et al. (1993). Neural induction by the secreted polypeptide noggin. *Science (New York, N.Y.)*, *262*(5134), 713–718. http://doi.org/10.1126/science.8235591

Launay, S., Maubert, E., Lebeurrier, N., Tennstaedt, A., Campioni, M., Docagne, F., et al. (2008). HtrA1-dependent proteolysis of TGF-β controls both neuronal maturation and developmental survival. *Cell Death and Differentiation*, *15*(9), 1408–1416. http://doi.org/10.1038/cdd.2008.82

Lawson, K. A., Dunn, N. R., Roelen, B. A., Zeinstra, L. M., Davis, A. M., Wright, C. V., et al. (1999). Bmp4 is required for the generation of primordial germ cells in the mouse embryo. *Genes & Development*, *13*(4), 424–436. http://doi.org/10.1101/gad.13.4.424

Lee, J. Y., Dominguez, A. A., Nam, S., Stowers, R. S., Qi, L. S., & Chaudhuri, O. (2019). Identification of cell context-dependent YAP-associated proteins reveals β1 and β4 integrin mediate YAP translocation independently of cell spreading. *Scientific Reports*, *9*(1), 17188–11. http://doi.org/10.1038/s41598-019-53659-4

Lee, J., Son, M. J., Woolard, K., Donin, N. M., Li, A., Cheng, C. H., et al. (2008). Epigenetic-mediated dysfunction of the bone morphogenetic protein pathway inhibits differentiation of glioblastoma-initiating cells. *Cancer Cell*, *13*(1), 69–80. http://doi.org/10.1016/j.ccr.2007.12.005

Lee-Hoeflich, S. T., Causing, C. G., Podkowa, M., Zhao, X., Wrana, J. L., & Attisano, L. (2004). Activation of LIMK1 by binding to the BMP receptor, BMPRII, regulates BMP-dependent dendritogenesis. *The EMBO Journal*, *23*(24), 4792–4801. http://doi.org/10.1038/sj.emboj.7600418

Lei, Q.-Y., Zhang, H., Zhao, B., Zha, Z.-Y., Bai, F., Pei, X.-H., et al. (2008). TAZ promotes cell proliferation and epithelial-mesenchymal transition and is inhibited by the hippo pathway. *Molecular and Cellular Biology*, *28*(7), 2426–2436. http://doi.org/10.1128/MCB.01874-07

Lein, E. S., Hawrylycz, M. J., Ao, N., Ayres, M., Bensinger, A., Bernard, A., et al. (2007). Genome-wide atlas of gene expression in the adult mouse brain. *Nature*, *445*(7124), 168–176. http://doi.org/10.1038/nature05453

Leone, D. P., Relvas, J. B., Campos, L. S., Hemmi, S., Brakebusch, C., Fässler, R., et al. (2005). Regulation of neural progenitor proliferation and survival by beta1 integrins. *Journal of Cell Science*, *118*(Pt 12), 2589–2599. http://doi.org/10.1242/jcs.02396

Levison, S. W., & Goldman, J. E. (1993). Both oligodendrocytes and astrocytes develop from progenitors in the subventricular zone of postnatal rat forebrain. *Neuron*, *10*(2), 201–212. http://doi.org/10.1016/0896-6273(93)90311-e

Li, W., Cogswell, C. A., & LoTurco, J. J. (1998). Neuronal differentiation of precursors in the

neocortical ventricular zone is triggered by BMP. *The Journal of Neuroscience : the Official Journal of the Society for Neuroscience*, *18*(21), 8853–8862. http://doi.org/10.1523/JNEUROSCI.18-21-08853.1998

Liddelow, S. A., Guttenplan, K. A., Clarke, L. E., Bennett, F. C., Bohlen, C. J., Schirmer, L., et al. (2017). Neurotoxic reactive astrocytes are induced by activated microglia. *Nature*, *541*(7638), 481–487. http://doi.org/10.1038/nature21029

Liem, K. F., Jessell, T. M., & Briscoe, J. (2000). Regulation of the neural patterning activity of sonic hedgehog by secreted BMP inhibitors expressed by notochord and somites. *Development (Cambridge, England)*, *127*(22), 4855–4866.

Liem, K. F., Tremml, G., Roelink, H., & Jessell, T. M. (1995). Dorsal differentiation of neural plate cells induced by BMP-mediated signals from epidermal ectoderm. *Cell*, *82*(6), 969–979. http://doi.org/10.1016/0092-8674(95)90276-7

Lillien, L. E., Sendtner, M., Rohrer, H., Hughes, S. M., & Raff, M. C. (1988). Type-2 astrocyte development in rat brain cultures is initiated by a CNTF like protein produced by type-1 astrocytes. *Neuron*, *1*(6), 485–494. http://doi.org/10.1016/0896-6273(88)90179-1

Lim, D. A., Tramontin, A. D., Trevejo, J. M., Herrera, D. G., Garcia-Verdugo, J. M., & Alvarez-Buylla, A. (2000a). Noggin Antagonizes BMP Signaling to Create a Niche for Adult Neurogenesis. *Neuron*, *28*(3), 713–726. http://doi.org/10.1016/S0896-6273(00)00148-3

Lim, D. A., Tramontin, A. D., Trevejo, J. M., Herrera, D. G., García-Verdugo, J. M., & Alvarez-Buylla, A. (2000b). Noggin antagonizes BMP signaling to create a niche for adult neurogenesis. *Neuron*, *28*(3), 713–726. http://doi.org/10.1016/s0896-6273(00)00148-3

Lin, C.-C. J., Yu, K., Hatcher, A., Huang, T.-W., Lee, H. K., Carlson, J., et al. (2017). Identification of diverse astrocyte populations and their malignant analogs. *Nature Neuroscience*. http://doi.org/10.1038/nn.4493

Liu, F., Hata, A., Baker, J. C., Doody, J., Cárcamo, J., Harland, R. M., & Massagué, J. (1996). A human Mad protein acting as a BMP-regulated transcriptional activator. *Nature*, *381*(6583), 620–623. http://doi.org/10.1038/381620a0

Liu, F., Ventura, F., Doody, J., & Massagué, J. (1995). Human type II receptor for bone morphogenic proteins (BMPs): extension of the two-kinase receptor model to the BMPs. *Molecular and Cellular Biology*, *15*(7), 3479–3486. http://doi.org/10.1128/mcb.15.7.3479

Liu, Z., Osipovitch, M., Benraiss, A., Huynh, N. P. T., Foti, R., Bates, J., et al. (2019). Dysregulated Glial Differentiation in Schizophrenia May Be Relieved by Suppression of SMAD4- and REST-Dependent Signaling. *Cell Reports*, *27*(13), 3832–3843.e6. http://doi.org/10.1016/j.celrep.2019.05.088

Lois, C., & Alvarez-Buylla, A. (1993). Proliferating subventricular zone cells in the adult mammalian forebrain can differentiate into neurons and glia. *Proceedings of the National Academy of Sciences*, *90*(5), 2074–2077. http://doi.org/10.1073/pnas.90.5.2074

Long, K., Moss, L., Laursen, L., Boulter, L., & Ffrench-Constant, C. (2016). Integrin signalling regulates the expansion of neuroepithelial progenitors and neurogenesis via Wnt7a and Decorin. *Nature Communications*, *7*, 10354. http://doi.org/10.1038/ncomms10354

Low, B. C., Pan, C. Q., Shivashankar, G. V., Bershadsky, A., Sudol, M., & Sheetz, M. (2014). YAP/TAZ as mechanosensors and mechanotransducers in regulating organ size and tumor growth. *FEBS Letters*, *588*(16), 2663–2670. http://doi.org/10.1016/j.febslet.2014.04.012

Lui, J. W., Xiao, S., Ogomori, K., Hammarstedt, J. E., Little, E. C., & Lang, D. (2019). The Efficiency of Verteporfin as a Therapeutic Option in Pre-Clinical Models of Melanoma.

Journal of Cancer, *10*(1), 1–10. http://doi.org/10.7150/jca.27472
Lü, H.-Z., & Hu, J.-G. (2009). Expression of bone morphogenetic proteins-2/4 in neural stem cells and their lineages. *Acta Neurobiologiae Experimentalis*, *69*(4), 441–447.
Marignier, R., Nicolle, A., Watrin, C., Touret, M., Cavagna, S., Varrin-Doyer, M., et al. (2010). Oligodendrocytes are damaged by neuromyelitis optica immunoglobulin G via astrocyte injury. *Brain : a Journal of Neurology*, *133*(9), 2578–2591. http://doi.org/10.1093/brain/awq177
Marom, B., Heining, E., Knaus, P., & Henis, Y. I. (2011). Formation of stable homomeric and transient heteromeric bone morphogenetic protein (BMP) receptor complexes regulates Smad protein signaling. *The Journal of Biological Chemistry*, *286*(22), 19287–19296. http://doi.org/10.1074/jbc.M110.210377
Martin, K., Pritchett, J., Llewellyn, J., Mullan, A. F., Athwal, V. S., Dobie, R., et al. (2016). PAK proteins and YAP-1 signalling downstream of integrin beta-1 in myofibroblasts promote liver fibrosis. *Nature Communications*, *7*, 12502. http://doi.org/10.1038/ncomms12502
Matsuura, I., Taniguchi, J., Hata, K., Saeki, N., & Yamashita, T. (2008). BMP inhibition enhances axonal growth and functional recovery after spinal cord injury. *Journal of Neurochemistry*, *105*(4), 1471–1479. http://doi.org/10.1111/j.1471-4159.2008.05251.x
McCarthy, K. D., & de Vellis, J. (1980). Preparation of separate astroglial and oligodendroglial cell cultures from rat cerebral tissue. *The Journal of Cell Biology*, *85*(3), 890–902. http://doi.org/10.1083/jcb.85.3.890
Meyers, E. A., Gobeske, K. T., Bond, A. M., Jarrett, J. C., Peng, C.-Y., & Kessler, J. A. (2016). Increased bone morphogenetic protein signaling contributes to age-related declines in neurogenesis and cognition. *Neurobiology of Aging*, *38*, 164–175. http://doi.org/10.1016/j.neurobiolaging.2015.10.035
Mira, H., Andreu, Z., Suh, H., Lie, D. C., Jessberger, S., Consiglio, A., et al. (2010). Signaling through BMPR-IA regulates quiescence and long-term activity of neural stem cells in the adult hippocampus. *Cell Stem Cell*, *7*(1), 78–89. http://doi.org/10.1016/j.stem.2010.04.016
Mishina, Y., Hanks, M. C., Miura, S., Tallquist, M. D., & Behringer, R. R. (2002). Generation of Bmpr/Alk3 conditional knockout mice. *Genesis (New York, N.Y. : 2000)*, *32*(2), 69–72. http://doi.org/10.1002/gene.10038
Mishina, Y., Suzuki, A., Ueno, N., & Behringer, R. R. (1995). Bmpr encodes a type I bone morphogenetic protein receptor that is essential for gastrulation during mouse embryogenesis. *Genes & Development*, *9*(24), 3027–3037. http://doi.org/10.1101/gad.9.24.3027
Monsoro-Burq, A., & Le Douarin, N. (2000). Left-right asymmetry in BMP4 signalling pathway during chick gastrulation. *Mechanisms of Development*, *97*(1-2), 105–108. http://doi.org/10.1016/s0925-4773(00)00417-2
Monsoro-Burq, A., & Le Douarin, N. M. (2001). BMP4 plays a key role in left-right patterning in chick embryos by maintaining Sonic Hedgehog asymmetry. *Molecular Cell*, *7*(4), 789–799. http://doi.org/10.1016/s1097-2765(01)00223-4
Montagne, A., Barnes, S. R., Sweeney, M. D., Halliday, M. R., Sagare, A. P., Zhao, Z., et al. (2015). Blood-brain barrier breakdown in the aging human hippocampus. *Neuron*, *85*(2), 296–302. http://doi.org/10.1016/j.neuron.2014.12.032
Morell, M., Tsan, Y.-C., & O'Shea, K. S. (2015). Inducible expression of noggin selectively

expands neural progenitors in the adult SVZ. *Stem Cell Research*, *14*(1), 79–94. http://doi.org/10.1016/j.scr.2014.11.001
Moser, J. J., Fritzler, M. J., & Rattner, J. B. (2009). Primary ciliogenesis defects are associated with human astrocytoma/glioblastoma cells. *BMC Cancer*, *9*(1), 448–12. http://doi.org/10.1186/1471-2407-9-448
Mueller, T. D., & Nickel, J. (2012). Promiscuity and specificity in BMP receptor activation. *FEBS Letters*, *586*(14), 1846–1859. http://doi.org/10.1016/j.febslet.2012.02.043
Muramatsu, T., Imoto, I., Matsui, T., Kozaki, K.-I., Haruki, S., Sudol, M., et al. (2011). YAP is a candidate oncogene for esophageal squamous cell carcinoma. *Carcinogenesis*, *32*(3), 389–398. http://doi.org/10.1093/carcin/bgq254
Nakamura, T., Takio, K., Eto, Y., Shibai, H., Titani, K., & Sugino, H. (1990). Activin-binding protein from rat ovary is follistatin. *Science (New York, N.Y.)*, *247*(4944), 836–838. http://doi.org/10.1126/science.2106159
Nakao, A., Afrakhte, M., Morén, A., Nakayama, T., Christian, J. L., Heuchel, R., et al. (1997). Identification of Smad7, a TGFbeta-inducible antagonist of TGF-beta signalling. *Nature*, *389*(6651), 631–635. http://doi.org/10.1038/39369
Nakashima, K., Wiese, S., Yanagisawa, M., Arakawa, H., Kimura, N., Hisatsune, T., et al. (1999a). Developmental requirement of gp130 signaling in neuronal survival and astrocyte differentiation. *The Journal of Neuroscience : the Official Journal of the Society for Neuroscience*, *19*(13), 5429–5434. http://doi.org/10.1523/JNEUROSCI.19-13-05429.1999
Nakashima, K., Yanagisawa, M., Arakawa, H., & Taga, T. (1999b). Astrocyte differentiation mediated by LIF in cooperation with BMP2. *FEBS Letters*, *457*(1), 43–46. http://doi.org/10.1016/s0014-5793(99)00997-7
Nakashima, K., Yanagisawa, M., Arakawa, H., Kimura, N., Hisatsune, T., Kawabata, M., et al. (1999c). Synergistic signaling in fetal brain by STAT3-Smad1 complex bridged by p300. *Science (New York, N.Y.)*, *284*(5413), 479–482. http://doi.org/10.1126/science.284.5413.479
Nakayama, T., Gardner, H., Berg, L. K., & Christian, J. L. (1998a). Smad6 functions as an intracellular antagonist of some TGF-beta family members during Xenopus embryogenesis. *Genes to Cells : Devoted to Molecular & Cellular Mechanisms*, *3*(6), 387–394. http://doi.org/10.1046/j.1365-2443.1998.00196.x
Nakayama, T., Snyder, M. A., Grewal, S. S., Tsuneizumi, K., Tabata, T., & Christian, J. L. (1998b). Xenopus Smad8 acts downstream of BMP-4 to modulate its activity during vertebrate embryonic patterning. *Development (Cambridge, England)*, *125*(5), 857–867.
Newfeld, S. J., Mehra, A., Singer, M. A., Wrana, J. L., Attisano, L., & Gelbart, W. M. (1997). Mothers against dpp participates in a DDP/TGF-beta responsive serine-threonine kinase signal transduction cascade. *Development (Cambridge, England)*, *124*(16), 3167–3176.
Nguyen, V. H., Trout, J., Connors, S. A., Andermann, P., Weinberg, E., & Mullins, M. C. (2000). Dorsal and intermediate neuronal cell types of the spinal cord are established by a BMP signaling pathway. *Development (Cambridge, England)*, *127*(6), 1209–1220.
Niwa, R., Nagata-Ohashi, K., Takeichi, M., Mizuno, K., & Uemura, T. (2002). Control of actin reorganization by Slingshot, a family of phosphatases that dephosphorylate ADF/cofilin. *Cell*, *108*(2), 233–246. http://doi.org/10.1016/s0092-8674(01)00638-9
Nohe, A., Hassel, S., Ehrlich, M., Neubauer, F., Sebald, W., Henis, Y. I., & Knaus, P. (2002). The mode of bone morphogenetic protein (BMP) receptor oligomerization determines different BMP-2 signaling pathways. *The Journal of Biological Chemistry*, *277*(7), 5330–

5338. http://doi.org/10.1074/jbc.M102750200
Nohno, T., Ishikawa, T., Saito, T., Hosokawa, K., Noji, S., Wolsing, D. H., & Rosenbaum, J. S. (1995). Identification of a human type II receptor for bone morphogenetic protein-4 that forms differential heteromeric complexes with bone morphogenetic protein type I receptors. *The Journal of Biological Chemistry*, *270*(38), 22522–22526. http://doi.org/10.1074/jbc.270.38.22522
North, H. A., Pan, L., McGuire, T. L., Brooker, S., & Kessler, J. A. (2015). β1-Integrin alters ependymal stem cell BMP receptor localization and attenuates astrogliosis after spinal cord injury. *The Journal of Neuroscience : the Official Journal of the Society for Neuroscience*, *35*(9), 3725–3733. http://doi.org/10.1523/JNEUROSCI.4546-14.2015
Oka, C., Tsujimoto, R., Kajikawa, M., Koshiba-Takeuchi, K., Ina, J., Yano, M., et al. (2004). HtrA1 serine protease inhibits signaling mediated by Tgfbeta family proteins. *Development (Cambridge, England)*, *131*(5), 1041–1053. http://doi.org/10.1242/dev.00999
Okawa, S., Nicklas, S., Zickenrott, S., Schwamborn, J. C., & Del Sol, A. (2016). A Generalized Gene-Regulatory Network Model of Stem Cell Differentiation for Predicting Lineage Specifiers. *Stem Cell Reports*, *7*(3), 307–315. http://doi.org/10.1016/j.stemcr.2016.07.014
Oshimori, N., & Fuchs, E. (2012). Paracrine TGF-β signaling counterbalances BMP-mediated repression in hair follicle stem cell activation. *Cell Stem Cell*, *10*(1), 63–75. http://doi.org/10.1016/j.stem.2011.11.005
Pan, L., North, H. A., Sahni, V., Jeong, S. J., McGuire, T. L., Berns, E. J., et al. (2014). β1-Integrin and integrin linked kinase regulate astrocytic differentiation of neural stem cells. *PloS One*, *9*(8), e104335. http://doi.org/10.1371/journal.pone.0104335
Panchision, D. M., Pickel, J. M., Studer, L., Lee, S. H., Turner, P. A., Hazel, T. G., & McKay, R. D. (2001). Sequential actions of BMP receptors control neural precursor cell production and fate. *Genes & Development*, *15*(16), 2094–2110. http://doi.org/10.1101/gad.894701
Parikh, P., Hao, Y., Hosseinkhani, M., Patil, S. B., Huntley, G. W., Tessier-Lavigne, M., & Zou, H. (2011). Regeneration of axons in injured spinal cord by activation of bone morphogenetic protein/Smad1 signaling pathway in adult neurons. *Proceedings of the National Academy of Sciences of the United States of America*, *108*(19), E99–107. http://doi.org/10.1073/pnas.1100426108
Park, J. S., Kim, M., Song, N.-J., Kim, J.-H., Seo, D., Lee, J.-H., et al. (2019). A Reciprocal Role of the Smad4-Taz Axis in Osteogenesis and Adipogenesis of Mesenchymal Stem Cells. *Stem Cells (Dayton, Ohio)*, *37*(3), 368–381. http://doi.org/10.1002/stem.2949
Peng, C.-Y., Mukhopadhyay, A., Jarrett, J. C., Yoshikawa, K., & Kessler, J. A. (2012). BMP receptor 1A regulates development of hypothalamic circuits critical for feeding behavior. *The Journal of Neuroscience : the Official Journal of the Society for Neuroscience*, *32*(48), 17211–17224. http://doi.org/10.1523/JNEUROSCI.2484-12.2012
Pera, M. F., Andrade, J., Houssami, S., Reubinoff, B., Trounson, A., Stanley, E. G., et al. (2004). Regulation of human embryonic stem cell differentiation by BMP-2 and its antagonist noggin. *Journal of Cell Science*, *117*(Pt 7), 1269–1280. http://doi.org/10.1242/jcs.00970
Petersen, M. A., Ryu, J. K., Chang, K.-J., Etxeberria, A., Bardehle, S., Mendiola, A. S., et al. (2017). Fibrinogen Activates BMP Signaling in Oligodendrocyte Progenitor Cells and Inhibits Remyelination after Vascular Damage. *Neuron*, *96*(5), 1003–1012.e7. http://doi.org/10.1016/j.neuron.2017.10.008
Piccirillo, S. G. M., Reynolds, B. A., Zanetti, N., Lamorte, G., Binda, E., Broggi, G., et al.

(2006). Bone morphogenetic proteins inhibit the tumorigenic potential of human brain tumour-initiating cells. *Nature*, *444*(7120), 761–765. http://doi.org/10.1038/nature05349

Piccolo, S., Agius, E., Leyns, L., Bhattacharyya, S., Grunz, H., Bouwmeester, T., & De Robertis, E. M. (1999). The head inducer Cerberus is a multifunctional antagonist of Nodal, BMP and Wnt signals. *Nature*, *397*(6721), 707–710. http://doi.org/10.1038/17820

Piccolo, S., Sasai, Y., Lu, B., & De Robertis, E. M. (1996). Dorsoventral patterning in Xenopus: inhibition of ventral signals by direct binding of chordin to BMP-4. *Cell*, *86*(4), 589–598. http://doi.org/10.1016/s0092-8674(00)80132-4

Plouffe, S. W., Lin, K. C., Moore, J. L., Tan, F. E., Ma, S., Ye, Z., et al. (2018). The Hippo pathway effector proteins YAP and TAZ have both distinct and overlapping functions in the cell. *The Journal of Biological Chemistry*, *293*(28), 11230–11240. http://doi.org/10.1074/jbc.RA118.002715

Podkowa, M., Christova, T., Zhao, X., Jian, Y., & Attisano, L. (2013). p21-Activated kinase (PAK) is required for Bone Morphogenetic Protein (BMP)-induced dendritogenesis in cortical neurons. *Molecular and Cellular Neurosciences*, *57*, 83–92. http://doi.org/10.1016/j.mcn.2013.10.005

Pous, L., Deshpande, S. S., Nath, S., Mezey, S., Malik, S. C., Schildge, S., et al. (2020). Fibrinogen induces neural stem cell differentiation into astrocytes in the subventricular zone via BMP signaling. *Nature Communications*, *11*(1), 630–13. http://doi.org/10.1038/s41467-020-14466-y

Qi, X., Li, T.-G., Hao, J., Hu, J., Wang, J., Simmons, H., et al. (2004). BMP4 supports self-renewal of embryonic stem cells by inhibiting mitogen-activated protein kinase pathways. *Proceedings of the National Academy of Sciences of the United States of America*, *101*(16), 6027–6032. http://doi.org/10.1073/pnas.0401367101

Qin, L., Wine-Lee, L., Ahn, K. J., & Crenshaw, E. B. (2006). Genetic analyses demonstrate that bone morphogenetic protein signaling is required for embryonic cerebellar development. *The Journal of Neuroscience : the Official Journal of the Society for Neuroscience*, *26*(7), 1896–1905. http://doi.org/10.1523/JNEUROSCI.3202-05.2006

Raff, M. C., Abney, E. R., & Miller, R. H. (1984). Two glial cell lineages diverge prenatally in rat optic nerve. *Developmental Biology*, *106*(1), 53–60. http://doi.org/10.1016/0012-1606(84)90060-5

Rao, M. S., Noble, M., & Mayer-Proschel, M. (1998). A tripotential glial precursor cell is present in the developing spinal cord. *Proceedings of the National Academy of Sciences*, *95*(7), 3996–4001. http://doi.org/10.1073/pnas.95.7.3996

Reyes de Mochel, N. S., Luong, M., Chiang, M., Javier, A. L., Luu, E., Toshihiko, F., et al. (2015). BMP signaling is required for cell cleavage in preimplantation-mouse embryos. *Developmental Biology*, *397*(1), 45–55. http://doi.org/10.1016/j.ydbio.2014.10.001

Richards, L. J., Kilpatrick, T. J., Dutton, R., Tan, S. S., Gearing, D. P., Bartlett, P. F., & Murphy, M. (1996). Leukaemia inhibitory factor or related factors promote the differentiation of neuronal and astrocytic precursors within the developing murine spinal cord. *The European Journal of Neuroscience*, *8*(2), 291–299. http://doi.org/10.1111/j.1460-9568.1996.tb01213.x

Rockman, S. P., Currie, S. A., Ciavarella, M., Vincan, E., Dow, C., Thomas, R. J., & Phillips, W. A. (2001). Id2 is a target of the beta-catenin/T cell factor pathway in colon carcinoma. *The Journal of Biological Chemistry*, *276*(48), 45113–45119. http://doi.org/10.1074/jbc.M107742200

Roybon, L., Lamas, N. J., Garcia-Diaz, A., Yang, E. J., Sattler, R., Jackson-Lewis, V., et al. (2013). Human Stem Cell-Derived Spinal Cord Astrocytes with Defined Mature or Reactive Phenotypes. *Cell Reports*, *4*(5), 1035–1048. http://doi.org/10.1016/j.celrep.2013.06.021

Sabra, H., Brunner, M., Mandati, V., Wehrle Haller, B., Lallemand, D., Ribba, A.-S., et al. (2017). β1 integrin-dependent Rac/group I PAK signaling mediates YAP activation of Yes-associated protein 1 (YAP1) via NF2/merlin. *The Journal of Biological Chemistry*, *292*(47), 19179–19197. http://doi.org/10.1074/jbc.M117.808063

Sahni, V., Mukhopadhyay, A., Tysseling, V., Hebert, A., Birch, D., McGuire, T. L., et al. (2010). BMPR1a and BMPR1b signaling exert opposing effects on gliosis after spinal cord injury. *The Journal of Neuroscience : the Official Journal of the Society for Neuroscience*, *30*(5), 1839–1855. http://doi.org/10.1523/JNEUROSCI.4459-09.2010

Sakurai, H., Miyoshi, H., Mizukami, J., & Sugita, T. (2000). Phosphorylation-dependent activation of TAK1 mitogen-activated protein kinase kinase kinase by TAB1. *FEBS Letters*, *474*(2-3), 141–145. http://doi.org/10.1016/s0014-5793(00)01588-x

Samanta, J., & Kessler, J. A. (2004). Interactions between ID and OLIG proteins mediate the inhibitory effects of BMP4 on oligodendroglial differentiation. *Development (Cambridge, England)*, *131*(17), 4131–4142. http://doi.org/10.1242/dev.01273

Samanta, J., Alden, T., Gobeske, K., Kan, L., & Kessler, J. A. (2010). Noggin protects against ischemic brain injury in rodents. *Stroke; a Journal of Cerebral Circulation*, *41*(2), 357–362. http://doi.org/10.1161/STROKEAHA.109.565523

Samanta, J., Burke, G. M., McGuire, T., Pisarek, A. J., Mukhopadhyay, A., Mishina, Y., & Kessler, J. A. (2007). BMPR1a signaling determines numbers of oligodendrocytes and calbindin-expressing interneurons in the cortex. *The Journal of Neuroscience : the Official Journal of the Society for Neuroscience*, *27*(28), 7397–7407. http://doi.org/10.1523/JNEUROSCI.1434-07.2007

Sasai, Y., Lu, B., Steinbeisser, H., & De Robertis, E. M. (1995). Regulation of neural induction by the Chd and Bmp-4 antagonistic patterning signals in Xenopus. *Nature*, *376*(6538), 333–336. http://doi.org/10.1038/376333a0

Schachtrup, C., Ryu, J. K., Helmrick, M. J., Vagena, E., Galanakis, D. K., Degen, J. L., et al. (2010). Fibrinogen triggers astrocyte scar formation by promoting the availability of active TGF-beta after vascular damage. *The Journal of Neuroscience : the Official Journal of the Society for Neuroscience*, *30*(17), 5843–5854. http://doi.org/10.1523/JNEUROSCI.0137-10.2010

Schlange, T., Arnold, H.-H., & Brand, T. (2002). BMP2 is a positive regulator of Nodal signaling during left-right axis formation in the chicken embryo. *Development (Cambridge, England)*, *129*(14), 3421–3429.

Scholze, A. R., Foo, L. C., Mulinyawe, S., & Barres, B. A. (2014). BMP signaling in astrocytes downregulates EGFR to modulate survival and maturation. *PloS One*, *9*(10), e110668. http://doi.org/10.1371/journal.pone.0110668

See, J., Mamontov, P., Ahn, K., Wine-Lee, L., Crenshaw, E. B., & Grinspan, J. B. (2007). BMP signaling mutant mice exhibit glial cell maturation defects. *Molecular and Cellular Neurosciences*, *35*(1), 171–182. http://doi.org/10.1016/j.mcn.2007.02.012

Serrano, I., McDonald, P. C., Lock, F., Muller, W. J., & Dedhar, S. (2013). Inactivation of the Hippo tumour suppressor pathway by integrin-linked kinase. *Nature Communications*, *4*, 2976. http://doi.org/10.1038/ncomms3976

Setoguchi, T., Yone, K., Matsuoka, E., Takenouchi, H., Nakashima, K., Sakou, T., et al. (2001). Traumatic injury-induced BMP7 expression in the adult rat spinal cord. *Brain Research*, *921*(1-2), 219–225. http://doi.org/10.1016/s0006-8993(01)03123-7

Shibuya, H., Iwata, H., Masuyama, N., Gotoh, Y., Yamaguchi, K., Irie, K., et al. (1998). Role of TAK1 and TAB1 in BMP signaling in early Xenopus development. *The EMBO Journal*, *17*(4), 1019–1028. http://doi.org/10.1093/emboj/17.4.1019

Shibuya, H., Yamaguchi, K., Shirakabe, K., Tonegawa, A., Gotoh, Y., Ueno, N., et al. (1996). TAB1: an activator of the TAK1 MAPKKK in TGF-beta signal transduction. *Science (New York, N.Y.)*, *272*(5265), 1179–1182. http://doi.org/10.1126/science.272.5265.1179

Shiga, A., Nozaki, H., Yokoseki, A., Nihonmatsu, M., Kawata, H., Kato, T., et al. (2011). Cerebral small-vessel disease protein HTRA1 controls the amount of TGF-β1 via cleavage of proTGF-β1. *Human Molecular Genetics*, *20*(9), 1800–1810. http://doi.org/10.1093/hmg/ddr063

Shimizu, T., Osanai, Y., Tanaka, K. F., Abe, M., Natsume, R., Sakimura, K., & Ikenaka, K. (2017). YAP functions as a mechanotransducer in oligodendrocyte morphogenesis and maturation. *Glia*, *65*(2), 360–374. http://doi.org/10.1002/glia.23096

Shore, E. M., Xu, M., Feldman, G. J., Fenstermacher, D. A., Cho, T.-J., Choi, I. H., et al. (2006). A recurrent mutation in the BMP type I receptor ACVR1 causes inherited and sporadic fibrodysplasia ossificans progressiva. *Nature Genetics*, *38*(5), 525–527. http://doi.org/10.1038/ng1783

Simon, D. W., McGeachy, M. J., Bayır, H., Clark, R. S. B., Loane, D. J., & Kochanek, P. M. (2017). The far-reaching scope of neuroinflammation after traumatic brain injury. *Nature Reviews. Neurology*, *13*(3), 171–191. http://doi.org/10.1038/nrneurol.2017.13

Sosunov, A. A., Wu, X., Tsankova, N. M., Guilfoyle, E., McKhann, G. M., & Goldman, J. E. (2014). Phenotypic heterogeneity and plasticity of isocortical and hippocampal astrocytes in the human brain. *The Journal of Neuroscience : the Official Journal of the Society for Neuroscience*, *34*(6), 2285–2298. http://doi.org/10.1523/JNEUROSCI.4037-13.2014

Srikanth, M., Kim, J., Das, S., & Kessler, J. A. (2014). BMP signaling induces astrocytic differentiation of clinically derived oligodendroglioma propagating cells. *Molecular Cancer Research : MCR*, *12*(2), 283–294. http://doi.org/10.1158/1541-7786.MCR-13-0349

Stahl, N., Boulton, T. G., Farruggella, T., Ip, N. Y., Davis, S., Witthuhn, B. A., et al. (1994). Association and activation of Jak-Tyk kinases by CNTF-LIF-OSM-IL-6 beta receptor components. *Science (New York, N.Y.)*, *263*(5143), 92–95. http://doi.org/10.1126/science.8272873

Sterpka, A., & Chen, X. (2018). Neuronal and astrocytic primary cilia in the mature brain. *Pharmacological Research*, *137*, 114–121. http://doi.org/10.1016/j.phrs.2018.10.002

Sudol, M. (1994). Yes-associated protein (YAP65) is a proline-rich phosphoprotein that binds to the SH3 domain of the Yes proto-oncogene product. *Oncogene*, *9*(8), 2145–2152.

Sun, C., De Mello, V., Mohamed, A., Ortuste Quiroga, H. P., Garcia-Munoz, A., Bloshi, Al, A., et al. (2017). Common and Distinctive Functions of the Hippo Effectors Taz and Yap in Skeletal Muscle Stem Cell Function. *Stem Cells (Dayton, Ohio)*, *35*(8), 1958–1972. http://doi.org/10.1002/stem.2652

Sun, Y., Nadal-Vicens, M., Misono, S., Lin, M. Z., Zubiaga, A., Hua, X., et al. (2001). Neurogenin promotes neurogenesis and inhibits glial differentiation by independent mechanisms. *Cell*, *104*(3), 365–376. http://doi.org/10.1016/s0092-8674(01)00224-0

Supanji, Shimomachi, M., Hasan, M. Z., Kawaichi, M., & Oka, C. (2013). HtrA1 is induced by oxidative stress and enhances cell senescence through p38 MAPK pathway. *Experimental Eye Research*, *112*, 79–92. http://doi.org/10.1016/j.exer.2013.04.013

Suzuki, A., Chang, C., Yingling, J. M., Wang, X. F., & Hemmati-Brivanlou, A. (1997). Smad5 induces ventral fates in Xenopus embryo. *Developmental Biology*, *184*(2), 402–405. http://doi.org/10.1006/dbio.1997.8548

Takaesu, G., Kishida, S., Hiyama, A., Yamaguchi, K., Shibuya, H., Irie, K., et al. (2000). TAB2, a novel adaptor protein, mediates activation of TAK1 MAPKKK by linking TAK1 to TRAF6 in the IL-1 signal transduction pathway. *Molecular Cell*, *5*(4), 649–658. http://doi.org/10.1016/s1097-2765(00)80244-0

Takizawa, T., Nakashima, K., Namihira, M., Ochiai, W., Uemura, A., Yanagisawa, M., et al. (2001). DNA methylation is a critical cell-intrinsic determinant of astrocyte differentiation in the fetal brain. *Developmental Cell*, *1*(6), 749–758. http://doi.org/10.1016/s1534-5807(01)00101-0

Tang, C., Takahashi-Kanemitsu, A., Kikuchi, I., Ben, C., & Hatakeyama, M. (2018). Transcriptional Co-activator Functions of YAP and TAZ Are Inversely Regulated by Tyrosine Phosphorylation Status of Parafibromin. *iScience*, *2*, 103. http://doi.org/10.1016/j.isci.2018.03.023

Timmer, J. R., Wang, C., & Niswander, L. (2002). BMP signaling patterns the dorsal and intermediate neural tube via regulation of homeobox and helix-loop-helix transcription factors. *Development (Cambridge, England)*, *129*(10), 2459–2472.

Tsai, H.-H., Li, H., Fuentealba, L. C., Molofsky, A. V., Taveira-Marques, R., Zhuang, H., et al. (2012). Regional astrocyte allocation regulates CNS synaptogenesis and repair. *Science (New York, N.Y.)*, *337*(6092), 358–362. http://doi.org/10.1126/science.1222381

Urist, M. R. (1965). Bone: formation by autoinduction. *Science (New York, N.Y.)*, *150*(3698), 893–899. http://doi.org/10.1126/science.150.3698.893

Urist, M. R., & Strates, B. S. (1971). Bone morphogenetic protein. *Journal of Dental Research*, *50*(6), 1392–1406. http://doi.org/10.1177/00220345710500060601

Vives, V., Alonso, G., Solal, A. C., Joubert, D., & Legraverend, C. (2003). Visualization of S100B-positive neurons and glia in the central nervous system of EGFP transgenic mice. *The Journal of Comparative Neurology*, *457*(4), 404–419. http://doi.org/10.1002/cne.10552

Waltzer, L., & Bienz, M. (1999). A function of CBP as a transcriptional co-activator during Dpp signalling. *The EMBO Journal*, *18*(6), 1630–1641. http://doi.org/10.1093/emboj/18.6.1630

Wang, N., Eckert, K. A., Zomorrodi, A. R., Xin, P., Pan, W., Shearer, D. A., et al. (2012). Down-regulation of HtrA1 activates the epithelial-mesenchymal transition and ATM DNA damage response pathways. *PloS One*, *7*(6), e39446. http://doi.org/10.1371/journal.pone.0039446

Wang, Y., Cheng, X., He, Q., Zheng, Y., Kim, D. H., Whittemore, S. R., & Cao, Q. L. (2011). Astrocytes from the contused spinal cord inhibit oligodendrocyte differentiation of adult oligodendrocyte precursor cells by increasing the expression of bone morphogenetic proteins. *The Journal of Neuroscience : the Official Journal of the Society for Neuroscience*, *31*(16), 6053–6058. http://doi.org/10.1523/JNEUROSCI.5524-09.2011

Watanabe, Y., Duprez, D., Monsoro-Burq, A. H., Vincent, C., & Le Douarin, N. M. (1998). Two domains in vertebral development: antagonistic regulation by SHH and BMP4 proteins. *Development (Cambridge, England)*, *125*(14), 2631–2639.

Wegleiter, T., Buthey, K., Gonzalez-Bohorquez, D., Hruzova, M., Bin Imtiaz, M. K., Abegg, A., et al. (2019). Palmitoylation of BMPR1a regulates neural stem cell fate. *Proceedings of the National Academy of Sciences of the United States of America*, *116*(51), 25688–25696. http://doi.org/10.1073/pnas.1912671116

Weinstein, D. C., & Hemmati-Brivanlou, A. (1999). Neural induction. *Annual Review of Cell and Developmental Biology*, *15*(1), 411–433. http://doi.org/10.1146/annurev.cellbio.15.1.411

Wen, Z., Han, L., Bamburg, J. R., Shim, S., Ming, G.-L., & Zheng, J. Q. (2007). BMP gradients steer nerve growth cones by a balancing act of LIM kinase and Slingshot phosphatase on ADF/cofilin. *The Journal of Cell Biology*, *178*(1), 107–119. http://doi.org/10.1083/jcb.200703055

Wieser, R., Wrana, J. L., & Massagué, J. (1995). GS domain mutations that constitutively activate T beta R-I, the downstream signaling component in the TGF-beta receptor complex. *The EMBO Journal*, *14*(10), 2199–2208.

Wilson, P. A., & Hemmati-Brivanlou, A. (1995). Induction of epidermis and inhibition of neural fate by Bmp-4. *Nature*, *376*(6538), 331–333. http://doi.org/10.1038/376331a0

Wine-Lee, L., Ahn, K. J., Richardson, R. D., Mishina, Y., Lyons, K. M., & Crenshaw, E. B. (2004). Signaling through BMP type 1 receptors is required for development of interneuron cell types in the dorsal spinal cord. *Development (Cambridge, England)*, *131*(21), 5393–5403. http://doi.org/10.1242/dev.01379

Winnier, G., Blessing, M., Labosky, P. A., & Hogan, B. L. (1995). Bone morphogenetic protein-4 is required for mesoderm formation and patterning in the mouse. *Genes & Development*, *9*(17), 2105–2116. http://doi.org/10.1101/gad.9.17.2105

Wrana, J. L., Attisano, L., Wieser, R., Ventura, F., & Massagué, J. (1994). Mechanism of activation of the TGF-beta receptor. *Nature*, *370*(6488), 341–347. http://doi.org/10.1038/370341a0

Xia, H., Dai, X., Yu, H., Zhou, S., Fan, Z., Wei, G., et al. (2018). EGFR-PI3K-PDK1 pathway regulates YAP signaling in hepatocellular carcinoma: the mechanism and its implications in targeted therapy. *Cell Death & Disease*, *9*(3), 269–12. http://doi.org/10.1038/s41419-018-0302-x

Xia, P., Gütl, D., Zheden, V., & Heisenberg, C.-P. (2019). Lateral Inhibition in Cell Specification Mediated by Mechanical Signals Modulating TAZ Activity. *Cell*, *176*(6), 1379–1392.e14. http://doi.org/10.1016/j.cell.2019.01.019

Xie, C. (2020). Astrocytic YAP Promotes the Formation of Glia Scars and Neural Regeneration after Spinal Cord Injury. *Journal of Neuroscience*, *40*(13), 2644–2662. http://doi.org/10.1523/JNEUROSCI.2229-19.2020

Yamaguchi, K., Nagai, S. I., Tsuji, J. N., Nishita, M., Tamai, K., Irie, K., et al. (1999). XIAP, a cellular member of the inhibitor of apoptosis protein family, links the receptors to TAB1–TAK1 in the BMP signaling pathway. *The EMBO Journal*, *18*(1), 179–187. http://doi.org/10.1093/emboj/18.1.179

Yamaguchi, K., Shirakabe, K., Shibuya, H., Irie, K., Oishi, I., Ueno, N., et al. (1995). Identification of a member of the MAPKKK family as a potential mediator of TGF-beta signal transduction. *Science (New York, N.Y.)*, *270*(5244), 2008–2011. http://doi.org/10.1126/science.270.5244.2008

Yamauchi, K., Phan, K. D., & Butler, S. J. (2008). BMP type I receptor complexes have distinct activities mediating cell fate and axon guidance decisions. *Development (Cambridge,*

England), *135*(6), 1119–1128. http://doi.org/10.1242/dev.012989
Yamauchi, K., Varadarajan, S. G., Li, J. E., & Butler, S. J. (2013). Type Ib BMP receptors mediate the rate of commissural axon extension through inhibition of cofilin activity. *Development (Cambridge, England)*, *140*(2), 333–342. http://doi.org/10.1242/dev.089524
Yan, Y., Gong, P., Jin, W., Xu, J., Wu, X., Xu, T., et al. (2012). The cell-specific upregulation of bone morphogenetic protein-10 (BMP-10) in a model of rat cortical brain injury. *Journal of Molecular Histology*, *43*(5), 543–552. http://doi.org/10.1007/s10735-012-9431-1
Yang, N., Higuchi, O., Ohashi, K., Nagata, K., Wada, A., Kangawa, K., et al. (1998). Cofilin phosphorylation by LIM-kinase 1 and its role in Rac-mediated actin reorganization. *Nature*, *393*(6687), 809–812. http://doi.org/10.1038/31735
Yang, N., Morrison, C. D., Liu, P., Miecznikowski, J., Bshara, W., Han, S., et al. (2012). TAZ induces growth factor-independent proliferation through activation of EGFR ligand amphiregulin. *Cell Cycle*, *11*(15), 2922–2930. http://doi.org/10.4161/cc.21386
Yao, M., Wang, Y., Zhang, P., Chen, H., Xu, Z., Jiao, J., & Yuan, Z. (2014). BMP2-SMAD signaling represses the proliferation of embryonic neural stem cells through YAP. *The Journal of Neuroscience : the Official Journal of the Society for Neuroscience*, *34*(36), 12039–12048. http://doi.org/10.1523/JNEUROSCI.0486-14.2014
Yeh, T.-H., Lee, D. Y., Gianino, S. M., & Gutmann, D. H. (2009). Microarray analyses reveal regional astrocyte heterogeneity with implications for neurofibromatosis type 1 (NF1)-regulated glial proliferation. *Glia*, *57*(11), 1239–1249. http://doi.org/10.1002/glia.20845
Yi, S. E., Daluiski, A., Pederson, R., Rosen, V., & Lyons, K. M. (2000). The type I BMP receptor BMPRIB is required for chondrogenesis in the mouse limb. *Development (Cambridge, England)*, *127*(3), 621–630.
Yi, S. E., LaPolt, P. S., Yoon, B. S., Chen, J. Y., Lu, J. K., & Lyons, K. M. (2001). The type I BMP receptor BmprIB is essential for female reproductive function. *Proceedings of the National Academy of Sciences*, *98*(14), 7994–7999. http://doi.org/10.1073/pnas.141002798
Ying, Q.-L., Nichols, J., Chambers, I., & Smith, A. (2003a). BMP Induction of Id Proteins Suppresses Differentiation and Sustains Embryonic Stem Cell Self-Renewal in Collaboration with STAT3. *Cell*, *115*(3), 281–292. http://doi.org/10.1016/S0092-8674(03)00847-X
Ying, Q.-L., Nichols, J., Chambers, I., & Smith, A. (2003b). BMP induction of Id proteins suppresses differentiation and sustains embryonic stem cell self-renewal in collaboration with STAT3. *Cell*, *115*(3), 281–292. http://doi.org/10.1016/s0092-8674(03)00847-x
Yoon, B. S., Ovchinnikov, D. A., Yoshii, I., Mishina, Y., Behringer, R. R., & Lyons, K. M. (2005). Bmpr1a and Bmpr1b have overlapping functions and are essential for chondrogenesis in vivo. *Proceedings of the National Academy of Sciences of the United States of America*, *102*(14), 5062–5067. http://doi.org/10.1073/pnas.0500031102
Yu, F.-X., Zhao, B., & Guan, K.-L. (2015). Hippo Pathway in Organ Size Control, Tissue Homeostasis, and Cancer. *Cell*, *163*(4), 811–828. http://doi.org/10.1016/j.cell.2015.10.044
Yuhki, M., Yamada, M., Kawano, M., Iwasato, T., Itohara, S., Yoshida, H., et al. (2004). BMPR1A signaling is necessary for hair follicle cycling and hair shaft differentiation in mice. *Development (Cambridge, England)*, *131*(8), 1825–1833. http://doi.org/10.1242/dev.01079
Zeisberg, M., Hanai, J.-I., Sugimoto, H., Mammoto, T., Charytan, D., Strutz, F., & Kalluri, R. (2003). BMP-7 counteracts TGF-beta1-induced epithelial-to-mesenchymal transition and reverses chronic renal injury. *Nature Medicine*, *9*(7), 964–968. http://doi.org/10.1038/nm888

Zeisel, A., Muñoz-Manchado, A. B., Codeluppi, S., Lönnerberg, P., La Manno, G., Juréus, A., et al. (2015). Brain structure. Cell types in the mouse cortex and hippocampus revealed by single-cell RNA-seq. *Science (New York, N.Y.)*, *347*(6226), 1138–1142. http://doi.org/10.1126/science.aaa1934

Zhang, D., Mehler, M. F., Song, Q., & Kessler, J. A. (1998). Development of bone morphogenetic protein receptors in the nervous system and possible roles in regulating trkC expression. *The Journal of Neuroscience : the Official Journal of the Society for Neuroscience*, *18*(9), 3314–3326.

Zhang, R., Boareto, M., Engler, A., Louvi, A., Giachino, C., Iber, D., & Taylor, V. (2019). Id4 Downstream of Notch2 Maintains Neural Stem Cell Quiescence in the Adult Hippocampus. *Cell Reports*, *28*(6), 1485–1498.e6. http://doi.org/10.1016/j.celrep.2019.07.014

Zhang, Y., Chen, K., Sloan, S. A., Bennett, M. L., Scholze, A. R., O'Keeffe, S., et al. (2014). An RNA-sequencing transcriptome and splicing database of glia, neurons, and vascular cells of the cerebral cortex. *The Journal of Neuroscience : the Official Journal of the Society for Neuroscience*, *34*(36), 11929–11947. http://doi.org/10.1523/JNEUROSCI.1860-14.2014

Zhou, J., Lee, P.-L., Lee, C.-I., Wei, S.-Y., Lim, S. H., Lin, T.-E., et al. (2013). BMP receptor-integrin interaction mediates responses of vascular endothelial Smad1/5 and proliferation to disturbed flow. *Journal of Thrombosis and Haemostasis : JTH*, *11*(4), 741–755. http://doi.org/10.1111/jth.12159

Zhou, M., Schools, G. P., & Kimelberg, H. K. (2006). Development of GLAST(+) astrocytes and NG2(+) glia in rat hippocampus CA1: mature astrocytes are electrophysiologically passive. *Journal of Neurophysiology*, *95*(1), 134–143. http://doi.org/10.1152/jn.00570.2005

Zhu, G., Mehler, M. F., Mabie, P. C., & Kessler, J. A. (1999a). Developmental changes in progenitor cell responsiveness to cytokines. *Journal of Neuroscience Research*, *56*(2), 131–145. http://doi.org/10.1002/(sici)1097-4547(19990415)56:2<131::aid-jnr3>3.0.co;2-i

Zhu, G., Mehler, M. F., Zhao, J., Yu Yung, S., & Kessler, J. A. (1999b). Sonic hedgehog and BMP2 exert opposing actions on proliferation and differentiation of embryonic neural progenitor cells. *Developmental Biology*, *215*(1), 118–129. http://doi.org/10.1006/dbio.1999.9431

Zimmerman, L. B., De Jesús-Escobar, J. M., & Harland, R. M. (1996). The Spemann organizer signal noggin binds and inactivates bone morphogenetic protein 4. *Cell*, *86*(4), 599–606. http://doi.org/10.1016/s0092-8674(00)80133-6

Zode, G. S., Clark, A. F., & Wordinger, R. J. (2009). Bone morphogenetic protein 4 inhibits TGF-beta2 stimulation of extracellular matrix proteins in optic nerve head cells: role of gremlin in ECM modulation. *Glia*, *57*(7), 755–766. http://doi.org/10.1002/glia.20803

Zou, H., & Niswander, L. (1996). Requirement for BMP signaling in interdigital apoptosis and scale formation. *Science (New York, N.Y.)*, *272*(5262), 738–741. http://doi.org/10.1126/science.272.5262.738

Zou, H., Wieser, R., Massagué, J., & Niswander, L. (1997a). Distinct roles of type I bone morphogenetic protein receptors in the formation and differentiation of cartilage. *Genes & Development*, *11*(17), 2191–2203. http://doi.org/10.1101/gad.11.17.2191

Zou, H., Wieser, R., Massagué, J., & Niswander, L. (1997b). Distinct roles of type I bone morphogenetic protein receptors in the formation and differentiation of cartilage. *Genes & Development*, *11*(17), 2191–2203.

Zudaire, E., Gambardella, L., Kurcz, C., & Vermeren, S. (2011). A computational tool for

quantitative analysis of vascular networks. *PloS One*, *6*(11), e27385. http://doi.org/10.1371/journal.pone.0027385